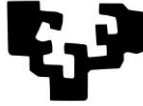eman ta zabal zazu

Universidad del País Vasco **Euskal Herriko Unibertsitatea**

TESIS DOCTORAL

Development of Plasma based surfaces, supported by Electro-Tribological studies

Iñigo Braceras Izaguirre

Donostia - San Sebastián, February 2019

ACKNOWLEDGEMENTS

I would like to thank everyone that has made it possible the preparation of this PhD dissertation.

LABURPENA

Tesi honetako lanen **helburua**, elektro-tribologia erabiliz bi gai ezberdinetan, gainazal-tratamendu eta estalduren garapenean datza.

Tribologia mugitzen diren elementuen arteko marruskadura, higadura eta lubrifikazioa aztertzen duen zientzia da. Tribologia saiakuntzak tribometroetan egin ohi dira, eta bertan ukitzen diren bi laginen arteko marruskadura koefizientea (CoF) etengabe neurtzen da. Kasu batzuetan, higidura ere neurtzen da, baino normalean saiakuntzaren ondoren. CoF-aren etengabeko segimenduaz gain, kontaktu elektrikoaren erresistentziarena (ECR) ere egiten bada, **elektro-tribologia** esaten zaio.

Tesi honen kasuan, elektro-tribologia honako puntu hauek ikertzeko erabili da: i) kualitatibo eta kuantitatiboki ukitze-azaleraren degradazio mekanismoak; ii) kontaktore elektrikoetan erabili daitezkeen eroale elektriko eta dielektriko estalduren eraginkortasuna; eta iii) elektro-tribologiaren gaitasuna ukitzen diren elementuen etengabeko egoeraren segimendua egiteko on-line moduan.

Aurreneko gaiaren kasuan, bi altzairu herdoilgaitz aleazioetan, gainazalaren propietate tribologikoak hobetzeko gainazal tratamenduen garapenean jarri da arreta, betiere korrosio erresistentzia galdu gabe. Bi geometria ezberdin ikertu dira: i) **AISI 316L** altzairu herdoilgaitz austenikoaren kasuan, hodien barruko gainazala; ii) **15-5PH** altzairu herdoilgaitz martensitikoaren kasuan, zilindroen gainazala. Aleazioen eta laginen geometriaren aukeraketa gerta daitezkeen industria aplikazioen ara behera egin da. Arlo medikuan (kanulak, trefinak,…), kimikoan eta elikadura industrian altzairu herdoilgaitz austenitikoa erabiltzen duten hodi geometria duten elementu asko dago. Ordea, ez dago hodien barruan propietate tribologikoak hobetzeko eman daitekeen gainazal-tratamendu egokirik. Bestalde, korrosioari erresistentzia behar denean propietate mekaniko altuekin batera, altzairu herdoilgaitz martensitikoak erabili ohi dira, maiz zilindro geometria duten elementuetan. Adibidez aeronautika arloan (lurreratze-trenaren elementuetan), lur-garraio arloan (meategietako kamioien karga sentsoreak daramaten elementuetan), medikuntza produktuetan (harraskagailu femoraletan). Kasu hauetan ere, propietate tribologikoak hobetzeko, korrosioarekiko erresistentzia kaltetuko ez duen gainazal tratamendu egokirik ez dago industria mailan.

Bigarren gaiaren kasuan, propietate elektro-tribologiko hobeagoak dituzten **estaldura eroale elektriko eta dielektrikoetan** jarri du arreta garapenak. Denbora asko baino lehen hemen izango ditugun ibilgailu elektrikoak edo sare elektriko azkarrak (Smart grids) kontaktore elektriko ugari beharko dituzte, orain baino eragiketa nabarmen gehiago jasan behar izango dituztelarik. Gaur egungo estaldurak lan baldintza hauek ezin dituzte jasan ordea, gertatzen diren degradazio elektro-tribologikoengatik (CoF, ECR eta higidura).

Altzairu herdoilgaitzen kasuan gainazal-tratamenduen garapena **Active Screen Plasma (ASP) teknologian eta Hollow Cathode (HC) efektuan** oinarritu da. Ohiko nitrurazio teknologiekiko ASP teknologiak baditu abantaila zehatz batzuk: ASP instalakuntzek sare metaliko (screen) bat dute tratamendu gunearen inguruan, hutsune kameran. Hau plasma eta bero iturri bezala erabili daiteke, tratatu nahi diren laginei ezartzen zaien parametro elektrikoengandik (bias voltage) guztiz bananduta. Honek

tratamendu prozesuan malgutasun handiagoa dakar, laginari aplikatutako plasmak ez bait du nitrurazioa difusio termo-kimiko bidez gerta dadin behar den tenperaturara igotzeko ardura guztia. Honekin ohiko plasma nitrurazioek dituzten mugak (hertz efektuak, homogeneotasun eza, arku elektrikoen arriskua, e.a.) gainditu daitezke.

Bestalde, Hollow Cathode efektua zirrikituetan (zuloetan, hodietan, e.a.) gertatu ohi da, plasma barruan kate erreakzioak gertatzen direnean. Ondorioz, zirrikitu hauetan plasma dentsitatea handiagoa izaten da, eta inguruko tenperatura igo ohi da. Sarri, Hollow Cathode efektua kaltegarritzat hartzen da, saihestu behar den arriskua. Dena den, beste kasu batzuetan onuragarria suertatu daiteke, modu egokian erabiltzen bada.

Tesi honetan aurkezten diren lanak argi uzten dute ASP teknologia eta HC efektuak lagungarriak izan daitezkela, nitruratutako bi altzairu herdoilgaitzen aleazioetan, gain-azalerak korrosio erresistentzia galdu gabe, tribologia propietateak hobetzeko. Gainazal tratamendu hauen gakoa leku aproposetan (hodi barruan edo zilindroen inguruan) dentsitate handiko plasmak lortzean datza, eta horren bidez tratamendu denbora laburrak tenperatura moderatu edo ertainetan ahalbidetzea. Honekin kromo nitruroen hauspeatzea mugatzen da, eta gainazalaren zati zehatzetan nahiko kromo askea geratzen da, altzairuen heldoilgaitzatasunaren arrazoia. Dena den, tratamendu baldintzen leihoa mugatuta da. Altzairu herdoilgaitz martensitikoen kasuan adibidez, tratamenduak eragindako tentsioen pilaketak, pitzadurak eragin ditzake, eta honek korrosioa ahalbideratzen du.

Elektro-tribologi ikerketak tratatutako aleazioen tribologia propietateen hobekuntza erakutsi dute. Gainera, ERC eta CoF bilakaeraren datuak, gain-azalaren degradazioaren ikerketan sakontzea ahalbideratu du. Honek ECR parametroaren etengabeko segimendua egitearen potentzialtasuna erakutsi du. Bestalde, CoF-ak tratatu gabeko gain-azalerak baino balio altuagoak erakutsi ditu gainazal tratatuetan, baino hasiera batetik balio egonkorrekin. Hau baliagarria izan daiteke elementuak , irristaka baino, errodadura moduan mugitzea ziurtatu nahi den aplikazioetan. ECR kasuan, bere bilakaera gainazal tratatuetan eta tratatu gabeetan oso ezberdina izan da. Beraz gainazalaren egoeraren segimendua egiteko parametro aproposa izan daiteke. Dena den ECR-aren bilakaeran beste parametro batzuk ere eragina izan

dezakete, i.e. hezetasunak, bai gainazal tratatuan bai ez tratatuan. Ondorio bezala honek konplexutasun handiagoa dakar, eta agian potentzialtasun handiagoa ere, inguruko baldintzetara sentikorra izatea interesgarria den aplikazioetan.

Funtzio elektrikoa duten estaduren kasuan, garapen eta ikerketak **Magnetron Sputtering – Physical Vapor Deposition (MS-PVD) teknologia**n oinarritu dira. Alde batetik, eroankortasun elektrikoa duten estalduren kasuan, zilar-aluminio (**AgAl**) aleazioak ikertu dira. Estaldura dielektrikoen kasuan, Diamond Like Carbon (**DLC**) geruzak. Bi kasutan, kobrearen gainean ezarri dira estaldurak, bien artean nikelezko eta WC-Co geruzak ezarri direlarik, estalduren atxikidura hobetzearren.

Gaur egun aplikazio elektriko askotan, kontaktoreetan elektrolitikoki ezarritako **zilarrezko estaldurak** erabili ohi dira. **Eroankortasun elektriko** ona dute, baino bere portaera tribologikoa oso eskasa da. Hau arazo larri bat da, bereziki era fidagarri eta iraunkorrean konexio – deskonexio elektriko asko jasan behar duten aplikazioetan (esate baterako, smart grid-etan). Egindako ikerketan, higidura modu ezberdinak nabarmendu dira, estalduran aluminio portzentaia, aleazioaren fase eta inguruko baldintzen arabera. ECR dinamiko eta estatikoen arteko ezberdintasunak ere egiaztatu dira. Estaldura hauen beste propietate garrantzitsu bat zufrearekiko (eta kloro eta oxigenoarekiko) erresistentzia da, zufrea duten olio isolatzaileetan egin ohi bait dute lan. Egindako ikerketek estalduraren aleazioan aluminioa sartzeak onurak ekarri dituela erakutsi dute, zufrearekiko degradazioa mugatuz. Dena den, gainazalaren oxidatzeko joera ere handitu egin da, eta honek tamalez ECR balioen igoera ekarri du.

AgAl estalduren kasuan, elektro-tribologia ikerketak baliagarriak izan dira estalduren funtzionaltasuna aztertzerakoan, estaldura hauen baliozko aplikazioa kontuan hartu, gainazal eroale-elektrikoak kontaktoreetan. Dena den, elektro-tribologia aplikazio bertan etengabeko estalduren segimendua egiteko baliagarria izan daitekeen zehaztu ahal izateko, ikerketa sakonagoak beharrezkoak dira. Ikerketa hauek sufrearekin eta kloroarekin gerta daitezkeen estalduren degradazioak, elektro-tribologia saiakuntzen baldintzetara gehitu beharko lirateke.

DLC estaldurak oso propietate ezberdinak izan ditzakete, bai tribologikoak bai elektrikoak. Tesian egindako lanetan DLC **dielektrikoak** ikertu dira.

Garatutako estalduretan propietate dielektrikoa ikerketa elektro-tribologikoetan egiaztatu da. Izan ere, hasierako ERC balioak erabilitako multimetroaren neurtzeko duen mugaren goitik suertatu dira. Bestalde, ikerketa elektro-tribologikoak oso baliagarriak izan dira saiakuntzen zehar degradazio mekanismoak zehaztu eta ulertu ahal izateko. Degradazioa fase ezberdinetan gertatu da. Lehendabizi estalduretan pitzadurak agertu dira. Puntu honetan estalduren barru-tentsioak rol garrantzitsua jokatu dute. Pitzadurak hedatzen joan dira saiakuntzek aurrera egin duten neurrian, betiere estalduren ezaugarri dielektrikoa mantenduz. Dena den, une batetik aurrera estaldurak zartatu eta altxatu egin dira, higidura arrastoen hainbat puntutan, kontrako aluminiozko laginetik materialaren transferentzia erraztuz eta higidura itsaskorra (adhesive wear) eraginez. Honekin batera, estalduren ECR-ek behera egin dute pixkanaka. Estalduren erdiko WC-Co geruzetara edo/eta kobrera heldutakoan higidura itsaskorra nabarmen handitu da, eta oxidazio fenomenoak agertu dira. Puntu hauetan, CoF eta ECR-ak gora behera handiak jasan dituzte, era kontrajarrian, i.e. oxidazioarekin CoF-ak behera eta ECR-ak gora. Bestalde, elektro-tribologia ikerketek DLC estalduren jardueran inguruko hezetasunaren garrantzia argi erakutsi dute, bati bat estalduren iraunkortasunean.

Tesian egindako lanetan **hipotesi nagusia** ikerketa elektro-tribologikoak baliagarriak izan daitezkeelakoan datza, lotuak dauden helburu ezberdinetarako: i) gainazal tratamendu eta estalduren garapenean; eta ii) gainazalen segimendua egiteko eta beraien funtzionaltasuna eta/edo degradazioari buruzko momentuan momentuko datuak jaso ahal izateko.

Gainerako hipotesiak honako beste puntu hauetan dautza: i) Hollow Cathode fenomenoa baliagarria izan daiteke altzairu herdoilgaitzen gainazal tratamenduetan korrosioarekiko erresistentzia eta propietate tribologikoen arteko konpromezu egokia lortu ahal izateko; ii) AgAl estaldurak gaur egungo zilarrezko estalduren portaera tribologikoa nabarmen hobetu ditzakete; eta iii) DLC estaldurak baliagarriak izan daitezke mugimenduan dauden kontaktu dielektrikoetan.

Burututako ikerketen emaitzek hasierako hipotesien egokitasuna neurri ezberdinetan baieztatu dute.

ASP teknologiaren eta HC efektuaren konbinazioa baliagarria dela ikusi da altzairu herdoilgaitz martensitiko eta austenitikoen nitrurazio gainazal tratamenduen garapenean, bai geometria zilindrikoan bai hodien barne gainazalean. Plasma dentsitate handiak ahalbideratu du lorpen hau. Honek tratamendu denbora laburrekin eta tenperatura moderatuekin, posible egin du aleazio hauetan korrosioaren erresistentzia ez galtzea, baino aldi berean propietate tribologikoak hobetzea.

Bestalde, MS-PVD teknologiak, propietate tribologiko onak dituzten estaldura dielektriko eta eroaleak ahalbidetu ditu. AgAl aleazio eroaleen kasuan gainera, sufrea duten inguruneekiko degradazioari erresistentzia hobetu dela ere agirian utzi da.

Azkenik, gauzatutako garapenetan saiakuntza elektro-tribologikoak gain-azalen degradazio mekanismoak ikertzeko baliagarriak direla egiaztatu da. Beraz tresna aproposa da estalduren garapenerako. Funtzio elektrikoa duten estalduren kasuan, CoF-ak edo ECR estatikoak eman dezaketen informaziotik areago eskaini ditzake etengabeko ECR dinamikoak, estalduren eta funtzionaltasunaren segimendua ahalbideturik, eta beraien degradazio mekanismoei buruz (higidura, pitzadurak, oxidazioak, e.a.) datu baliagarriak emanez. Ondorioz, gainazalen egoeraren monitorizazio edo etengabeko segimendua egiteko aukera eskaintzen du, mantenu beharrak iragarri edo aurreikusteko gaitasuna duten sistemetan erabiliz, betiere.

RESUMEN

Los **objetivos** de los trabajos de esta tesis se han centrado en el desarrollo de tratamientos de superficie y recubrimientos en dos campos diferenciados, apoyados en estudios electro-tribológicos.

La **tribología** es la ciencia que estudia la fricción, el desgaste y la lubricación que tienen lugar durante el contacto entre superficies sólidas en movimiento. Las herramientas clásicas en los estudios tribológicos consisten en tribómetros que registran de manera continua el coeficiente de fricción (CoF) entre los componentes o muestras en contacto. El desgaste, se mide también en algunos casos de forma continua, o frecuentemente tras la finalización de los ensayos. Si además de monitorizar de forma continua el CoF, se monitoriza también la resistencia eléctrica de contacto (ECR – Electrical Contact Resistance), hablamos de electro-tribología.

El apoyo de estos **estudios electro-tribológicos** realizados en la tesis se ha centrado en su uso como herramienta para el estudio cuantitativo y cualitativo de los mecanismos de degradación paulatina de las superficies en contacto; el estudio operativo de recubrimientos conductores y aislantes eléctricos orientados a su uso en contactores eléctricos; y el estudio de su potencialidad como herramienta de monitorización continua, en línea, de componentes en operación.

El primero de los campos de desarrollo de tratamientos de superficie se ha centrado en mejorar las propiedades tribológicas de las superficies de dos aleaciones de **aceros inoxidables** en dos geometrías diferentes, sin comprometer su resistencia a la corrosión: la aleación **AISI 316L**, un acero inoxidable austenítico, y la aleación **15-5PH**, un acero inoxidable endurecible por precipitación (PH) martensítico. En el primer caso, se ha trabajado sobre superficies en interiores de conductos o geometrías tubulares. En el segundo, sobre geometrías cilíndricas. La selección tanto de la aleación como de las geometrías obedece a potenciales aplicaciones industriales que puedan beneficiarse de los desarrollos en un futuro. Así, existen multitud de aplicaciones en el campo biomédico (cánulas, trefinas, etc.), químico, alimentación, etc. que emplean aleaciones de aceros inoxidables austeníticos, presentan una geometría tubular, pero no existen tratamientos satisfactorios que se puedan aplicar en los interiores de los mismos para dotarles de mejores propiedades tribológicas. Por otra parte, en muchas aplicaciones donde las exigencias mecánicas y de resistencia a la corrosión son máximas, en el campo aeronáutico (p.ej. componentes en los trenes de aterrizaje), transporte (p.ej. componentes sensores de camiones de carga en minería) o biomédico (p.ej. raspas femorales), etc. se emplean aceros inoxidables PH martensíticos, en componentes de geometrías cilíndricas o semi-cilíndricas, donde otra vez, la disponibilidad de tratamientos que mejoren sus prestaciones tribológicas no es satisfactoria.

El segundo de los campos de desarrollo se ha centrado en mejorar las propiedades electro-tribológicas de **recubrimientos** delgados **conductores eléctricos** y capas finas **dieléctricas** respectivamente. Amplias tecnologías de futuro como las redes inteligentes (smart grids), los vehículos eléctricos, etc. conllevan el uso de un mayor número de contactos eléctricos con un mayor número de operaciones que los materiales y recubrimientos que se emplean en la actualidad no son capaces de soportar, por su deterioro electro-tribológico.

En el caso de los **aceros inoxidables**, el desarrollo de los tratamientos de superficie se ha basado en la tecnología de nitruración de plasma de rejilla activa (ASP - **Active Screen Plasma**) y el efecto de cátodo hueco (HC – **Hollow Cathode**). La ventaja del ASP respecto a las tecnologías convencionales de nitruración por plasma reside en la posibilidad de emplear la rejilla externa en la cámara de tratamiento como fuente de calor y como generador de especies de plasma, de forma independiente a los parámetros eléctricos (Fuente de BIAS) aplicados directamente al componente a tratar. Ello permite una mayor flexibilidad de la definición de los tratamientos, ya que el plasma aplicado directamente a la pieza no asume toda la responsabilidad de elevar la temperatura de la pieza al nivel necesario para que tenga lugar la reacción termo-química de nitruración. Con ello, potencialmente, se pueden superar limitaciones típicas de los plasmas convencionales como los efectos de borde (i.e. tratamiento irregular), riesgo de arcos, etc.

Por otra parte, el efecto de cátodo hueco se produce por un efecto cascada en el plasma cuando éste se halla localizado en una geometría confinada (orificios, agujeros pasantes, etc.), que da lugar a plasmas de mayor densidad que conducen a un calentamiento local de dicha región. Normalmente, el efecto de cátodo hueco se considera un efecto pernicioso, a evitar. No obstante, en determinadas situaciones, puede hacerse uso del mismo de forma provechosa.

Los desarrollos acometidos en este trabajo han puesto de manifiesto la potencialidad de la tecnología ASP y el efecto de HC para generar superficies nitruradas, preservando la resistencia a la corrosión de los dos aceros inoxidables estudiados. La clave de los tratamientos reside en generar plasmas de alta densidad en las zonas deseadas, i.e. en el interior de los tubos o en torno a los cilindros, que posibiliten tratamientos de nitruración breves (en comparación con los tratamientos convencionales) a temperaturas moderadas. Con ello se limita la precipitación de nitruros de cromo, conservando regiones de la sección superficial con suficiente cromo libre, detrás de la resistencia a la corrosión de los aceros inoxidables. No obstante, se ha demostrado también que la ventana de tratamiento es reducida, porque, por ejemplo, en el caso de los aceros PH martensíticos, la acumulación de tensiones

causadas por el tratamiento genera grietas transversales, que dan lugar a puntos de corrosión localizados.

Los estudios electro-tribológicos han puesto de manifiesto la mejora del comportamiento tribológico de las aleaciones tratadas. Además, la información de la evolución del ECR (y del CoF) ha permitido profundizar en el estudio de los mecanismos de degradación de las superficies en contacto, poniendo de relieve con ello la potencialidad de dicho parámetro para monitorizar en línea de forma continua o discontinua la condición de la superficie tratada. El CoF en general aumenta respecto a las superficies no tratadas y muestra unos valores muy estables desde etapas tempranas de los ensayos. Esta característica presenta potencial interés en aquellos casos donde por ejemplo se requiere garantizar regímenes de funcionamiento en rodadura (evitando el deslizamiento o fenómenos de "derrapaje"). En cuanto al ECR, la evolución del mismo fue muy diferente en las superficies nitruradas respecto a las no tratadas, lo que abriría la puerta para su uso como parámetro de monitorización del estado de las superficies. No obstante, cabe resaltar también que la evolución del ECR se mostró dependiente de las condiciones ambientales (humedad) de trabajo, tanto en las superficies tratadas como no tratadas. Esto implica una mayor complejidad, y una mayor potencialidad en aquellas aplicaciones que sean sensibles al medio de trabajo.

En cuanto a los **recubrimientos** con **funcionalidad eléctrica**, la tecnología empleada en su desarrollo se basó en la deposición en fase vapor por pulverización catódica (Magnetron Sputtering Physical Vapor Deposition – **MS-PVD**). Se estudiaron tanto el caso de recubrimientos conductores eléctricos, en la forma de aleaciones de plata aluminio (**AgAl**), como recubrimientos dieléctricos carbonáceos (Diamond Like Carbon - **DLC**). En ambos casos las deposiciones se realizaron sobre cobre, utilizando una intercapa de anclaje de níquel en el primer caso, y de metal duro, WC-Co, en el segundo.

En muchas aplicaciones en componentes eléctricos se utilizan en la actualidad recubrimientos de plata depositados vía electrolítica. Sin embargo, aunque presentan buenas propiedades de conductividad eléctricas de origen, su comportamiento tribológico es deficiente. Esto es especialmente el caso en aplicaciones (p.ej. Smart

grids) que requieren de un número elevado de operaciones de conexión / desconexión de forma duradera y fiable. Las aleaciones **AgAl** desarrolladas han demostrado presentar un mejor comportamiento tribológico, en funcionamiento tanto al aire como bajo aceite aislante (condición de trabajo habitual en estos casos). Un aspecto por destacar ha consistido en la identificación de distintos mecanismos de desgaste, en función del porcentaje de aluminio, la fase de la aleación, y del medio de trabajo. Se ha constatado así mismo las diferencias en cuanto a los valores de ECR estático y dinámicos. Otro aspecto relevante de las prestaciones de estos recubrimientos consiste en su resistencia a la degradación en medios con presencia de compuestos de azufre (y clorados u oxígeno), dada la reactividad de la plata, y el aluminio en este caso, con los mismos. Los estudios realizados han puesto de manifiesto el beneficio de la incorporación de aluminio en la resistencia del recubrimiento a la degradación por reacción con el azufre. No obstante, la incorporación de aluminio en la aleación también ha aumentado la tendencia a la oxidación de la superficie. Este último punto, ha supuesto desafortunadamente un moderado aumento en los valores de ECR.

En el caso de los recubrimientos de AgAl, los estudios electro-tribológicos se han mostrado de utilidad en el análisis de la operatividad (bajos CoF y ERC) de los recubrimientos, dada su funcionalidad en contactores eléctricos. Respecto a su posible uso como herramienta de monitorización, más allá de la utilidad directa para monitorizar el correcto funcionamiento de los contactores recubiertos, se requieren estudios más extensos y amplios que incorporen los mecanismos de degradación por reacción con el azufre o la oxidación de las superficies a los ensayos electro-tribológicos.

Los recubrimientos **DLC** representan una amplia gama de capas con propiedades muy distintas, p.ej. tribológicas y eléctricas. En los trabajos realizados se han estudiado recubrimientos de DLC con carácter dieléctrico.

Se ha comprobado en efecto el carácter dieléctrico de los recubrimientos desarrollados, con valores de ECR por encima de los límites de medida del multímetro

empleado en el tribómetro. Por otra parte, los estudios electro-tribológicos se han demostrado de gran utilidad en la identificación e interpretación de los mecanismos de degradación del recubrimiento. Este se da en varias etapas, que se inician con el agrietamiento de la capa, en el que las tensiones residuales del recubrimiento juegan un papel importante, la propagación de las grietas, el desconche de secciones del recubrimiento en combinación con fenómenos de adhesión del aluminio proveniente de la contraparte, llegándose eventualmente a la intercapa de WC-Co y el sustrato, momento a partir del cual predomina el desgaste adhesivo, en combinación con fenómenos de oxidación superficial del cobre. Se ha constatado así mismo en estos estudios, la sensibilidad de la vida de los recubrimientos a la humedad del medio tribológico.

La **hipótesis principal** de los trabajos de esta tesis han consistido en asumir que los estudios electro-tribológicos proporcionan una información útil y relevante i) en el marco del desarrollo de los recubrimientos y tratamientos de superficie, y ii) para la monitorización de su estado operativo o grado de degradación.

Hipótesis adicionales han consistido en asumir que i) el fenómeno de cátodo hueco, HC, puede resultar de utilidad para alcanzar compromisos satisfactorios entre la resistencia a la corrosión y las prestaciones tribológicas en aleaciones de aceros inoxidables; ii) recubrimientos base plata aluminio pueden mejorar el comportamiento electro-tribológico de los recubrimientos de plata utilizados actualmente; y iii) recubrimientos base DLC pueden ser una opción prometedora en contactos dieléctricos en deslizamiento relativo.

Con todo ello, los resultados de los estudios realizados han corroborado la **validez** de las hipótesis iniciales, en distinto grado.

La combinación de la tecnología ASP con fenómenos de HC se ha mostrado útil en el desarrollo de tratamientos de nitruración sobre aleaciones de aceros inoxidables, austeníticos y martensíticos, tanto en geometrías internas tubulares como cilíndricas, gracias al empleo de plasmas de alta densidad y tratamientos breves a temperaturas

moderadas, que presentan propiedades tribológicas mejoradas sin comprometer la resistencia a la corrosión propia de estas aleaciones.

Por otra parte, la tecnología de MS-PVD ha permitido desarrollar procesos de deposición de recubrimientos conductores eléctricos y dieléctricos, con buenas o mejores propiedades tribológicas, que además presentan una mejor resistencia a la degradación en medios ricos en azufre en el caso de las aleaciones conductoras de AgAl.

Finalmente, el empleo de **estudios electro-tribológicos** en los desarrollos acometidos, se ha demostrado como una herramienta útil en la evaluación y conocimiento de los mecanismos de degradación de los recubrimientos en condiciones de contacto y movimiento relativo, apoyando con ello la optimización de los procesos de tratamiento y recubrimiento. Además, en el caso de los recubrimientos con funcionalidad eléctrica, han aportado información relevante, más allá de la que puedan aportar la evolución del CoF o los valores de ECR estáticos. Por último, se ha explorado la utilización de la evolución del ECR como parámetro clave en la monitorización del estado de las superficies en deslizamiento, en cuanto a su nivel de degradación por desgaste, oxidación, agrietamiento, etc., concluyéndose que cuenta con potencialidad para ser utilizado en sistemas predictivos de mantenimiento, siempre en base a futuras investigaciones en este campo.

INDEX

FIGURE INDEX

TABLE INDEX

LIST OF ACRONYMS

AgAl	Silver-Aluminum
AISI	American Iron and Steel Institute
ASPN	Active Screen Plasma Nitriding
BCC	Body Centered Cubic
BES	Backscatter Electron Signal
BET	Backscattered Electron Topographic (image)
CAPEX	Capital Expenditure
CM	Condition Monitoring
CoF	Coefficient of Friction
CVD	Chemical Vapor Deposition
DLC	Diamond Like Carbon
ECR	Electrical Contact Resistance
EDS	Energy Dispersive Spectroscopy
FCC	Face Centered Cubic
HC	Hollow Cathode
HCP	Hexagonal Close-Packed
MS-PVD	Magnetron Sputtering Physical Vapor Deposition
OM	Optical Microscopy
OPEX	Operating Expense
PH	Precipitation Hardening
PLD	Pulsed Laser Deposition
PVD	Physical Vapor Deposition
RF	Radio Frequency
RT	Room Temperature

RTD	Research and Technical (or Technological) Development
SEI	Secondary Electron Image
SEM	Scanning Electron Microscopy
SST	Salt Spray Tests
XRD	X-Ray Diffraction

1.   INTRODUCTION

1.1. MOTIVATION

Tribology can be defined as the science and technology of interacting surfaces in relative motion and of the practices related thereto; or the science concerned with the design, friction, lubrication, and wear of contacting surfaces that move relative to each other (ASM International Handbook Committee 1994). The term dates back to 1966, when Peter Jost coined the word highlighting tribology related costs in the economy (Jost 1966). The word tribology derives from classic Greek: τρίβω, tribo or "to rub", and -λογία, "study of" or "knowledge of" (Tzanakis, et al. 2012).

If electrical properties of the sliding surfaces are also made part of the tribological studies, the term can be expanded to **Electro-Tribology**. (Not to be confused with Triboelectricity, a type of contact electrification by which certain materials become electrically charged after frictional contact with another material).

The concept of friction and wear has concerned great scientists since the time of Aristotle (384–322 BC). Leonardo Da Vinci found that the friction force is proportional to the normal load and independent of the contact area, and formulated empirical laws of friction. Nowadays tribology is a wide-ranging multi-disciplinary field of study and research investigating the lifecycle, durability, reliability and efficiency, of many mechanical systems worldwide (Tzanakis, et al. 2012).

Tribological issues are ubiquous and represent a heavy cost to the economy. Any moving parts are subject to wear phenomena, which eventually will lead to the failure or miss performance of the system or equipment. This makes it necessary to incur on maintenance and operation costs, also known as OPEX, to assure that the systems are kept operative.

The benefits of tribology have been estimated in several countries, claiming potential savings if tribology solutions were to be fully adopted of 1.1 to 1.5% UK Gross National Product, or 1.55% Gross Domestic Product in China (just in six industries). In 1976, economic losses caused by friction and wear were estimated to be around 1% of the Gross National Product in West Germany. More recently, in 1999, it has also been estimated that approximately 11% of the total energy annually consumed in the U.S.A. in the four major areas of transportation, turbomachinery, power generation and industrial processes could be saved through new developments in lubrication and tribology. (Tzanakis, et al. 2012) (S. Zhang 2009) (Tribology Science Industrial Application Status and Development Strategy. The investigation on position and function of tribology in industrial energy conservation, consumption and emission reduction. 2009) (Bundesministerium Für Förschung und Technologie 1976) (Bronshteyna and Kreiner 1999).

Besides the economic costs, an additional complexity of tribology lies in the fact that tribological phenomena are not defined only by the materials used in the system. Unlike other mechanical, chemical or electrical properties, tribological properties are a system dependent phenomenon, i.e. tribological performance is determined by the materials of the surfaces on relative motion and a number of other equally relevant properties: magnitude and direction of the relative motion, contact load, media (e.g. humidity, temperature, presence or absence of liquids of different nature including lubricants,…), geometries of the parts in contact (micro: surface finishing, and macro-geometry), etc.

The role of the tribologist, could thus be described as to reduce the inefficient systemic losses through friction and wear, which reduce the performance of the machines, while often simultaneously developing low-impact alternatives to the often environmentally damaging current practices (Tzanakis, et al. 2012).

Traditionally, the industry has addressed tribological issues most often with the selection and application of proper materials and lubrication, with the aim of limiting friction, reducing wear and extending part operational lives. This involves often using costly materials, and those that present a good tribological performance often do not possess other adequate mechanical properties such as toughness.

These issues have been addressed by either applying **surface treatments** or depositing **coatings**, with properties different from those of the bulk material on which the parts are manufactured, but with improved tribological properties.

Surface engineering has thus been and is the field of intensive and extensive research, aiming typically at cost reduction and performance improvement of systems with moving parts. The study and development of new surfaces looks for extension of operational lives of the parts, reduction of the environmental impact of the adopted solutions (during the part manufacturing: coating deposition or surface treatment processes; during service: use of toxic lubricants; and after service: frequent part replacement and recycling), and cost reduction by either reduction in maintenance costs or use of less expensive materials and solutions, i.e. OPEX and CAPEX reduction.

The development of tribological solutions has made extensive use of different **tribotesters** and **tribometers**. A tribotester is the general name given to a machine or device used to perform tests and simulations of wear, friction and lubrication. A tribometer is an instrument that measures tribological quantities, such as the coefficient of friction, friction force, and wear volume, between two surfaces in contact.

As mentioned before, tribological properties not being intrinsic properties of the sliding materials, but properties dependent on the whole system, tribometers often are extremely specific in their function, e.g. tribotesters that accurately reproduce the motions and forces that occur in human hip joints to perform accelerated wear tests.

The key concept here is accelerated. As performing field tests takes long times, and is often costly, cumbersome or impractical, laboratory tests are performed in the initial

study of tribological studies. One should be aware nevertheless that performing accelerated tests always involve a compromise, some parameter of the "real" tribological system must be adapted in the tribometer to make the tribological tests more aggressive, i.e. accelerated. Therefore, shorter standing (no movement) times, higher speed or contact loads are typically applied to make for faster tests. This should always be considered in the analyses of the results, and make a consideration as to how accurately the lab system represents reliably the real tribological system.

Linked to this field of research in the realm of surface engineering, is the **monitoring** of the degradation of the systems, in service, on-line. The final aim is not just to learn about the condition of the sliding surfaces, but to foresee when the tribological performance will be non-acceptable, putting in risk the whole system, and thus plan in-advance system halts and part replacements in economical optimal ways (Figure 1.1).
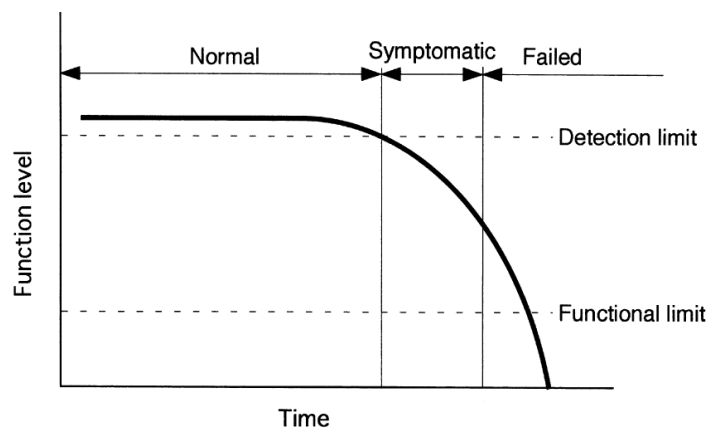
Figure 1.1. Deterioration pattern (Kimura 1997)

Different strategies are being explored to monitor the degradation of surfaces by wear or corrosion. One of such, is based on the surface electrical properties. In particular, the Electrical Contact Resistance (**ECR**) could be a valuable monitoring parameter. The ECR is dependent, among others, of both the surface material and surface geometry.

Therefore, if the material degrades, e.g. by oxidation, it should appear in the value of the ECR. Likewise, if the surface coating gets thinner by wear, if should also show up in the ECR value.

Not only can the ECR be a valuable **monitoring parameter**, but in some applications, such as sliding electrical contacts, the ECR is a key **operational parameter**. In conductive sliding contacts, if the ECR rises, it signals the degradation of the surfaces. Likewise, in dielectric sliding contact, if the ECR decreases, it also signals the degradation of the sliding surfaces. Therefore, the study of the ECR along the operational lives of the sliding parts could be valuable to learn about the material degradation mechanisms of the surfaces, the operational stages of the same, and the monitoring of the part conditions to foresee when the sliding surface performance will become non-acceptable.

1.2. OBJECTIVES AND HYPOTHESIS

The objective of the thesis consists on the development of plasma based surface treatments and coatings with specific functionalities, supported by electro-tribology studies, as a tool to study the degradation mechanisms of selected surfaces, their operative lives in electrical applications, and eventually explore the potential of electro-tribology as monitoring tool of parts and components in operation.

One of such functionality consists on the surface treatment of stainless steel parts without loss of their initial corrosion resistance. The other, the deposition of dielectric and electrically conductive coatings for electrical sliding applications.

In the former case, the "beauty" of **stainless steel** is based on its corrosion resistance. This has made it to be used across multiple sectors such as aeronautics, marine applications, food and biomedical devices, architecture, chemical processing and a

diversity of machinery, consumer goods, etc. But, its tribology performance at most is poor. Improving the tribology with the application of surface treatments without a deleterious effect on the corrosion resistance has typically been a challenge.

In this thesis, the application of hollow cathode plasmas is studied in two distinct stainless steel alloys and geometries:

- austenitic and precipitation hardening martensitic alloys,
- inner tube surfaces and outer cylindrical surfaces.

Austenitic stainless steel alloys typically present a good corrosion resistance, but are prone to wear and high friction coefficients. Furthermore, commercial solutions in the form of coatings often find it challenging their application to inner geometries. One of the objectives of the work therefore has focused on the development of plasma based nitriding process for the inner surfaces of a commonly used stainless steel, AISI 316, improving thus the tribological performance without compromising the corrosion resistance of the alloy.

In applications where the mechanical stresses are demanding, martensitic stainless steel alloys are preferred, although the corrosion resistance is often lower than in the case of the austenitic stainless steel alloys. This is the case in components of the landing gears in aeronautics, surgical tools or sensing and transmission parts in the automotive industry. These parts are typically cylindrical in shape. This is why a second objective of the work has aimed at developing plasma nitriding processes on cylindrical geometries to improve the tribological properties without compromising the corrosion resistance of the alloy.

In the other case, the electro-tribological functionality of a couple of thin films deposited in cooper has been studied. One, Diamond Like Carbon (DLC) based, is originally dielectric. The other, based on silver-aluminum alloy coatings, is originally electrically conductive.

The development of both coatings is oriented towards sliding electrical contacts, such as those that can be found in electrical transformers, engines, transportation vehicles,

etc. In those sectors, technology trends (smart grids, the electric car…) demand higher frequency of operation, without detriment of the operational lives of the components. This requires coatings with higher wear resistance, maintaining low friction values and good electrically conductive or insulating properties.

In the whole study, the **main hypothesis** consists on the assumption that electro-tribology studies will provide useful information towards the development of the coatings and nitriding surface treatments, and the monitoring of their operative status.

Additional hypotheses are based on the expectation that i) hollow plasma can be useful in reaching valuable compromises between the corrosion resistance and tribological performance of stainless steel alloys; ii) silver-aluminum based coatings can improve the electro-tribological performance of current silver coatings; and iii) DLC based coatings are a promising option for dielectric sliding contacts.

1.3. THESIS METHODOLOGY AND STRUCTURE

As described in the previous section, the objectives of the work are clearly divided (Figure 1.2), so they are going to be presented in different chapters.

- Chapter 2: Experimental Techniques.

- Chapter 3: Plasma Nitriding of Stainless Steel.

- Chapter 4: Conductive and dielectric PVD coatings.

- Chapter 5: Conclusions.

- Chapter 6: Future research directions.
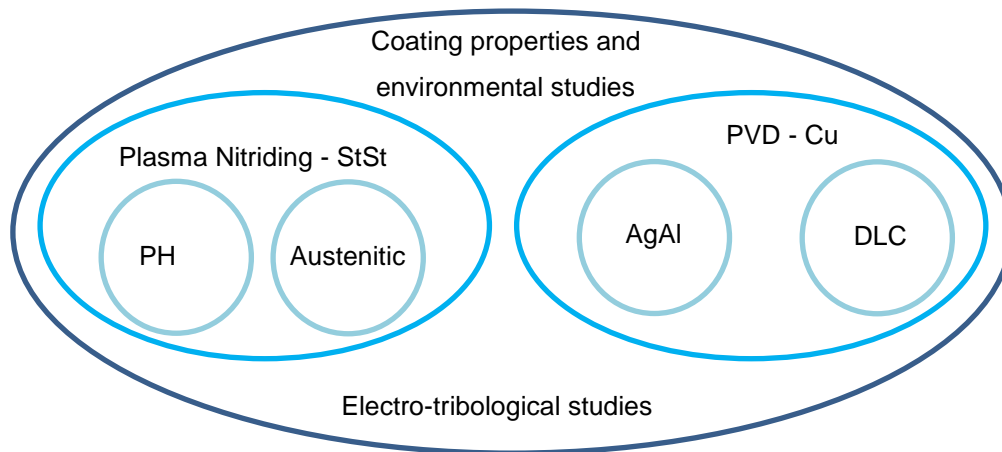
Figure 1.2. Thesis structure

In **Chapter 2** a review is presented of plasma based surface engineering technologies, and more specifically nitriding and PVD/CVD technologies. A review is also presented of the monitoring techniques used in condition monitoring, including those involving electrical conductance. This is followed by a detailed description of the materials and methods used in this work. The method comprises the coating deposition and surface plasma treatment equipment used for the development of the surfaces studied in the work, and the techniques and equipment used for the analyses of their properties as well as for the environmental resistance studies. These properties include the surface finishing, the thickness of the coatings and layers, their hardness, internal stresses, chemical composition, etc. The environmental studies include degradation resistance tests against salt spray, SH2 and thermal cycling in oil. Additionally, the methods used include also a tribometer where all the electro-tribological studies of all the surfaces studied here have been performed.

In the following section, **Chapter 3**, a review on the Plasma Nitriding of Stainless Steel is presented first, specifically concerning the Hollow Cathode and Active Screen Plasma technologies and both the alloys studied: austenitic and precipitation hardening martensitic. Then the experimental studies are presented for each alloy and geometry,

first around the properties of the surfaces and then the electro-tribological and environmental evaluation of the same.

Chapter 4, which is devoted to the Conductive and dielectric PVD coatings, is organized in a similar way. Here, unlike in the previous chapter, the electro-tribological studies include the study of the operational performance of the coatings, as well as the potential use as a monitoring tool.

Finally, in **Chapter 5**, the conclusions of the studies are presented, concerning each of the developed surfaces, as well as common and general ones. This is also the case on **Chapter 6**, which focuses on the future research directions in the fields studied in this work.

It should also be noted that partial results of the presented work have been published or accepted for publication, or submitted to international scientific journals. Furthermore, some results have also already been presented as contributions in scientific international journals (See **Chapter 7**: Publications).

- Plasma nitriding of PH alloys, Chapter 3, Section 3.3. (Braceras, Ibáñez and Domínguez-Meister, et al. 2018).

- Plasma nitriding of inner surfaces of austenitic alloys, Chapter 3, Section 3.4. (Braceras, Ibáñez and Dominguez-Meister, et al. 2018).

- AgAl PVD coatings, Chapter 4, Section 4.2. (Braceras, Ibáñez and Taher, et al. 2018).

- Dielectric DLC coatings, Chapter 4, Section 4.3. (Braceras, Ibañez, et al.).

2. EXPERIMENTAL TECHNIQUES

2.1. INTRODUCTION TO THE EXPERIMENTAL TECHNIQUES

Tribological interactions have a profound impact on many areas of engineering and everyday life. Accordingly, much research has taken place with the aim of reducing friction and wear, through the development of new additives and lubricants, surface treatment and coatings, to improve the performance of interfaces. (Vakis, et al. 2018)

There exist many classifications of surface treatments and coating deposition technologies. Among others, they could be classified as follows (Figure 2.1).

Surface treatments can be performed **without changing the material surface chemically, modifying the nano/microstructure**. These include techniques such as laser, flame or induction surface hardening that induce surface phase transformations. Other techniques are based on mechanical processes that induce compressive stress, changes in the microstructure, increasing hardness and fatigue resistance e.g. by peening, shot blasting, explosive hardening; or only modify the surface texture, e.g. by machining or blasting. Other techniques do also only modify the surface texture, often

on selected sections of the part surfaces, e.g. by chemical/electro-etching or laser engraving.

Other surface treatments cause the **modification of the surface chemistry**. Among others, these techniques include:

- Thermochemical Diffusion Processes, such as carburizing, carbonitriding, **nitriding**, boronising, oxidizing or a combination thereof.

- Ion Implantation Processes.

SURFACE TREATMENT	
MICROSTRUCTURAL: THERMAL	CHEMICAL: IMPLANTATION
INDUCTION	ION IMPLANTATION
LASER	ION BEAM MIXING
FLAME	…
ELECTRON BEAM	**CHEMICAL: DIFFUSION**
WORK HARDENING	CARBURIZING
…	CARBONITRIDING
MICROSTRUCTURAL: MECHANICAL	**NITRIDING**
COLD WORKING	NITROCARBURIZING
BLASTING	BORIDING
…	ALUMINIZING
MICROSTRUCTURAL: CHEMICAL	…
ETCHING	
…	

COATING DEPOSITION	
SOLID STATE	**GASEOUS STATE**
CLADDING	CVD - CHEMICAL VAPOUR DEPOSITION
…	PVD - PHYSICAL VAPOUR DEPOSITION
MOLTEN STATE	**PLASMA ASSISTED - CVD / PVD**
LASER	IBAD - ION BEAM ASSISTED DEPOSITION
THERMAL SPRAYING	…
WELDING	
…	
SOLUTION STATE	
CHEMICAL DEPOSITON	
CHEMICAL CONVERSION	
ELECTROCHEMICAL DEPOSITION	
SOL-GEL	
…	

Figure 2.1. Classification of Surface treatment and coating deposition techniques (Podgornik and Vižintin 2002)

Other family of surface modification techniques consist on the addition of new materials onto the surface, i.e. the deposition of **coatings**. Among others, these techniques include:

- Welding Type Processes, e.g. surface hardening.

- Thermal Spray Process

- Electroplating, Electroless plating

- Galvanizing

- Physical Vapor Deposition (PVD)

- Chemical Vapor Deposition (CVD)

- Painting

- Cladding

- Chemical Conversion Coatings, e.g. phosphating, chromating, …

- Electrochemical Processes: e.g. Anodizing (anodizing)

Among all of the above techniques, several are **plasma based** technologies, which offer many advantages as compared with more traditional treatments and coating deposition technologies. Among other aspects, these technologies are typically environmentally friendly, very flexible (e.g. almost any chemistry can be produced in the coatings), very controllable (i.e. reproducible) and scalable (for industrial applications).

2.2. REVIEW OF PLASMA BASED SURFACE ENGINEERING

Plasma (from Ancient Greek πλάσμα, meaning 'moldable substance') is one of the four fundamental states of matter. Plasma presents properties and behaviors different from those of the other states: solid, liquid, and gas. However, unlike the other three states, plasma does not exist freely on the Earth's surface under normal natural non-artificial conditions, but can be found on phenomena such as lightning (Figure 2.2).

Figure 2.2. Lightning associated plasma discharge (Wikipedia, 2016).

Nevertheless, plasma is the most abundant state of the matter in the universe as far as we know (leaving apart dark matter/energy), e.g. the main constituent of stars. However, plasma can be artificially generated, by heating or subjecting a neutral gas to a strong electromagnetic field, by which positive charges in ions are achieved by stripping away orbiting electrons. This generates an increasingly electrically conductive ionized gaseous substance, which reacts to and interacts with electromagnetic fields.

Many modern technologies, including the surface engineering, take advantage of this feature.

Plasma is used in surface treatments without change of the material surface chemistry (e.g. some plasma etchings), in surface treatments that modify the surface chemistry (e.g. plasma nitriding), and in coating deposition treatments (e.g. thin films deposited by Physical Vapor Deposition - PVD or Chemical Vapor Deposition - CVD, and thick films by plasma thermal spraying).

In this thesis, two of such technologies are studied: plasma nitriding and PVD/CVD.

2.2.1. PLASMA NITRIDING

Nitriding is a thermo-chemical case-hardening surface treatment process that involves the diffusion of nitrogen into the surface of a metal to create a nitride layer at the surface. Nitrided cases provide, in addition to very high hardness, increased wear resistance and antiscuffing properties, improved fatigue life, and improved corrosion resistance in plain steels (ASM International Handbook Committee 1994). Nitriding is extensively applied on steels, especially on nitriding alloys, whose composition include nitride forming elements such as aluminum, chromium, molybdenum and titanium.

The mechanism of nitriding is generally known, but the specific reactions that occur in different steels are not always known. Nitrogen has partial solubility in iron. It can form a solid solution with ferrite at nitrogen contents up to about 6%. At about 6% N, Fe_4N forms, a compound called γ' (Figure 2.3). At nitrogen contents greater than 8%, the Fe_3N compound, known as ε, forms.
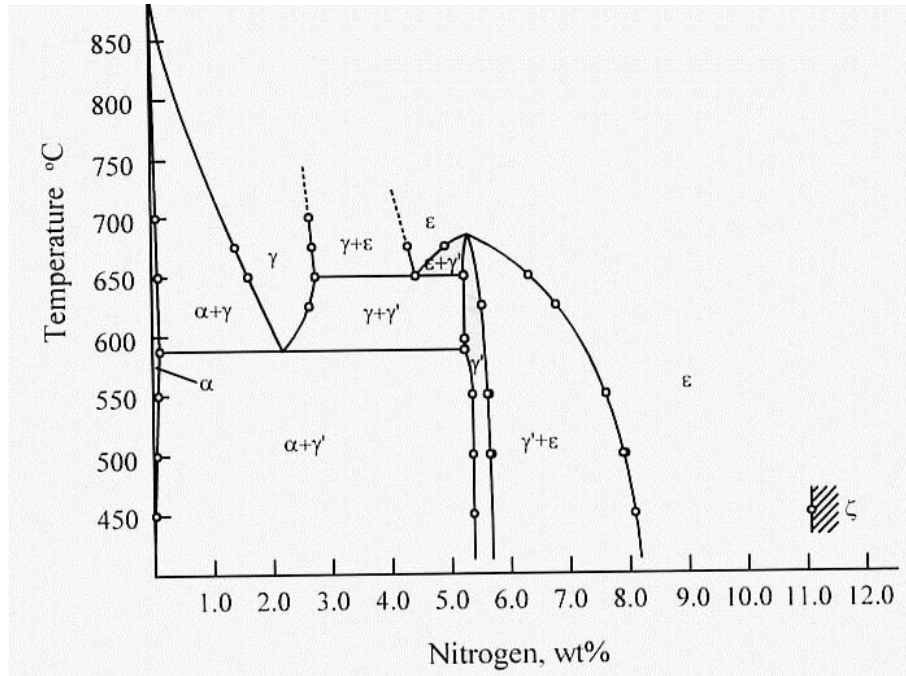
Figure 2.3. Fe-N phase diagram (Darken and Gurry 1953).

The outermost surface can be all γ' and when this occurs it is referred to as the white layer, because it etches white in metallographic preparation. Such a surface layer is very hard but so brittle that it may spall in use. Thus, it is usually avoided, removed or special nitriding processes are applied to make it less brittle. The main zone of the nitrided case is hardened by the formation of the Fe_3N compound, and below this layer there is some solid solution strengthening from the nitrogen in solid solution (Figure 2.4) (ASM International Handbook Committee 1991).
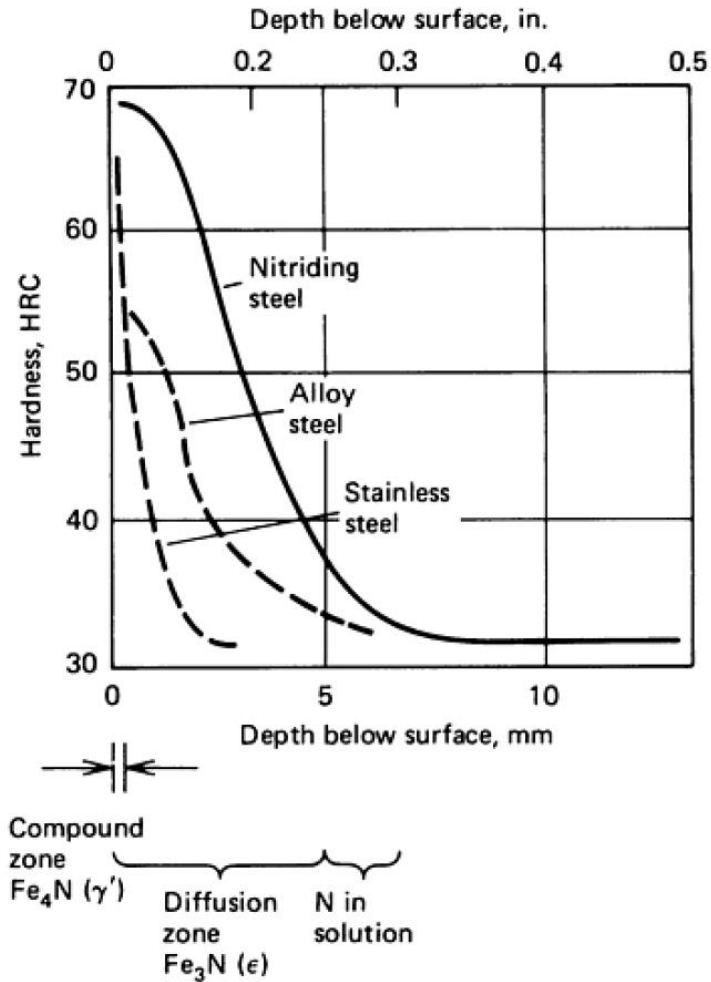
Figure 2.4. Nitride case profiles for various steels (Budinski 1988).

Different media are typically used to donate nitrogen to the steel substrate (ASM International Handbook Committee 1994) during the treatment process. The three main methods involving different media are: gas nitriding, salt bath nitriding, and plasma nitriding (Figure 2.5).

Process	Nature of case	Process temperature, °C (°F)	Case hardness, Typical case depth	HRC	Typical base metals	Process characteristics
Nitriding						
Gas	Diffused nitrogen, nitrogen compounds	480-590 (900-1100)	125 µm-0.75 mm (5-30 mils)	50-70	Alloy steels, nitriding steels, stainless steels	Hardest cases from nitriding steels, quenching not required, low distortion, process is slow, is usually a batch process
Salt	Diffused nitrogen, nitrogen compounds	510-565 (950-1050)	2.5 µm-0.75 mm (0.1-30 mils)	50-70	Most ferrous metals including cast irons	Usually used for thin hard cases <25 µm (1 mil), no white layer, most are proprietary processes
Ion	Diffused nitrogen, nitrogen compounds	340-565 (650-1050)	75 µm-0.75 mm (3-30 mils)	50-70	Alloy steels, nitriding steels, stainless steels	Faster than gas nitriding, no white layer, high equipment costs, close case control

Figure 2.5. Typical characteristics of nitriding treatments (ASM International Handbook Committee 1994).

Salt bath nitriding. In salt bath nitriding the nitrogen donating medium is a nitrogen-containing salt (e.g. cyanide salt). The surface treatment process is typically performed at approx. 510-565 °C. The main advantage of salt nitriding is that it achieves faster treatments as compared with the other treatments, in a simple immersion process. On the other hand, the salts used are highly toxic, and their disposal is strictly regulated, which rises the cost of the treatments. This is the main reason why the use of this method is decreasing, and other alternatives are often preferred.

Gas nitriding. In gas nitriding the nitrogen donor is a nitrogen rich gas, typically ammonia, NH_3. When ammonia comes into contact with the heated part, at approx. 480 – 590 ºC, it dissociates into nitrogen and hydrogen. The nitrogen then diffuses onto the surface of the part creating a nitride layer.

The advantages of gas nitriding include the possibility of a precise control of the process and of treating relatively large batch sizes, and an all part nitriding effect. This can be an advantage or disadvantage depending on the desired effect. On the other

hand, disadvantages comprise the use of ammonia and the dependence of the treatment final results on the surface condition (e.g. presence of thick oxides or oil is detrimental), which makes it necessary an initial surface activation treatment (e.g. to treat stainless steel alloys or high chromium alloys). Moreover, ammonia can be harmful inhaled in large quantities and the possibility of explosions exist when heating in presence of oxygen.

Plasma nitriding. Plasma nitriding is also known as ion nitriding, plasma ion nitriding or glow-discharge nitriding.

In plasma nitriding, the nitrogen donor is the residual nitrogen gas in the vacuum treatment chamber, where electric fields are used to generate ionized molecules, i.e. the plasma.

Plasma nitriding treatments can be carried out at a wider temperature range than either salt bath nitriding or gaseous nitriding, from 260 °C to more than 600 °C (Zagonel, et al. 2006). This makes it possible for instance to apply nitriding treatments at moderate temperatures on stainless steel without formation of chromium nitride precipitates, which is detrimental for their corrosion resistance (Larisch, Brusky and Spies 1999).

The base gas used for plasma nitriding is usually pure nitrogen. Other gasses like Hydrogen or Argon are also used in the gas mix. This is for instance the case in the plasma pre-treatment, performed in the same treatment chamber to remove surface oxide layers, surface solvents and pollutants that might interfere afterwards with the nitriding process. During the plasma nitriding process itself, H_2 is also typically added to the N_2 gas, which allows to keep the surface free of oxides and a faster treatment process.

However, standard plasma nitriding of steel part faces many problems and limitations (Janosi, Kolozsvary and Kis 2004):

- The parts that act as cathodes, are heated as a result of ion bombardment of the surface. Besides inhomogeneous batches heat up non-uniformly. Problems arise with batches with varying surface mass ratios.

- An "anomalous" glow discharge can become an electric arc due to avalanche formation of particles and thus damage the treated parts.

- An "edge effect" may arise, because differing growth rates of the nitrided layer on the edges and flat regions of the surface of a part.

- The part, as the cathode, is subjected to sputtering, which might assist in cleaning and surface activation (positive), but induces surface roughness and contamination from surrounding materials (negative).

- Hollow cathode effects might occur in an uncontrolled way, causing nonuniform heating of the treated part, resulting in thermal stresses, varying thickness of the nitrided layer and nonuniform hardness and structure.

In the field of plasma treatments, different techniques are being studied to overcome these problems and limitations, to improve process productivity and surface quality. Among them, **Active Screen Plasma Nitriding** (ASPN) and **Hollow Cathode** (HC) assisted plasma nitriding can be cited.

Active screen plasma nitriding offers many advantages over conventional plasma nitriding. The active screen acts as both a generator of plasma species and source of radiation that acts as a heater, thus enabling a better process temperature control, independent from the voltage bias applied to the treated part acting as a cathode. This reduces the edge effects, arcing risk, etc. However, some investigations have suggested that the properties of active screen nitriding layer might be affected by the part position relative to the screen (de Sousa, et al. 2009).

On the other hand, the **hollow cathode** (HC) effect produces denser plasmas, by means of the "pendulum", photoionization and stepwise ionization (Figure 2.6) (Muhl and Pérez 2015). The hollow cathode effect is a special case of glow discharge, that appears when the surfaces of holes, channels, or closely located parts facing each other (e.g. tubes) are placed at such a short distance that negative glows (discharges)

contact each other or even overlap (Janosi, Kolozsvary and Kis 2004). In these regions electrons are caught and oscillate, causing additional ionization and excitation of atoms, which leads to an intensified ion bombardment of the cathode and subsequent rapid growth in the temperature. Additionally, in such regions the radiation heat losses are very low due to the geometry constrains. However, only limited information has been reported about the application of HC effect as a heating source in plasma nitriding (Shen, Wang and Xu 2013).
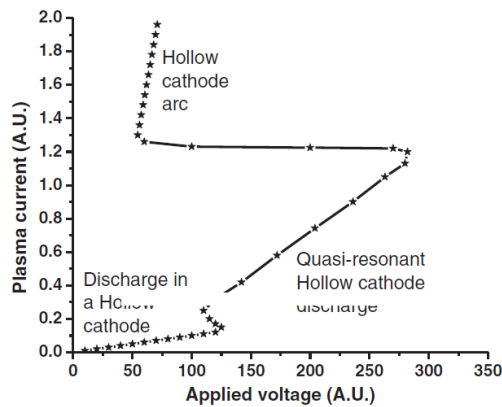
Figure 2.6. Schematic drawing of the I-V characteristic of a hollow cathode system (Muhl and Pérez 2015).

The combination of both, ASP and HC, has been studied recently on austenitic stainless steel, aiming at rapid nitriding processes in short times, the key to preserve the corrosion resistance of the alloys (Li, et al. 2014) (Yang W.J. 2016) (Shen, Wang and Xu 2013) (Nikolov, Bunk, et al. 2014).

Chapter 3 details the study of nitriding processes, combining ASP and HC, performed on two distinct geometries and stainless steel alloys: cylindrically shaped 15-5PH precipitation hardening martensitic alloy and inner surfaces of tubes manufactured on the AISI 316L austenitic stainless steel.

2.2.2. PHYSICAL VAPOR DEPOSITION, PVD, AND CHEMICAL VAPOR DEPOSITION, CVD.

In the PVD process, a material is vaporized from a solid or liquid surface, then transported through a low-pressure (vacuum) gaseous or plasma environment to a surface where the material condenses and possibly reacts with a gaseous material or co-deposited material to form a compound.

PVD itself describes a variety of vacuum deposition methods, that include sputtering, cathodic arc deposition (or Arc-PVD) and evaporation as the most used processes on an industrial basis (BCC Research 2016).

BASIC PHYSICAL VAPOR DEPOSITION TECHNOLOGIES

Type	Source
Thermal evaporation	Resistively heated Electron beam (e-beam) heated
Sputtering	Magnetron Radio frequency (RF) and direct current (DC) diode Reactive
Ion beam-assisted deposition	Ion particles
Pulsed laser deposition	High-powered pulsed laser
Cathodic arc deposition	Vacuum arcs

Figure 2.7. Basic industrial physical vapor deposition technologies (BCC Research 2016).

In the Arc-PVD technique a high-power electric arc is used to vaporize material from a cathode target or source, which blasts away into a highly ionized vapor, and is deposited onto the part as a coating.

In evaporation-PVD technique, the source material is heated in vacuum to a high vapor pressure by electrical resistance, an electron beam or other heating source, and then deposited onto the parts in the coating chamber.

Other PVD includes techniques such as Pulsed Laser Deposition (PLD), where a high-power laser ablates material from the target into a vapor, which is deposited in the part as a coating.

In **Sputtering-PVD** a glow plasma discharge bombards the target source material, sputtering away some of it as a vapor, which subsequently deposits as a coating. Usually, for a higher deposition efficiency, the plasma is forced to be localized and concentrated around the target by a magnet. This is then known as **Magnetron Sputtering PVD** or MS-PVD (Figure 2.8).
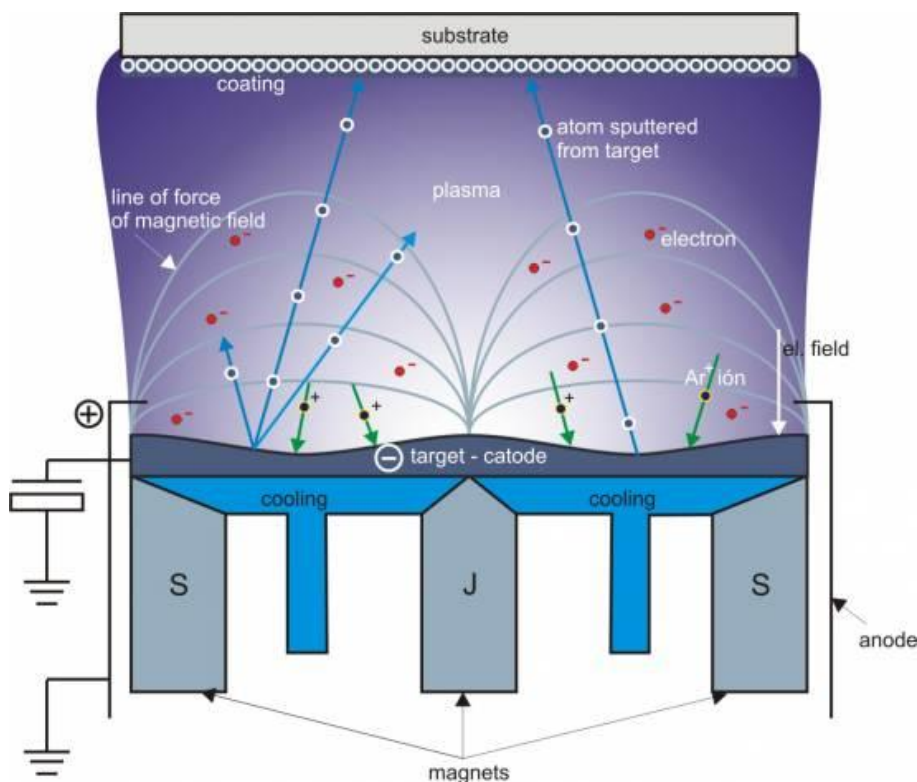
Figure 2.8. Magnetron Sputtering principle (Institute of materials and machine mechanics SAS 2016).

One of the main advantages of the PVD technology consists on the possibility to deposit virtually any type of inorganic and some organic coating materials on any substrate material. Additionally, this technique is more environmentally friendly than traditional wet chemistry based coating processes such as electroplating and conversion coatings.

The Chemical Vapor Deposition or CVD process can be defined as the deposition of a solid on a heated surface via a chemical reaction from the vapor or gas phase. Although CVD competes directly with PVD, an important recent trend is the merging of these two techniques. For instance, CVD now makes extensive use of plasma (a physical phenomenon), whereas PVD is often carried out in a chemical environment (reactive evaporation and reactive sputtering). Likewise, CVD and PVD operations are often processed in the same integrated equipment in a sequential fashion without breaking the vacuum (thus minimizing contamination), and the distinction between the two basic processes has become blurred (Bader, Hall and Strasser 1990) (ASM International Handbook Committee 1994). This is the case for instance of the deposition process of Diamond Like Carbon or DLC coatings from C_2H_2 gas precursors, over a previously MS-PVD deposited bonding interlayer.

PVD/CVD coatings are deposited over many substrates and parts, aiming at different surface properties, which are used in multiple industries. PVD/CVD coatings can be thus applied on metal, ceramic, polymeric and polymeric parts, provided the substrate material can properly withstand PVD/CVD process vacuum and temperatures without degradation, outgassing, etc. The surface properties pursued with the coating of the parts include wear resistance, corrosion and oxidation resistance, aesthetic and optical properties (in terms of reflectance, absorbance, etc.), biologic interactions (biocompatibility, osseointegration, anti-microbial properties, etc.), catalytic reactions, or electromagnetic properties (electrical conductivity, insultation, electromagnetic interference shielding, etc.). These coatings have seen industrial applications in a wide variety of sectors: manufacturing industries, biomedical products, watch and jewelry industries, microelectronics, electro-mechanical applications, food and chemical transforming industries, automotive parts and components, energy power facilities (e.g. solar energy), etc.

Presently research on new PVD/CVD coatings typically goes hand by hand with the research in key sector technologies: efficient cars, efficient energy production, smart

grids, implantable devices, etc. Another key feature in the research field of PVD/CVD coatings is the demand for multi-functional coatings.

This is actually the case of the coatings developed and studied in this work. As described in **Chapter 4**, the work has focused on the study of two tribological coatings (wear resistant low friction coatings), with good dielectric properties or electrical contact resistance respectively. In the latter case, good environmental resistance was also pursued. The two coating variants have consisted of PVD/CVD DLC and PVD AgAl coatings respectively.

2.3. REVIEW OF MONITORING TECHNIQUES OF TRIBOLOGICAL SYSTEMS

As mentioned before, frictional losses have been assessed to cost more than 1% of GDP in advanced economies (Tzanakis, et al. 2012). Thus, **tribology related problems** are very relevant for the economic activity of any modern economy. Besides, it plays a very relevant role on the safety of many systems and equipment, often with serious implications also on human and environmental safeties. This is specially the case in remote (e.g. aerospace, off-shore (Kusiak, Zhang and Verma 2013) (Salameh, et al. 2018) (Nie and Wang 2013),…) and / or critical applications (e.g. transport equipment (Trinh, et al. 2015); medical devices or hospital facilities, nuclear energy power stations) (Helmi Attia 2006).

Consequently, **monitoring** the **tribological performance** and status of the surfaces, materials, components and equipment is of paramount interest.

The monitoring of the surface degradation is also of interest and relevance in the case of the study and **development** of new **coatings** or surfaces. The after tribotest or after service / operation analyses frequently provide limited information. Ideally, the on-line availability of parameters other than the CoF could be useful on understanding the degradation mechanisms of the surfaces and coatings in a plurality of environments and situations. As it has been mentioned before, tribological performance in not only a property of the counterpart materials, but depends on the whole tribological system, thus increasing exponentially the potential cases of interest and the variables that might have an effect.

Associated to this, **condition monitoring** (CM) has become essential in maintaining and extending the health of rotating and reciprocating machinery used in many sectors. The real-time condition monitoring of a machine's health status can significantly reduce the operation cost by eliminating the need for costly machine shutdowns for inspection, which would otherwise be needed to avoid the possibility of catastrophic component

failure during operation. Accurate condition monitoring methodologies are being sought to facilitate the effective scheduling of maintenance and repair downtime, and manage safety risks (Zhu, Zhong and Zhe 2017).

A key aspect in any monitoring device is the **property to monitor**, and the **associated technology** to makes it possible. Related to this, the monitoring technology should allow for its implementation on-line. Often off-line analysis techniques offer greater accuracy and richer information, but the likely costs associated to delays in the acquisition of data and its analysis should outweigh these advantages. Therefore, an **on-line** monitoring system is much more desirable.

One option is the monitoring of the Coefficient of Friction, **CoF,** or the forces applied on the parts to make them move or keep moving. But this is not always an option or even meaningful. The CoF might happen to show increasingly less distinct changes over time, or even keep the same after the surface treatment or coating is removed, and wear keeps progressing, or other function such as electrical conductance, electrical insulation or corrosion protection are removed (Y.-P. Chang 2009) (Y. Chang 2007). Monitoring of **other** tribology related **parameters** such as wear debris (Beebe 2004) (Agoston, Ötsch and Jakoby 2005) (Hong, et al. 2018) (Vakis, et al. 2018), vibration, changes in temperatures (Zhu, Zhong and Zhe 2017), optics, and electric properties has also been explored, both in lubricated (Tandon, Ramakrishna and Yadava 2007) and unlubricated systems (Hasea and Mishina 2018).

The work carried out in this thesis has focused on the potential of acquiring tribological and electrical monitoring data from four different material / surface pairs. In the case of the **electrical properties**, ideally, they could provide info about the degree of oxidation, cracking, contact surface, wear… on a continuous and even remote way.

Properties such as the **ECR** have already been included in other multiple tribological studies (See references below). Monitoring systems based on the ECR are thus aligned with current research efforts, are relevant and could be of interests, among others in:

> The study and deeper understanding of tribological **degradation mechanisms** (Trinh, et al. 2015) (Yang, et al. 2004) (Keller, et al. 2009) (Yu, et al. 2016) (Minfray, et al. 2003) (Wahl, Belin and Singer 1998) (Chu and Lin 2000). (Hong, et al. 2018) (Booth, et al. 2010) (Zhang, et al. 2009).

> The development and study of **tribology coatings** and materials with **electrical functionalities**, especially in the case of those applications where the electrical properties under sliding i.e. tribological conditions are key. (Takeno, et al. 2013), (André, et al. 2011), (He and Manory 2001), (Bouchoucha, Chekroud and Paulmier 2004), (Argibay, et al. 2013), (Nedfors, et al. 2015), (Nygren, et al. 2014), (Chen, et al. 1997), (Hombo, et al. 2013).

> The study of **condition monitoring** of tribological or electro-tribological systems (Laporte, Perrinet and Fouvry 2015) (Y.-P. Chang 2009) (Y. Chang 2007). (Chang, Chiou and Lee 2008) (Torres Pérez, et al. 2011) (Helmi Attia 2006) (Belin 1999) (Ye, et al. 2014) (Liu, Liu, et al. 2000).

2.4. MATERIALS AND METHODS

In this section the materials used in the studies and the methods applied for the deposition of the coatings, the implementation of the surface treatments as well as the characterization of the resulting surfaces are detailed. The characterization encompasses the study of electro-tribological properties together with finishing, chemical, microstructural properties and resistance to environmental degradation studies.

2.4.1. SURFACE TREATMENT AND COATING DEPOSITION TECHNIQUES

2.4.1.1. Plasma Surface Treatments.

Substrates.

Two different stainless steel alloys and geometries have been studied in relation with the plasma nitriding treatment developments.

- Firstly, the study has focused on the **15-5PH** or **1.4545 grade** precipitation hardening martensitic stainless steel, on long cylindrically shaped geometries.

- Secondly, the study has focused on the inner surfaces of tubes manufactured on the **AISI 316L** or **1.4404** grade or austenitic stainless steel.

The selection of the geometries for each alloy was based on potential applications. **Cylindrically shaped 15-5PH** grade made parts are found in many critical applications, in the aeronautical (e.g. landing gear components), ground transportation (e.g. load sensing components) and biomedical (e.g. surgical tools) fields (Figure 2.9).

Figure 2.9. Parts manufactured on precipitation hardening stainless steel alloys: landing gear parts (above), load sensing in mining trucks (middle), and femoral rasps surgical tool (below).

The samples used in this work were 10mm in diameter and 80mm long cylinders, manufactured on grade 1.4545.3 stainless steel (15-5PH in the H1100 condition (AMS5659)), with a surface finishing of Ra 1.0 μm. The chemical composition of such an alloy is detailed in Table 2-1.

Table 2-1. Chemical composition of the 1.4545 stainless steel (15-5PH) alloy, in wt%.

C	Si	Mn	P	S	Cr	Ni	Mo	Cu	Nb
≤0.07	≤1.00	≤1.00	≤0.03	≤0.015	15.0-15.5	3.00-5.50	≤0.50	2.50-4.50	≥5×C

Inner surfaces of 316L tubes.

There are numerous applications also that could benefit from a corrosion resistant inner surface with good tribo-mechanical properties, e.g. multiple sleeves in the engineering field, or cannulas, trephine tips, reamers, in the biomedical field, etc. (Figure 2.10). Alloys such as AISI316L are typically used in these cases.

Figure 2.10. Medical devices manufactured on austenitic stainless steel alloys: trephine tips, reamers, cannulas and pin inserters (from left to right, top to bottom).

210 mm long tube samples manufactured in 1.4404 stainless steel (AISI 316L) with different inner diameters have been used in the microstructural and environmental studies:

- 12mm inner diameter (solderless DIN 17458),
- 25mm and 45mm inner diameters (welded EN 10217-7 TC1) (Table 2-2).

For the tribological studies, discs of 50mm diameter of the same alloy have been used.

Tubes were studied in the as received condition, which presented an initial surface roughness on the inner diameter of Ra 0.24 µm. Discs were grinded to a surface roughness of Ra 0.20 µm.

Table 2-2. Chemical composition of the 1.4404 stainless steel (AISI 316L) tubes, in wt%.

ID	C	Si	Mn	P	S	Cr	Ni	Mo	N
45 mm	0.020	0.36	1.31	0.0025	0.001	16.55	10.04	2.02	0.029
25 mm	0.021	0.42	1.87	0.0032	0.001	16.5	10.0	2.03	0.04

In both cases, before nitriding, all the samples were ultrasonically cleaned sequentially in acetone and ethanol bath (> 10 min) and air-dried.

Objectives.

The main aim of the study for both alloys has been achieving good tribological properties, preserving good corrosion resistance and with no delamination risk (no proper coating). An additional objective has consisted on defining a methodology to monitor the on-service degradation of the surfaces in moving parts (Table 2-3).

In one case, good mechanical and tribological properties have been considered to be provided by the 15-5PH grade alloy with a thick nitride layer (above 50 µm), while a good compromise concerning the corrosion resistance has been considered to require resistance to more than 48 h at Salt Spray Test (SST) without red corrosion. [1]

The objective and challenge in the second case has been achieving a good compromise between tribological properties and corrosion resistance in the inner diameter of long tubes.

---

[1] *Specifications defined by CESA, Compañía Española de Sistemas Aeronáuticos, S.A. in the framework of the projects PROSAVE and PROSURFACE.*

Regarding the monitoring of the status of the surface on service, i.e. in moving parts subjected to wear, the property studied in both cases has been the evolution of the Electrical Contact Resistance, ECR.

Table 2-3. Summary of the objectives.

Objective	Technique	
Corrosion	SST	*: >48h
Mechanical properties and Tribology	Cylinder on cylinder* Ball on disc**	*: >50µm
Monitoring	ECR	-

*: Precipitation Hardening 1.4545 grade alloy.
**: AISI 316L.

Equipment.

The plasma nitriding experiments were carried out in the self-built plasma equipment at the laboratory of Surface Engineering in Tecnalia (Figure 2.11).

The combination of active screen plasma nitriding (ASPN) and the hollow cathode (HC) effect were used in both stainless steel alloys. In the active screen plasma treatments, the outer screen is subjected to a voltage, while the samples are immersed in plasma and biased to a lower potential (Figure 2.12). If the sample is a tube or the sample occurs to be surrounded by an open-ended tube, in some cases, a hollow cathode might happen inside such a tube.

Figure 2.11. Plasma treatment facility at Tecnalia's Surface Engineering Lab.
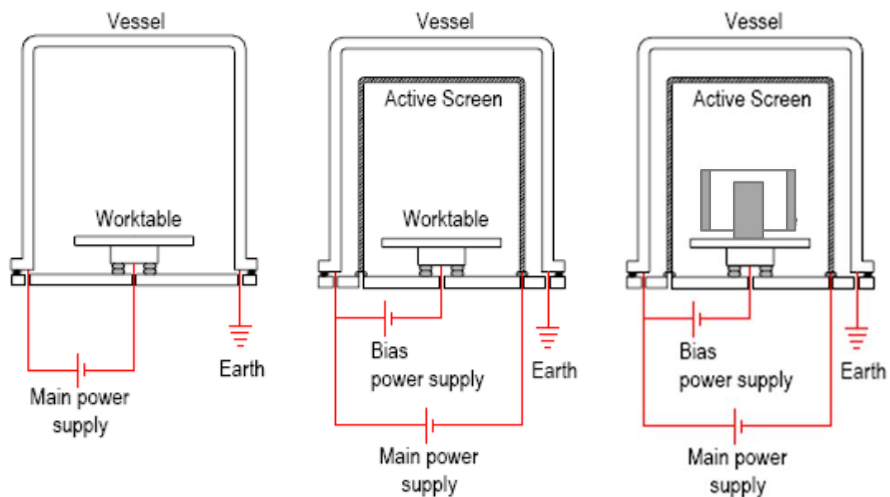
Figure 2.12. Schematic of a conventional plasma nitriding (left), active screen plasma nitriding (middle) and combined active scree plasma and hollow cathode nitriding (right) equipment lay-out.

34

Process **temperature** was monitored with thermocouples placed into bulk dummy cylinders.

In the treatments processes applied on tubes, thermocouples were also placed in dummy tubes with the same inner diameter of the samples, to learn about the chamber temperature and the temperature of the tubes along the plasma processes. Among other things, this allowed to confirm unmistakably the presence of denser plasmas inside the tubes, i.e. the hollow cathode effect, and later study their effect in the resulting nitride surfaces.

2.4.1.2. Physical Vapor Deposition, PVD.

Substrates.

The AgAl PVD coatings studied were deposited on top of:

- 3 mm thick and 76 mm (3-inch) diameter copper half discs coated with 10μm electrolytic nickel, with a roughness of Ra 10nm,
- 76 mm (3-inch) diameter p-doped single-crystal Si (100) wafers.

The DLC coatings were deposited on:

- electrical grade mirror polished copper disks, 50mm in diameter and 5 mm thick, Cu-Etp EN-13601 R250 from Bronmetal, Spain,
- 8 x 40 mm silicon coupons.

Equipment.

The Ag-Al PVD coatings were deposited by means of **DC magnetron sputtering** from Ag and Al metal targets in the facilities at the University of Uppsala (Sweden). The coating composition was controlled in this equipment by increasing the power at the Al target and / or by shifting the position of the substrate closer to the Ag target.

The DLC coatings were deposited in a CEMECON CC800/8 plus (Germany) Physical Vapor Deposition Magnetron Sputtering (**PVD-MS**) unit in Tecnalia, with acetylene, C_2H_2, as the carbon source gas (Figure 2.13).

Figure 2.13. CEMECON CC800/8 plus PVD equipment.

2.4.2. CHARACTERIZATION, EVALUATION AND TESTING TECHNIQUES

In the case of the 15-5PH samples, the studies were performed directly on the cylindrical samples. In the case of the 316L treatments, they were applied on tubes, which were cut in two halves longitudinally. In one of the halves, surface analyses were performed by X-Ray Diffraction (XRD), surface roughness was measured by contact profilometry, and cross-section samples were prepared for metallographic analyses. In the other half tubes, Salt Spray Tests (SST) were performed to assess the corrosion resistance of the treated surfaces. The electro-tribological test were performed on 316L flat samples. Similarly, the studies on the PVD coatings were performed on Cu and Si flat samples.

Next the characterization, evaluation and testing techniques used in each case are described in detail.

2.4.2.1. Surface Profilometry and Wettability

The Surface Finishing of the original samples (control samples), and the resulting surface treated or coated samples was measured by contact profilometry in a Veeco Dektak 150 profilometer (Figure 2.14). In contact profilometry technique, a diamond stylus is moved vertically in contact with a sample, which moves laterally for a determined distance.

Mean values were calculated together with the standard deviation for each analyzed surface.

After the tribology tests, wear tracks were also assessed by profilometry to quantify the wear rates for each test samples and test condition.

In the case of the DLC coatings, the coating thickness and residual stresses were also determined by profilometry on coatings deposited onto silicon coupons. In the latter case, both the length (L) and the height (H) of the curvature were measured, and the residual stresses calculated according to the Stoney formula.
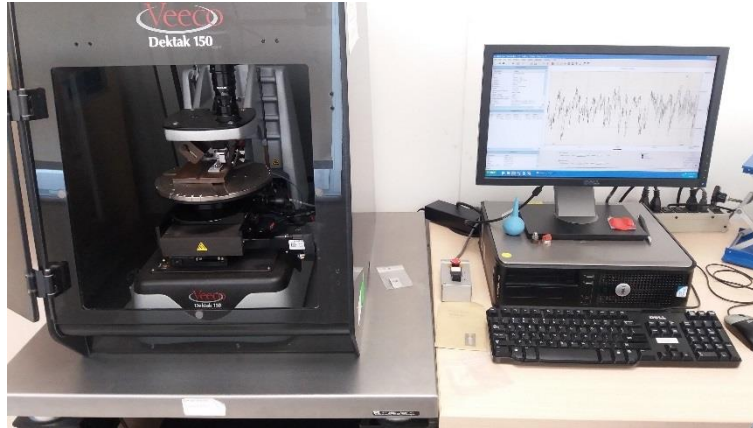
Figure 2.14. Veeco Dektak 150 profilometer.

Additionally, also in the case of the DLC coatings, surface wettability was quantified by contact angle, following standard IEC TS 62073, in a Digidrop, GBX contact angle equipment (Figure 2.15).
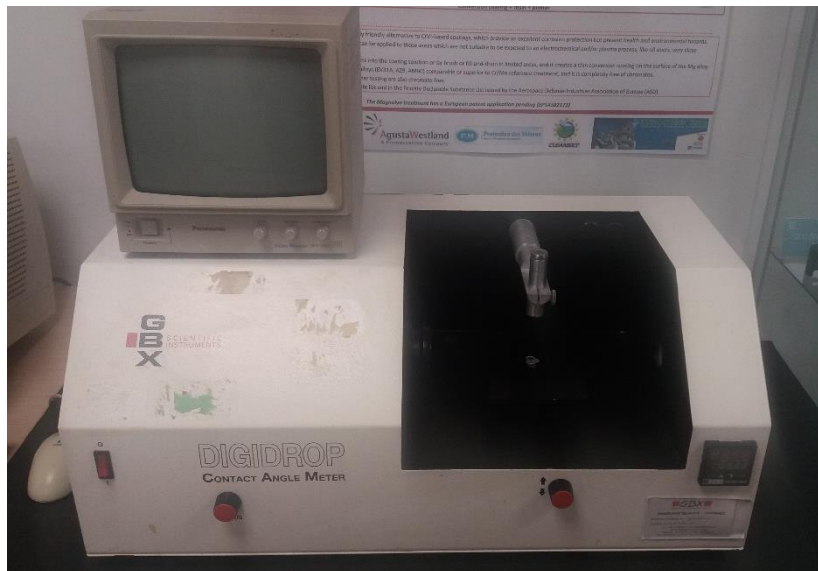
Figure 2.15. Digidrop, GBX contact angle equipment.

2.4.2.2. Coating Structural Analysis: X-Ray Diffraction, XRD, and Raman Spectroscopy.

X-Ray Diffraction, is a technique used for determining the atomic and molecular structure of a crystal, in which the crystalline structure causes a beam of incident X-rays to diffract into many specific directions, by measuring the angles and intensities of these diffracted beams.

In this work, XRD analyses of the treated 316L tubes, 15-5PH cylinders and DLC coated Cu samples were performed in a D8 Advance, Bruker Diffractometer, using Cu-Kα radiation (λ=1.544 Å) at glance angle of incidence of 2º (Figure 2.16).

The XRD phase composition analyses of the AgAl coatings were performed in a Bruker D8 Discover diffractometer, with θ - 2θ scans using Cu Kα radiation (λ = 1.541 Å).

Figure 2.16. X-Ray D8 Advance, Bruker Diffractometer.

Additionally, in the case of the DLC coatings, coating composition and structure were analyzed by Raman spectroscopy. Raman is a non-destructive tool commonly used to provide a structural fingerprint by which molecules can be identified. In the case of DLCs, any mixture of sp3, sp2 and sp1 carbon atoms always have a gap whose energy range matches that of IR-vis-UV Raman spectrometers.

In this study, Raman analyses were performed at 1000 to 1900 cm^{-1} with an excitation wave length of 514 nm, 50 seconds of exposure times, in a In via Reflex, Renishaw equipment (Figure 2.17). Interpretation of the results was done following relevant scientific bibliography: (Robertson 2012) (Ferrari and Robertson 2000).

Figure 2.17. In via Reflex, Renishaw, Raman Spectrometer.

2.4.2.3. Metalographic estudies.

Cross-sections of each sample were prepared, by cutting, embedding and polishing (Figure 2.18). These sections were analyzed at the Optical Microscope (OM) and / or in the Scanning Electron Microscope (SEM) and Energy Dispersive Spectrometer (EDS).

After OM and / or SEM analyses, in some cases, in the nitrided surfaces, the cross-sections were chemically etched (Beraha etching) to reveal the micro-structure of the treated surfaces or coatings.

Figure 2.18. Cutting and polishing equipment.

2.4.2.4. Optical and Electronic Scanning Microscopy.

The determination of the nitride layer **thickness** in the surface treated stainless steel alloys was performed on Optical Microscopes (OM) at different magnifications: Nikon Eclipse MA200, Olympus BX51M or / and Zuzi – Moticam 2.0MP (Figure 2.19). Additionally, hardness HV depth profiles were performed in the nitrided cross sections to determine the thickness of the hardened layer (Figure 2.20).

Figure 2.19. Optical Microscopes.

The determination of the **thickness** in the PVD coated samples was performed by Electron Scanning Microscopy (SEM) (Figure 2.21).

Elemental chemical composition of the cross-sections in the plasma nitrided samples was analyzed by Energy Dispersive Spectroscopy (EDS) (JEOL JSM-5910LV), before and / or after etching. In the case of the AgAl PVD coatings, these elemental chemical analyses were performed at three random points at the surface of the coatings, with the signal acquired at a magnification of x100.
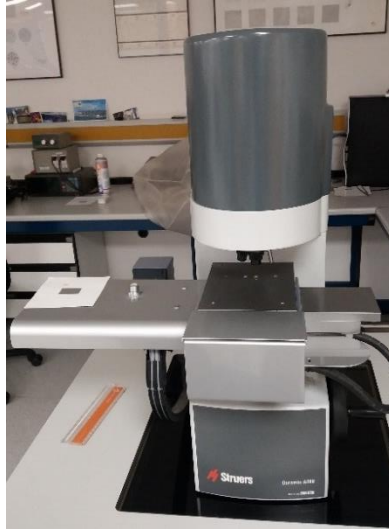
Figure 2.20. HV hardness measurement equipment.

Figure 2.21. Scanning Electron Microscope.

2.4.2.5. Electro-Tribometer.

The electro tribology tests were performed on different configurations and conditions, as defined by the possible industrial applications of surface treatments and coatings (Table 2-4).

Table 2-4. Summary of the electro-tribology test configuration and conditions.

Material / treatment	Test configuration	Counterpart	Test conditions
316L / plasma nitriding	Ball on Disc (rotating)	WC-Co balls	1 N, 50% RH, RT, 0.3 m/s
15-5PH / plasma nitriding	Cylinder on Cylinder reciprocating.	15-5PH cylinder	5 and 15N, 18 and 80%RH, 0.020 m/s
Cu-Ni / AgAl	Pin on Half-Disc reciprocating.	Ag coated Cu pin (Figure 2.25)	2N, 50%RH or immersed in oil, 0.002 m/s
Cu / DLC	Pin on Disc (rotating)	Al balls	3N, RT, 0.500 m/s

All the electro-tribology tests were performed in a MT4002 MICROTEST tribometer (Figure 2.22). Both the evolution of the Coefficient of Friction (CoF) and the Electrical Contact Resistance (ECR) were registered, the later as measured by a "4 wire" Keithley 2100 Multimeter (Figure 2.23).
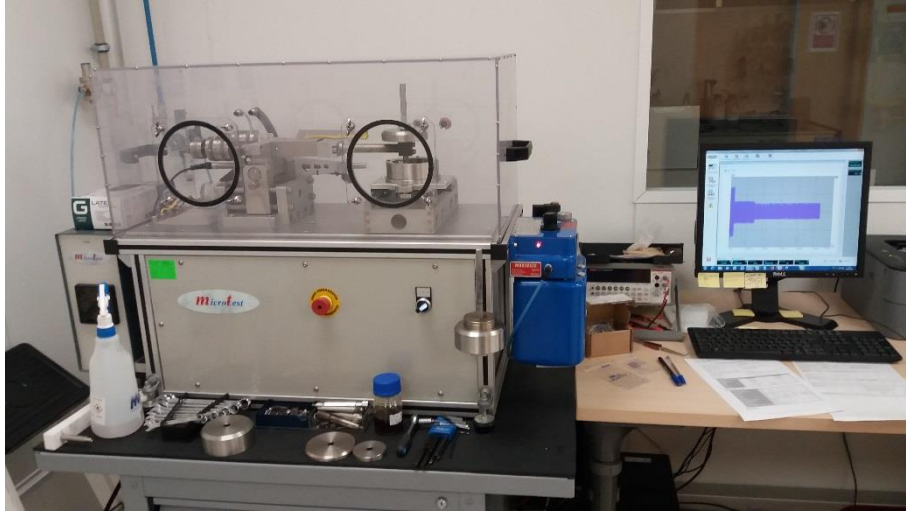
Figure 2.22. MT4002 MICROTEST tribometer.

Figure 2.23. Keithley 2100 Multimeter.

In the case of the nitrided **15-5PH** cylinders, a cylinder on cylinder reciprocating configuration was adopted, where one of the cylinders had either a plasma treated or an untreated surface, and the other had an untreated surface. The tests were performed at room temperature, at different loads, 5 and 15 N, low and high humidity, 18% and 80%RH respectively, and a mean speed of 0.020 m/s.

In the case of the nitrided **316L** surfaces, a ball on disc configuration was adopted, i.e. nitrided 316L discs against WC-Co balls. The tests were performed at a load of 1 N,

50% relative humidity, at room temperature and at a speed of 0.3 m/s. In this case, the tribological studies were not performed on the inner surfaces of the tubes, because the tests could not be implemented in the tribometer used in this work.

In the case of the **AgAl coatings**, a pin on (half) disc reciprocating configuration was adopted (Figure 2.24). The counter surface in the tribological studies was a copper pin plated with 20μm Ag, with a semispherical tip 10 mm in diameter (Figure 2.25). This counterpart was selected because is the material of choice currently used in many electrical contacts, and the set up used in previous studies (Mao, Taher and Kryshtal, et al. 2016), (Mao, Taher and Berastegui, et al. 2018), (Taher, et al. 2018).
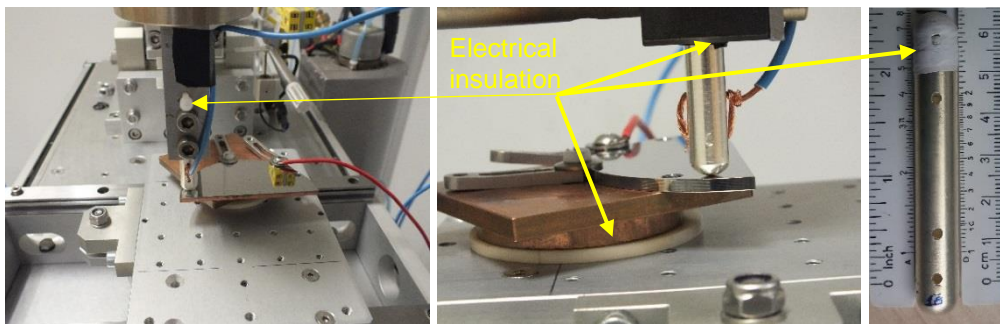
Figure 2.24. Tribometer set up in the "in air" tests: details of the electrical connection set up (blue and red wires) between the MT4002 MICROTEST tribometer and the Keithley 2100 Multimeter for measurement of the Electrical Contact Resistance (ECR).

Figure 2.25. Image of one of the Ag coated Cu pins used as counterparts in the electro-tribological studies against AgAl coatings.

The tests were performed under 2 N, mean speed of 2 mm/s, at room temperature, in air at a relative humidity of 50% or immersed in insulating oil (Nytro 10XN, Nynas). Tests were carried out at sequentially diminishing track lengths of 50, 40, 30, 20 and 10 mm (Figure 2.26), and repeated twice. This way the evolution of wear could be assessed and measured at different number of cycles.
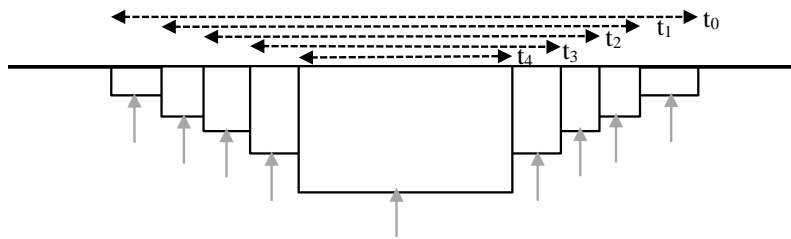
Figure 2.26. Decreasing test track lengths and wear assessment points (↑).

The electro-tribology studies with the **DLC coatings** were performed against 6 mm diameter aluminum (99,7%) balls, being aluminum used frequently in electrical and electronic gear, although its tribology is typically quite poor.

The tests were performed on a pin-on-disk (PoD) configuration, in controlled humidity environments, with the same Microtest MT4002 tribometer and micro-ohmmeter, Keithley K2100, used in the previous studies. Main test conditions consisted of a load of 3N, a speed of 50 cm/s and room temperature.

2.4.2.6. Environmental Tests.

Salt Spray Tests (SST) were performed in accordance to ASTM B117 and ISO 9297 to study the corrosion resistance of the samples to chloride rich environments (Figure 2.27).

Figure 2.27. Salt Spray Test Chamber and sample lay-out.

Additionally, in the case of the AgAl coatings, because of the foreseen application in electrical sliding contacts under insulating oil, two distinct complementary environmental degradation tests were carried out.

The **H₂S gas test,** which exposed the coated Si samples for 24, 48 and 96 hours at room temperature to the atmosphere produced by 1.14g/L Na2S in 50mL deionized water. Samples were arranged vertically above the solution (Figure 2.28).
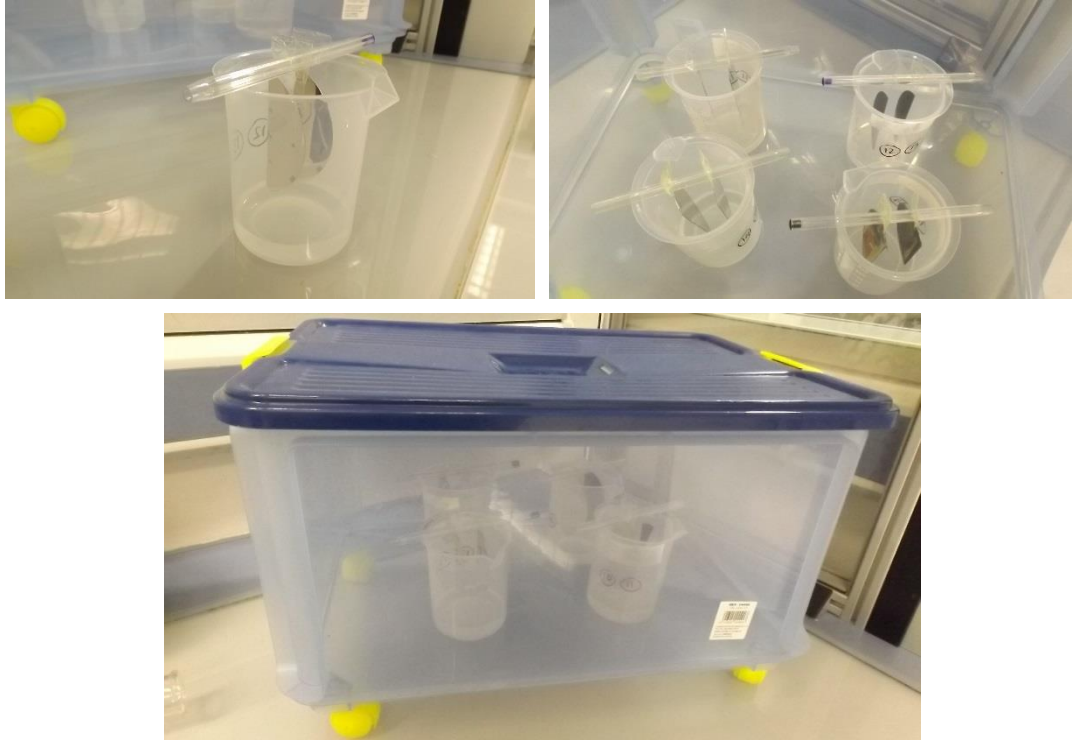
Figure 2.28. Images of the SH$_2$ test arrangement.

Additionally, an **oil immersion test** was performed on the coated Cu samples. They were first annealed at 135ºC for 24 hours in air, and then, immersed in insulating oil (Nytro 10XN, Nynas) for 30 days and subjected to the following thermal cycle: 120ºC for 18h, cooling to 70ºC, followed by heating back to 120ºC after 6h (CTS GmbH, C-40/200). After the oil immersion test cycles were completed, the surfaces were rubbed with dry soft paper tissue to remove the oil, and the surface degradation was quantified in terms of the areas that had kept the initial brightness, i.e. had not suffered tarnishing, and through the evaluation of the electrical contact resistance, ECR. The assessment of the percentage of tarnished surface was performed through visual inspection with a transparent grid pattern in an illumination controlled room (Figure 2.29).

The evaluations of the coatings after the tests were performed by visual inspection, OM, SEM and EDS.
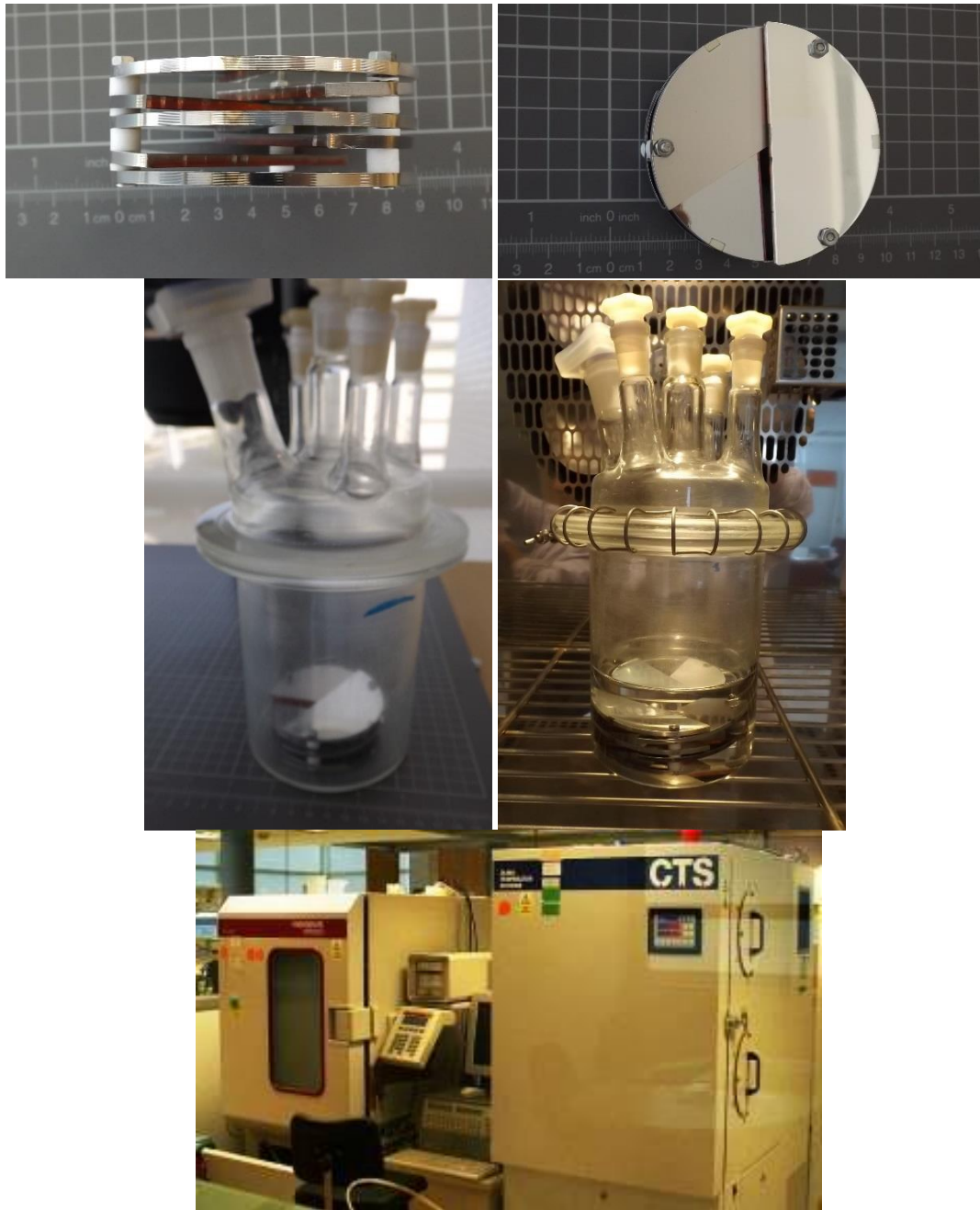
Figure 2.29. Images of the oil immersion test sample arrangement and the climatic chamber were the tests were performed.

3.   PLASMA NITRIDING OF STAINLESS STEEL

3.1. PROBLEM STATEMENT

Stainless steels, especially the austenitic grades, present overall a good **corrosion resistance** but poor **tribo-mechanical** properties.

Nitriding is often used to improve tribological properties and wear resistance of stainless steels (Lo, Shek y Lai 2009), (Ou, et al. 2011), (Köster, et al. 2013). Nevertheless, preserving the corrosion resistance of stainless steels, while producing hardened surfaces with good tribological properties, often lead to not fully satisfactory compromises. This is especially the case with the treatment of martensitic stainless steels (Lo, Shek y Lai 2009).

However, in many critical applications, in the aeronautical (e.g. landing gear components), ground transportation (e.g. load sensing components) and biomedical (e.g. surgical tools) fields, good mechanical properties are mandatory in combination with good tribological and corrosion resistance properties. In such cases, precipitation hardening martensitic stainless steels are often the material of choice. Precipitation-hardening stainless steels have actually been developed to provide high strength and toughness while maintaining the corrosion resistance of stainless steels.

Nitriding of stainless steel must overcome, among others, **two main challenges:** the removal of the naturally occurring passive oxide film and the precipitation of chromium carbides.

In the first case, the stable surface chromium oxide film actually provides the alloys with their corrosion resistance. However, the oxide layer impairs the diffusion of nitrogen and, consequently, needs to be removed before the nitriding process.

In the latter case, as described in the previous chapter (2.2.1.), traditional nitriding treatments are conducted at high temperatures, around 500ºC - 600ºC, which causes chromium to precipitate as chromium nitrides. This has a deleterious effect on the corrosion resistance of the alloys. Therefore, the objective is to devise processes that produce a layer of precipitation free austenite o martensite depending on the corresponding alloy, supersaturated with nitrogen, which are usually referred to as S-phase or expanded austenite ('γ_N-phase') and expanded martensite (α'_N-phase').

Among the nitriding techniques, **plasma nitriding** is a well stablished, environmentally friendly and energy efficient technique. This method allows for an easy removal of the naturally occurring passive layer from the stainless steel surface, as described above necessary prior to the nitriding, which is often a challenge in gas nitriding processes.

It has been actually reported that low temperature (<450 ºC) **plasma nitriding** can produce a new phase with high hardness and good corrosion resistance on austenitic stainless steel surfaces, by the formation of a nonequilibrium supersaturated layer, called 'S-phase' or expanded austenite 'γ_N-phase'. Thus, nitrogen remains in solid solution without removing chromium from the austenitic structure by precipitation of Cr nitrides, and thus lowering the corrosion resistance. However, a long nitriding time is necessary to obtain a sufficiently thick γ_N-phase layer by low temperature nitriding techniques (Dong 2010) (Li, et al. 2014).

Therefore, research continues into new treatment techniques able to produce better compromises between tribological properties and corrosion resistance features. Along these lines, the **active screen plasma** (ASP) nitriding offers many advantages over conventional plasma nitriding. The generation of the plasma in the outer screen, which serves also as a radiation source, allows for a more flexible process, where the part to be treated can be subjected to an independent bias potential, thus reducing edge effects, arcing risk, etc. As the active screen acts as both a generator of plasma species and source of radiation that acts as

a heater, this enables a better process temperature control, independent from the voltage bias applied to the treated part.

It is also known that the **hollow cathode** (HC) effect produces denser plasmas, by means of the "pendulum", photoionization and stepwise ionization (Muhl and Pérez 2015).

Nitriding of austenitic stainless steels.

Several authors have indeed reported the advantages of the active screen plasma nitriding of austenitic stainless steels (Corujeira Gallo and Dong 2009), (Corujeira Gallo and Dong 2012), (Li and Bell 2004), (Hoshiyama, Mizobata and Miyake 2016), (Lin, et al. 2014).

The combination of both, ASP and HC, has also been studied recently on austenitic stainless steel, aiming at rapid nitriding processes in short times (Li, et al. 2014), (Yang W.J. 2016), (Shen, Wang and Xu 2013), (Nikolov, Bunk, et al. 2014).

However, plasma nitriding of inner geometries still represents a challenge (Kim and Han 2003), (Fernández de Ara, et al. 2017). Few authors have indeed studied this field, although there are numerous applications that could benefit from a corrosion resistant inner surface with good tribo-mechanical properties, e.g. multiple sleeves in the engineering field, or cannulas, trephine tips, reamers, in the biomedical field, etc. The plasma nitriding of inner surfaces is nevertheless conditioned, among others, by geometric features that can cause at the extremes absence of plasma or the occurrence of high density plasmas due to hollow cathode effects (Muhl and Pérez 2015), (Nikolov, Köster, y otros 2014).

Nitriding of precipitation hardening martensitic stainless steels.

Relatively little research has been carried out on the effect of plasma nitriding on martensitic precipitation hardening (PH) stainless steels. Some good results have been found regarding surface hardness and α'_N (nitrogen supersaturated expanded martensite) layer thickness, but most often with poor corrosion behavior because of the formation of chromium nitrides during the plasma nitriding process (Leyland, et al. 1993), (Barua, Kim and Lee 2016), (Sun 2016), (Brühl, et al. 2010), (Esfandiari and Dong 2007), (Dong, Esfandiari and Li 2008), (Barua, Kim and Lee 2016), (Pinedo, et al. 2016).

In this work, the combination of the active screen plasma nitriding and hollow effect has been studied on both the inner surfaces of AISI 316L austenitic stainless steel and the 15-5PH grade precipitation hardening martensitic stainless steel, on long cylindrically shaped geometries.

The idea was to develop a plasma based surface treatment with a a good **compromise** between **tribological properties and corrosion resistance**.

In the case of the Precipitation Hardening martensitic alloy, this objective was more narrowly defined (by an industrial collaborator) as achieving a thick nitride layer above 50μm, with good tribological properties and a corrosion resistance of more than 48h at Salt Spray Test (SST).

In the case of the austenitic stainless steel, the work has focused on the development of active screen plasma nitriding processes of the inner surfaces of tubes manufactured on the widely used AISI 316L alloy, with the assistance of the hollow cathode effect.

At the same time, the electro-tribology properties as a way of **monitoring** the status of the nitrided stainless steel surfaces have also been investigated.

3.2. HOLLOW CATHODE AND ACTIVE SCREEN PLASMA

Firstly, details of the occurrence of the HC effect and its intensity in Tecnalia's ASP equipment were studied. Thus, a screening of the process temperatures of different open-ended tube diameters were carried out as compared with the temperatures measured in a dummy bulk cylinder.

It soon became evident that the HC was present, and it had an effect in the process temperature. Among other process parameters, the following were identified as key:

- The tube inner diameters, i.e. Figure 3.1 vs. Figure 3.2.
- The gas mix, e.g. Figure 3.3.

In Figure 3.1 the evolution of the temperature on a 45mm diameter dummy bulk cylinder (black line) and 45mm diameter tube (red line) are shown for a typical gas mix of N_2:H_2 1:3. A larger temperature, with an increase in 80ºC, was observed in the tube due to the HC effect.

In Figure 3.2 the temperature evolution, for the same gas mix, corresponds to a 25mm diameter tube. In this case, a larger temperature increase was observed: 120ºC higher in the tube that in the bulk dummy.

In both cases, the plasma process temperature, as measured in the dummy, was of 350ºC. So, it can be concluded that the plasma was denser in the 25mm diameter tube than in the 45mm one.
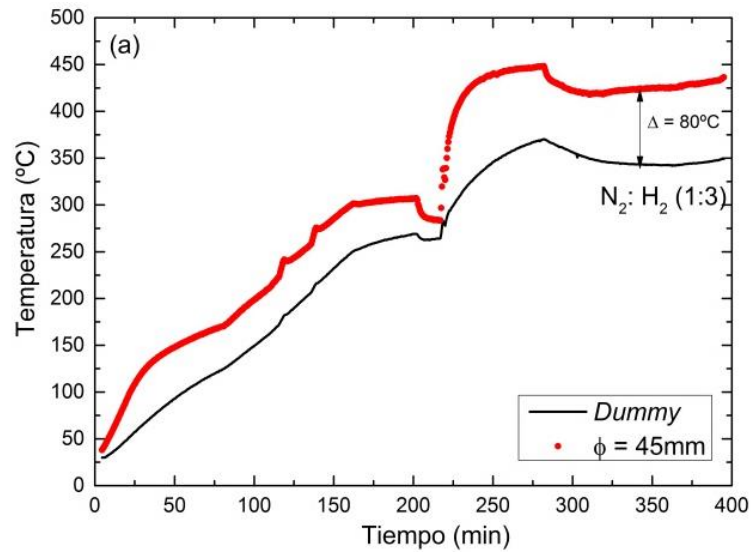
Figure 3.1. Evolution of the temperature along the ASP process on a dummy bulk cylinder (black line) and 45mm diameter tube (red line).
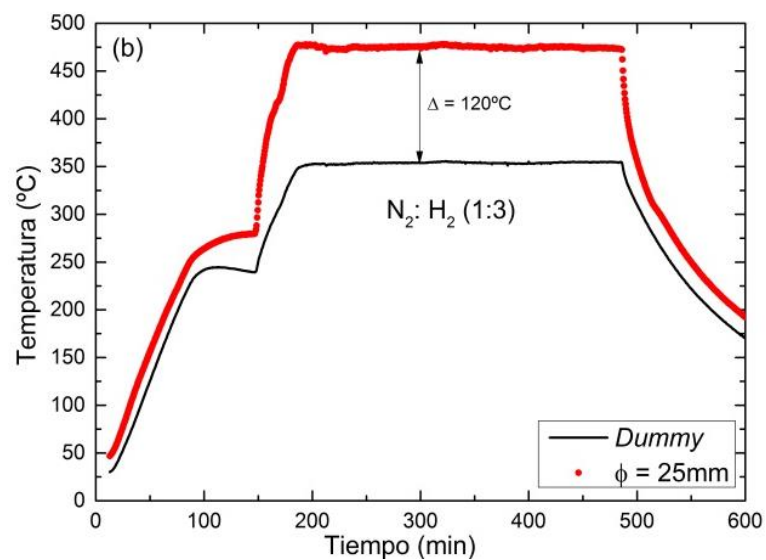
Figure 3.2. Evolution of the temperature along the ASP process on a dummy bulk cylinder (black line) and 25mm diameter tube (red line).

These preliminary studies were also carried out at different N_2-H_2 gas mixes in the 45mm diameter tubes (Figure 3.3). The experiments confirmed that the HC effect is dependent on the nature of the ion mix in the plasma. The higher the percentage of hydrogen in the gas mix, the larger was the temperature increase in the tube.
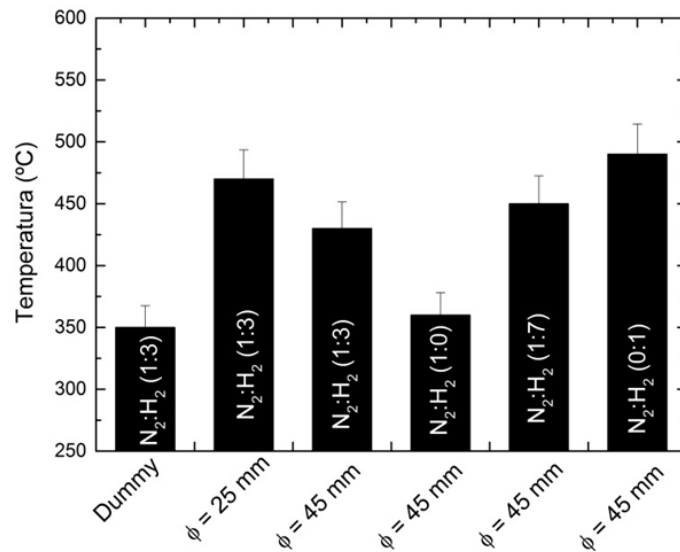
Figure 3.3. Process temperatures for different geometries (dummy bulk cylinder and 25 and 45 mm tubes) and gas mixtures.

3.3. PLASMA NITRIDING OF PH ALLOYS

3.3.1. PLASMA NITRIDED 15-5 PH

As mentioned before, the active screen plasma nitriding technique in combination with the hollow cathode effect was studied in this work, with the aim of obtaining thick nitride layers (50μm), with good corrosion resistance (>48h in STT) and tribological properties.

In the active screen plasma treatments, the outer screen is subjected to a voltage, while the samples are immersed in plasma and biased to a lower potential. Furthermore, if the sample is surrounded by an open-ended tube, in some cases, a hollow cathode occurs inside the tube.

A schematic of the technique used for the plasma treatments is shown in Figure 3.4. In this work the screen and the sample were each connected to independent DC power supplies. The nitrided samples consisted of 10 mm in diameter and 80 mm long 15-5PH made cylinders. The surrounding tube was manufactured on austenitic stainless steel, AISI 316L, with a height of 120mm and 45mm in diameter, and was open-ended in both ends.
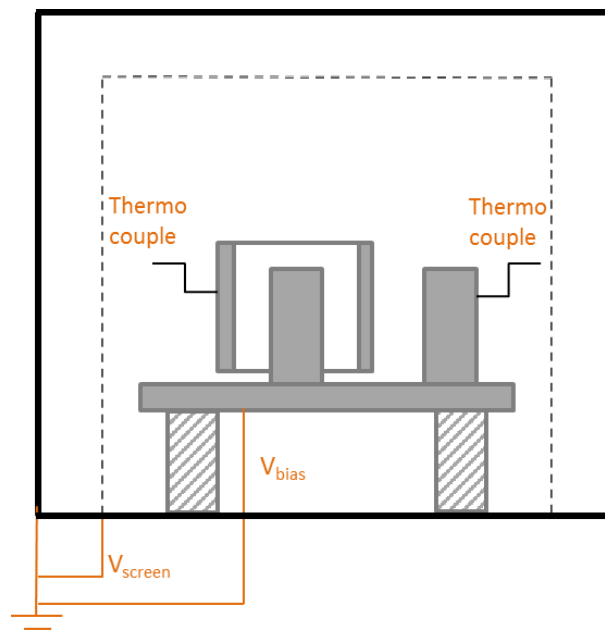
Figure 3.4 Equipment layout during the PH alloy plasma treatments.

Firstly, the samples were plasma cleaned with 50/50 Ar/H_2 for a minimum of 1h to remove residual surface contaminants and the naturally occurring surface oxides, using a bias voltage of 250 V (and 210 V in the screen).

The nitriding surface treatments were subsequently applied at a pressure of 120 Pa, with a gas mixture of 3/1 H_2/N_2, according to the parameters detailed in Table 3-1. The process temperatures were monitored with a thermocouple in an adjoining bulk dummy cylinder, and later in the study also by another thermocouple inserted in the tube surrounding the sample. After the treatment, the samples cooled in vacuum down to room temperature, RT.

Table 3-1. Plasma process parameters.

Reference	Process Temperature at dummy (ºC)	Process Temperature at the tube (ºC)	Process duration (h)	Nitride layer thickness (µm)
#350.5	350	-	5	4
#350.25	350	-	25	8
#350HC5	350	-	5	100-110
#350HC2.5	350	-	2.5	140
#275HC5	275	370	5	155
#275HC2.5	275	350	2.5	100
#275HC1	275	365	1	60

Nitride layer thickness

Conventional plasma nitriding treatments, i.e. with no surrounding tube and thus no hollow cathode effect, produced thin nitride layers, 4 and 8 μm thick respectively for 5 and 25 h treatment times at 350 ºC (Ref. #350.5 and #350.25; Table 3-1; Figure 3.5 and Figure 3.6 respectively).

Figure 3.5. Cross sections of reference #350.5.
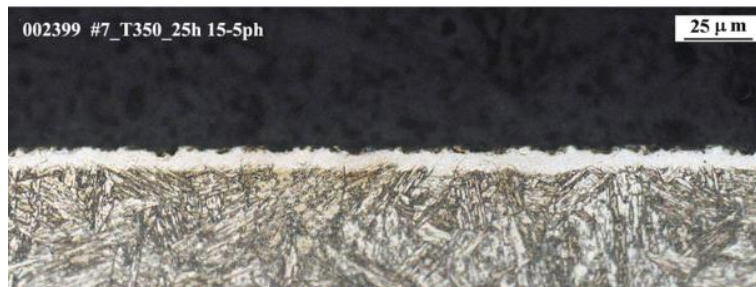
Figure 3.6. Cross sections of reference #350.25.

On the other hand, the same process time and temperature accompanied by the hollow cathode effect showed a nitride layer thickness above 100 μm (Ref. #350HC5; Figure 3.8).
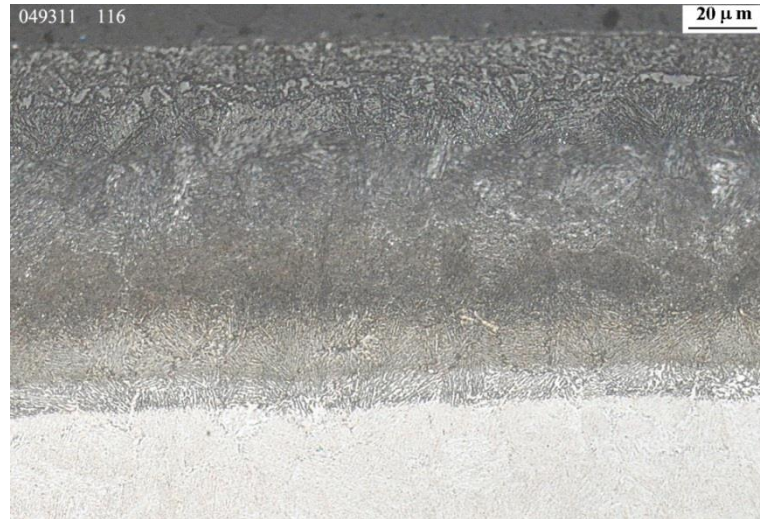
Figure 3.7. Cross sections of reference #350HC5.

When milder treatment conditions were applied, in the form of shorter nitriding treatments, 2.5h, or treatment at lower temperature, 275 ºC (370ºC at the tube), radial cracks were detected at the surface, which presented a nitride layer thickness of 140 and 155 µm respectively (Ref. #350HC2.5 and 275HC5; Figure 3.9 and Figure 3.8 respectively). At even milder conditions, 2.5h and 275 ºC (350º at the tube), the nitride layer thickness was reduced to ~100µm, but still cracks were present (Ref. #275HC2.5; Figure 3.10).
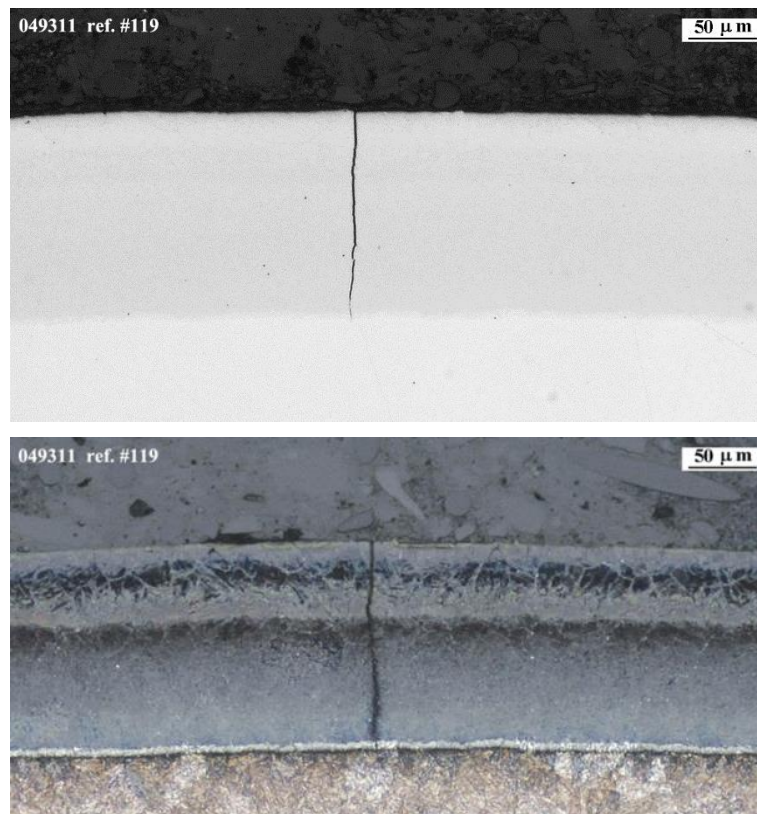
Figure 3.8. Cross sections of reference #275HC5.
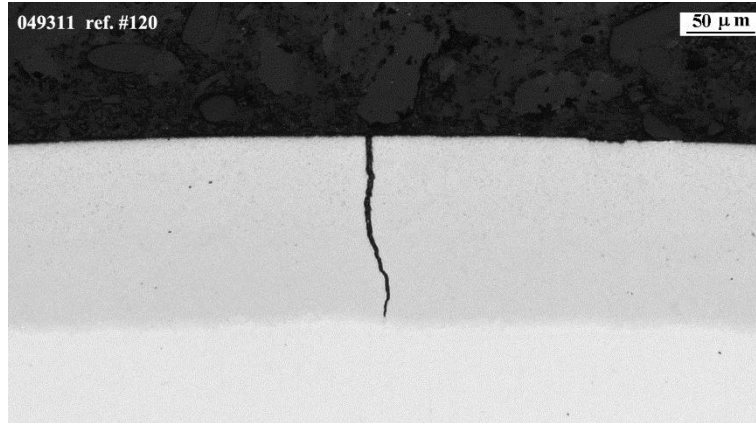
Figure 3.9. Cross sections of reference #350HC2.5.

Figure 3.10. Cross sections of reference #275HC2.5.

At slightly higher temperature but shorter treatment time, 1h and 270 ºC (365º at the tube), the nitride layer thickness was reduced to ~ 60µm, and no cracks were apparent in the surface cross sections prepared (Figure 3.11).

Figure 3.11. Cross sections of reference #275HC1.

Overall, when measured, it was observed that the presence of the hollow cathode effect produced an increase in the temperature of 75 to 95ºC in the surrounding tube comparing with the adjoining cylindrical dummy.

3.3.2. ENVIRONMENTAL STUDIES OF PLASMA NITRIDED 15-5 PH.

The corrosion resistance of the treated surfaces was assessed in Salt Spray Tests (SST) performed following the ISO 9297 standard (International Organization for Standarization 2012).

The limitations of accelerated corrosion testing are well known, specifically concerning salt spray tests. The standard itself mentions that there is seldom a direct relation between resistance to the action of salt spray and resistance to corrosion in other media, and therefore, the test results should not be regarded as a direct guide to the corrosion resistance in all environments. Nevertheless, the method gives a means of checking that the comparative quality of a metallic material, with or without corrosion protection, is maintained. Thus, this test

method was selected to assess the damage inflicted in the substrate material by the plasma nitriding treatment and because, despite all the limitations, it is still widely used in many industrial fields.

Conventional plasma nitriding treatments (with no hollow cathode effect) had produced 4 and 8 μm quite thin nitride layers, (Ref. #350.5 and #350.25; Table 3-1). However, these surfaces already showed red rust at the SST tests at 4h (Figure 3.12).

Figure 3.12 Samples #350.5 (left) and #350.25 (right) at the SST test after 4h.

The same process time and temperature accompanied by the hollow cathode effect (Figure 3.13) (100 μm thick nitride layer) showed also red rust at the SST tests at 4h (Ref. #350HC5).
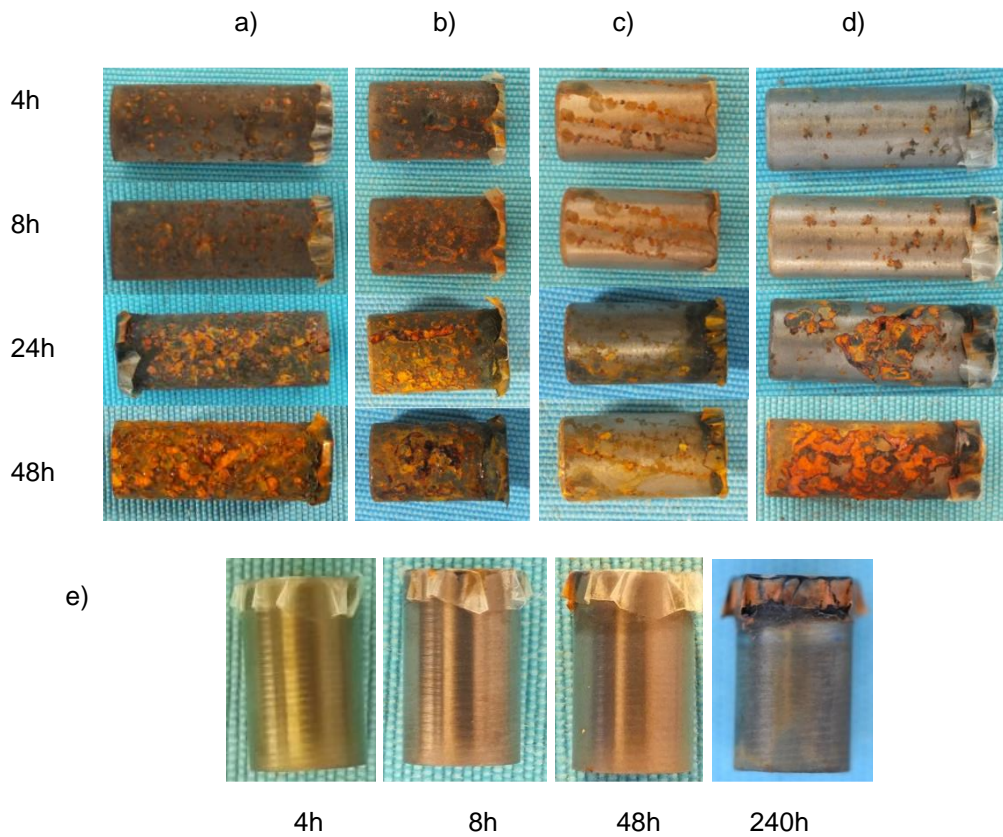
Figure 3.13 Samples Ref. #350HC5 (a), #350HC2.5 (b), #275HC5 (c) and #275HC2.5 (d) at the SST test after 4h, 8h, 24h and 48h, and Ref. #275HC1 (e) after 4h, 8h, 48h and 240h.

Milder treatment conditions, with shorter nitriding treatments, 2.5h, did not improve the corrosion resistance (Ref.#350HC2.5). Conversely, treatment at lower temperature, 275 ºC (370ºC at the tube), showed better corrosion resistance with sections of the surface showing resistance after 48h at SST, though others showed red rust before 4h (Ref.#275HC5). This can be assigned to a great extent to the fact that in both treatments radial cracks were detected at the surface (Ref. #350HC2.5 and 275HC5). At even milder conditions, 2.5h and 275 ºC (350º at the tube) saw a further improvement of the corrosion resistance, but still presence of cracks (Ref. #275HC2.5).

However, at slightly higher temperature but shorter treatment time, 1h and 270 ºC (365º at the tube), the SST test showed a corrosion resistance above 240h (Ref. ##275HC1), and the nitrided layer was above the target at ~ 60μm.

Surface structure

Selected surface cross sections were analyzed by EDS and phases present at the surface by XRD, to learn about the reasons behind the remarkable differences in corrosion resistance.

Big differences in corrosion resistance were observed between references #350HC2.5 and #275HC5, although they presented quite similar nitride layer thicknesses. Therefore, these surfaces were analyzed in detail by SEM and EDS, together with ref. #275HC1, which had shown the best corrosion resistance performance.

i) EDS

EDS showed the same initial elemental composition in all references (Figure 3.14, <). On the other hand, after surface etching, differences appeared: while ref. #350HC2.5 showed an increasing displacement of Cr concentration towards the surface (Figure 3.14, yellow line, a,>), ref. #275HC5showed an intermediate region with lower Cr content (Figure 3.14, yellow line, b,>), and ref. #275HC1 showed no apparent change (Figure 3.14, yellow line, c,>).
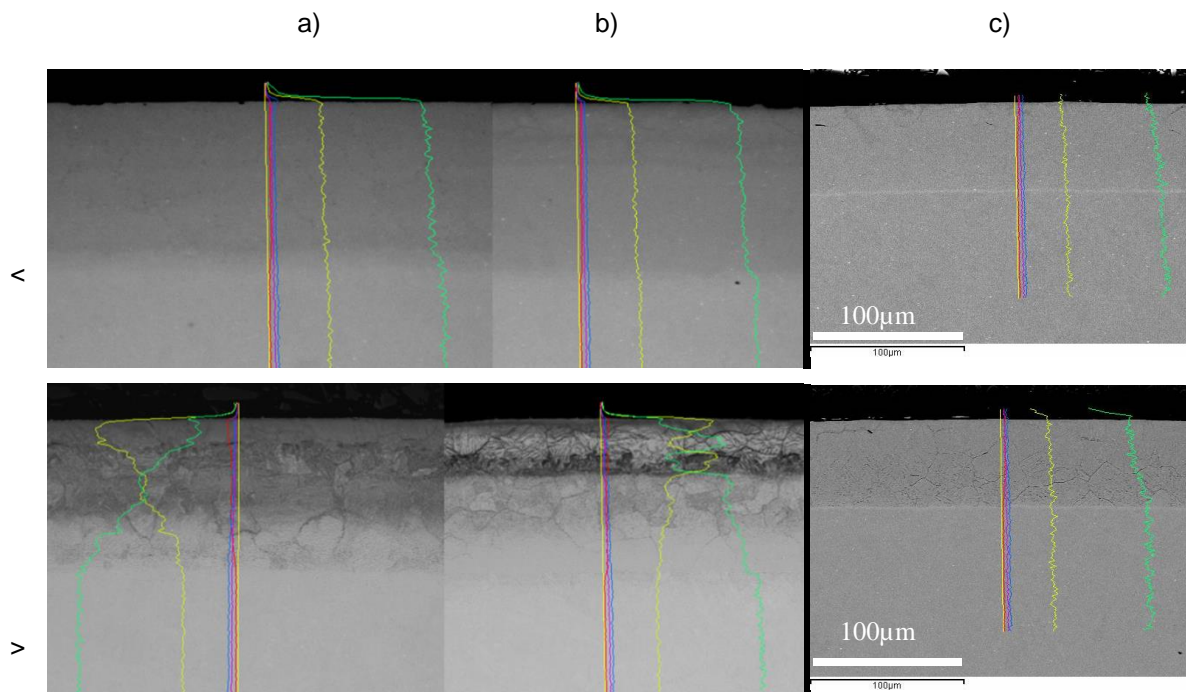
Figure 3.14 EDS depth profiles of references #350HC2.5 (a), #275HC5 (b) and #275HC1(c), before (<) and after (>) etching: Fe in green and Cr in yellow. SEM images, x500.

ii) XRD

XRD spectra of ref #275HC5, #350HC2.5, #275HC1 and the untreated steel are shown in Figure 3.15. These surfaces, which have showed remarkably different corrosion resistances, also presented differences in the XRD spectra.

The untreated surface presented a single diffraction peak of the martensite phase ($\alpha'Fe$) (Figure 3.15.). CrN and α'_N peaks were much lower in the case of reference #275HC1 as compared with #350HC2.5, and even lower for ref. #275HC1 (Dong, Esfandiari and Li 2008).
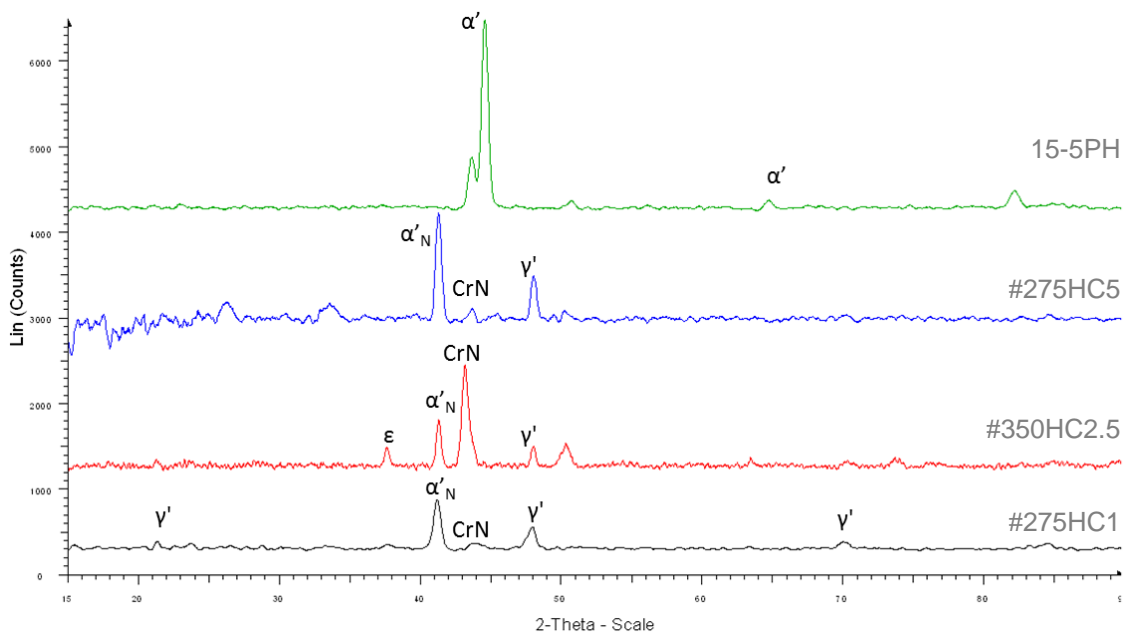
Figure 3.15. XRD spectra of references: untreated 15-15PH steel, #275HC5, #350HC2.5 and #275HC1.

Overall, results show that process temperature, duration and plasma density are key parameters in the resulting nitride layers and their performance. Conventional plasma treatments typically applied on stainless steels, i.e. at 350ºC process temperature, produce a very thin nitride layer (ref. #350.5: 4µm), even if the process duration is prolonged (ref. #350.25: 8µm). Increasing treatment time produces diminishing increases in the nitride layer thickness. This is in accordance with results reported elsewhere (Leyland, et al. 1993), (Brühl, et al. 2010), (Esfandiari and Dong 2007), (Muhl and Pérez 2015)]. Besides, it basically destroys the corrosion resistance ability of the alloy.

The hollow cathode effect increases the nitride layer thickness remarkably, i.e. above 100µm. This thickness is much larger than that achieved by Li et al. on stainless steel, albeit with a different configuration (Li, et al. 2014).

This is due mainly to two related reasons: increase in both the process temperature and the plasma density. The former can be observed on the temperatures measured on the treatment chamber by means of thermocouples in a dummy bulk cylinder and in the tube surrounding the 15-5PH samples (Table 3-1), with increases in the range of 75 to 95ºC. The influence of the latter is clear comparing the thicknesses achieved at nitriding temperatures of 350ºC for 5h with conventional plasma and hollow cathode presence: 4µm at ref. #350.5 as compared with 155µm at ref. #275HC5. The increasing nitride layer thickness with increasing N_2 percentage and ion spices in the plasma has actually been reported, though with much thinner thicknesses, ≤ 20µm, the opposite effect on corrosion resistance due to Cr_2N formation, and no hollow cathode effect involved (Leyland, et al. 1993).

However, the hollow cathode effect does not preclude the precipitation of Cr nitrides, the main reason behind the loss of corrosion resistance. This is clearly evident in surface ref.#350HC2.5, where the XRD spectrum shows presence of peaks corresponding to Cr nitrides as well as α'_N nitrogen supersaturated expanded martensite (Figure 3.15), while red corrosion is already present in 4h at the SST (Figure 3.13, b).

However, thanks to the hollow cathode effect, thicker thicknesses can be achieved in shorter treatment times, with potentially less precipitation of Cr nitrides.

This has been observed in the EDS depth profile analyses. Ref #275HC5 shows a lesser increase in the near surface of Cr than ref. #350HC2.5 (Figure 3.14, a) after etching, especially

in an intermediate region of the nitride layer, possibly indicating a lower degree of precipitates, i.e. chromium nitrides, deleterious for the corrosion resistance, because the degree of free metallic chromium diminishes. Ref. #275HC1 shows actually no such increase. These differences in the severity of the etching can also be observed in the optical microscope (Figure 3.11).

Concerning the XRD analysis, Dong et al. already reported in his systematic microstructure characterization of plasma nitrided precipitation hardening PH alloy (Esfandiari and Dong 2007), that surface phase constituents, highly treatment temperature dependent, presented nitrogen supersaturated martensite (α'_N-expanded martensite); Nitrogen S-phase grains, if there is some pre-existent retained austenite, γ'–Fe_4N compound layer and CrN precipitates. Thus, the results obtained (Figure 3.15) of the glancing angle XRD analysis were consistent with several papers that reported that the white layer in nitride martensitic steels is mainly a stressed structure called "expanded martensite" (Brühl, et al. 2010), where nitrogen is present on interstitial sites of the bcc ferrite tetragonally distorted. On the other hand, the higher the temperature and nitriding time, the more CrN was present, #350HC2.5 >#275HC5 > #275HC1.

Naeem et al. have recently reported in the nitriding of AISI 304 austenitic stainless steel that when cathodic cage diameter is decreased and consequently a more reactive plasma is generated, a phase transformation from conventionally reported γ_N-phase to iron nitrides ($Fe_{2-3}N$, Fe_4N) occurs without precipitation of chromium nitrides, which is behind the improvement of corrosion resistance (Naeem, et al. 2016). Esfandiari et al. have also reported that formation of γ'-Fe_4N in precipitation hardening stainless steels can enhance their corrosion properties, being a face centered cubic (fcc) phase as in austenite, although they report no γ'-Fe_4N in low temperature nitriding at 350°C (Esfandiari and Dong 2007).

This interpretation is further confirmed in process ref. #275HC2.5, where the process duration has been halved. In this case, the nitride layer is still relatively thick, ~100μm, and the corrosion resistance is only hindered by the presence of surface cracks (Figure 3.11 and Figure 3.13). It has also been explored modifying the heating and cooling speeds to avoid the formation of these cracks (results not reported here), but to no effect.

A further halving of the process duration to 1h and slightly higher temperature, ref. #275HC1, has rendered much improved results: absence of red rust up to 240h at the SST test (Figure

3.13), associated with absence of cracks (Figure 3.11) and much lower precipitation of Cr (Figure 3.15), with still a thick nitride layer, ~ 60 µm.

In conclusion, preserving the corrosion resistance is proven to be associated to the absence of surface cracks and reduced precipitation of chromium nitrides.

3.3.3. ELECTRO-TRIBOLOGICAL OF PLASMA NITRIDED 15-5 PH.

Electro-tribology studies were performed with the surface showing better corrosion resistance (#275HC1) and control untreated surfaces, at different loads (5 and 15N) and humidity (18 and 80 %RH), on a cylinder on cylinder reciprocating configuration (Figure 3.16). Both the coefficient of friction (CoF) and electrical contact resistance (ECR) were monitored along the tests (Figure 3.17 to Figure 3.19).
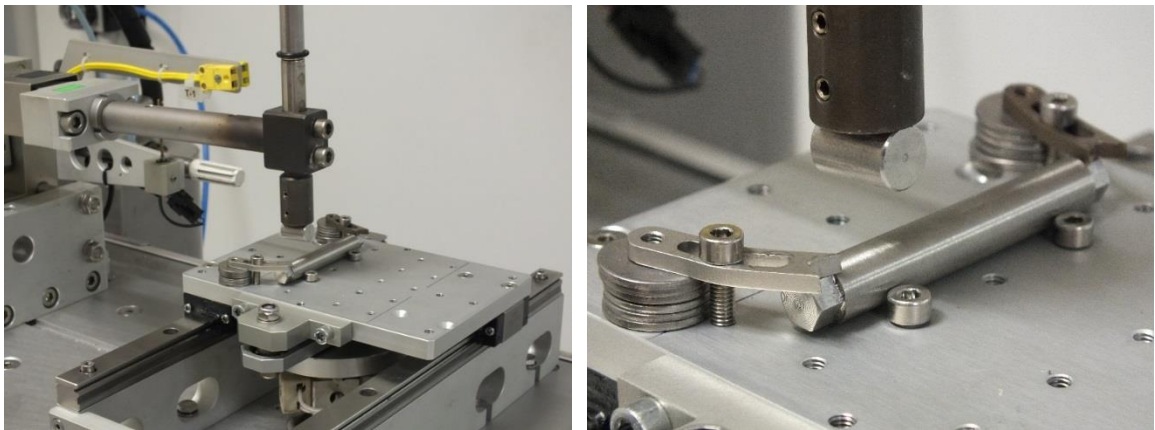
Figure 3.16 Tribometer set up for the cylinder on cylinder reciprocating tests.

The 15-5PH against 15-5PH pair at low humidity showed two distinct patterns: first low friction and high ECR, then higher CoF and low ECR (Figure 3.17, above). In the case of the 15-5PH against plasma nitrided #275HC1 pair, the ECR remained low and the CoF rose to high values faster (Figure 3.17, below).

At larger loads, results were similar, but the second region of higher CoF occurred before, with less test cycles (Figure 3.18).

Conversely, at high humidity, the 15-5PH against 15-5PH pair showed low ECR but increasing CoF, while the 15-5PH against plasma nitrided #275HC1 pair still showed high CoF and two distinct regions of ERC values (Figure 3.19).
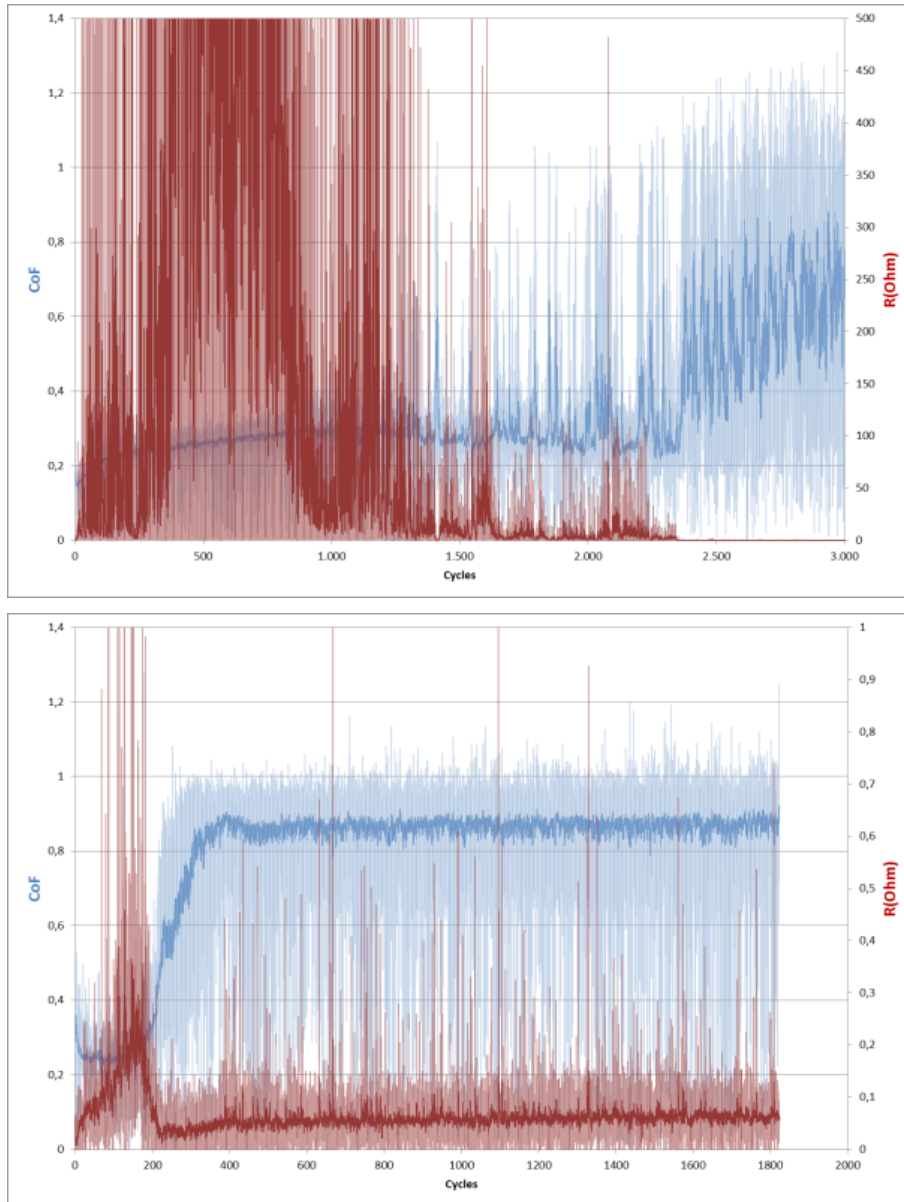
Figure 3.17 CoF (blue; average of 100 data points in dark blue) and ECR (red; average of 100 data points in dark red) of 15-5PH against 15-5PH pair (above) and 15-5PH against ref. #275HC1 pair (below), at **5N** and **18%RH**. Note: No all ECR in the same scale.
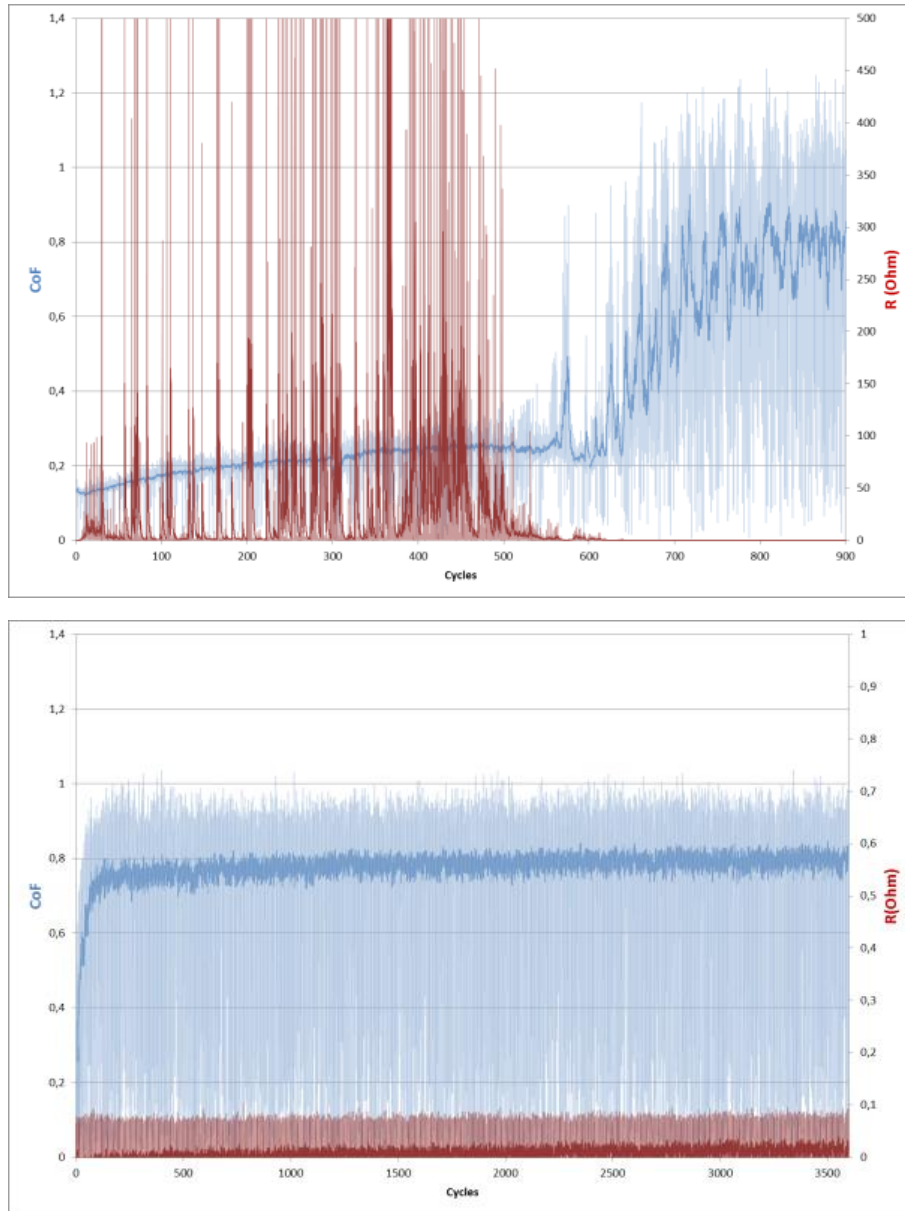
Figure 3.18 CoF (blue; average of 100 data points in dark blue) and ECR (red; average of 100 data points in dark red) of 15-5PH against 15-5PH pair (above) and 15-5PH against ref. #275HC1 pair (below), at **15N** and **18%RH**. Note: no all ECR in the same scale.
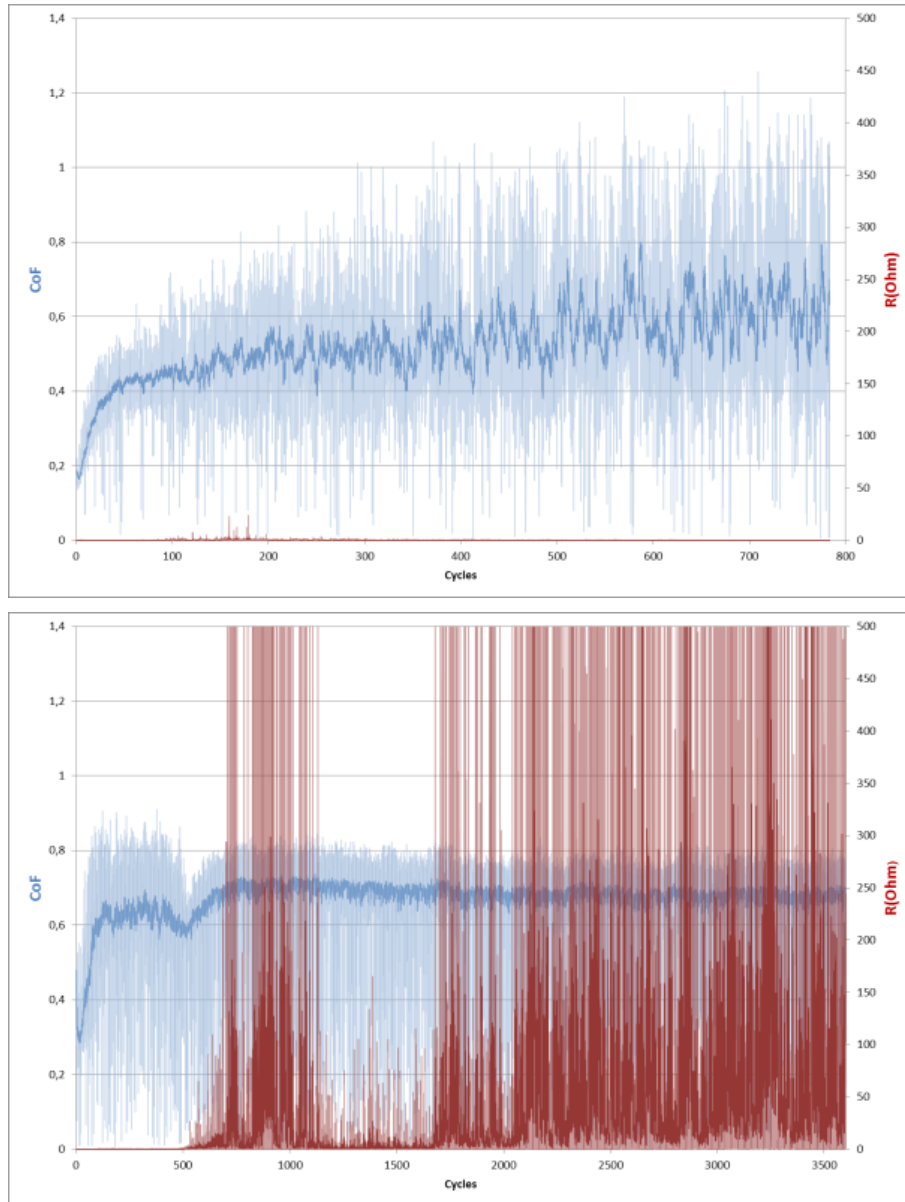
Figure 3.19 CoF (blue; average of 100 data points in dark blue) and ECR (red; average of 100 data points in dark red) of 15-5PH against 15-5PH pair (above) and 15-5PH against ref. #275HC1 pair (below), at **5N** and **80%RH**. Note: no all ECR in the same scale.

Therefore, different patterns can be distinguished in the tribological performance of the studied surfaces (Figure 3.19). As a rule, there is an initial rise in CoF due to the enlargement of the contact surfaces, including the reduction of the surface roughness. Then typically two different patterns occur.

At low humidity, a relatively steady regime with low CoF, <0.3, ensues. It is known that oxidation effects in dry sliding are generally beneficial because they reduce wear by forming compact layers of oxide particles on the surface which act as lubricant.

The 15-5PH against 15-5PH pair shows an oscillating ECR. This is also related to the surface oxide layer, continuously thickening and wearing out. At some point, the oxide layer is removed, a rise in CoF and drop in ECR follows, and the system enters an adhesive wear regime (Figure 3.20, a). In the case of the #275HC1 against 15-5PH pair, the ECR stays permanently very low, because the oxide layer is removed in the very first cycles, and probably also because the nitride layer conserves enough amount of free Cr. This also causes the CoF to rise, and adhesive wear to occur earlier, i.e. by ~200cycles instead of by ~2000-2500 cycles. The regime transition occurs sooner for larger loads, 15N, i.e. almost immediately and by ~600cycles respectively. In both conditions and pairs the CoF ends up close to ~0.8. These CoF values are in line with values reported elsewhere, albeit not in a like on like configuration (Pantazopoulos, et al. 2004), (Dalibon, et al. 2014). This might be associated with metal on metal sliding conditions.

a)   b)
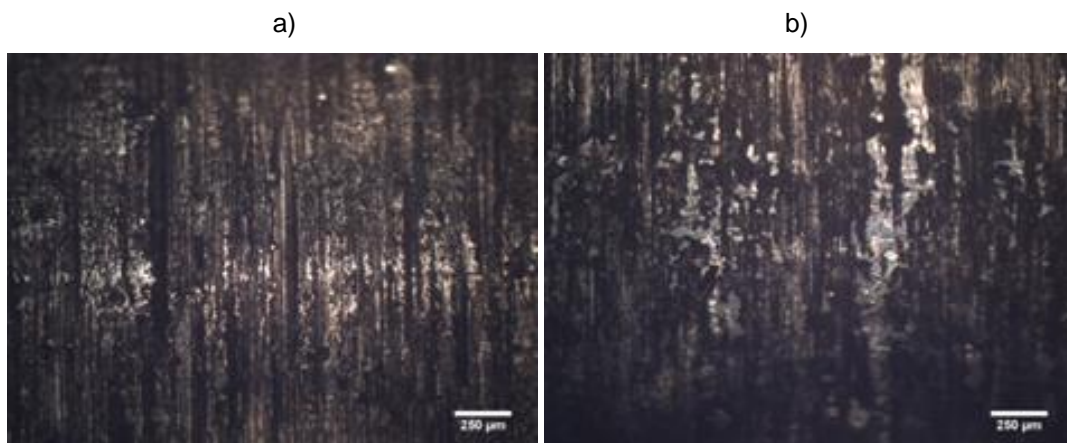
Figure 3.20 Wear tracks of untreated 15-5PH (a) and ref. #275HC1 (b), after the tribology tests at 5N and 18%RH.

These patterns change with high humidity, 80% RH. In the like on like pair, the ECR remains low, while the CoF keeps rising. In the case of the #275HC1 against 15-5PH pair, there is an initial regime, like the one at low humidity, i.e. high but steady CoF and low ECR. This is followed by a regime with a slightly larger but still steady CoF and higher and oscillating ECR. This could be linked to the generation of wear debris that gets oxidized and trapped in the hard #275HC1 surface, unlike in the like on like condition. At high humidity conditions the CoF shows lower values than for lower humidity, i.e. close to ~0.7.

Having applied and studied the treatments on cylindrical parts, the steady and relatively high CoF could be valuable in applications where rolling between the parts, but not sliding, is desired. Likewise, monitoring of the ECR could provide information concerning the tribological regime of the parts, e.g. persistent presence of high ECR warning of lower CoFs and thus higher risk of losing rolling conditions.

Therefore, the combination of active screen plasma nitriding with the hollow cathode effect produces thicker nitride layers as compared with conventional plasma nitriding for similar process times.

Besides, when the plasma density is high, the process duration short enough, and the process temperature is kept low, thick nitride layers can still retain good corrosion resistance, as measured by SST. This is linked to the fact that the level of chromium precipitates in some outer regions of the nitrided layer is limited, i.e. enough free chromium is present to form a passivated corrosion protective surface.

Additionally, these surfaces present steady and high CoF. This could be useful, in applications where rolling regimes are preferred in opposition to sliding regimens, e.g. cylindrical rolling wheel systems.

Finally, continuous or periodic monitoring of the ECR can provide insightful information about the system status, evolution and conditions of the tribological regime.

However, it should always consider that both the CoF and the ECR are sensitive to variations in the humidity and contact pressure.

3.4. PLASMA NITRIDING OF THE INNER SURFACES OF AUSTENITIC ALLOYS

3.4.1. PLASMA NITRIDED 316L

As mentioned before, this work has focused on the development of active screen plasma nitriding processes of inner geometries of the widely used AISI 316L austenitic stainless steel, with good tribological properties but preservation of the corrosion resistance. The structure and composition of the nitrided surfaces were studied and corrosion resistance of the inner surfaces assessed. Electro-tribological studies have also been performed, both to confirm the improvement of the tribological performance of the treated samples and to explore the potential of ECR as a monitoring tool.

The ASP nitriding processes were applied on 210mm long AISI 316L stainless steel tubes with different inner diameters (12 mm, 25 mm and 45 mm) and on 50mm diameter discs. The tubes were studied in the as received condition, which presented an initial surface roughness on the inner diameter of Ra 0.24 µm. Discs were grinded to a surface roughness of Ra 0.20 µm.

Active Screen Plasma Nitriding (ASPN) experiments were carried out in the self-built nitriding equipment at the Surface Engineering laboratory in Tecnalia (Figure 2.11). Process temperature was monitored with thermocouples placed into bulk dummy cylinders and into tubes with the same inner diameter of the samples, to learn about the chamber temperature and the temperature of the tubes along the plasma processes, to assess the occurrence and intensity of the hollow cathode effect and study their effect in the resulting nitride surfaces.

Before nitriding, all the samples were ultrasonically cleaned sequentially in acetone and ethanol bath (>10 min.) and air-dried. Then an Ar/H$_2$ plasma etching was carried out at 230-250ºC (temperatures in this section refer to measurements in the bulk dummy cylinder unless is stated otherwise). Subsequently, the nitriding process was performed in a nitrogen–hydrogen atmosphere under a pressure of 200±30 Pa. The bias voltage applied to the

samples was kept at 580V on all the processes. Process durations, gas mixtures and temperatures are detailed in Table 3-2.

Table 3-2. Nitriding plasma process parameters and resulting nitride layer thickness and surface roughness.

Ref.	Gases N_2:H_2 (%)	Duration (h)	T_{bulk} (ºC)	(µm) Flat	TØ25 (ºC)	(µm) Ø25 Out/in	TØ45 (ºC)	(µm) Ø45 Out/in	Ra (µm)
S#350/5	25:75	5	350	*3.6*	470	*47/55*	395	*6/6*	*0.24±0.02*
S#350/10	25:75	10	350				395	*13/15*	*0.25±0.03*
S#350/25	25:75	25	350	*7*			395	*28/34*	*0.31±0.03*
13#350/10	13:87	10	350		430		410	*10.5±2.5 /12.5±4.5*	-
100#350/5	100:0	5	350		385		370	*0/12*	*0.30±0.03*
M#350/10	25:75 0:100	1.25x4 1.25x4 Total 10	350		490		435	*15±2/ 20.5±7.5*	-
S#450/5	25:75	5	450		505	*36/65*	510	*38/39*	*0.32±0.04*

NOTE: Process temperatures: measured in the bulk dummy cylinder (T_{bulk}), a tube with an inner diameter of 25mm (TØ25) and 45mm (TØ45). Along the process, these temperatures oscillated in the ±5ºC range of the indicated temperature.

Thickness: maxima corresponds to the centre of the tube and the minima to the edges.

M#350/10*: variation in the gas mix every 1.25 hour during the process: 25:75 N_2:H_2 (%) for 1.25h, followed by 0:100 N_2:H_2 (%) for 1.25h, 25:75 for 1.25h, 0:100 for 1.25h, 25:75 for 1.25h, 0:100 for 1.25h, 25:75 for 1.25h, and finally 0:100 for 1.25h.

Treated tubes were cut in two halves longitudinally. In one of the halves, X-Ray Diffraction (XRD) surface analyses were performed and cross-sections of each sample were prepared, polished and chemically etched (Beraha) to study the nitride layers.

The nitride layer thicknesses at the inner and outer diameter of the tubes and in the flat samples are shown at Table 3-2. Thickness along the tube was homogeneous, other than in

ref. 13#350/10 and M#350/10. In these cases, the nitride layer thickness fell from 17µm and 28 µm, in the inner diameter at the tube center, to 8µm and 13µm respectively at the extremes of the tubes. This might be related to the non-homogeneity of the plasma with hydrogen rich atmospheres in configurations such as the ones studied.

The effect of the hollow cathode (Figure 3.21) in the effective process temperature is critical, and geometry dependent, as seen in the previous section. In the case of a 350ºC typical stainless steel treatment temperature (as measured in the bulk dummy cylinder) with a 25:75 N_2 to H_2 ratio, the effective temperature increased in 45ºC and 120ºC in the 45mm and 25mm tubes respectively. This effect changed with the geometry and the hydrogen content in the plasma gas mixture, e.g. 395ºC with a 25:75 N_2 to H_2 ratio, raised to 410ºC with a 13:87 N_2 to H_2 ratio, and to 435ºC with 100% H_2, in the 45mm diameter tubes, but decreased to 370ºC with 100% N_2. 470ºC also rises to 490ºC with 100% H_2, in the 25mm diameter tubes, but decreased to 430ºC and 385ºC with a 13:87 N_2 to H_2 ratio and with 100% N_2 respectively (Table 3-2).
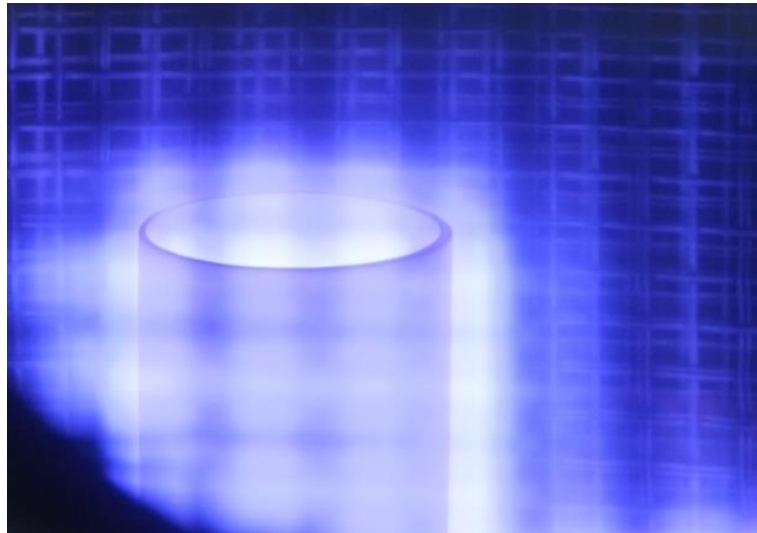
Figure 3.21. Hollow cathode effect on a 45mm tube.

The resulting surfaces were very different for the same process, e.g. ref. S#350/25 (Figure 3.22, right) depending on the sample geometry. The flat sample (Figure 3.22, right) presented a nitride layer thickness of 7µm. This thickness was relatively similar to that measured by Li et al. (10µm) albeit with higher process temperature (420ºC) but shorter treatment time (20h) (Li and Bell 2004). On the other hand, the inner and outer surfaces of a 45mm tube presented a nitride layer thickness of 34 and 28 µm respectively. The consequences of the hollow cathode effect were crystal clear. The hollow cathode effect caused the part temperature to rise from 350ºC in the flat sample to 395ºC, originating a far thicker nitride layer, 28µm vs. 7µm. Furthermore, the more intense plasma present in the inner volume of the tube made the nitride layer to grow even thicker, to 34 µm. Actually, there were differences not only in the nitride layer thickness, but also in the composition, as revealed by the different degree of etching in the outer and inner diameter (Figure 3.22, left). Both the process temperature and plasma density due to the hollow cathode had a remarkable effect in the nitride layer produced.
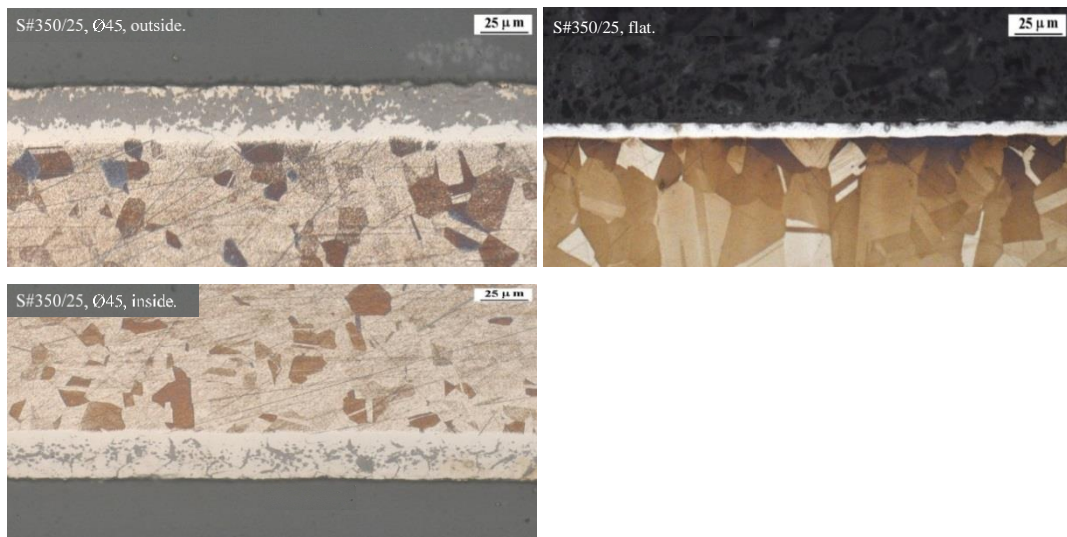
Figure 3.22 Micrographs of the surfaces of ref. S#350/25, outside and inside a 45mm diameter sample (left above and below respectively) and on a flat disc (right).

Variation of the tube diameter, from 45mm to 25mm (Ref. S#350/5), with an increase of the process temperature as measured in the tubes of 45ºC and 120ºC respectively, produced nitride layer thicknesses of 6 and 55µm respectively (Figure 3.23.a). On the other hand, in similarly long 12mm diameter tubes, no plasma was generated and the inner surface was not nitrided.

The increase in the N_2 content in the gas mixture, e.g. from 25% to 100%, refs. S#350/5 and 100#350/5, caused a lesser increase in the temperature at the tubes, 45ºC vs. 20ºC, but nevertheless the nitride layer thickness increased, 6µm to 12µm (Figure 3.23.a and b, left). Therefore, there was a contradictory effect in the amount of H_2 in the gas mixture, which originated a more intense hollow cathode effect, but a slower growth of the nitride layer.

Decreasing the N_2 content in the gas mixture, e.g. from 25% to 13% and 0%, while rising the H_2 content from 75% to 87% and 100% (refs. S#350/10, 13#350/10 and M#350/10), caused an increasing rise in the temperature at the tubes of 45ºC vs. 60ºC and 85ºC respectively, producing an augmentation in the nitride layer thickness from 15 µm, to 17 µm and 28 µm (Figure 3.23.a and c). Therefore, the optimum gas mixture might vary for each geometry.

The effect of the hollow cathode on the resulting nitride layer thickness was made only more apparent as the plasma treatment process duration increased (S#350/5, S#350/10 and S#350/25; Figure 3.23.a and d; Figure 3.24).

Finally, it should be noted that at higher processing temperatures, e.g. ref. S#350/5 and S#450/5, a relatively lesser temperature increase was observed, and dependent on the tube diameter: rising from 350ºC to 470ºC and 395ºC in the 25mm and 45 mm diameter tubes in the first case, and from 450ºC to 505ºC and 510ºC in the latter. This allowed for a much faster growth of the nitride layer in the larger diameter, i.e. from 6µm to 39µm, and a more modest one in the 25mm diameter tube, i.e. from 55µm to 65µm (Figure 3.23.b right).
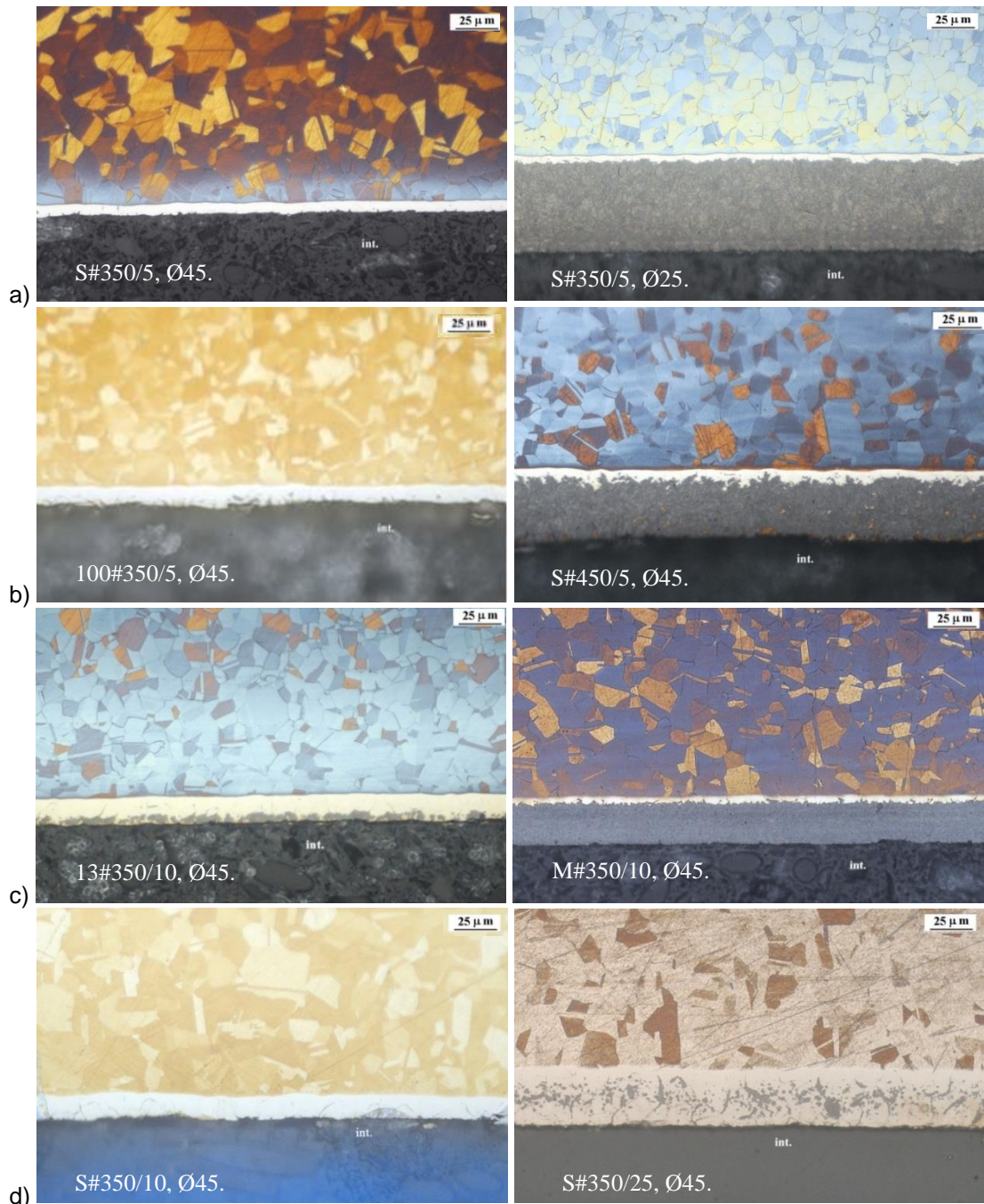
Figure 3.23. Micrographs of the following processes: a) Ref. S#350/5 inside a 45mm (left) and 25mm (right) diameter tubes; b) Ref. 100#350/5 (left); Ref. S#450/5 (right) (inside 45mm tubes); c) Ref. 13#350/10 (left) and M#350/10 (right) (inside 45mm tubes); d) Refs. S#350/10 (left) and S#350/25 (right) (inside 45mm tubes).
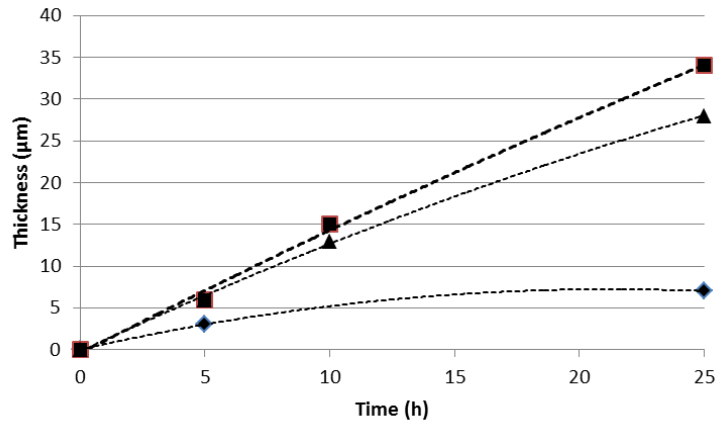
Figure 3.24. Nitride layer thickness at flat (♦), outer tube (▲) and inner tube (■) surfaces of 45mm diameter tubes vs. plasma process duration, corresponding to S#350/5, S#350/10 and S#350/25.

As for the surface roughness, the initial on the inner diameter of the tubes did not change in the milder treatment conditions (S#350/5 and S#350/10: Ra 0.24 and 0.25µm respectively as compared with Ra 0.24µm in the control sample), but became rougher in harsher treatment conditions (longer treatment times, S#350/25, 100% nitrogen plasma, 100#350/5, or higher temperature, S#450/5: Ra 0.31, 0.30 and 0.31µm respectively) (Table 3-2). The surface roughness in the flat samples stayed unchanged at Ra 0.20 µm.

Finally, Figure 3.25 shows the XRD spectra of selected treatments and untreated surfaces in 45mm diameter tubes.
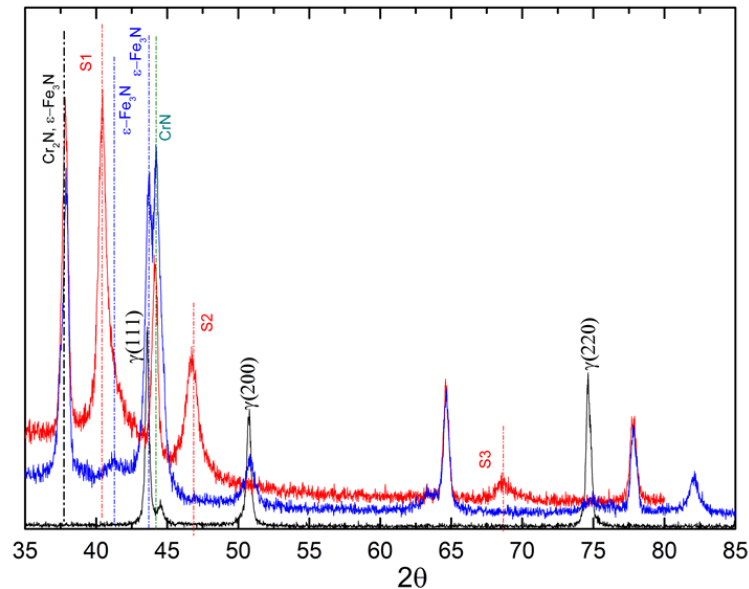
Figure 3.25. XRD spectra of ref. S#350/5 (above), M#350/10(middle) and untreated (below) surfaces in 45mm diameter tubes.

3.4.2. ELECTRO-TRIBOLOGICAL AND ENVIRONMENTAL STUDIES OF PLASMA NITRIDED 316L.

Environmental tests.

Treated tubes were cut in two halves longitudinally. In one of the halves, X-Ray Diffraction (XRD) surface analyses were performed and cross-sections of each sample were prepared, polished and chemically etched (Beraha) to study the nitride layers. In addition, the corrosion resistance was studied on SST in the other half tubes.

Concerning the corrosion resistance of the inner surfaces, the performance varied remarkably. Some surfaces were totally covered by red rust by 24h, while others were rust free after 1000h (Figure 3.26). Ref. S#350/5 was remarkable in this aspect, as the 25mm diameter sample showed very low corrosion resistance, while that of the 45mm sample went beyond 1000h (Figure 3.26 a and b). Li et al. have actually reported recently, albeit in a different alloy (AISI 304) and configuration, that high temperature plasma nitriding for a short treatment time (0.5

h) with hollow cathode discharge can produce a phase layer without precipitation of chromium nitride, leading to the preservation of the corrosion resistance (Li, et al. 2014). The same mechanism could be at play here.

XRD spectra of references S#350/5 and M#350/10 (Figure 3.26.g), showed that actually the amount of precipitates present in the first were much lower than in the latter (Figure 3.25).
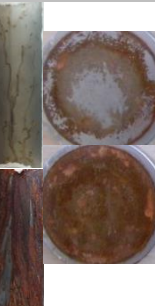
a	b		c	d		e	f	g	h	i
	S#350/5		S#350/10	S#350/25		S#450/5		M#350/10	100#350/10	13#350/10
Ø45	Ø25	flat	Ø45	Ø45	flat	Ø45	Ø25	Ø45	Ø45	Ø45
24h /312h	24h	24h	4h / 168h	4h / 168h	4h / 24h	24h	24h	24h	24h / 168h	24 / 120h

Figure 3.26. Aspect of the inner surface of the tubes and flat samples at the SST test.

This contrasting performance of the different geometries repeated at ref. S#450/5 (Figure 3.26. e and f). On the other hand, there was a basic correlation between the nitride layer thickness and the corrosion resistance, ref. S#350/5 with 6µm presenting the best performance (Figure 3.26. a). Actually, extending the duration of the processes from 5h to 10h and 25h, caused a reduction in the corrosion resistance, with some signs of red rust already as early as at 4h of SST in the latter case (Figure 3.26. a, c and d).

Decreasing the N_2 content in the gas mixture was also detrimental for the corrosion resistance, i.e. ref 13#350/10 with 13% of N_2 and 410ºC tube temperature presented a big proportion of the inner surface covered by red rust at 24h of SST (Figure 3.26. i), while ref. S#350/10 with 25% of N_2 and 395ºC tube temperature was unscathed at 24h of SST and showed little

corrosion spots at 168h of SST (Figure 3.26. c). In both cases, they had quite similar nitride layer thicknesses at the center of the tube: 17μm and 15μm respectively. On the other hand, at the extremes of the tube, where ref 13#350/10 presented a thinner thickness, 8μm, the corrosion resistance was better than in the tube center. Mingolo et al. have also reported that more chromium nitride precipitates happen at lower N_2 contents (75:25 N_2:H_2 vs. 25:75 N_2:H_2) during conventional plasma nitriding of AISI 316L (400ºC; 12h) (Mingolo, Tschiptschin and Pinedo 2006).

It is also worth mentioning that those surfaces that showed a darker aspect in the metallographic preparations after etching in Figure 3.23 (S#350/5 in 25mm; Ref. S#450/5 and M#350/10 in 45 mm tubes), have also shown by far the worse corrosion resistance, indicating a massive precipitation of chromium nitrides (Figure 3.26. b, e and g).

Electro-Tribology studies.

Reliable tribology testing on the inner surface of the tubes is complex. An alternative approach consists on looking at a different though related parameter, i.e. the Electrical Contact Resistance (ECR). While monitoring the CoF in a geometry such as that of the inner tube is complicated, especially on site, monitoring the ECR is much easier, and feasible in many geometries and applications, where often the components are, part of the time, on stand-by or getting refurbished. Thus, in this work, electro – tribology studies were performed on flat samples, to investigate if the ECR could be related to the performance of the surfaces (Figure 3.27).

The electro-tribology tests were performed on a pin on disc configuration against WC-Co balls at 1N, 50% humidity and room temperature, at 0.3 m/s, with the evolution of both the Coefficient of Friction (CoF) and the Electrical Contact Resistance (ECR) registered.
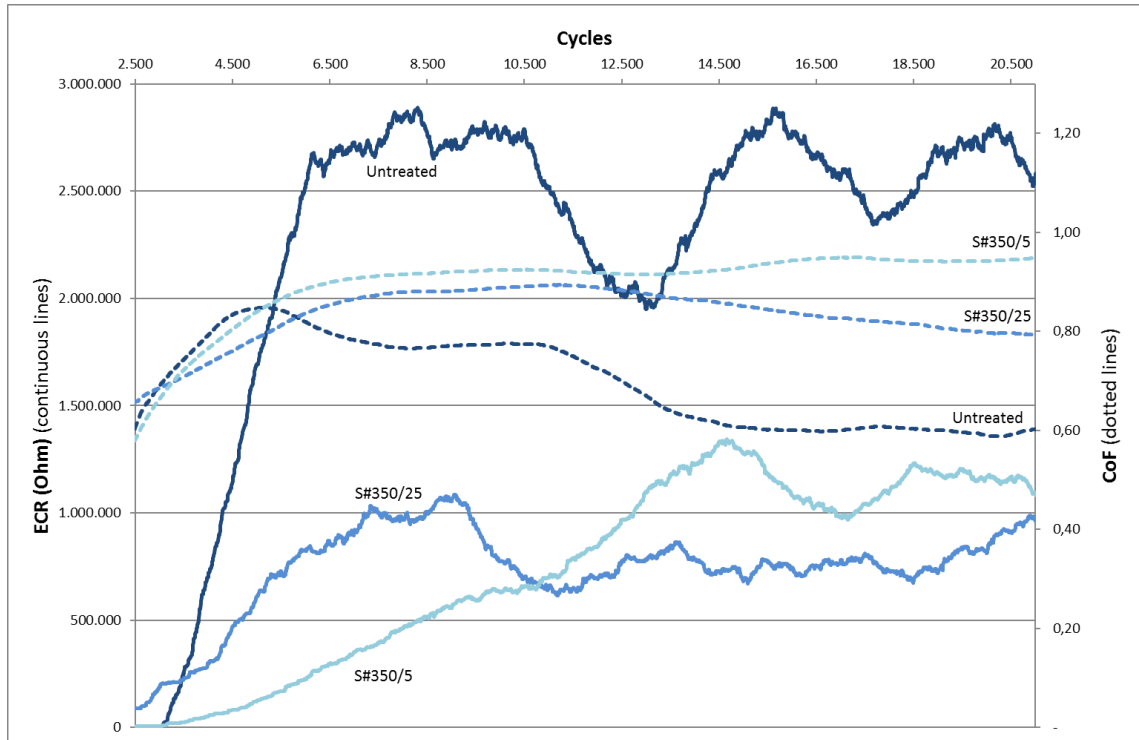
Figure 3.27. Evolution of the ECR (left scale; continuous lines) and CoF (right scale; dotted lines) of an untreated 316L sample, an active screen plasma nitride 316L sample showing good corrosion resistance (>720h SST; ref. S#350/5), and an active screen plasma nitride 316L sample showing very poor corrosion resistance (<24h SST; ref. S#350/25).

In all cases the evolution of the ECR showed an initial increase associated with the formation of surface oxides (Figure 3.28). Then, after it peaked, an oscillating ECR followed, where the dominance of oxide formation and its removal due to wear varied alternatively. This was coupled in some cases with the variation in the contact surface due to the transfer of material as adhesive wear occurred. Two references, S#350/5 and S#350/25, showing very different corrosion resistance were studied, together with the untreated material as control surface.
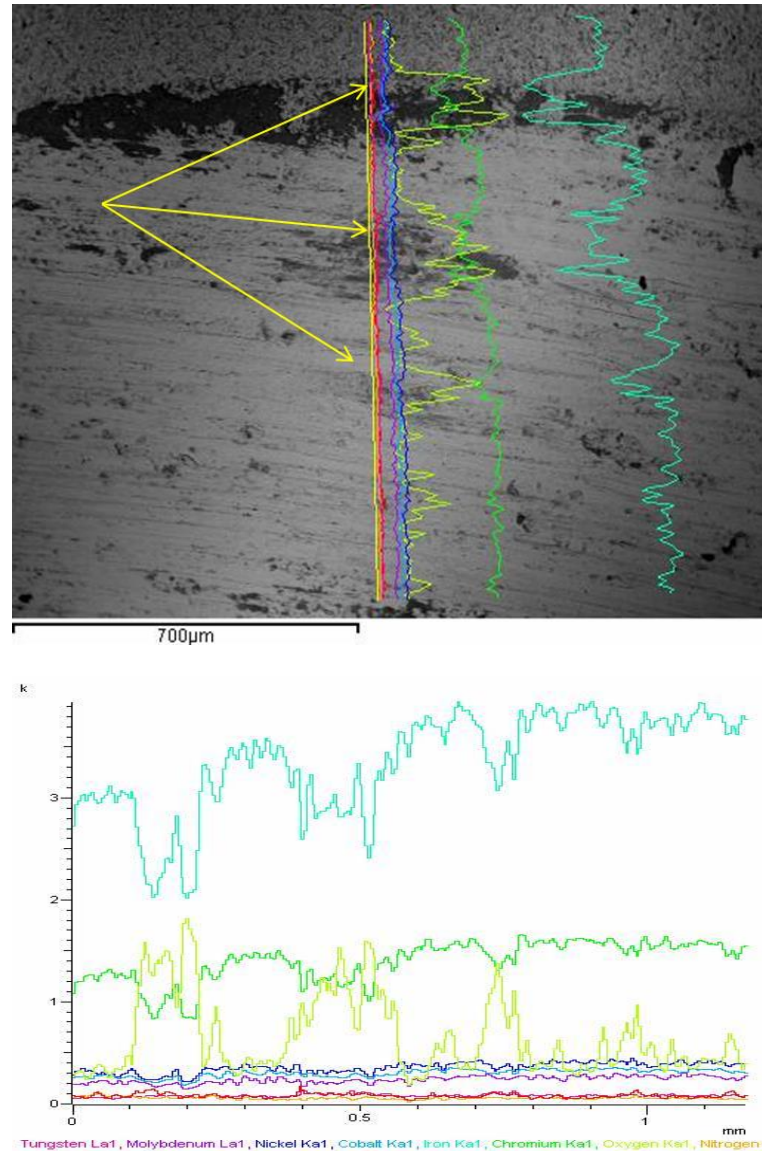
Figure 3.28. SEM and EDS wear track analysis (untreated 316L).

Initially, ref. S#350/25 showed a slightly larger ECR than the S#350/5 and untreated samples, possibly due to a large presence of precipitated nitrides at the surface and an initial larger surface roughness (Ra 0.31±0.03μm vs.0.24±0.02μm and 0.20μm respectively). The untreated AISI316L surface showed the largest ECR increase rate, followed by ref. S#350/25.

This might be due to the fact that oxides were more easily formed on the untreated AISI316L surface. At some point nevertheless the ever-thicker oxide layer broke down and adhesive wear followed. Both phenomena could be observed in Figure 3.29, as black spots (oxides) and spread out grey areas (adhesive wear). The adhesive wear was reflected as an oscillating ECR, as material was constantly pull out and transferred back to the surface (lowering ECR values), which was then oxidized (rising ECR values as the oxide layer thickens). This was coupled with a less stable effective contact area, which also caused the ECR to oscillate. On the other hand, the presence of more abundant oxide caused the CoF to be smaller than in the case of the nitrided samples.

Ref. S#350/25 showed quite a similar behavior, but larger CoF, lower ECR (though the starting ERC was larger, due to a smaller effective contact area caused by a larger surface roughness), and less pronounced oscillations in the ECR after it peaked. Overall lower ECR values were linked to formation of less oxide at the sliding surfaces, as there was less free metallic Cr and Fe, due to the precipitation of nitrides in the treatment. Additionally, the hardening effect of the nitriding process limited the adhesive wear.

Finally, ref. S#350/5 showed one remarkable difference. The ECR kept rising, after the CoF had peaked. This signaled the presence of a more stable oxide layer, which would also be in accordance with the better corrosion resistance offered by this surface. Nonetheless, the oxide layer kept thickening and peaked at a higher value than ref. S#350/25, though after approximately twice the number of cycles.
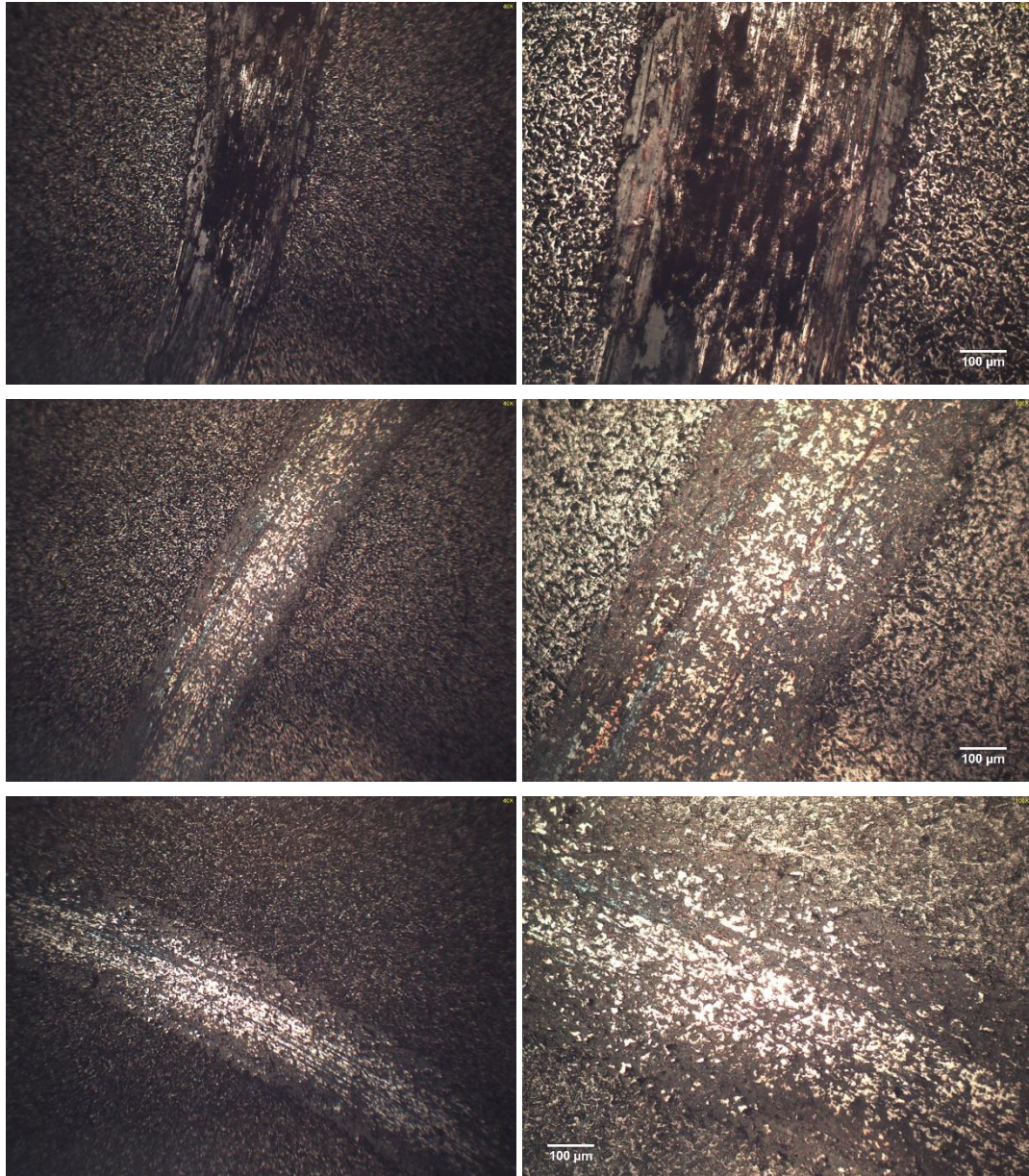
Figure 3.29. Wear tracks of ref. untreated, above; S#350/5, middle; and S#350/25, below.

ERC values might be of value to monitor the status of components in service, as peaking ERC values indicate that the oxide layer is been worn out and corrosion might ensue. This could

be used to stablish a component maintenance, refurbishing or replacement plan, minimizing service disruptions, costs, etc. Besides, together with other surface characterization and testing results, ERC and equivalent electric circuit information could provide a more detailed understanding of the degradation mechanisms occurring at the surface, supporting the development and optimization of the surface treatment processes.

To sum up, the active screen plasma nitriding of stainless steel in certain geometries can be associated with hollow cathode effects. This might be beneficial or detrimental for the nitriding of the inner surfaces of stainless steel tubes with preservation of a good corrosion resistance.

This hollow cathode has two related main effects: denser plasma and a higher part temperature. The positive or negative effect conditions on the corrosion resistance depends on the plasma processing, which must be optimized for each geometry. E.g. it has been shown that similar processing conditions (outside the tube inner volume) have produced very different surfaces and corrosion resistance results in 25mm and 45mm diameter tubes.

Additionally, monitoring of the ECR in applications with tribological service conditions might be a good indicator and predictor with respect to the surface performance. This can be potentially useful in monitoring the surface status of devices in service, whose operative surface is in the inner diameter, which often does not present an easy access.

4. CONDUCTIVE AND DIELECTRIC PVD COATINGS

4.1. PROBLEM STATEMENT.

In a variety of electrical devices sliding contacts play a key role. This is the case for instance in electrical and hybrid transport vehicles, electronics, current collectors in rail systems or transformers in smart grids (Grill 1999) (Grill 1999) (Hombo, et al. 2013) (He, Lee and Yeo 2015) (Song and Schinow 2015) (He, Manory and Sinkis 2000), (Bouchoucha, Chekroud and Paulmier 2004) (Argibay, et al. 2013).

In some cases, contact materials must have a low electrical contact resistance while in others they should present a dielectric, very high ECR, non-conductive, property. Besides the electrical properties, the contact materials should also present a low coefficient of friction and wear rates, and high degradation resistance to the surrounding media.

Electrically conductive PVD coatings.

In the case of the **electrically conductive** materials, silver has been the material of choice in many of these applications, typically in the form of a coating due to their cost (Braunović, Konchits and Myshkin 2006) (Song and Schinow 2015) . Nevertheless, although silver presents a low electrical resistance, its tribological properties are poor, specially in terms of wear resistance. Silver is also sensitive to the surrounding media. The tarnishing process of silver, which affects negatively the electrical conductivity, depends on many factors, such as pH, humidity, temperature, exposure time, nature and concentrations of pollutants. Despite a relatively low tendency to oxidation, silver is prone to react with sulfur, which leads to the degradation of its surface properties (Braunović, Konchits and Myshkin 2006) (Graedel 1992) (Ben Amor, et al. 2014) (Rudolphi and Jacobson 1997). Natural sulfur compounds contribute to the intrinsic oxidation stability of mineral insulating oils, and although a higher refining of the insulating oil would remove sulfur to a high extent, it would also leave the oil without protection against oxidation (Holt, et al. 2013) (Minzari, et al. 2011). Moreover, silver sulphidation is further accelerated by presence of chlorine in hydrogen sulphide gas (Braunović, Konchits and Myshkin 2006) (Fiaud and Guinement 1986). Both shortcomings, poor tribology and limited degradation resistance, compromise the long term operational performance of silver coatings, a serious drawback in electrical devices subjected to many sliding cycles operating in challenging industrial environments (Braunović, Konchits and Myshkin 2006).

Different approaches have been explored to overcome these limitations. One consists on designing composite coatings incorporating dispersed particles or phases in a metallic matrix that would provide improved tribological properties and degradation resistance (Rigou, et al. 2012) (Grandin and Wiklund 2013) (André, et al. 2011) (Nedfors, et al. 2015) (Nygren, et al. 2014), (Chen, et al. 1997). Another consists on incorporating alloying elements into silver with the very same aim (Braunović, Konchits and Myshkin 2006), or using silver as the coating dopant (Takeno, et al. 2013). One such element is aluminum, which presents low electrical resistance, high degradation resistance to a variety of environments and is relatively inexpensive.

The tribology of Ag-Al alloys has recently been studied on both bulk samples and coatings deposited by magnetron sputtering (Mao, Taher and Kryshtal, et al. 2016) (Mao, Taher and Berastegui, et al. 2018). When Al is added to Ag a series of different phases are formed depending on the Al composition. One of these alloys is a disordered solid solution phase with a hexagonal close-packed (HCP) structure. The HCP phase starts to form at about 30 at% Al in bulk samples, but already at about 13-15 at% Al in magnetron sputtered coatings (Mao, Taher and Berastegui, et al. 2018). The presence of the HCP phase leads to a reduction of the friction coefficient and wear rate, suggesting a potential use of Ag-Al alloys in sliding electric contacts. This is due to the formation of easy-shearing planes in the hexagonal structure.

However, Al is prone to oxidation, which is detrimental for the electric properties (Mao, Taher and Berastegui, et al. 2018). Actually, AgAl alloys in a conductive environment will make up a galvanic couple, and cause for Al to oxidize (i.e. galvanic corrosion) (Acevedo-Hurtado, et al. 2008). The extent of this corrosion will be typically affected by the environment, the difference in the alloy potentials, the ratio and distance of the cathodic to the anodic areas. Although Al oxidation is a problem in ambient atmosphere, there are applications where the presence of oxygen or moisture is limited. One such example is electric contacts under an insulating oil, where the oil can protect the HCP alloy from oxidation.

Dielectric PVD coatings.

In the case of the dielectric sliding materials and among the solid lubricant coatings, one of the most promising alternative is diamond like carbon (DLC). The family of DLC coatings exhibits a wide variety of tribo mechanical and electrical properties, depending among others on their composition and structure (Vetter 2014).

The electrical properties of DLC coatings vary from that of a semimetal to that of an insulator (Hombo, et al. 2013) (Grandin and Wiklund 2018).

Moreover, it has been demonstrated multiple times that dielectric hard DLC coatings can be obtained with good tribological properties (Bewilogua, et al. 2009) (Field, Jarratt and Teer 2004) (Oñate, et al. 2001) (Brizuela, et al. 2002). Low steady friction

coefficients of DLC coatings have been related to the formation of a carbon-rich transfer layers on the counterface, caused by friction induced annealing by thermal and strain effects generated during sliding. It has also been proposed that bonding into the DLC surface of oxygen and hydrogen reduces the possibility for the formation of bonds between the DLC coating and its counterface, originating low friction forces. (Grill 1997) (Erdemir 2004) (Liu, Erdemir and Meletis 1996) (Liu, Erdemir and Meletis 1996)

However, aspects such as the internal stresses of the coatings or the relative humidity of the working environments are known to play an important role in their tribology performance (Liu, Erdemir and Meletis 1996) (Luo, Fridrici and Kapsa 2011) (Liu, Erdemir and Meletis 1997).

Electrical Contact Resistance.

Monitoring the coating status and evolution in either case of electrically conductive or dielectric coatings, can provide a valuable tool regarding the dependability of coatings/systems in critical applications and/or difficult to access locations (Vakis, et al. 2018) (Clarke, et al. 2016) (Bucca and Collina 2015). Along these lines, monitoring the degradation of the coatings in sliding conditions, due to wear or other coating degradation mechanisms, can be helpful in the framework of defining a predictive approach of a dependable coating operating life (Simonovic and Kalin 2017).

The coating monitoring can also be valuable in the framework of coating process development and optimization studies, as coating failure modes can be related to coating deposition process parameters, evolution and degradation of the dielectric properties, testing or operating conditions, etc. (Majdoub, et al. 2013).

Aligned with the previous points, the aim of the study presented in this chapter is to investigate the electro-tribological properties of silver aluminum alloy coatings under insulating oil and in air against Ag counterparts, and DLC coatings at different humidities against Al counterparts. The study focuses on the evolution of the degradation of the CoF and ECR along the coating operative lives. Aluminum is the

selected counterpart in the case of the DLC coatings, as one of the most used material in electric and electronic applications together with copper, and because typically presents a challenging tribology behavior. In the case of AgAl coatings, Ag coatings have been selected as the counterparts, being the coating of choice nowadays in many inner transformer connectors.

Besides, the study also includes, in the case of the AgAl coatings, the investigation of the degradation of such alloys in different sulfur and chloride rich environments.

Finally, the use of electro tribological data as a monitoring tool of the coating operative lives is assessed.

4.2. SILVER-ALUMINUM PVD COATINGS.

4.2.1. THE SILVER-ALUMINUM COATINGS.

The PVD coatings were deposited by means of DC magnetron sputtering from Ag and Al metal targets at 1.3 10^{-1} Pa Ar pressure and room temperature. No bias was applied during the sputtering process. The base pressure at the vacuum chamber was 10^{-8} Pa and the target to substrate distance 15 cm unless indicated otherwise, with the targets oriented at an angle of 39° from the substrate normal.

The coating composition was controlled by increasing the power at the Al target to obtain the film with the higher at% Al content and shifting the position of the substrate closer to the Ag target (by 10.5 mm) to obtain the films with the intermediate at% Al.

The substrates were RF etched clean for 20 minutes prior to the coating deposition. The RF etching conditions were: 13 mbar Ar with a 10 sccm gas flow at 310V (42W). Details of the coating deposition parameters are depicted in

Table 4-1.

Table 4-1. Coating deposition parameters.

Reference	Power (W)		Current (A)	
	Ag	Al	Ag	Al
Ag▼	75	-	0.26	-
Ag80Al20	50	45	0.17	0.16
Ag78Al22T	50	120	0.17	0.40
Ag78Al22	50	120	0.17	0.40
Ag63Al37	50	120	0.17	0.40

*: Sample position closer to the Ag target by 10.5 mm.

One of the coatings with a nominal 22 at% Al composition was deposited at 275°C, to produce the cubic-µ phase (Ref. Ag78Al22T). The deposition was carried out for 2 hours while rotating the substrate and resulted in 1.5 µm thick films.

The coating surface composition, surface finishing and thickness measured in the coating cross sections are detailed in Table 4-2. The coating thickness increased with the Al content for the same process duration. Cross sections of the coatings (Figure 4.1 to Figure 4.5), showed that the coating morphology is not homogeneous along the thickness.

The elemental chemical composition of the coatings detailed in Table 4-2 represent an average composition of the coating, as the EDS spectra showed some signal of the Ni interlayer below the AgAl coatings. Cross sectional EDS analysis presented a trend towards a higher Al content in the outer surface of the coating, as compared with the region close to the interface.

Addition of Al to the coating caused the surface roughness to increase (as compared to the Ag coating; Table 4-2), especially in the case of the coating deposited at high temperature in ref. Ag78Al22T.

Table 4-2. Surface roughness (Ra), coating thickness (μm) and elemental chemical composition (at %) as determined by EDS.

Reference	Ra (nm)	Thickness (μm)	Composition Ag/Al (at %)
Ag▼	11±2	1.8	100.0/0.0
Ag80Al20	20±7	1.8	80.3/19.7
Ag78Al22T	39±12	2.2	78.4/21.6
Ag78Al22	13±4	2.2	78.0/22.0
Ag63Al37	25±14	3.0	62.8/37.2

Ref. Ag, unlike in the alloyed samples, presented a uniform morphology and composition along the coating cross section (Figure 4.1). On the other hand, ref. Ag80Al20 presented a denser morphology in the deeper levels of the coating (Figure 4.2). The EDS profile shows that Al content keeps increasing along the coating thickness towards the outer surface, and that the later and outer section of the coating presents a larger oxygen content and a different morphology.

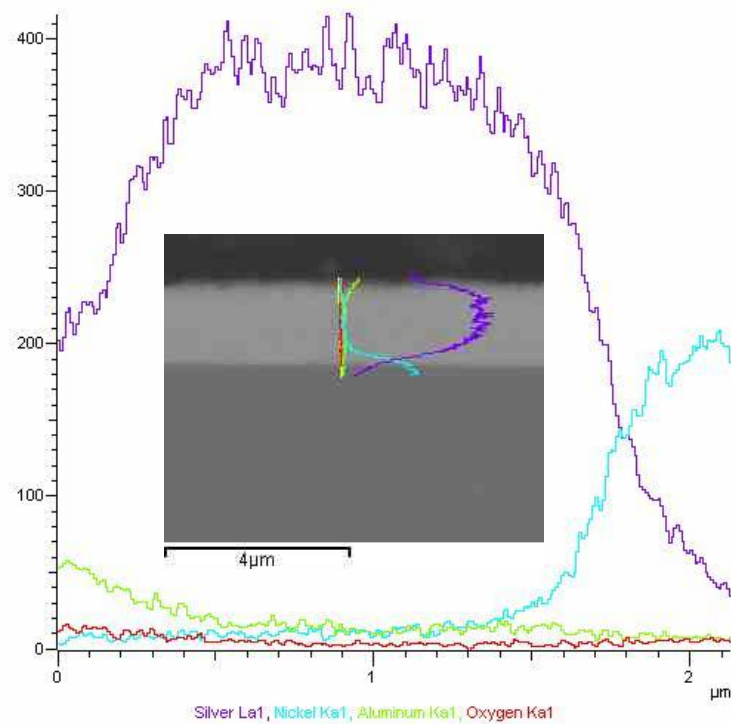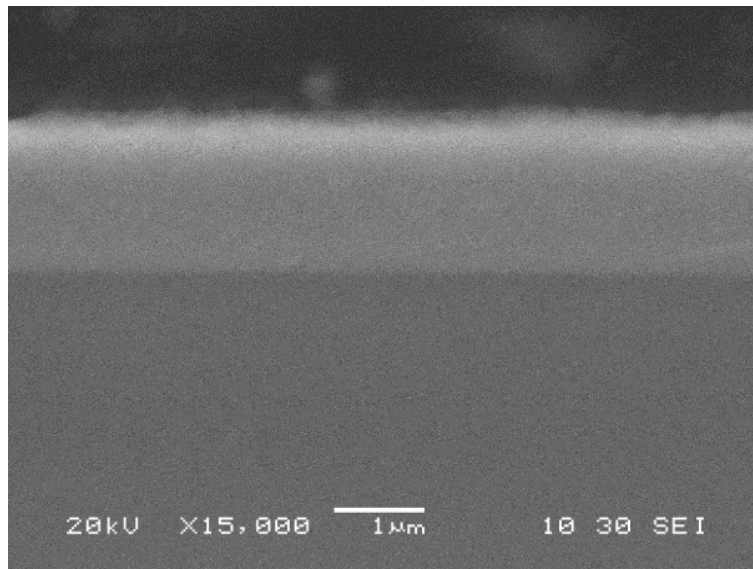Silver La1, Nickel Ka1, Aluminum Ka1, Oxygen Ka1

Figure 4.1. SEM image and EDS profile analyses of the cross-section of the coating ref. Ag.
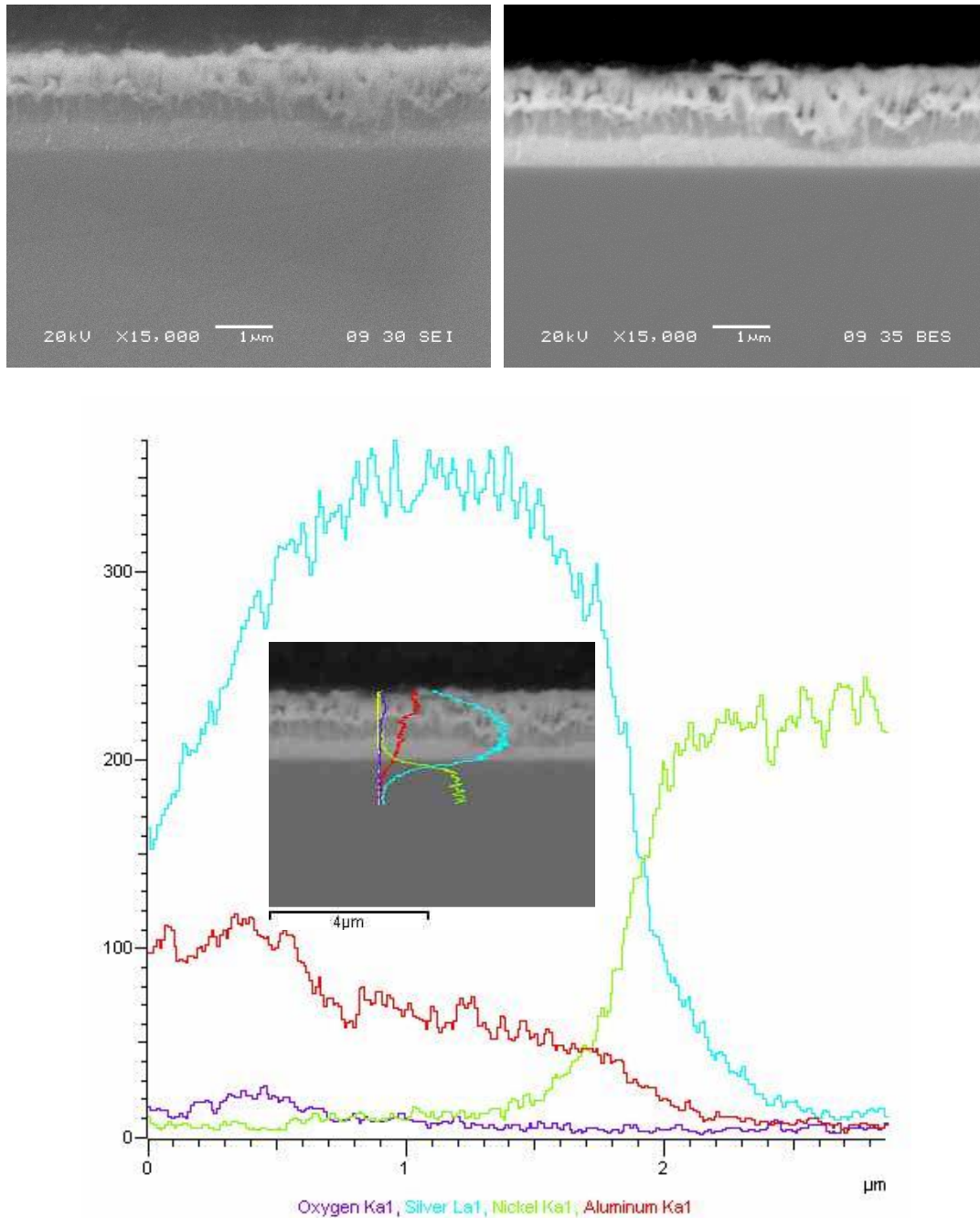
Figure 4.2. SEM (secondary electron and backscattering) images and EDS profile analyses of the cross-section of the coating ref. Ag80Al20.

Both ref. Ag78Al22 and Ag78Al22T were deposited in the same conditions, but for the process temperature. The resulting coating thickness and overall composition resulted similar. That was not the case for the surface roughness, which was much larger in the latter case (Table 4-2). This is apparent in the coating cross section morphology (especially apparent in the BES image), which shows a more porous outer layer (Figure 4.3), with lower Ag and Al content, but more C content, corresponding to the resin where the samples has been embedded during the metallographic preparation.

In ref. Ag78Al22, as was the case in ref. Ag80Ag20, there is an upward trend in the Al and O content towards the outer surface of the coating (Figure 4.4). However, it can be observed in the EDS profile spectra in both ref. Ag78Al22 and Ag78Al22T that there is a thin intermediate region within the coating with a lesser Al (and O) content, and larger Ag content. This is reflected in a more whitish intermediate layer in the corresponding BES images, being Ag a heavier element than Al (and O).

This phenomenon is repeated in ref. Ag63Al37 (Figure 4.5). This might be linked to the fact that the Al target presented initially an aluminum oxide surface layer, that was gradually eliminated by sputtering during the coating deposition process. This made the Al percentage in the coating to increase. Besides, a larger Al content in the coating incorporated more oxygen to the alloy, being Al much more oxygen reactive than Ag. This is reflected in larger oxygen counts in the outer regions of the oxygen profiles of ref. Ag63Al37 (Figure 4.5) as compared with Ag78Al22 and Ag78Al22T (Figure 4.4).

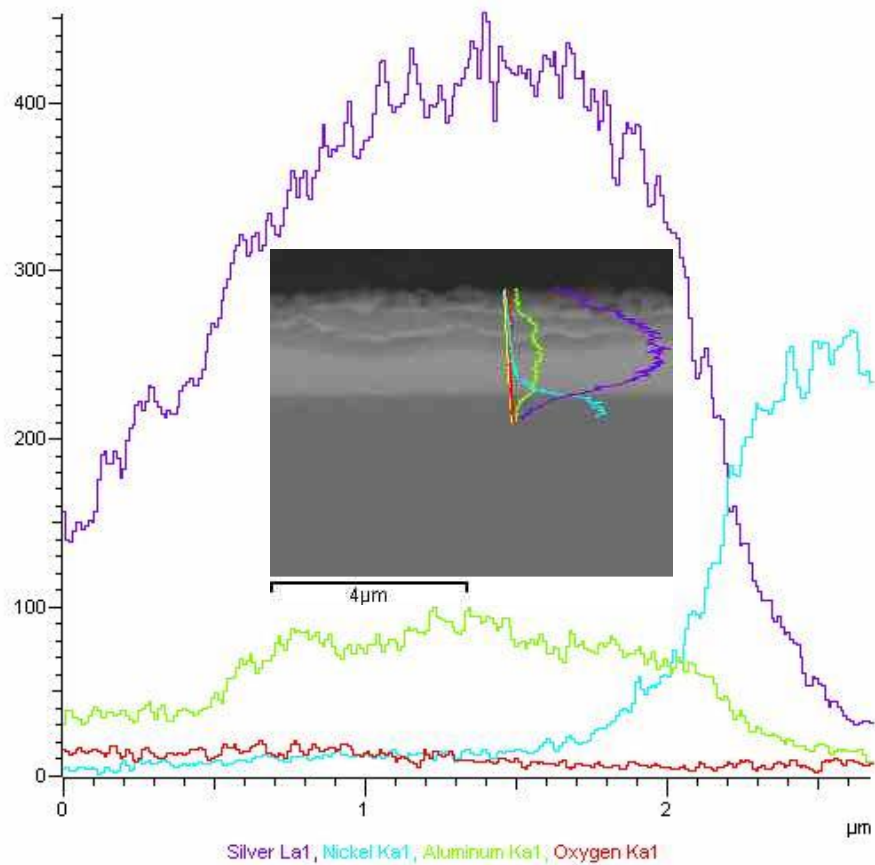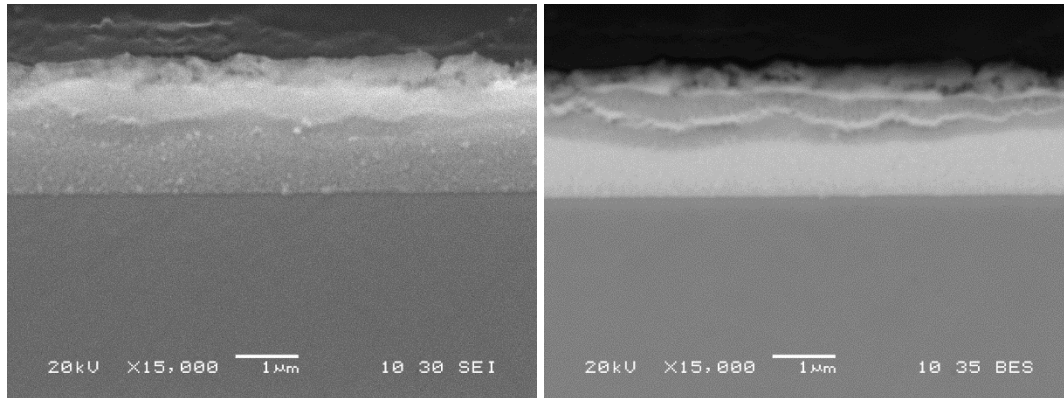Figure 4.3. SEM (secondary electron and backscattering) images of the cross-section of the coatings c) ref. Ag78Al22T.
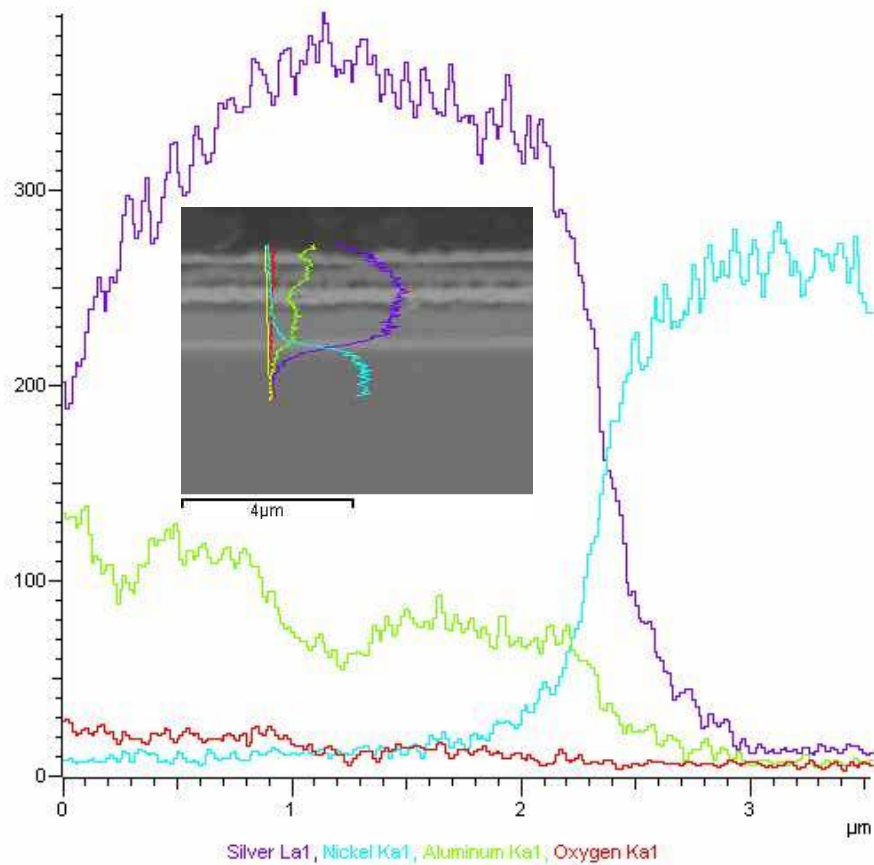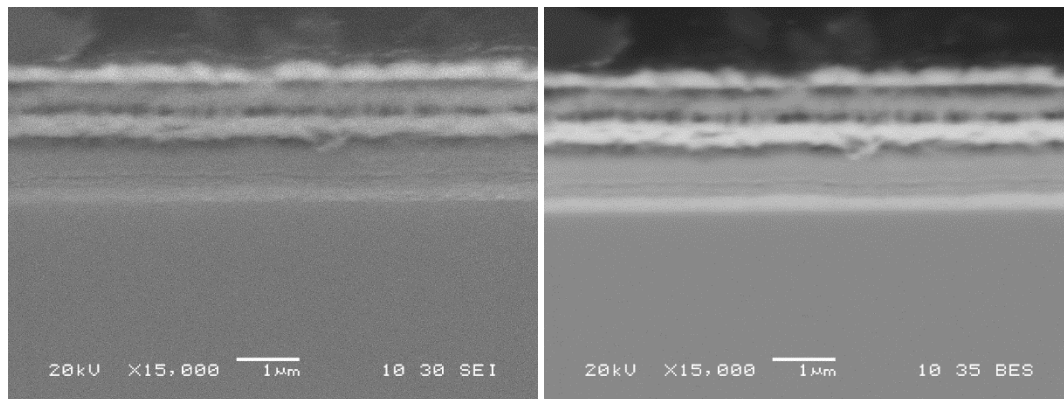
Figure 4.4. SEM (secondary electron and backscattering) images and EDS profile analyses of the cross-section of the coating ref. Ag78Al22.
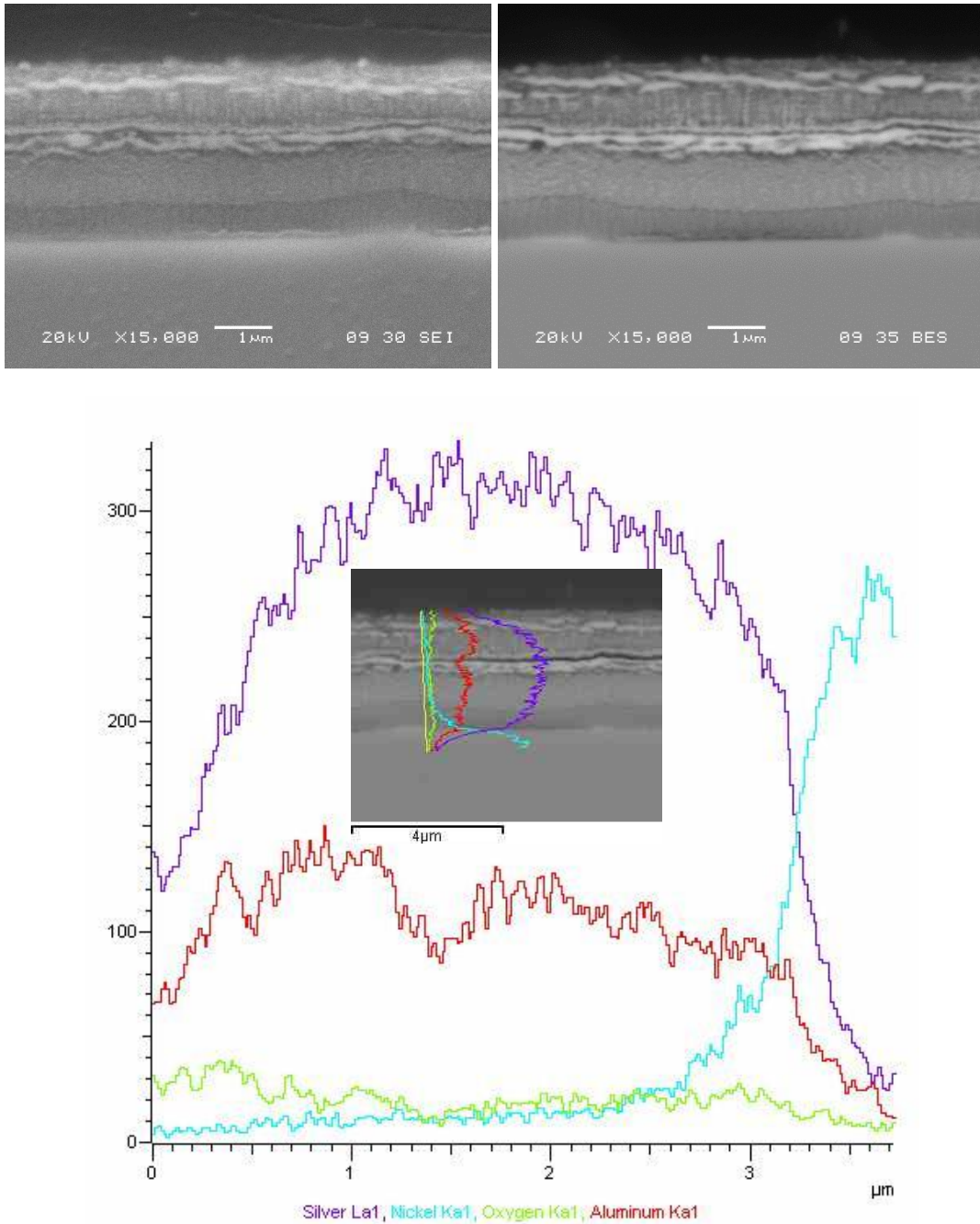
Figure 4.5. SEM (secondary electron and backscattering) images and EDS profile analyses of the cross-section of the coating ref. Ag63Al37.

According to the Ag-Al phase diagram there are four possible phases at room temperature: the Ag-FCC phase, with Al in solid solution; the cubic μ-phase; the HCP-δ phase, with Al in solid solution; and the Al-FCC phase, with Ag in solid solution (McAlister 1987).

Figure 4.6 shows the X-ray diffractograms of the AgAl coated samples studied after annealing (black lines) and in their initial untested condition (red lines), for the samples where a difference was observed. The peak positions for the sharp Cu and broad Ni peaks from the substrates are marked. Ref. Ag showed a strong texture and the (111) Ag peak at 38.1° corresponding to the Ag-FCC phase. References Ag80Al20 and Ag78Al22 presented the Ag-FCC phase before annealing and a mixture of Ag-FCC and μ-phase after annealing. In ref. Ag78Al22T these were transformed into the μ-phase because of the coating deposition at 275ºC. This can be attributed to the metastable non-equilibrium phases originated during the coating deposition, far from the equilibrium phase diagram conditions. The (111) peak from the FCC phase is however very weak in the diffractogram of the Ag78Al22 annealed sample, which suggests that the transformation to the μ-phase might not be complete after 24 hours at 135°C. Finally, ref. Ag63Al37 showed the (002) peak at 39.2° from the hexagonal phase. This all is in line with previous findings (Mao, Taher and Kryshtal, et al. 2016) (Mao, Taher and Berastegui, et al. 2018) (Taher, et al. 2018).

Figure 4.6. X-Ray diffractograms of ref. Ag; Ag80Al20; Ag78Al22; Ag78Al22T; Ag63Al37 (as prepared, red lines, and after 135⁰C annealing, black lines). Vertical lines indicate the position of the strongest peaks from the Ag-FCC and Ag-HCP phase, and the Ni plated Cu substrate. Red dots show the positions of the strongest peaks from the cubic Ag₃Al μ−phase.
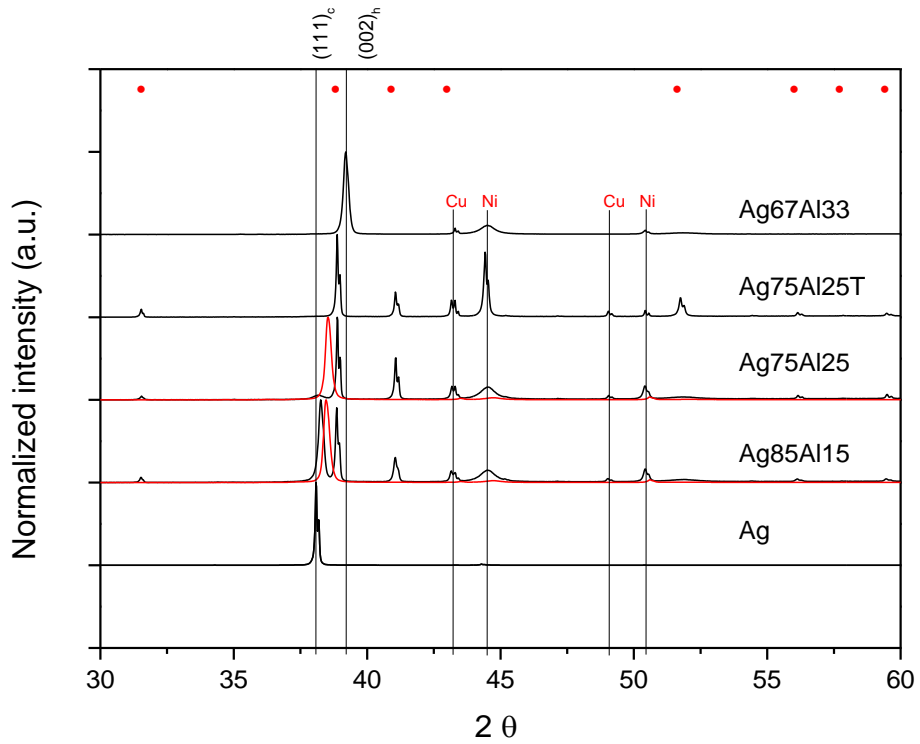
4.2.2. ELECTRO-TRIBOLOGICAL AND ENVIRONMENTAL STUDIES OF THE SILVER ALUMINUM COATINGS.

Electro-Tribology.

The tribological test were performed with a configuration of diminishing track lengths after several cycles (Figure 2.26), so as to allow the quantitative and qualitative study of the evolution of wear. The actual track length for each test cycle, test condition, and coating ref. is detailed in Table 4-3.

Table 4-3. Number of test cycles for each track length, coating, and test condition (in air or under oil). (1 and 2 denote two different tests and wear tracks in the same coated sample).

Track length	Ref. Ag		Ref. Ag80Al20				Ref. Ag78Al22				Ref. Ag78Al22T				Ref. Ag63Al37			
mm	Air	Oil	Air1	Air2	Oil1	Oil2	Air1	Air2	Oil1	Oil2	Air1	Air2	Oil1	Oil2	Air1	Air2	Oil1	Oil2
50	0	0	5	10	10	100	5	10	10	75	10	10	10	75	10	50	10	100
40	2	10	10	20	20	150	10	20	20	100	20	20	20	100	20	75	20	150
30	5	20	15	30	30	200	15	30	30	125	30	30	30	125	30	100	30	200
20			20	40	40	250	20	40	40	150	40	40	40	150	40	125	40	250
10			25	50	50	500	25	50	50	200	50	50	50	200	50	150	50	500

As mentioned before, tests were carried out both under oil and in air. It would typically be expected that the under-oil condition would reduce the tendency of oxide layers to regenerate after wear or thicken if some heating occurred during the tribogical tests. In sliding electrical contacts, this would diminish the risk of formation of less conductive compounds or even insulating layers. Additionally, the degree of local heating would also be decreased because the heat generated in the sliding surfaces might be distributed through diffusion in the oil phase (Grandin and Wiklund 2013).

In preliminary tests, where the coefficient of friction was monitored, a screening of the wear test conditions was performed, to determine those conditions that would allow a comparison between the different coating alloys and pure Ag.

The one test where the Ag based coating remained, in 15 to 40 at% Al-Ag coated samples, at least partially, was performed in the following conditions: reciprocating, 2N, immersed in oil, 0.002m/s, 1000 cycles (Figure 4.7). These test conditions, reciprocating, 2N and 0.002m/s were used all along the tests from this point onwards on the alloyed coatings ref. Ag78Al22, Ag80Al20, Ag63Al37, Ag78Al22T and Ag.

It should be mentioned that the CoF is measured with a load cell, which in reciprocating tests measures both positive and negative friction forces. This is why in CoF evolution graphics of reciprocating tests the CoF sometimes appears as changing from positive to negative values periodically.
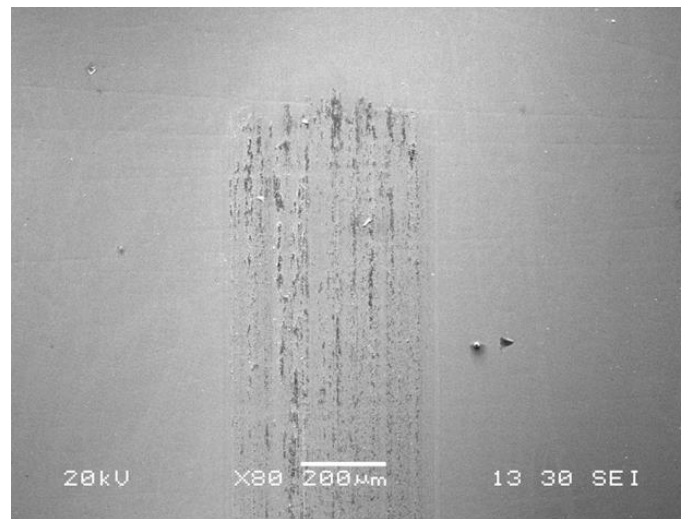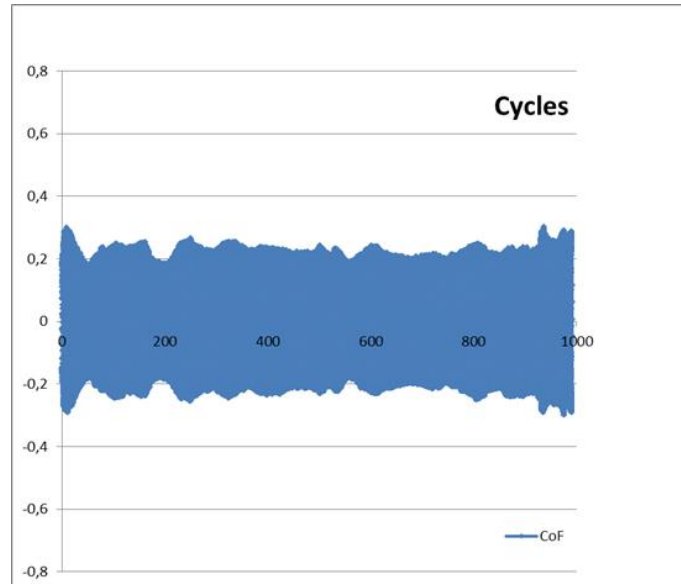
Figure 4.7 CoF and SEM image of wear track on 15 to 40 at% Al sample
(reciprocating, 2N, immersed in oil, 0.002m/s).

In the AgAl alloys studied, both the fact that aluminum is more prone to oxidation than silver, and the presence of different phases, had an effect in the tribological behavior of the coatings.

In the following figures, Figure 4.8 to Figure 4.31, the CoF evolution for each sequential track length is presented (in a different color), together with the aspect of the wear track after the number of cycles corresponding to the same track length.

In the case of the pure silver coating, **ref. Ag**, under oil conditions, the coating was not able to endure even 20 cycles. By cycle 10, plenty of adhesive wear was apparent, and by cycle 20 the Ni layer beneath the Ag coating was visible all along the track (Figure 4.8). The CoF raised to a value of approx. 1, though decreased down to 0.5, probably when the Ag – Ag interface was replaced by the Ni – Ag interface.

In the in air test conditions, the coating endurance was even shorter (Figure 4.9). Actually, by the third test cycle sections of the Ni underlayer were already visible, and the CoF reached a value >1.

Both the wear volume and depth were larger in air (Figure 4.10). The test had to be terminated prematurely because the high wear rate, as compared with the alloyed coating tests presented next.

Figure 4.8. Ref. Ag (2N; 0,002m/s; 10 reads/s), reciprocating test **under oil**, CoF and SEM images of the test tracks CoF and SEM images of the test tracks (downwards, sequentially correspond to the n of cycles in the CoF graphic).

Figure 4.9. Ref. Ag (2N; 0,002m/s; 10 reads/s), reciprocating test **in air**, test A (above) and B (below), CoF and SEM images of the test tracks (left to right, sequentially correspond to the n of cycles in the test B CoF graphic; BES image framed in orange, same spot as the previous SEI image).
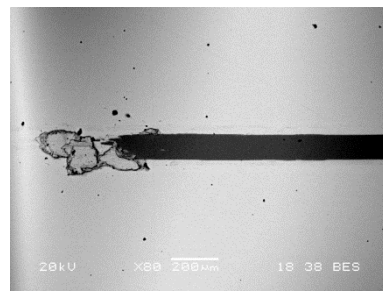
Figure 4.10. Ref. Ag (2N; 0,002m/s; 10 reads/s), reciprocating test **under oil** (thicker line) and **in air** (thinner line), wear and wear track depth evolution.

In the case of coating **ref. 85Al15Ag**, under oil, the CoF (around 0.3) was much lower than for ref. Ag (Figure 4.11 and Figure 4.12). The Ni interlayer was not reached till a larger number of cycles (around 150 cycles, Figure 4.12). Although to a lesser extent that in ref. Ag, still plenty of Ag coating material had been displaced, and there were plenty of adhesive wear signs.

In the in air test conditions, remarkably, the CoF first raised rapidly to around 0.4, but as the test progressed, already by cycle 10 to 15, it has decreased to around 0.2, below the value in the under oil conditions (Figure 4.13 and Figure 4.14). Additionally, the coating material displacement was much less evident than under oil conditions, and there was presence of some groves. On the other hand, the Ni underlayer was reached already by cycle 20, and was very apparent by cycle 50.

This was very apparent in the wear volume and depth evolution (Figure 4.15). While the wear rate in air was a little larger than under oil, the wear depth raised much faster, indicating a narrower wear track, with deeper groves.
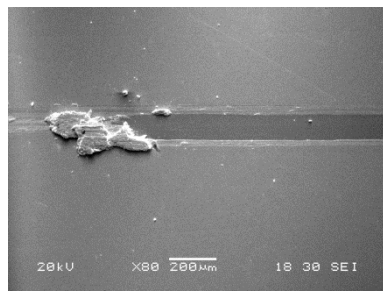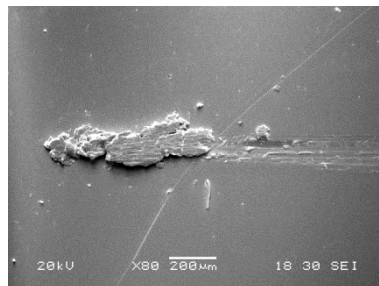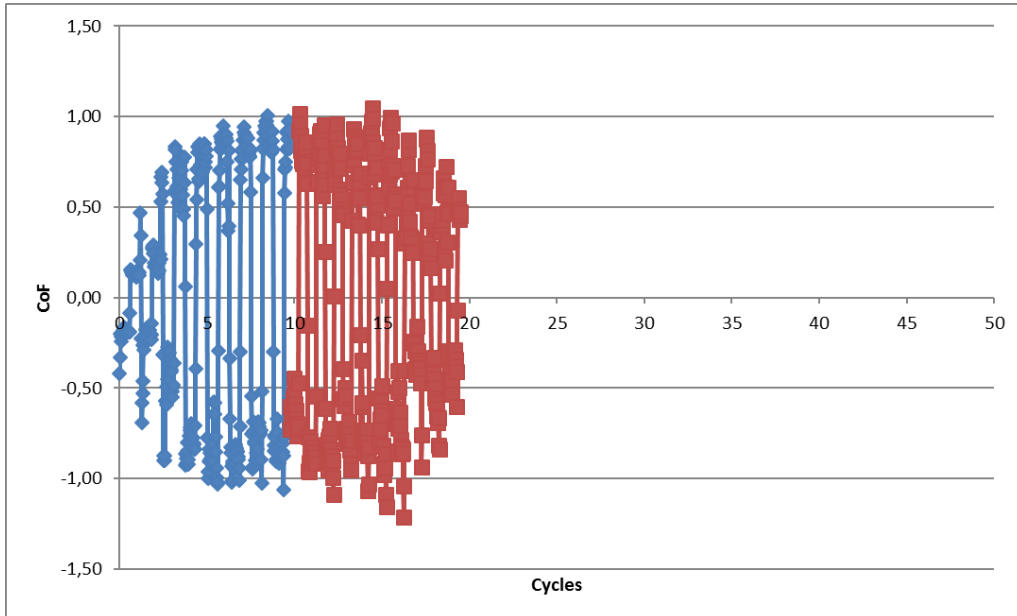
Figure 4.11. Ref. Ag80Al20 (2N; 0,002m/s; 10 reads/s), reciprocating test **under oil**, short test A. CoF and SEM images of the test tracks (left to right, sequentially correspond to the n of cycles in the CoF graphic).

Figure 4.12. Ref. Ag80Al20 (2N; 0,002m/s; 10 reads/s), reciprocating test **under oil**, test B, CoF and SEM images of the test tracks (left to right, sequentially correspond to the n of cycles in the CoF graphic).
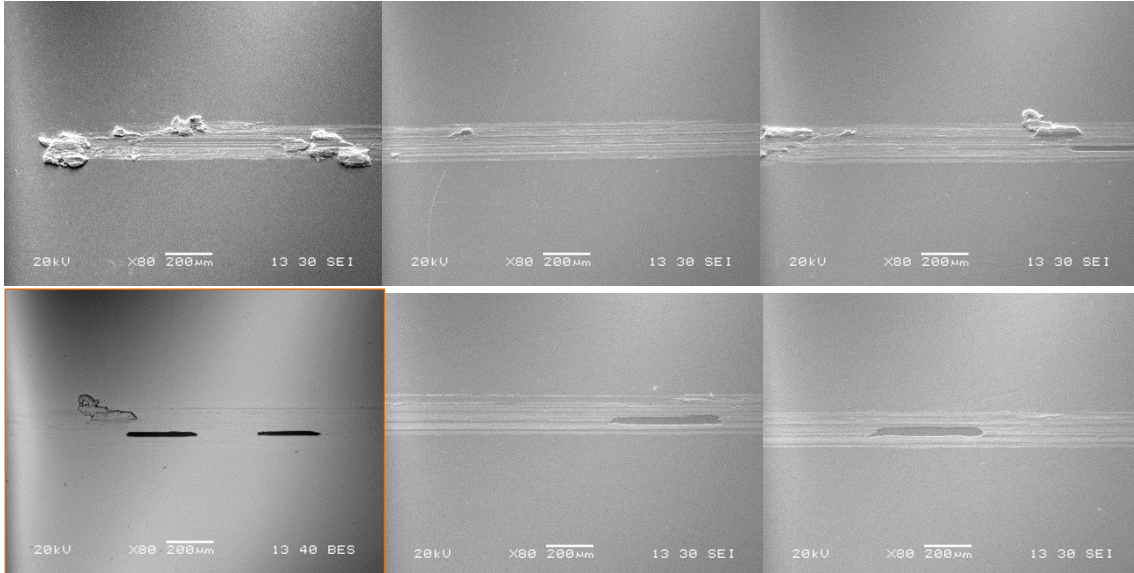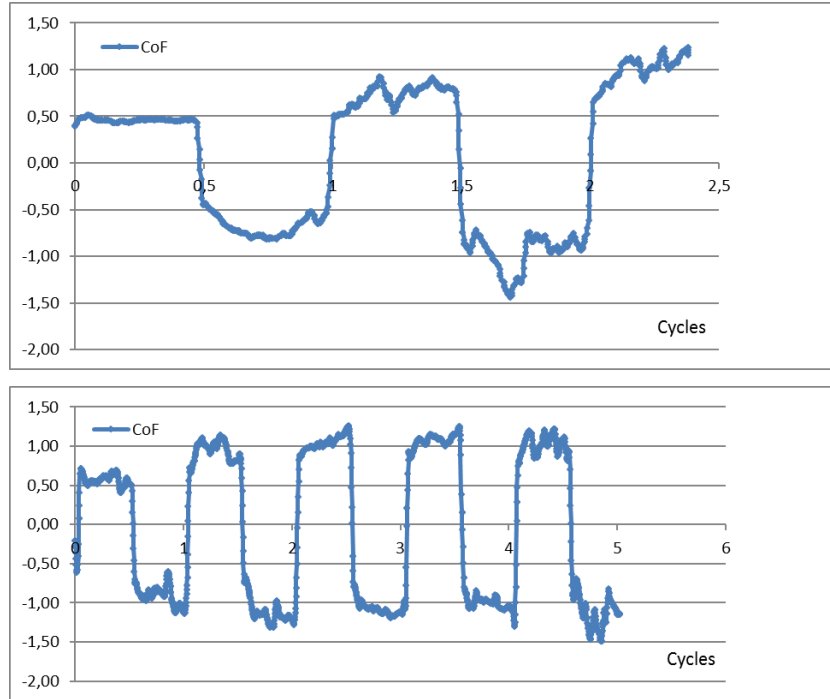
Figure 4.13. Ref. Ag80Al20 (2N; 0,002m/s; 10 reads/s), reciprocating test **in air**, test B, CoF and SEM images of the test tracks (left to right; up down).

Figure 4.14. Ref. Ag80Al20 (2N; 0,002m/s; 10 reads/s), reciprocating test **in air**, test A, CoF and SEM images of the test tracks (left to right, sequentially correspond to the n of cycles in the CoF graphic; BES image framed in orange, same spot as the previous SEI image).
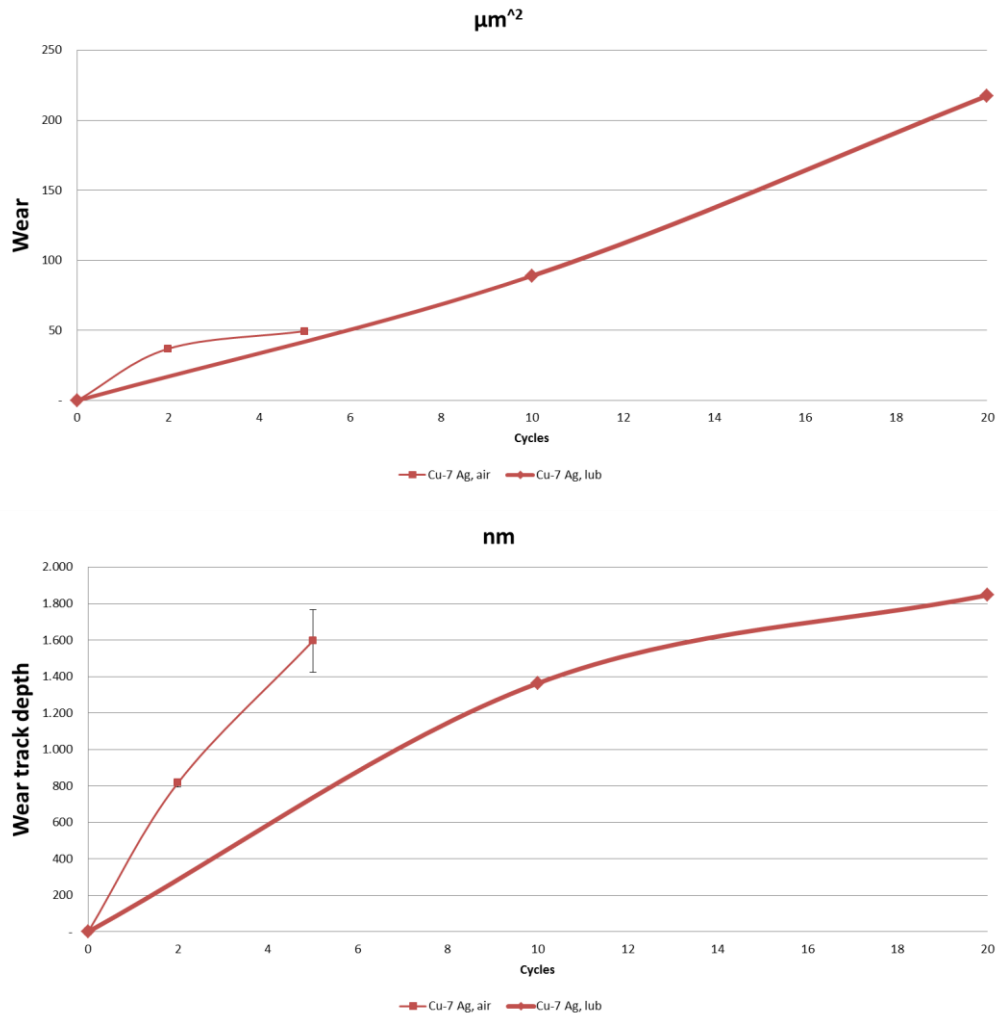
Figure 4.15. Ref. Ag80Al20 (2N; 0,002m/s; 10 reads/s), reciprocating test **under oil** (thicker line) and **in air** (thinner line), wear and wear track depth evolution.

In the case of coating **ref. Ag78Al22T**, as mentioned before, the surface, due to the deposition temperature, presents a larger surface roughness than all the other coatings (Figure 4.16; Table 4-2). This, together with the phase change, affect the tribological performance of the coating.

In the under oil test conditions, the CoF initially rises above 0.4, and then decreases to values just above 0.3 (Figure 4.17 and Figure 4.18). Above 30 test cycles, grooves are already visible in the coating surface, and they keep growing deeper, though the Ni underlayer is not reached by cycle 200. The wear track depth is thus less deep than for ref. Ag80Al20, though wear rates are quite similar. Also, unlike in the case of ref. Ag80Al20 there is no evidence of adhesive wear, which is more erosive or third body abrasive.

In the in air test conditions, the CoF observed are higher than under oil conditions, reaching a peak value above 0.6, that then decreases and stabilizes around 0.4 (Figure 4.19and Figure 4.20). It can also be noted, that unlike under oil conditions, there are some early sings of material adhesion and displacement. Contrary to under oil conditions, the Ni underlayer is reached in the in air conditions, tentatively by test cycle 40, but definitively by cycle 50.

This is evidenced by the wear track volume and depth evolution, where rates are much larger for the in air conditions as compared with the under oil ones (Figure 4.21).
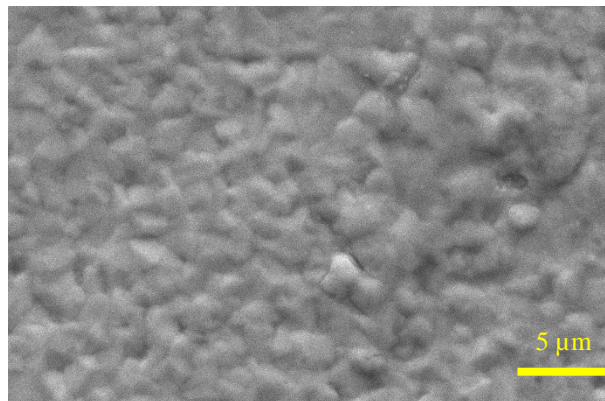
Figure 4.16. Scanning Electron Microscope image of the surface of ref. Ag78Al22T. (Not images shown for the other surfaces, where no feature was visible).
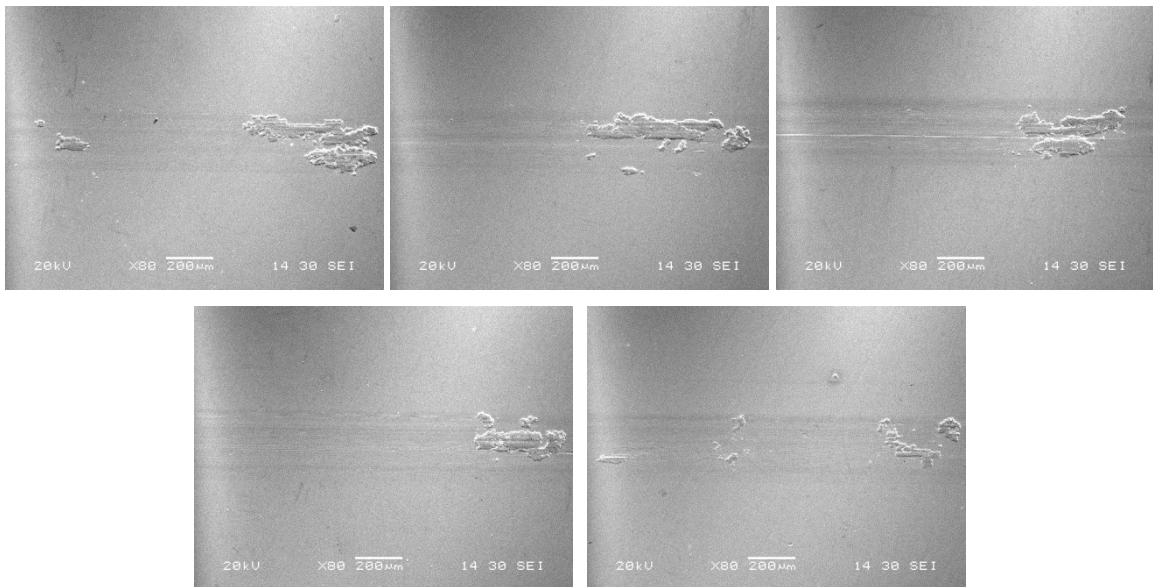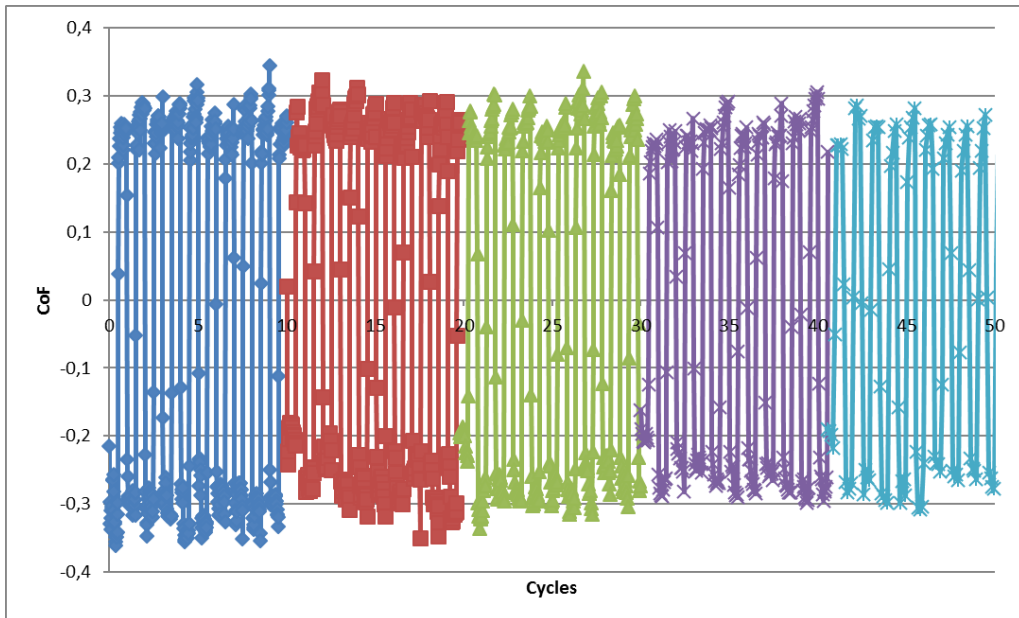
Figure 4.17 Ref. Ag78Al22T (2N; 0,002m/s; 10 reads/s), reciprocating test **under oil**, short test A. CoF and SEM images of the test tracks CoF and SEM images of the test tracks (left to right, sequentially correspond to the n of cycles in the CoF graphic).
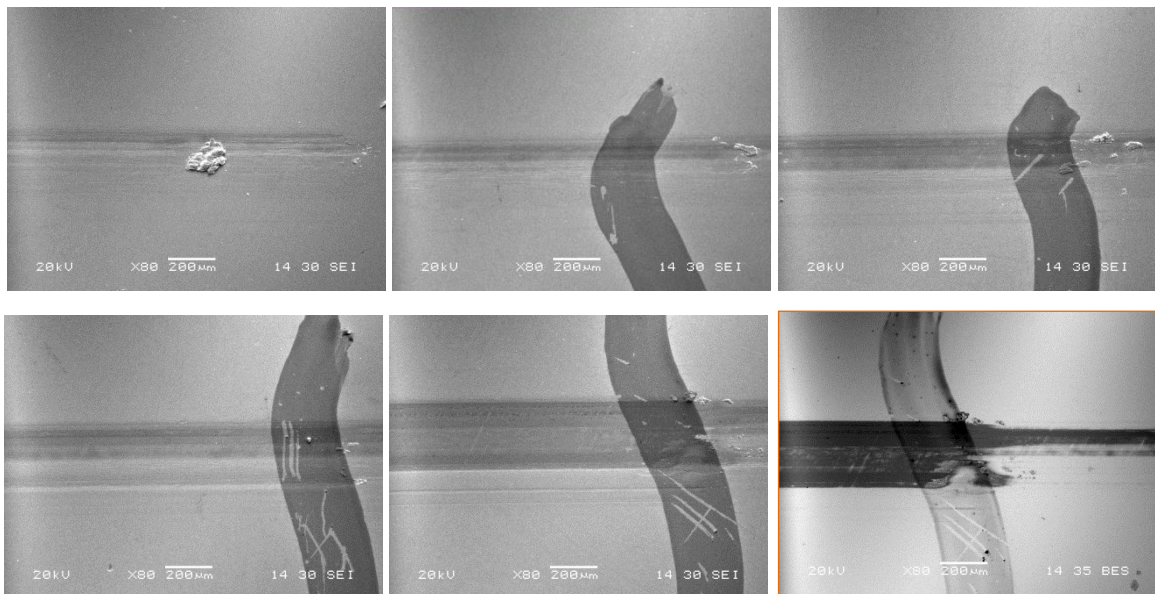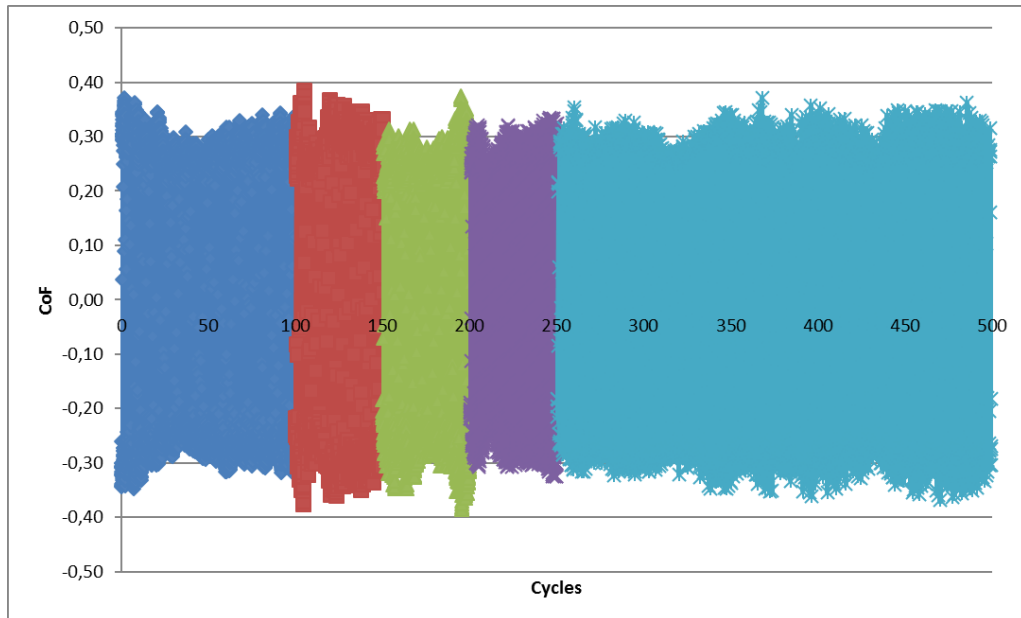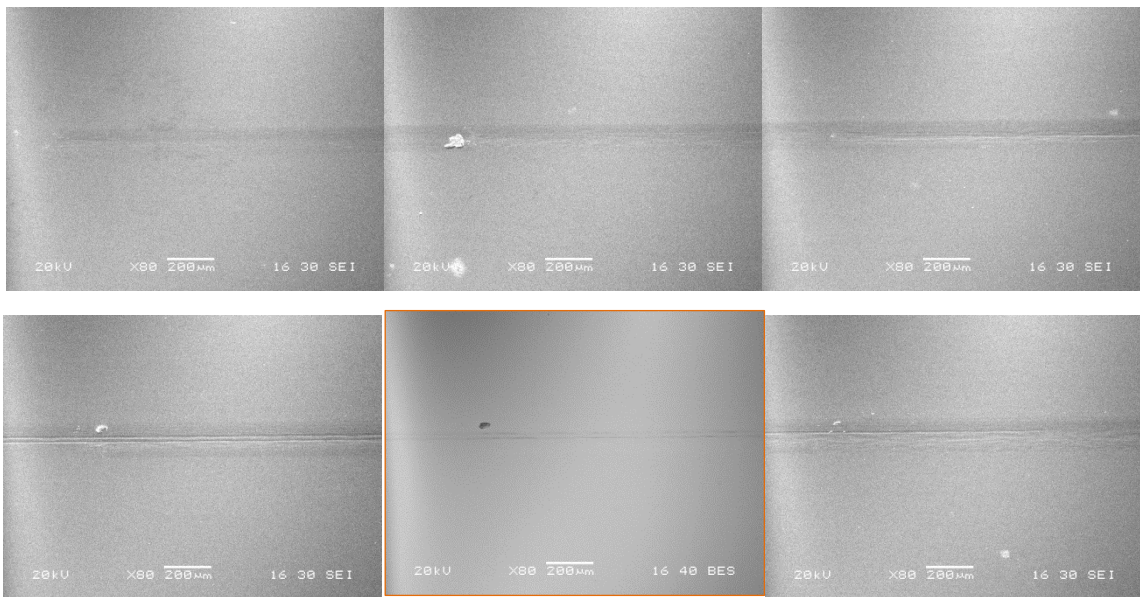
Figure 4.18. Ref. Ag78Al22T (2N; 0,002m/s; 10 reads/s), reciprocating test **under oil**, long test B. CoF and SEM images of the test tracks CoF and SEM images of the test tracks (left to right, sequentially correspond to the n of cycles in the CoF graphic).

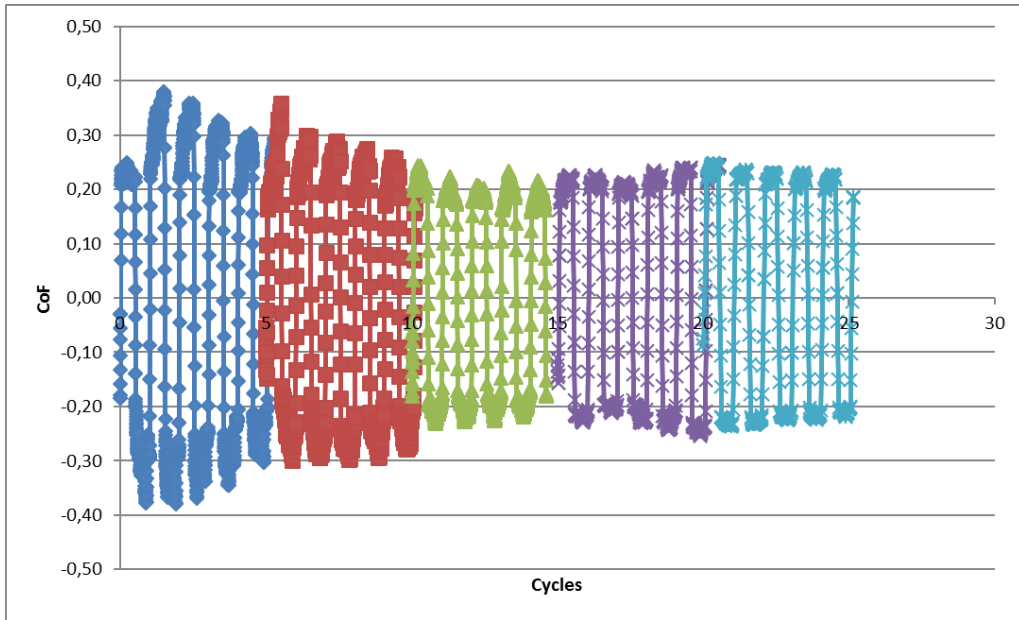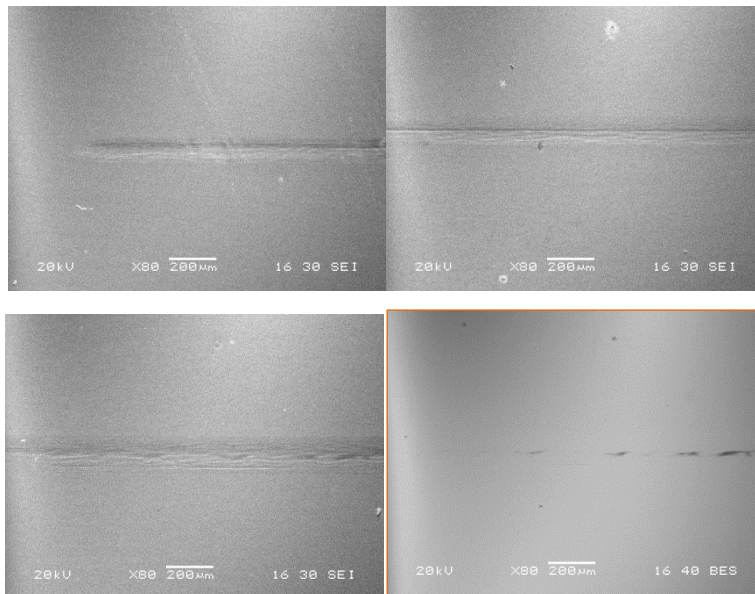Figure 4.19. Ref. Ag78Al22T (2N; 0,002m/s; 10 reads/s), reciprocating test **in air**, test A, CoF and SEM images of the test tracks (left t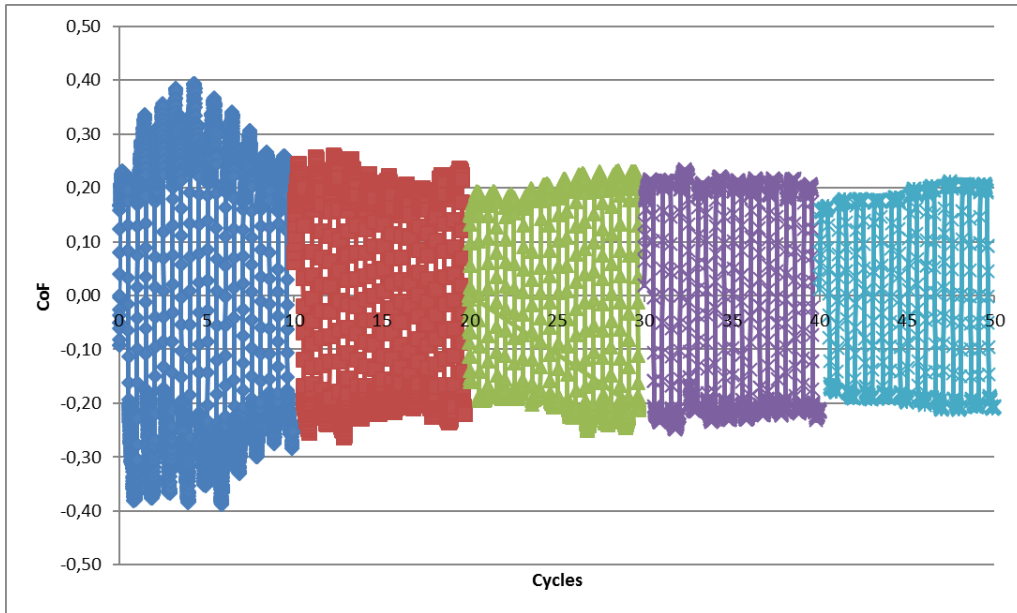o right, sequentially correspond to the n of cycles in the CoF graphic; BES image framed in orange, same spot as the previous SEI image).
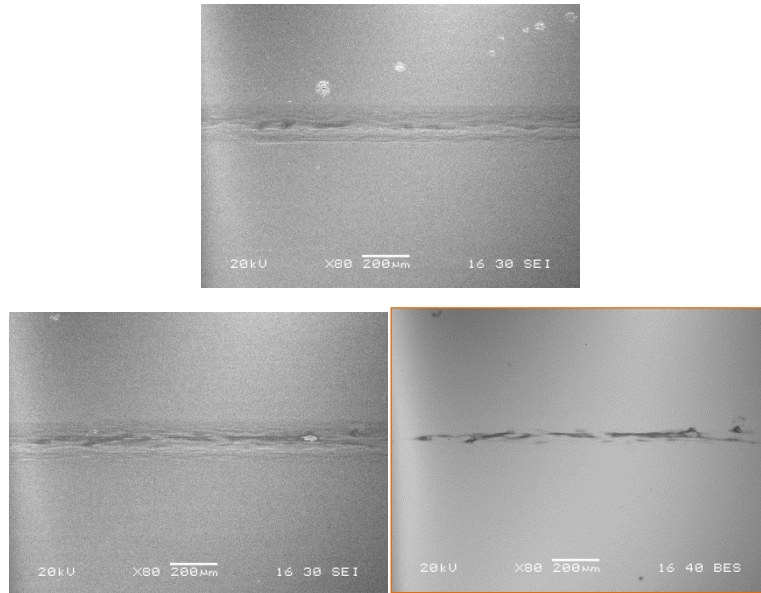
Figure 4.20. Ref. Ag78Al22T (2N; 0,002m/s; 10 reads/s), reciprocating test **in air**, test B, CoF and SEM images of the test tracks (left to right, sequentially correspond to the n of cycles in the CoF graphic; BES image framed in orange, same spot as the previous SEI image).
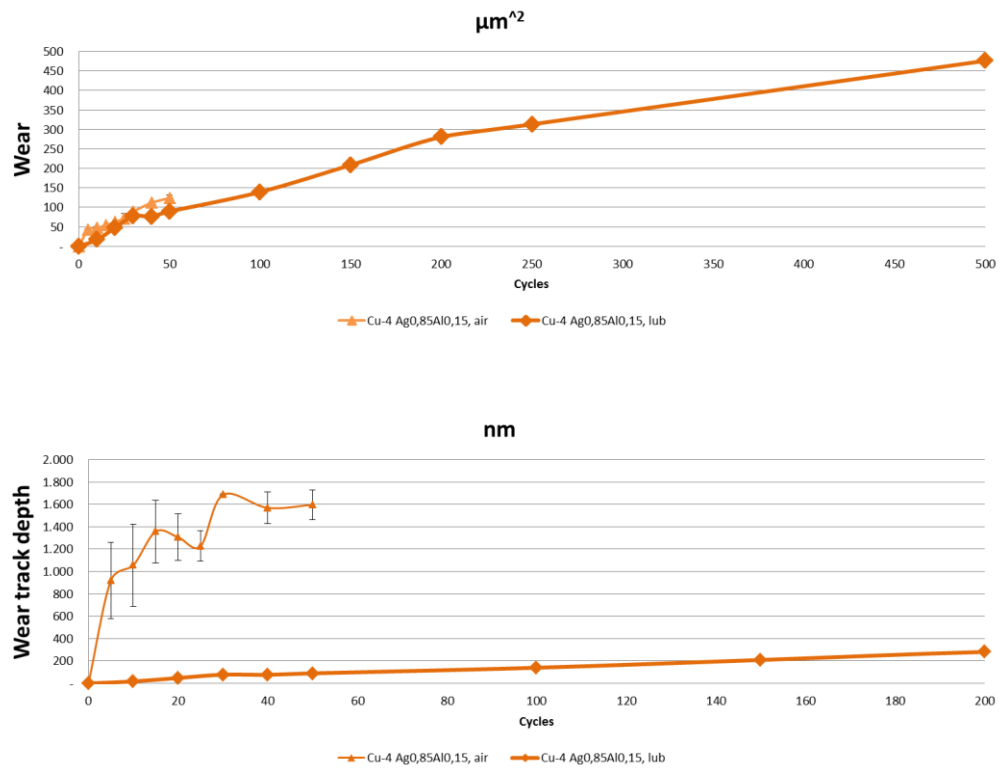
Figure 4.21. Ref. Ag78Al22T (2N; 0,002m/s; 10 reads/s), reciprocating test **under oil** (thicker line) and **in air** (thinner line), wear and wear track depth evolution.

Differences between ref. **Ag78Al22** and ref. **Ag78Al22T**, which have the same coating thickness and composition, though different surface roughness and microstructure phase, are evident in the tribological tests.

In the case of coating **ref. Ag78Al22,** in the under oil test conditions, the CoF shows initially values around peaking above 0.3, which subsequently decrease along the test cycles to 0.2 (Figure 4.22 and Figure 4.23). Those values are significantly lower than in the case of ref. Ag78Al22T, where CoF values move above 0.3 to reach 0.4 at longer test cycles. So, under oil conditions, CoF values are lower to those of ref. Ag78Al22T in the steady regime.

In the under oil test conditions, some material adhesion and displacement can also be observed in the wear track (as well as some scratch), which was not so apparent in ref. Ag78Al22T under oil. This might be due to the fact that a rougher outer surface of the coating offers better conditions to maintain a working oiled environment.

In the case of the test conditions in air, the CoF of ref. Ag78Al22 peaks first above 0.4, but then decreases to above 0.20-0.25 (Figure 4.24 and Figure 4.25). Those are again lower values than those corresponding to ref. Ag78Al22T in the same testing conditions.

Besides, in the in air tests, some grooving and scratches are apparent in the wear tracks.

Finally, as in the case of ref. Ag78Al22T, with ref. Ag78Al22 wear volumes and track depth are larger, in air conditions than under oil (Figure 4.26).
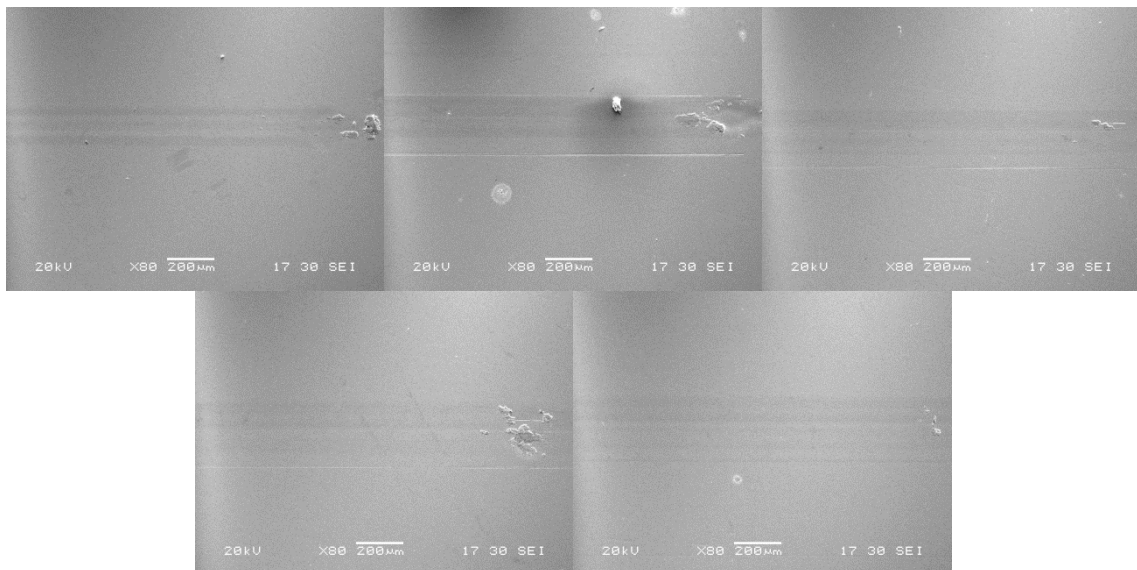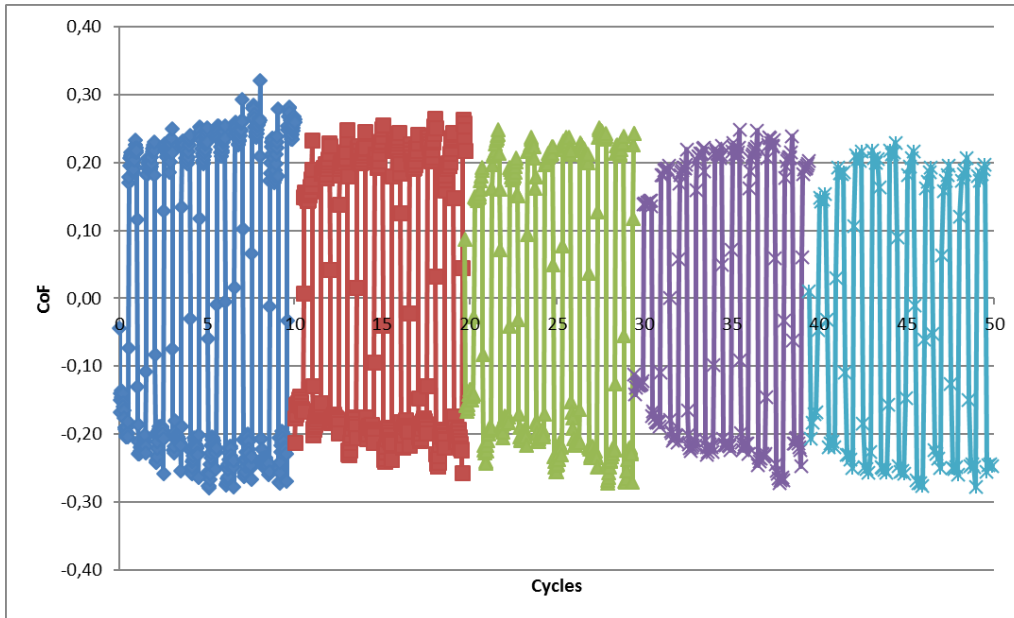
Figure 4.22. Ref. Ag78Al22 (2N; 0,002m/s; 10 reads/s), reciprocating test **under oil**, short test A. CoF and SEM images of the test tracks (left to right, sequentially correspond to the n of cycles in the CoF graphic).
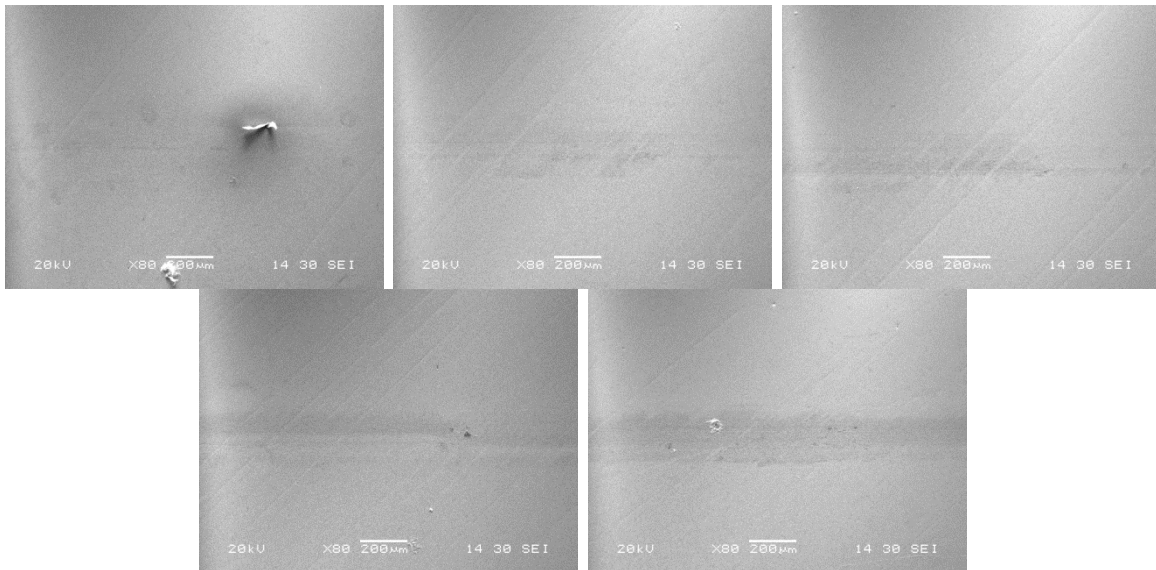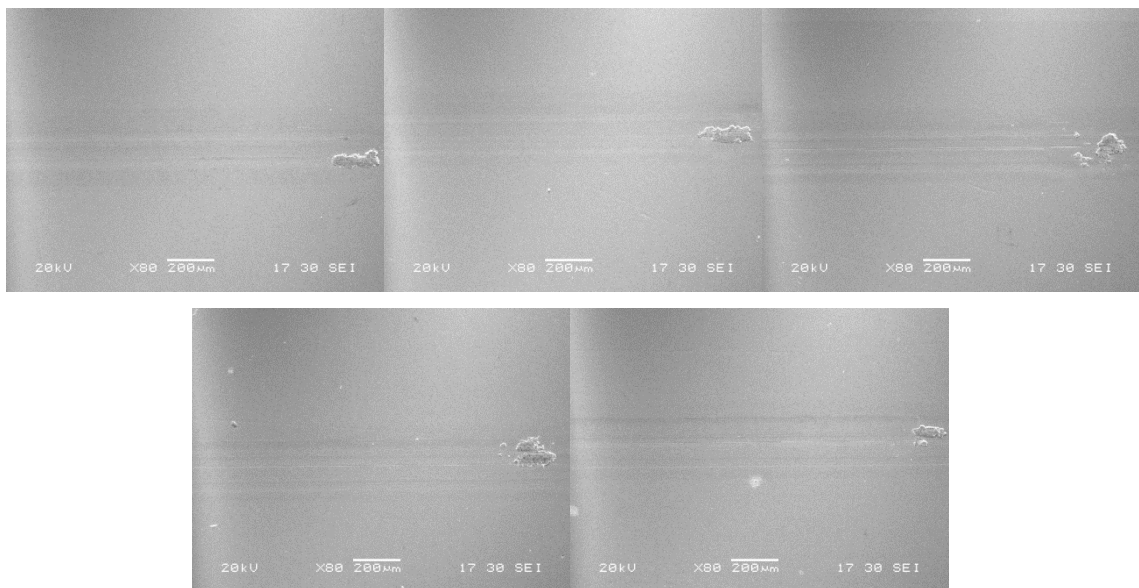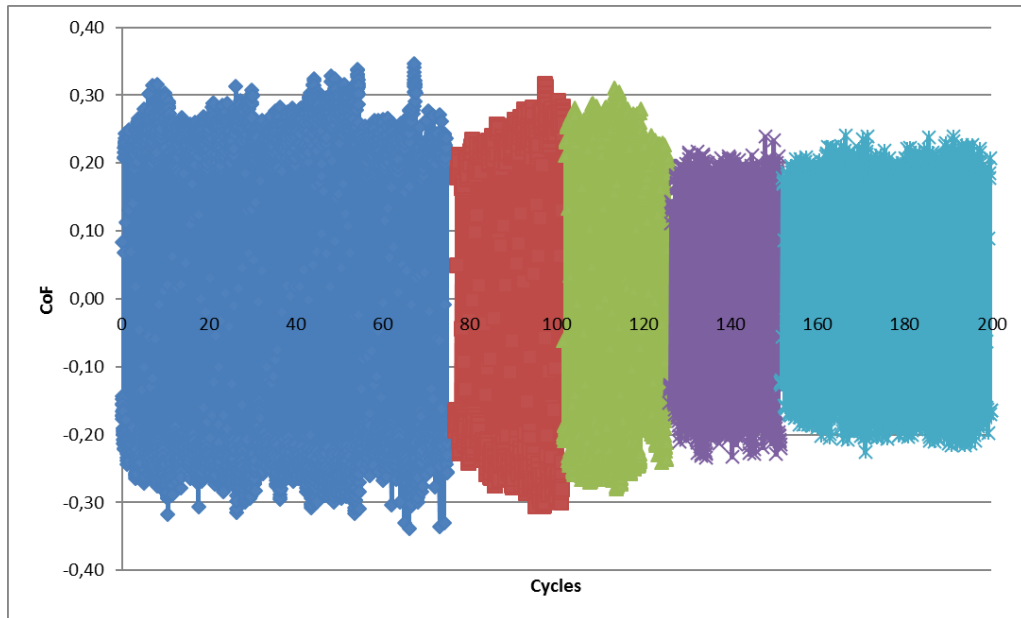
Figure 4.23. Ref. Ag78Al22 (2N; 0,002m/s; 10 reads/s), reciprocating test **under oil**, long test B. CoF and SEM images of the test tracks (left to right, sequentially correspond to the n of cycles in the CoF graphic).
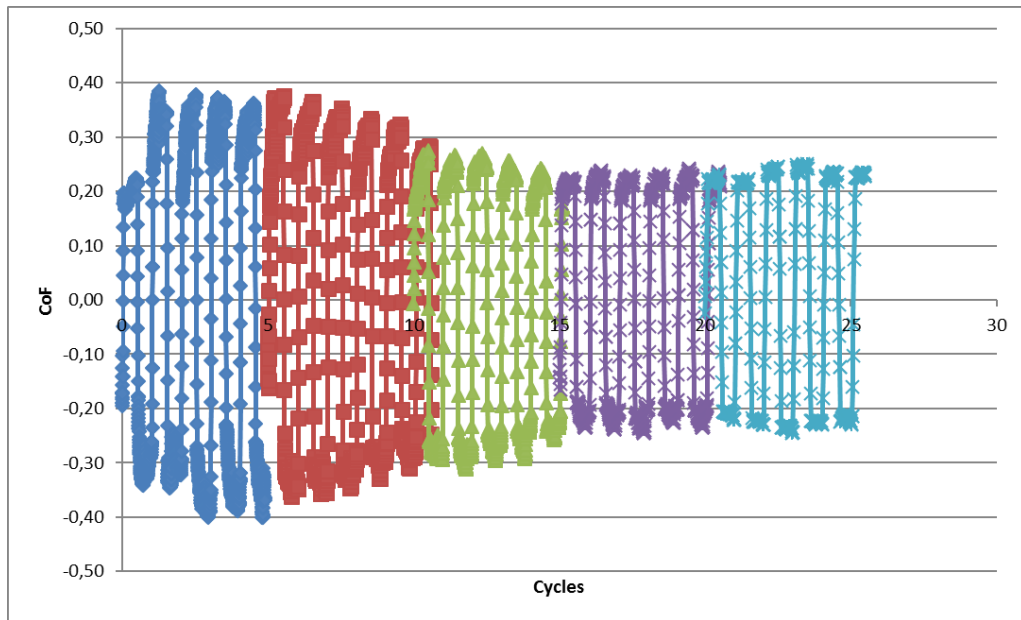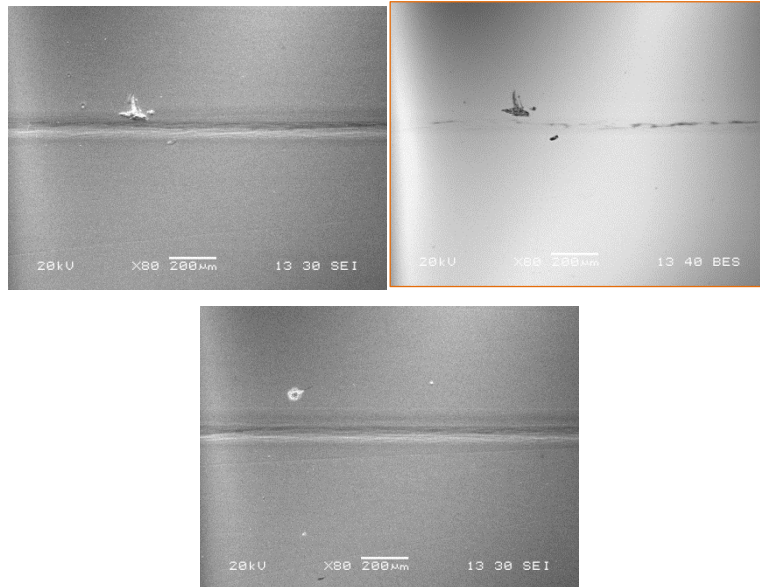
Figure 4.24. Ref. Ag78Al22 (2N; 0,002m/s; 10 reads/s), reciprocating test **in air**, test A, CoF and SEM images of the test tracks (left to right, sequentially correspond to the n of cycles in the CoF graphic; BES image framed in orange, same spot as the previous SEI image).
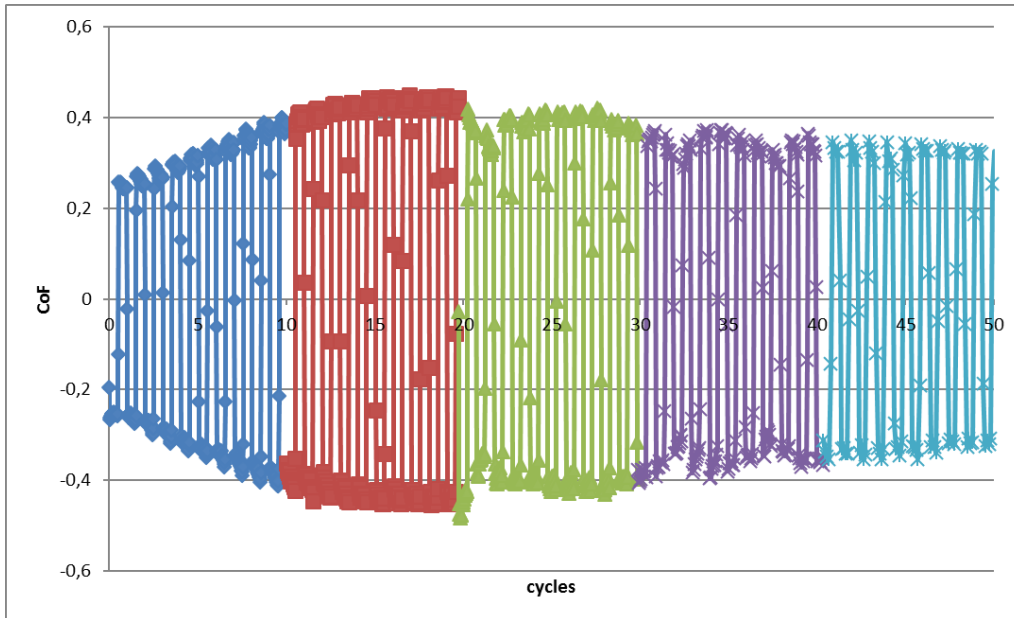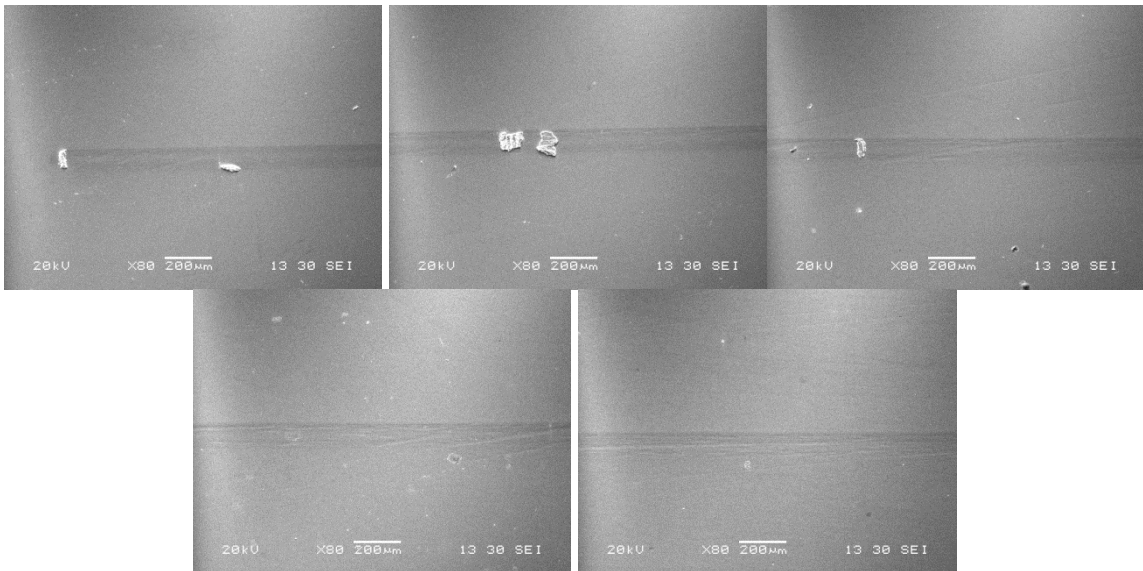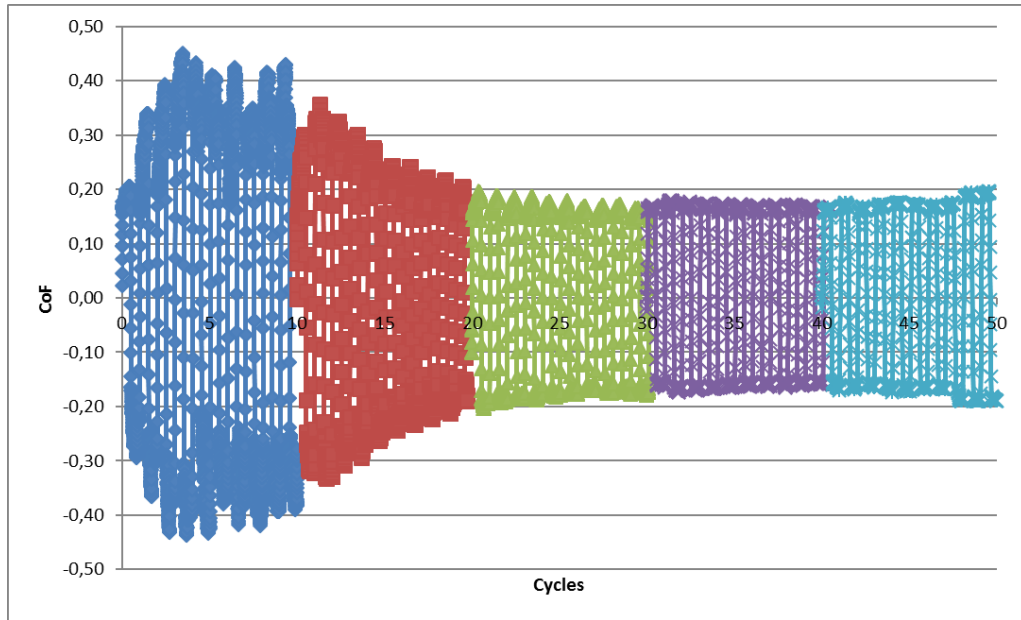
Figure 4.25. Ref. Ag78Al22 (2N; 0,002m/s; 10 reads/s), reciprocating test **in air**, test B, CoF and SEM images of the test tracks (left to right, sequentially correspond to the n of cycles in the CoF graphic).
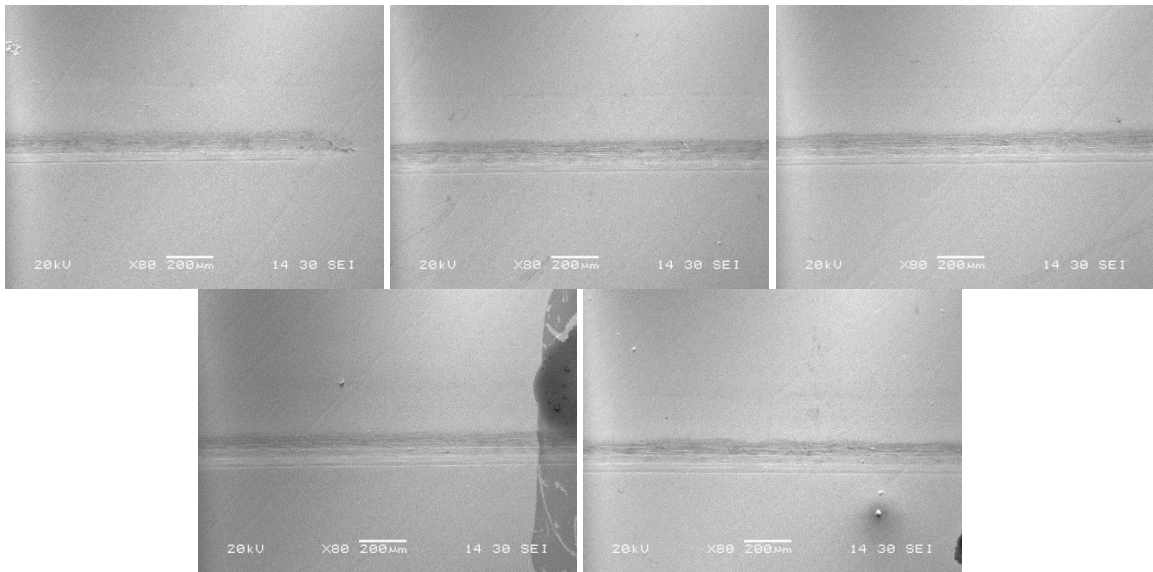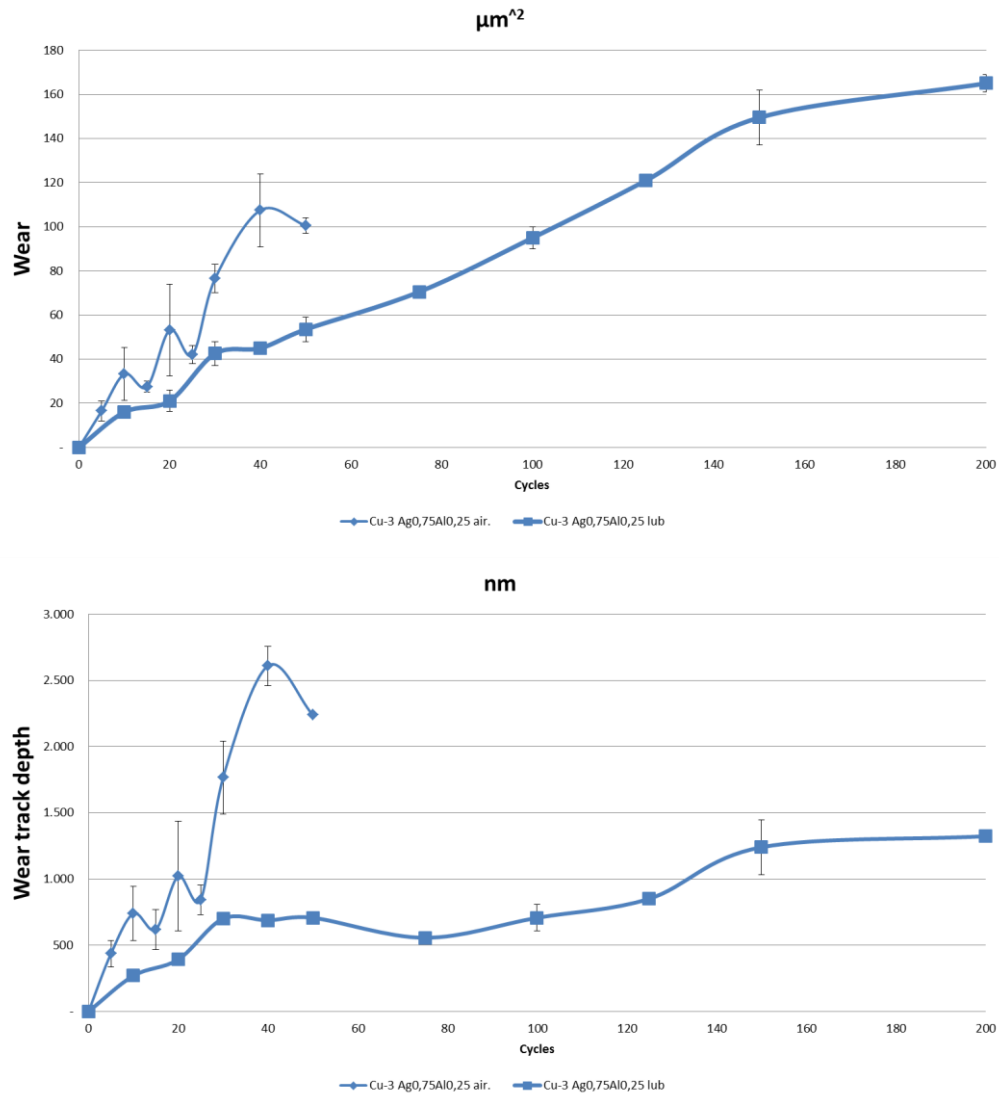
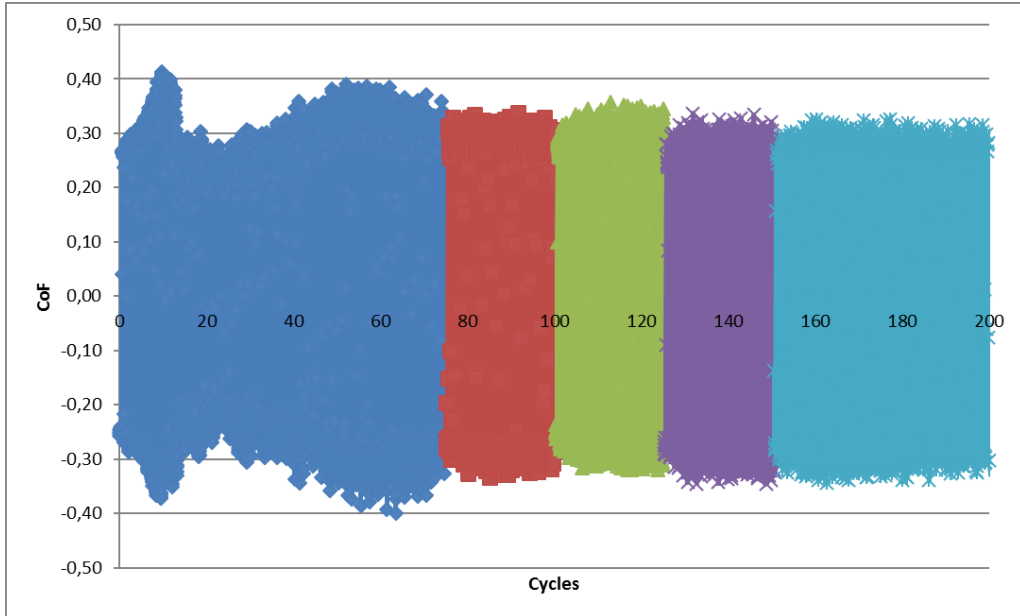Figure 4.26. Ref. Ag78Al22 (2N; 0,002m/s; 10 reads/s), reciprocating test **under oil** (thicker line) and **in air** (thinner line), wear and wear track depth evolution.

Finally, in the case of ref. Ag63Al37, under oil test conditions, the CoF increases from relatively initial low values, around 0.2, to larger values after 50 test cycles around 0.35. In the wear tracks, some scratches are visible, but no material adhesion or grooving (Figure 4.27 and Figure 4.28).

On the other hand, in air conditions, ref. Ag63Al37 shows initial peak CoF values above 0.6, that decrease eventually to values around 0.4 (Figure 4.29 and Figure 4.30). Unlike in the under oil conditions, some grooves and a little adhesion are present in the wear track, and the Ni underlayers seems to have been reached at some point.

As in all the previous cases, for coating ref. Ag63Al37 the wear track volume and depth evolution show larger values the in air conditions as compared with the under oil ones (Figure 4.31).

It should be also mentioned, that in none of the tests was apparent any coating failure because of poor adhesion. Therefore, the **coating adhesion** is at a minimum adequate for these working conditions.
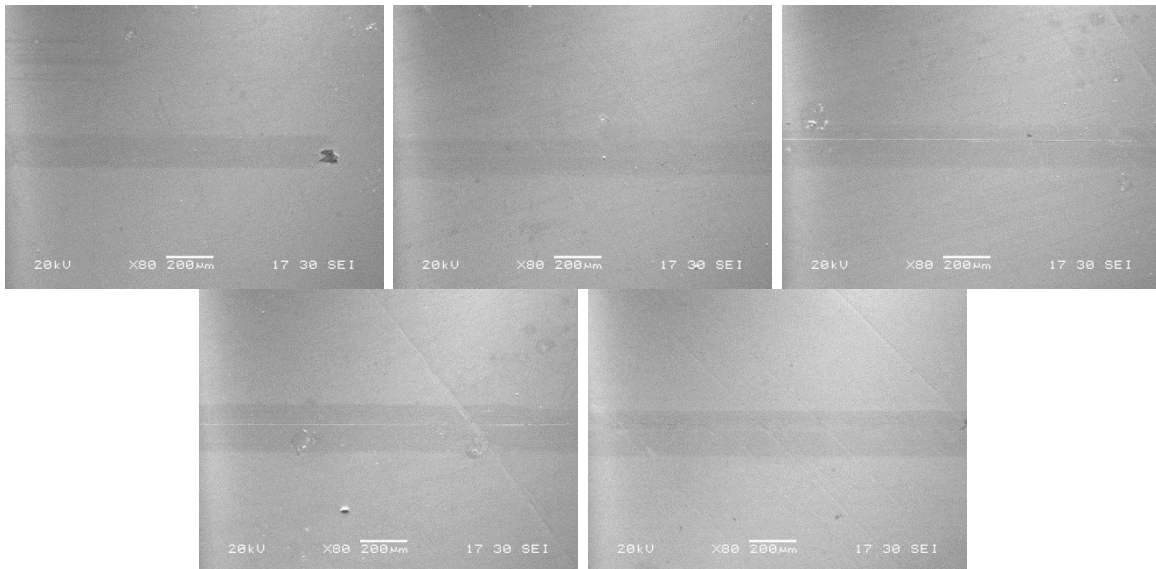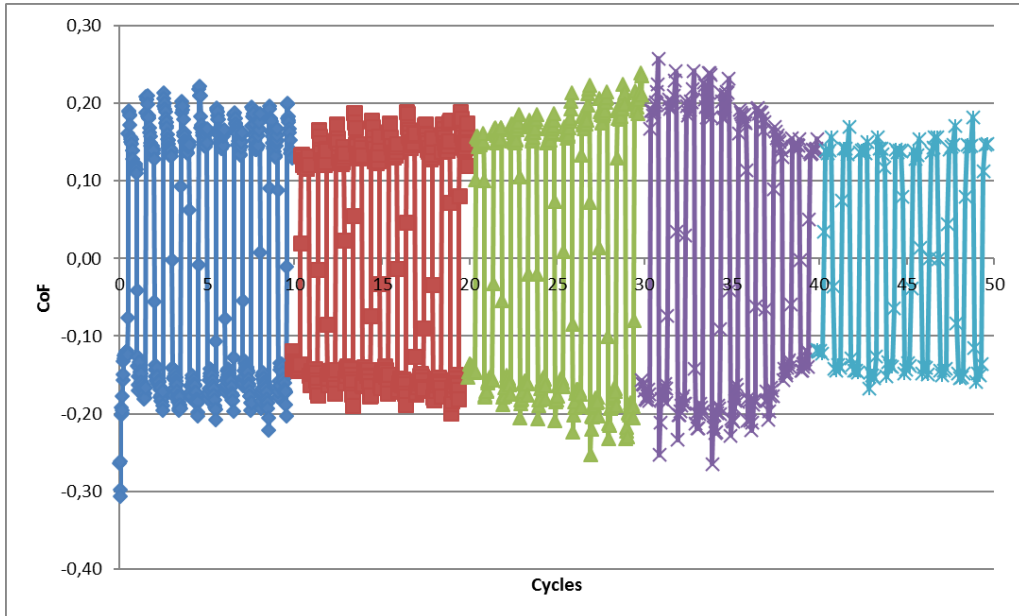
Figure 4.27. Ref.Ag63Al37 (2N; 0,002m/s; 10 reads/s), reciprocating test **under oil**, short test A. CoF and SEM images of the test tracks (left to right, sequentially correspond to the n of cycles in the CoF graphic).
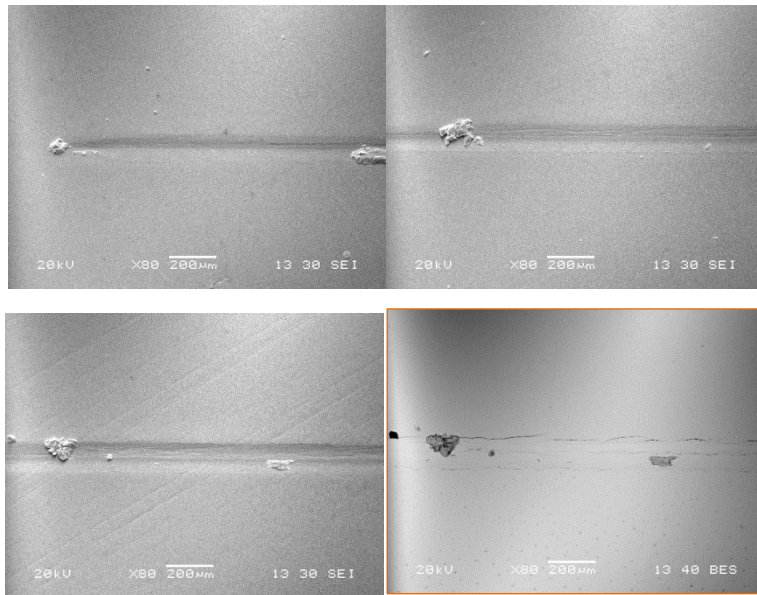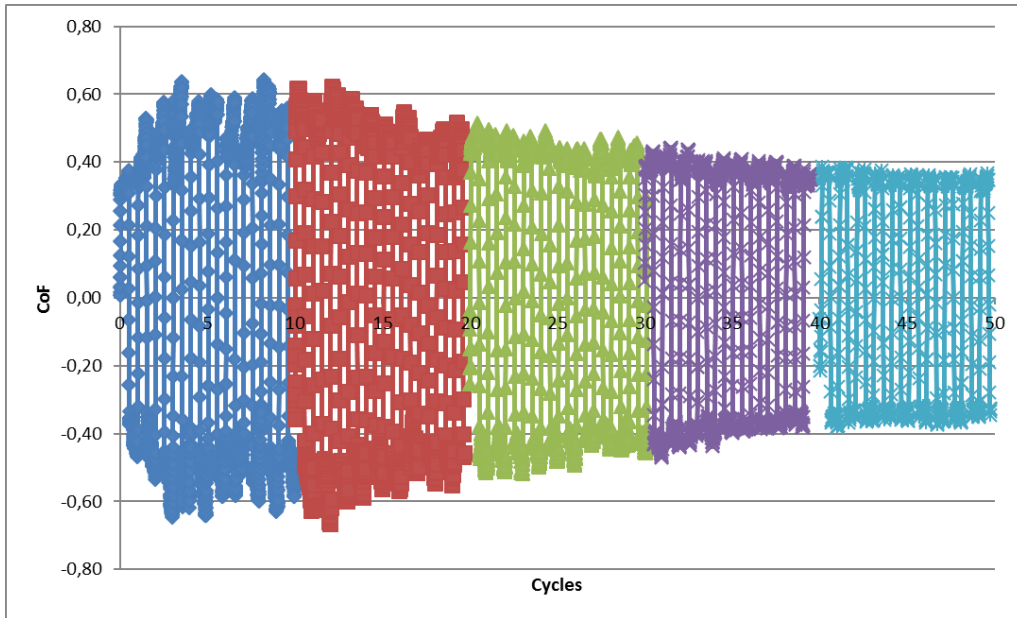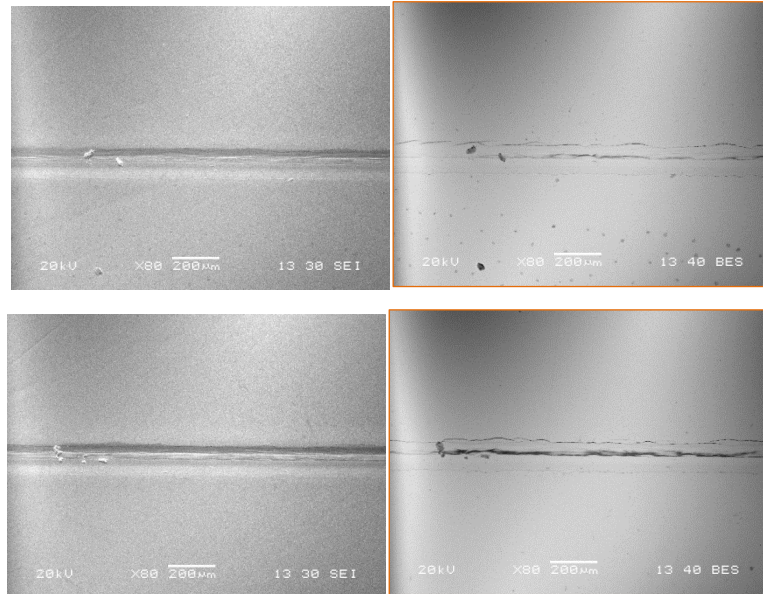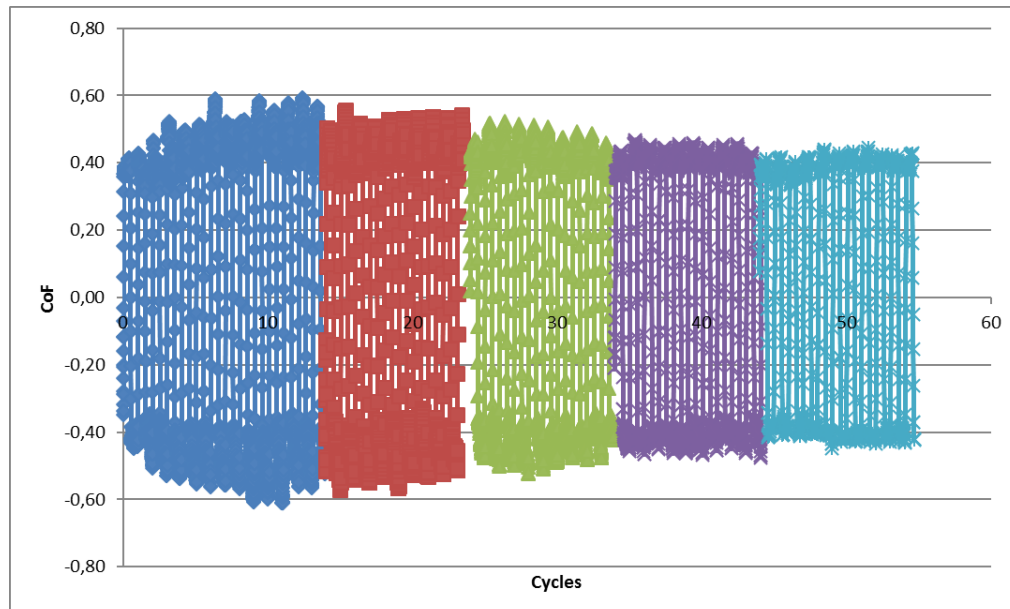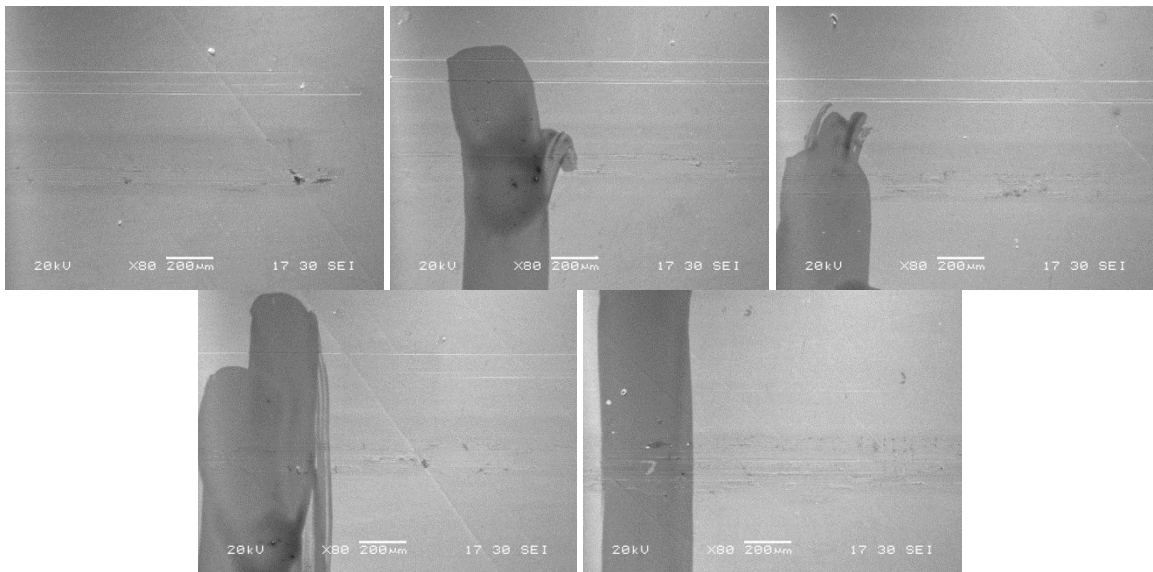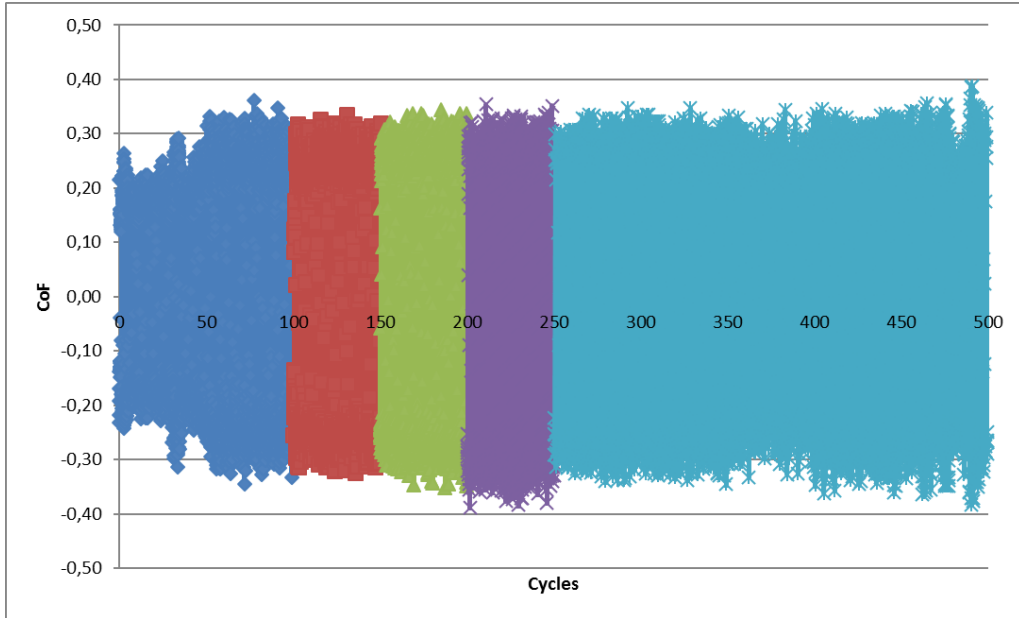
Figure 4.28. Ref. Ag63Al37 (2N; 0,002m/s; 10 reads/s), reciprocating test **under oil**, long test B. CoF and SEM images of the test tracks (left to right, sequentially correspond to the n of cycles in the CoF graphic).
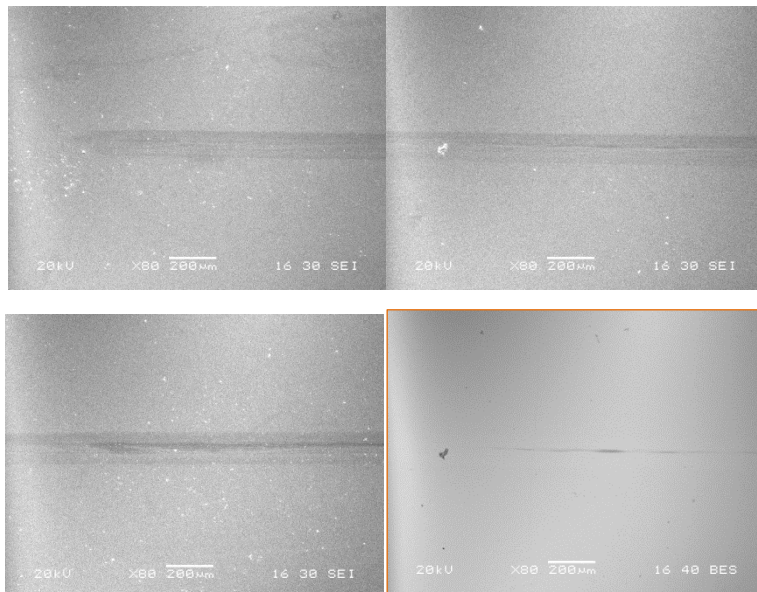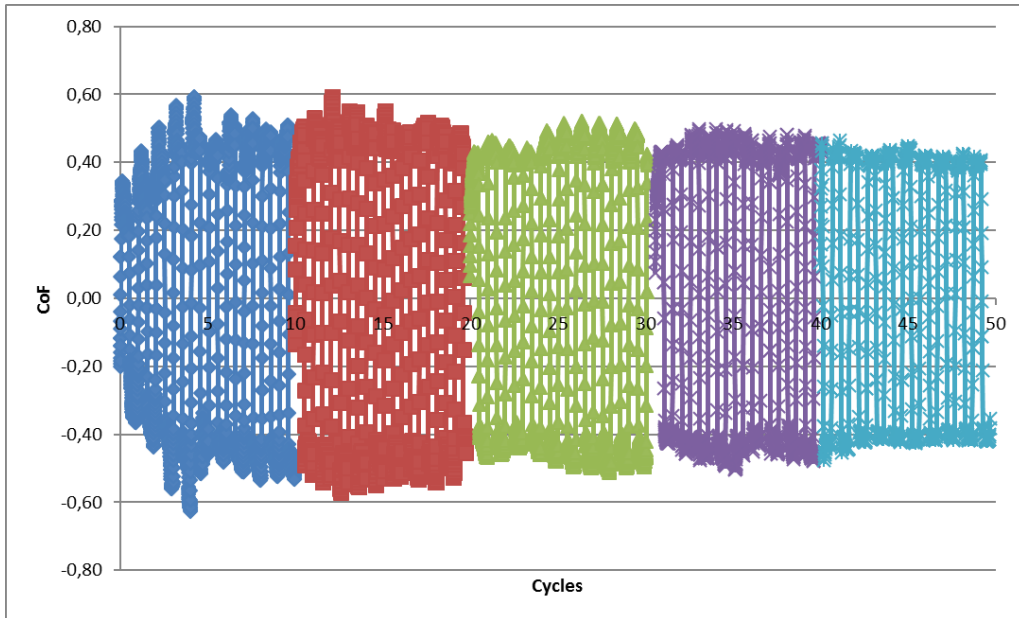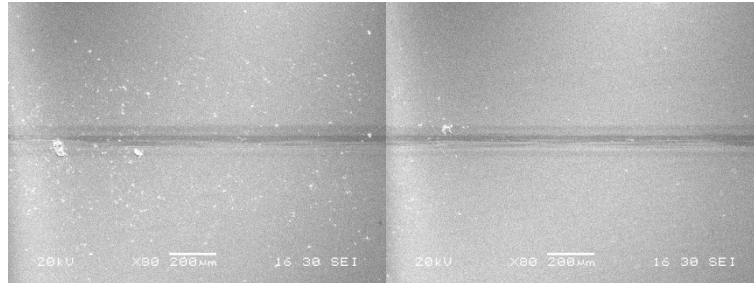
Figure 4.29. Ref. Ag63Al37 (2N; 0,002m/s; 10 reads/s), reciprocating test **in air**, test A, CoF and SEM images of the test tracks (left to right, sequentially correspond to the n of cycles in the CoF graphic; BES image framed in orange, same spot as the previous SEI image).
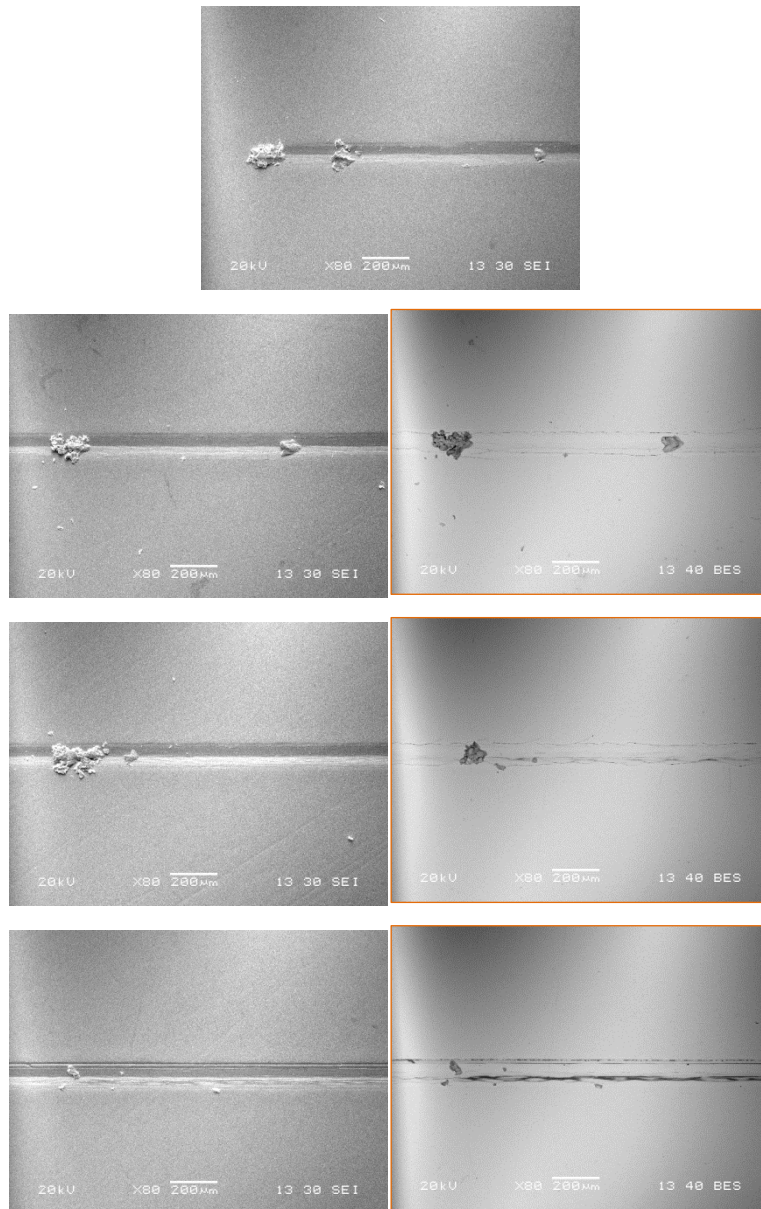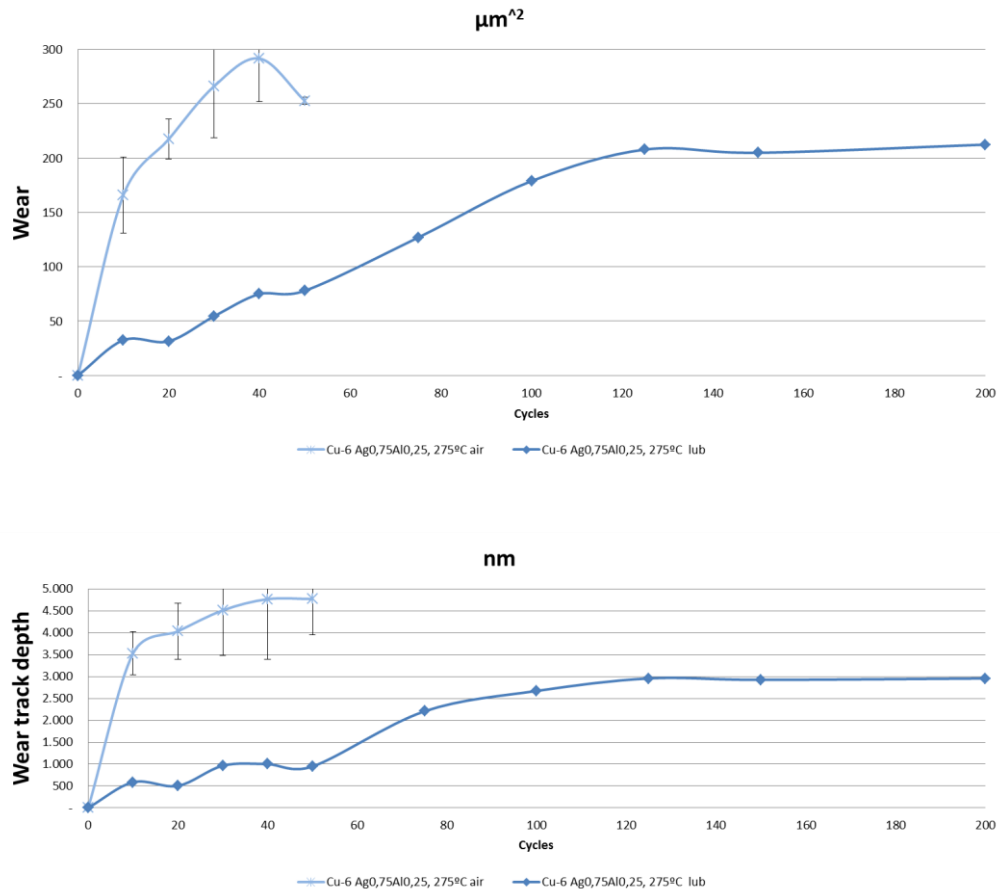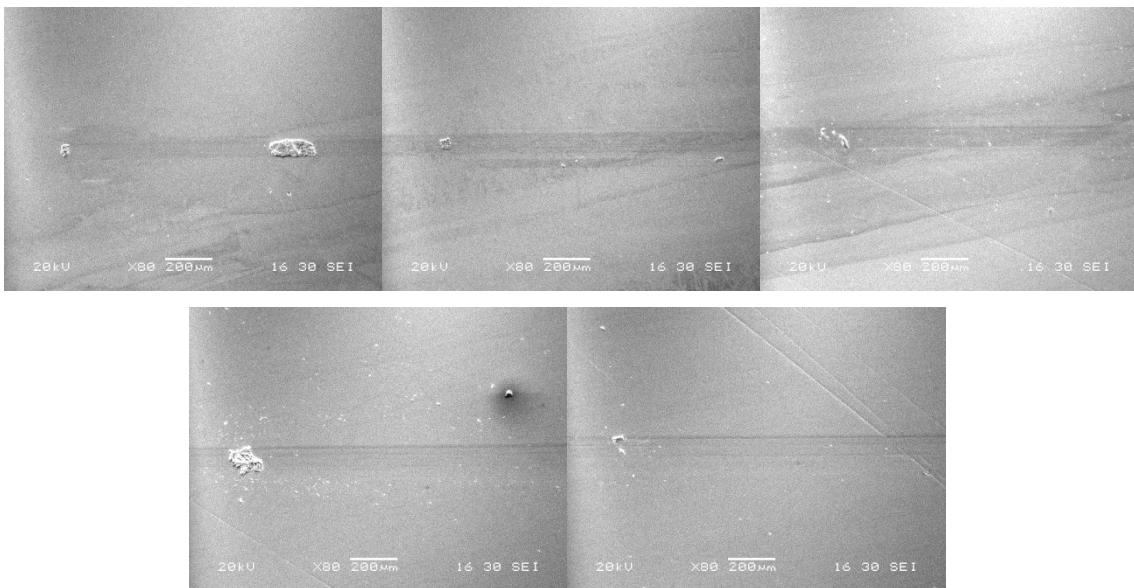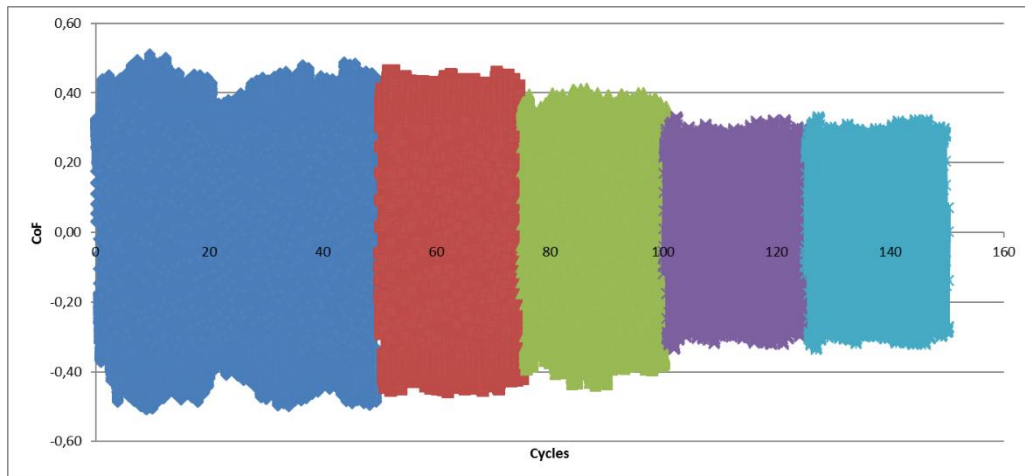
Figure 4.30. Ref. Ag63Al37 (2N; 0,002m/s; 10 reads/s), reciprocating test **in air**, test B, CoF and SEM images of the test tracks (left to right, sequentially correspond to the n of cycles in the CoF graphic).
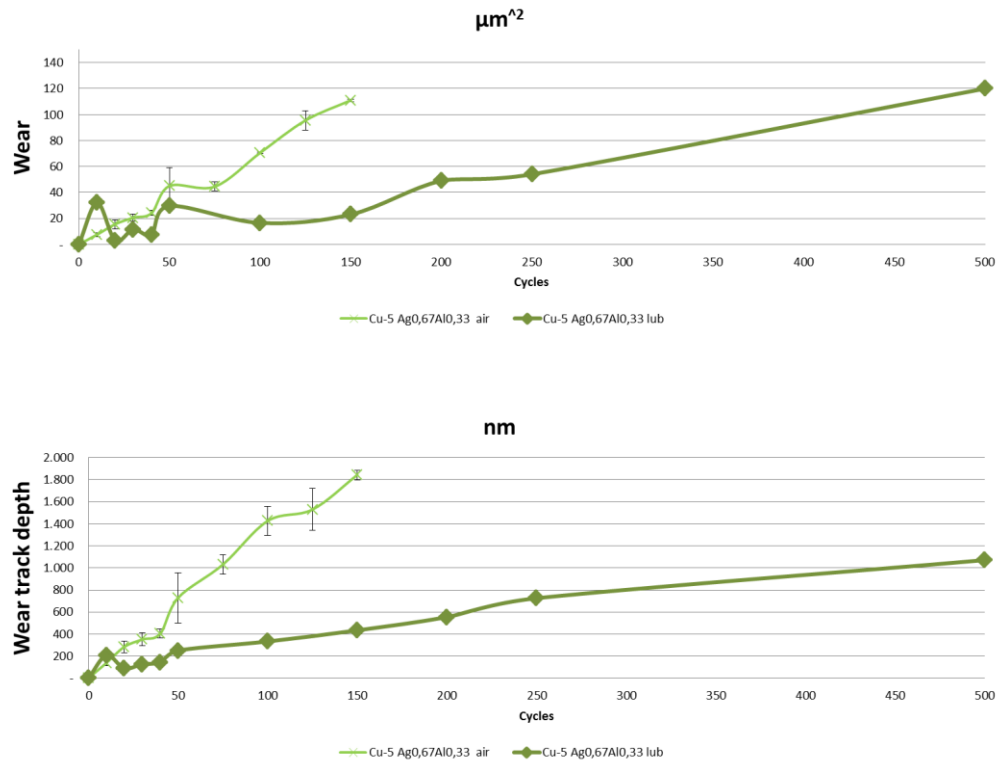
Figure 4.31. Ref. Ag63Al37 (2N; 0,002m/s; 10 reads/s), reciprocating test **under oil** (thicker line) and **in air** (thinner line), wear and wear track depth evolution.

So far, results of the analyses of the AgAl coated surfaces have been presented. It is also worth mentioning that the surface of the counterbody, the semi-spherical Ag coated Cu pins, were analyzed.

In none of the cases the wear level was such that the substrate was reached (Figure 4.32). However, there was always some deformation of the coating, and in some cases some cases, some adhesion of Ni, originating the Ni underlayer below the AgAl coatings.

Spectra	O	Al	Ni	Ag
Spectrum left	41.35			58.65
Spectrum right	81.40	0.94	16.23	1.44
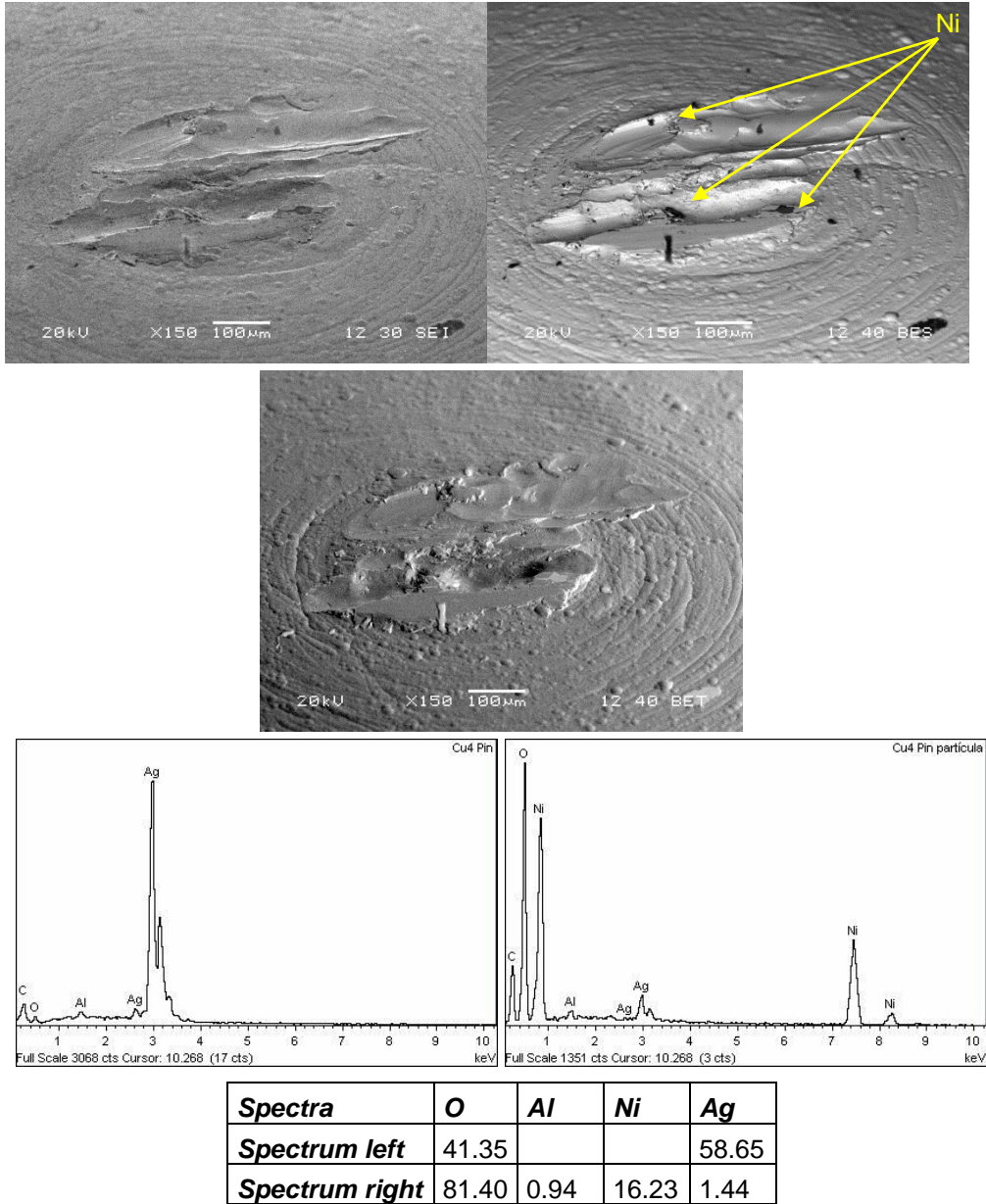
Figure 4.32. Scanning Electron Microscope images (SEI, BES and BET) of the wear tracks of the Ag coated Cu semispherical pin, used in the electro-tribology tests against ref. Ag80Al20 (above) and EDS spectra of the coating (below left) and some wear debris particle (below right), as well and the corresponding semi-quantitative elemental values.

For the sake of facilitating a direct comparison, images of the wear tracks are presented in Figure 4.33, corresponding to Scanning Electron Microscope images of the wear tracks after 30 test cycles (other than for ref. Ag), under oil and in air test conditions.

With the same aim, the mean average coefficient of friction for up to 50 cycles, the standard deviation of the mean CoF (and ECR) values corresponding to different wear tracks, and normalized wear rates (mm^3/Nm) x 10^{-9} are detailed at Table 4-4.

b)

c)

d)

e)
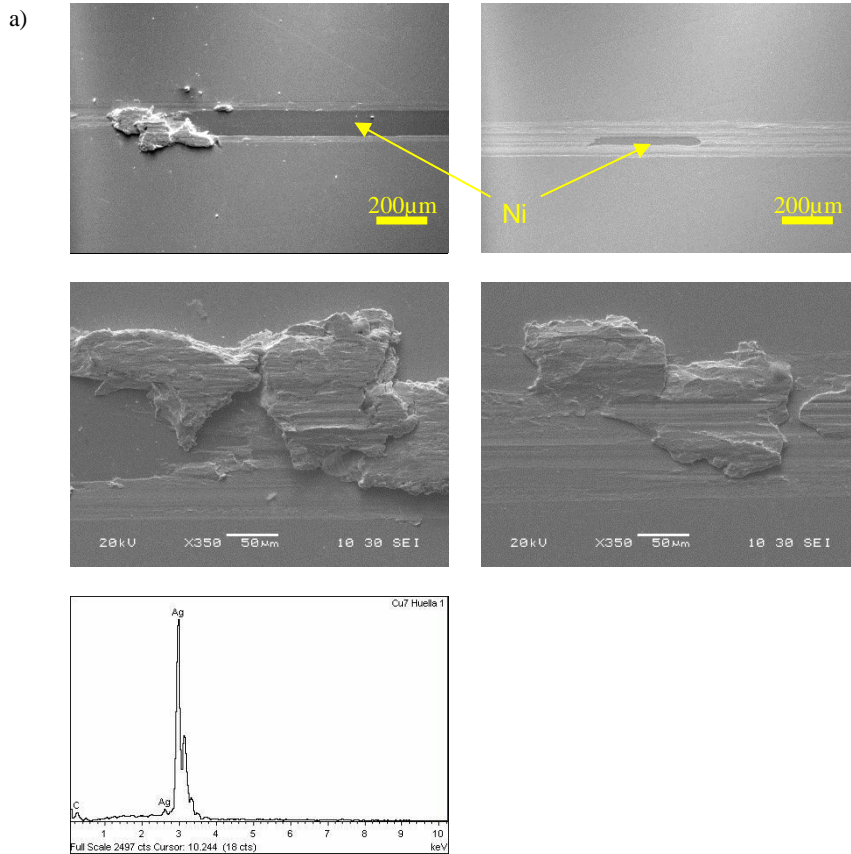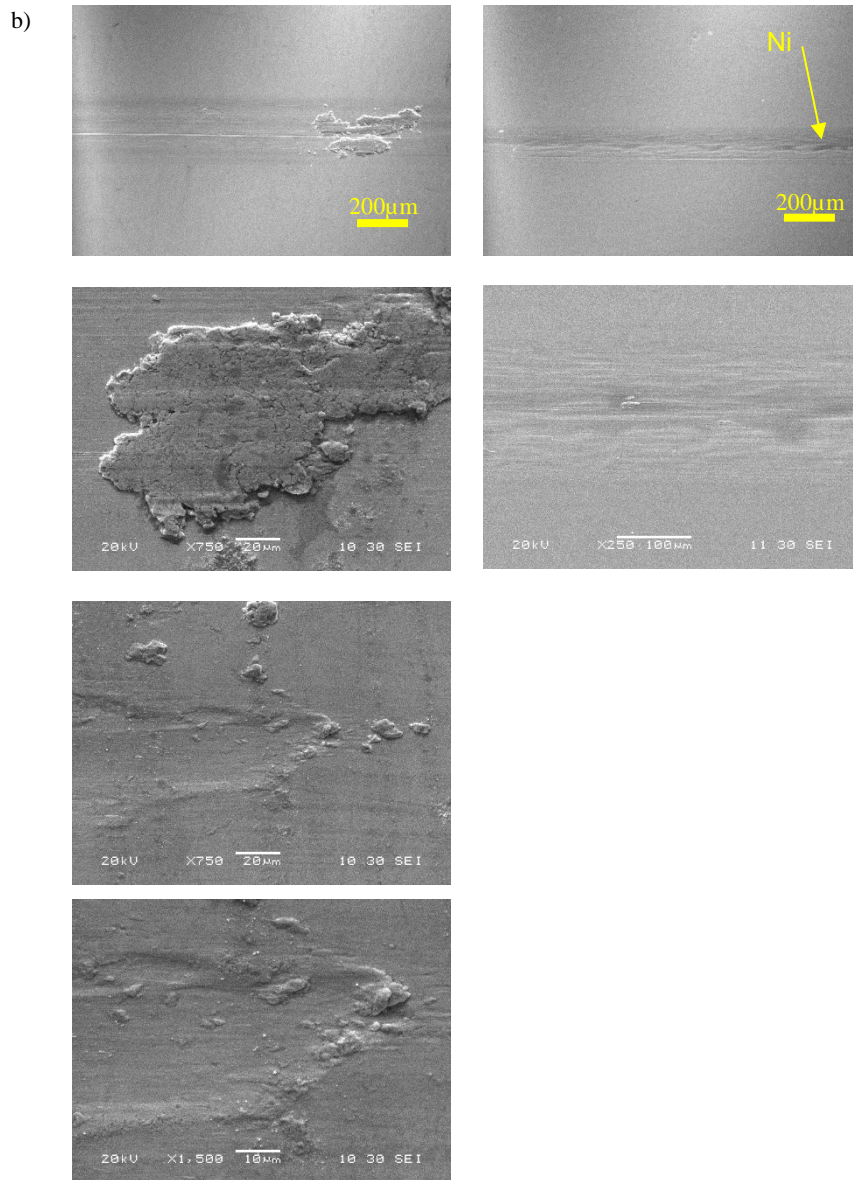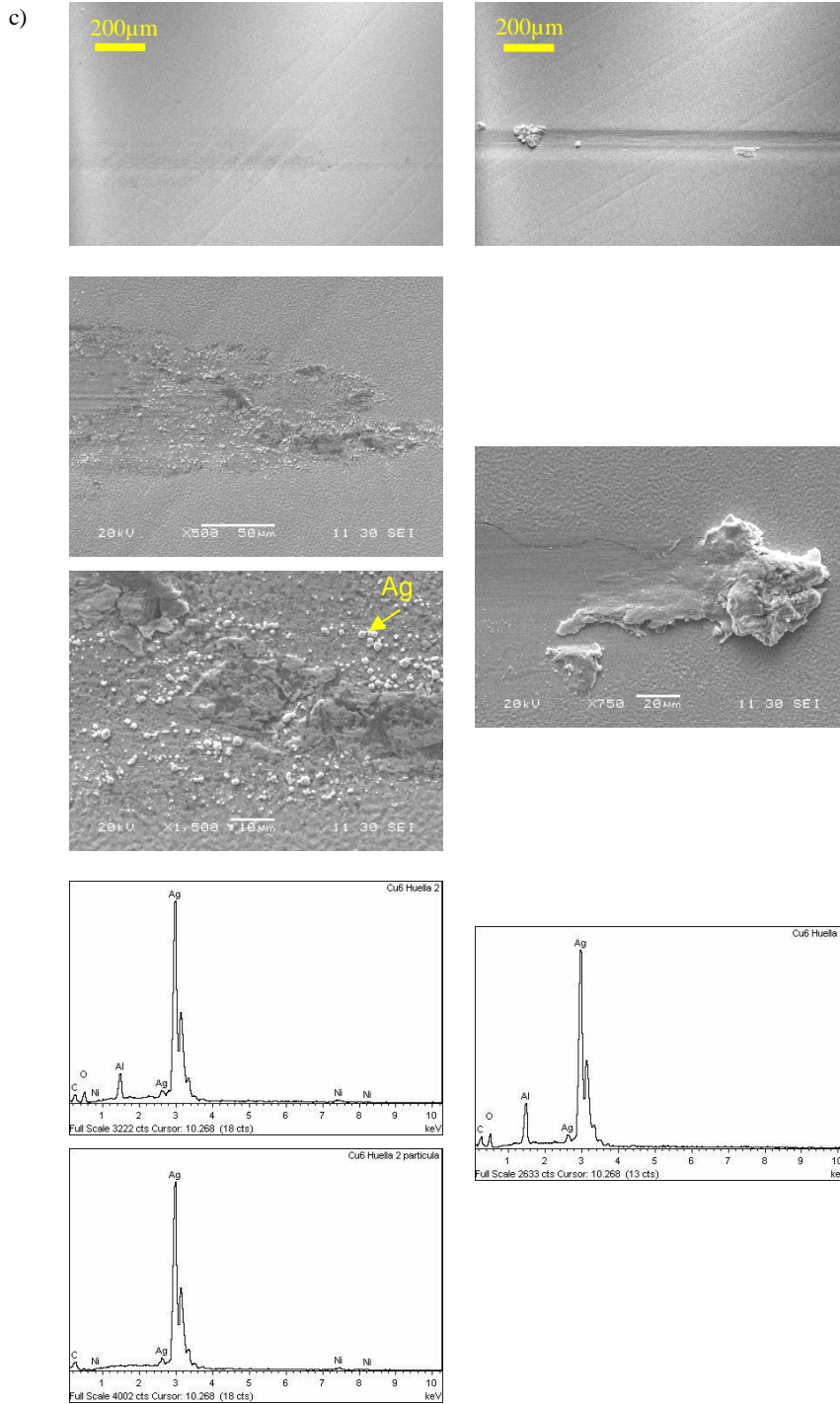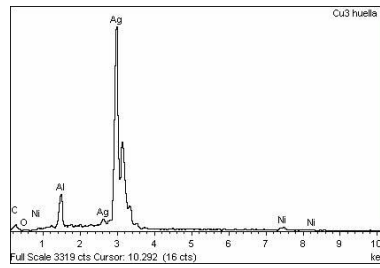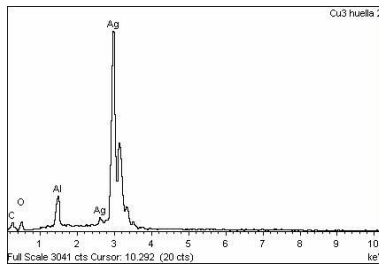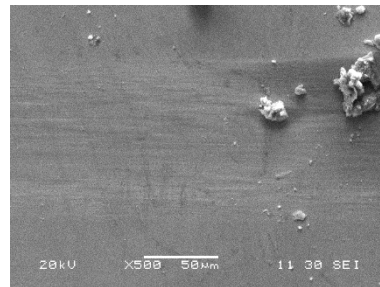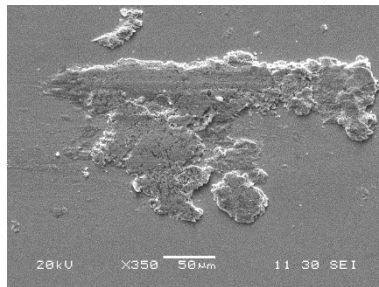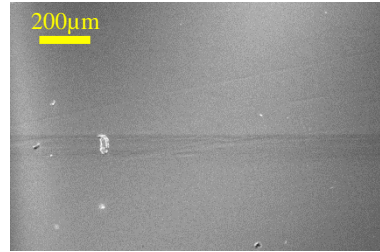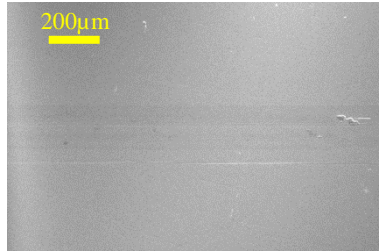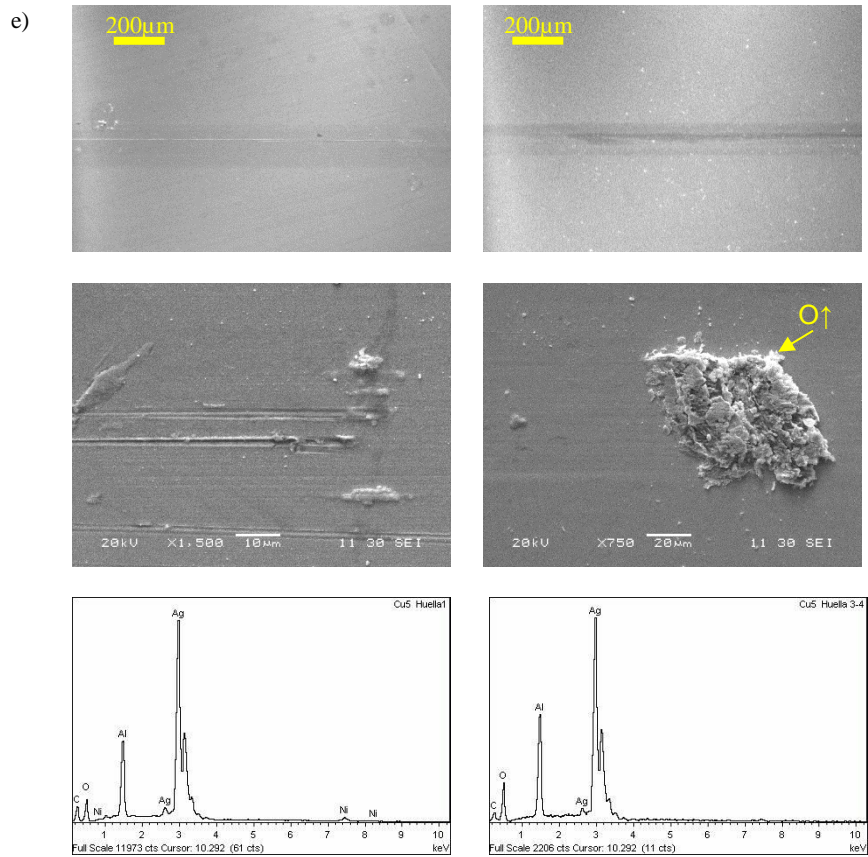
Figure 4.33. Scanning Electron Microscope images of the wear tracks (Secondary Electron Images; 20kV), under lubrication (left column) and in air (right column), after 30 cycles (two images above in each ref.; other than ref. Ag: after 20 and 5 cycles respectively), and magnifications of the wear track and debris (two or three images below in each ref.), and EDS spectra obtained in each wear track.
a)   ref. Ag; b) ref. Ag80Al20; c) ref. Ag78Al22T; d) ref. Ag78Al22; e) ref. Ag63Al37.

Table 4-4. Coefficient of friction (CoF) under oil and in air, wear rates and dynamic and static electrical contact resistance (ECR) for 2N contact load, as measured in air.

COF: average for the first 50 cycles; ▼:5 cycles in air and 20 cycles under oil for Ref. Ag; *: Long term average, 100 to 150 test cycles for ref. Ag63Al37 and Ag (with Ag coating already removed in ref. Ag); Standard deviation included as ± if more than one test data available.

Reference	CoF (oil)	Wear (mm³/Nm) x 10⁻⁹ (oil)	CoF (air)	Wear (mm³/Nm) x 10⁻⁹ (air)	Dynamic ECR (mΩ) (air)	Static ECR (mΩ) (air)
Ag▼	0.64 0.57±0.6*	83.3	0.96 0.67±0.1*	125.9	61	1.15
Ag80Al20	0.26±0.1	16.7	0.22	51.1	79	1.85
Ag78Al22T	0.35	17.4	0.42±0.2	137.2	62±0.0	1.52
Ag78Al22	0.22±0.3	10.9	0.20	35.0	64	1.08
Ag63Al37	0.17±0.2 0.24*	5.7	0.41±0.2 0.26*	6.5	63±0.3 0.64*	1.62

Comparing the quantitative and qualitative results for each coating depicted in Table 4-4 and Figure 4.33 respectively, the following points can be highlighted.

Under oil conditions the pure silver coating, **ref. Ag**, showed the highest wear rate by far, which caused the test to be prematurely terminated. In the case of in air test conditions, ref. Ag (together with ref. Ag78Al22T) showed the highest wear rates (Table 4-4). In ref. Ag under oil, the coating was already completely removed by cycle 20 (Figure 4.33a). In air tests, by cycle 5, the substrate, i.e. the nickel interlayer, was already visible. The surface of ref. Ag showed an adhesive wear mode, with plenty of coating material removed due to the shear stresses, both in air and under oil conditions (Figure 4.33a below). In both cases, deformed and thick lumps of material were pushed towards the ends of the sliding tracks, in accordance with observations elsewhere (Rudolphi and Jacobson 1997).

Ref. Ag did also show the highest CoF as compared with the AgAl coatings both under oil and in air, 0.64 and 0.96 respectively (Table 4-4). Once the Ag coating was removed, the CoF dropped from an average of 0.64 to 0.57 under oil and from 0.96 to 0.67 in air.

This performance is in accordance to that reported by other authors, where the initial coefficient of friction is highest, due to the increase in the contact area, with adhesive friction the main mechanism. This is followed by a reduction in friction, because wear particles in the contact area cause third body friction and the buildup of the surface oxide films (Song and Schinow 2015). Besides, in the case of pure Ag the prompt roughening by wear might had amplified the effect of the oil presence, which caused a reduction in CoF values as compared with the in air condition.

Along the tribological tests, ECR was also measured simultaneously with the CoF in the in air tests (Figure 4.34 to Figure 4.38). The average ECR obtained are detailed in Table 4-4 as dynamic ECR. Pure silver, ref. Ag, showed the lowest value, 61mΩ, as unlike in the other coatings, no aluminum oxide was present at the surface along the tests (Figure 4.34).
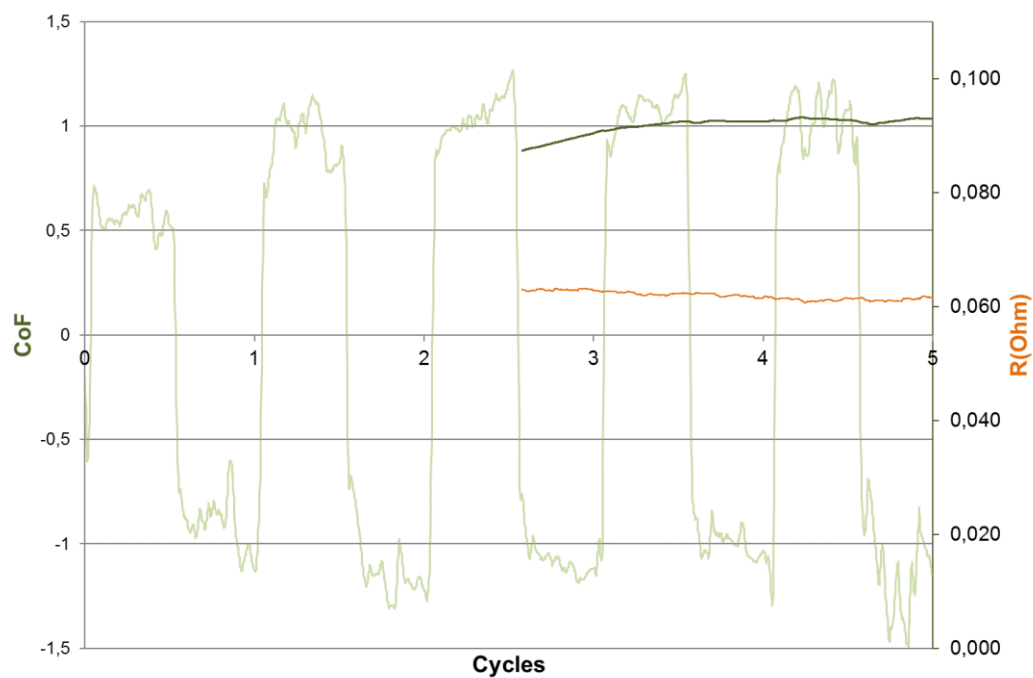
Figure 4.34. Left axis: evolution of the CoF of ref. **Ag** in air, raw data (light green) and average of 1000 absolute data points (dark green). Right axis: evolution of the ECR of ref. Ag in air, average of 1000 data points (orange).

On the other hand, the AgAl coatings saw overall a drop in both the wear rates and CoF, and an increase in the dynamic ECR.

Ref. **Ag63Al37** showed the highest wear resistance both under oil and in air test conditions, and the lowest CoF under oil, 0.17, but not under air, and a dynamic ECR similar to the other surfaces (other than Ag80Al20). In the case of Ag63Al37, an abrasive wear mode was present in both test conditions, with presence of grooves and scratches along the wear track (Figure 4.33e). In the case of the in air test wear tracks, the wear debris was oxidized, according to the EDS spectra (Figure 4.33e, right below). It should also be noted that due to the low wear rate of Ag63Al37, it took much longer to reach the steady CoF regime (Figure 4.35). For ref. Ag, Ag63Al37 the presence of oil also caused a reduction in CoF values. These results are in accordance with results previously reported, albeit corresponding to different tribological test conditions, where it was observed that the presence of the HCP phase is tribologically beneficial, causing a remarkable reduction of the friction as compared to values for the FCC and µ phases (Mao, Taher and Kryshtal, et al. 2016).
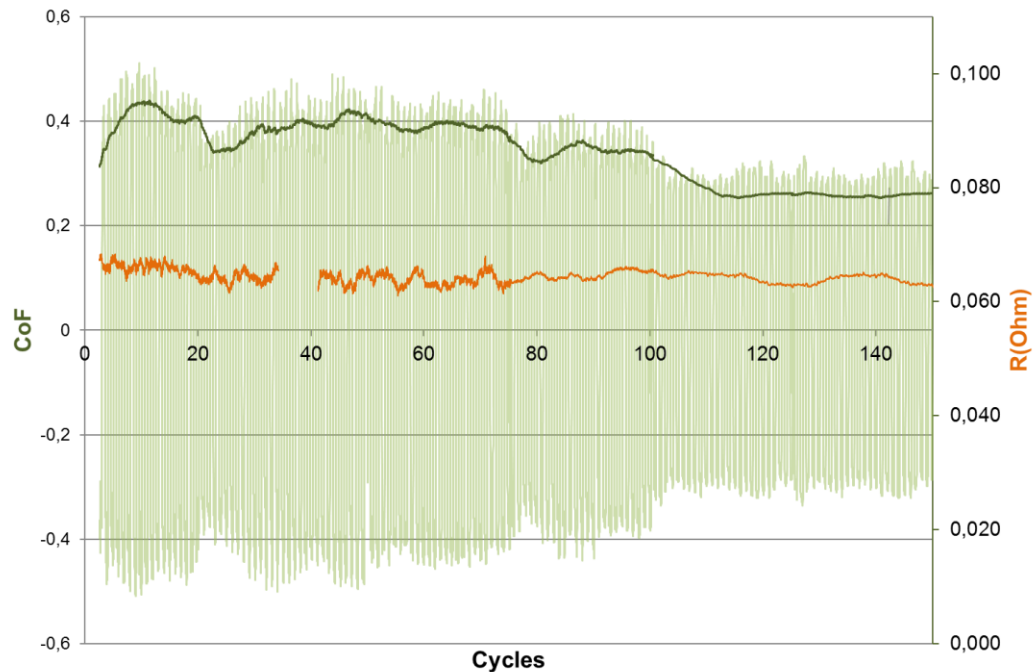
Figure 4.35. Left axis: evolution of the CoF of ref. **Ag63Al37** in air, raw data (light green) and average of 1000 absolute data points (dark green). Right axis: evolution of the ECR of ref. Ag63Al37 in air, average of 1000 data points (orange).

The high temperature coating deposition, and the associated change into cubic μ phase, had a deleterious effect on the wear resistance, i.e. **Ag78Al22T** showed higher wear rates than **Ag78Al22** both under oil and in air, though quite similar in air dynamic ECR (62 vs 64 mΩ) (Figure 4.36 and Figure 4.37). Actually, in air condition, wear rates for Ag78Al22T were close to that of ref. Ag. Under oil conditions, the presence of plenty of Ag rich particles were observed among the wear debris (Figure 4.33c; below left). Here, as has been mentioned elsewhere, a rougher surface, Ra 39 nm (Figure 4.16,Table 4-4), due to the high temperature coating deposition played also a role.
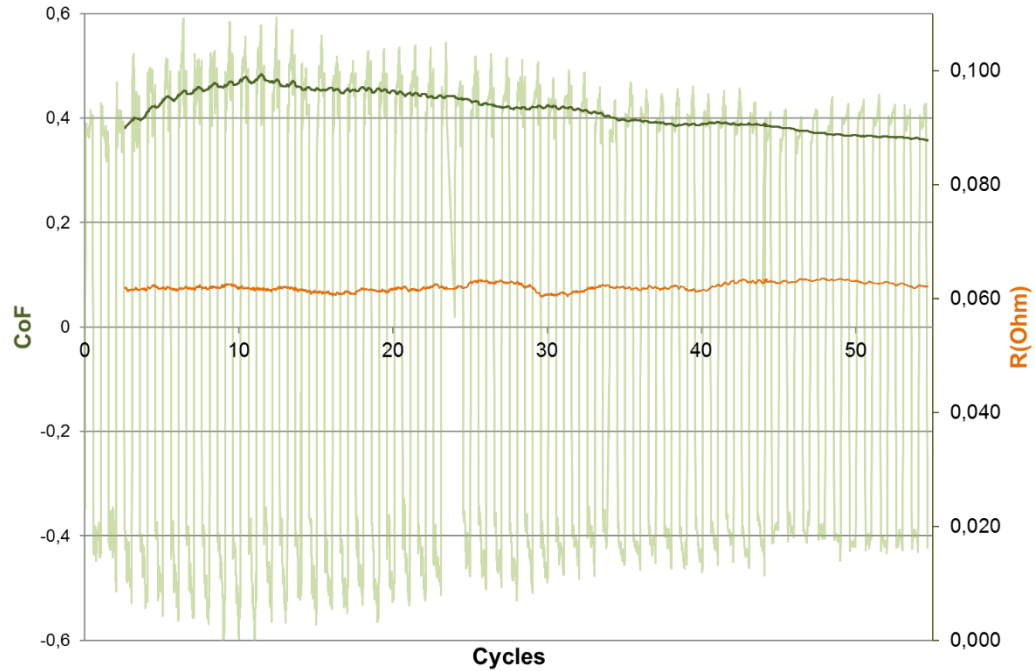
Figure 4.36. Left axis: evolution of the CoF of ref. **Ag78Al22T** in air, raw data (light green) and average of 1000 absolute data points (dark green). Right axis: evolution of the ECR of ref. Ag78Al22T in air, average of 1000 data points (orange).

Ref. Ag78Al22 showed less material adhesion than all references except Ag63Al37, with some in the under oil conditions and barely any in air conditions (Figure 4.33d). CoF in the case of Ref. Ag78Al22, unlike for the other coatings studied, showed no difference between in air and under oil conditions, corresponding to an intermediate behavior of that of ref. Ag63Al37 and Ag80Al20 (discussed next). On the other hand, for ref. Ag78Al22T (like ref. Ag and Ag63Al37) the presence of oil did cause a reduction in CoF values.
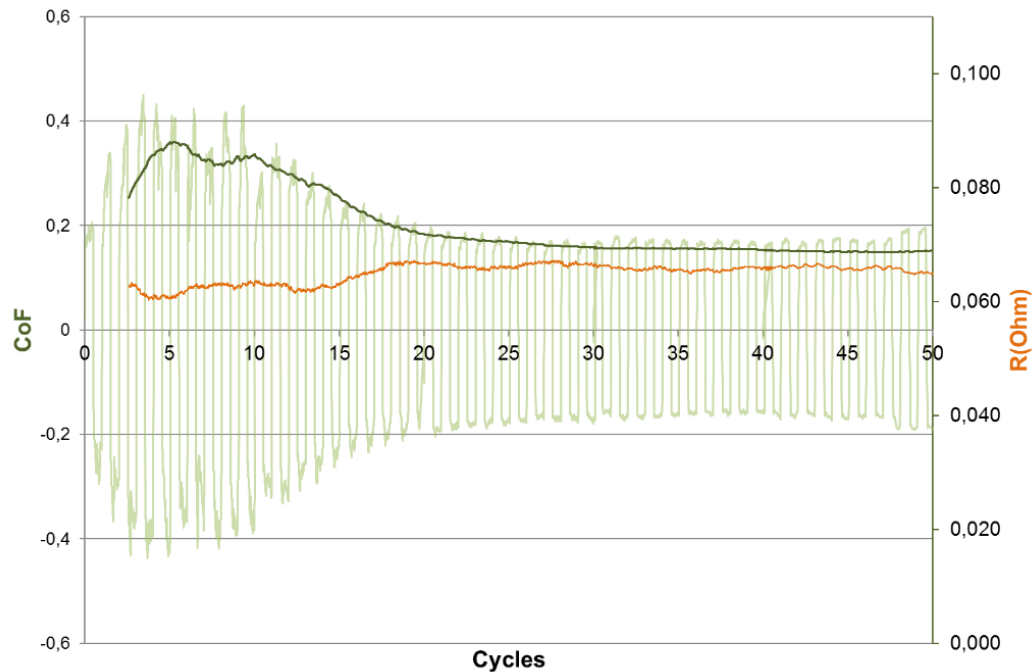
Figure 4.37. Left axis: evolution of the CoF of ref. **Ag78Al22** in air, raw data (light green) and average of 1000 absolute data points (dark green). Right axis: evolution of the ECR of ref. Ag78Al22 in air, average of 1000 data points (orange).

Ref. **Ag80Al20** showed an intermediate behavior, i.e. mostly adhesive wear mode under oil and a more abrasive wear mode in the air tests (Figure 4.33b). This trend was anyway present in all surfaces, i.e. a more adhesive wear mode under oil and a more abrasive mode in air. Whereas the wear rates under oil and in air and the CoF under oil for Ref. Ag80Al20 were intermediate, i.e. between those of ref. Ag and those of ref. Ag78Al22 and Ag63Al37, this was not the case for the CoF in air and the dynamic ECR in air.

This is linked to the fact that in the case of ref. Ag80Al20, a transition occurred from an adhesive wear mode under oil to a mildly abrasive mode in air. This caused the CoF in the former to be higher despite the presence of oil.

Ref. Ag80Al20 showed the highest in air dynamic ECR of all the coatings studied, and a low in air CoF (the lowest but for ref. Ag78Al22) (Figure 4.38). Concerning the in air

156

dynamic ECR, the oxide layer was not more abundant or thicker than in the other AgAl coatings, as assessed by EDS analyses, which showed a correlation between the O signal and the Al content of the coating alloy. Therefore, the larger ECR could be linked to a reduced surface contact, due to the deformation of the softer coating along the wear track (Figure 4.33b; right below), though the in air static ECR was also the largest for this coating.
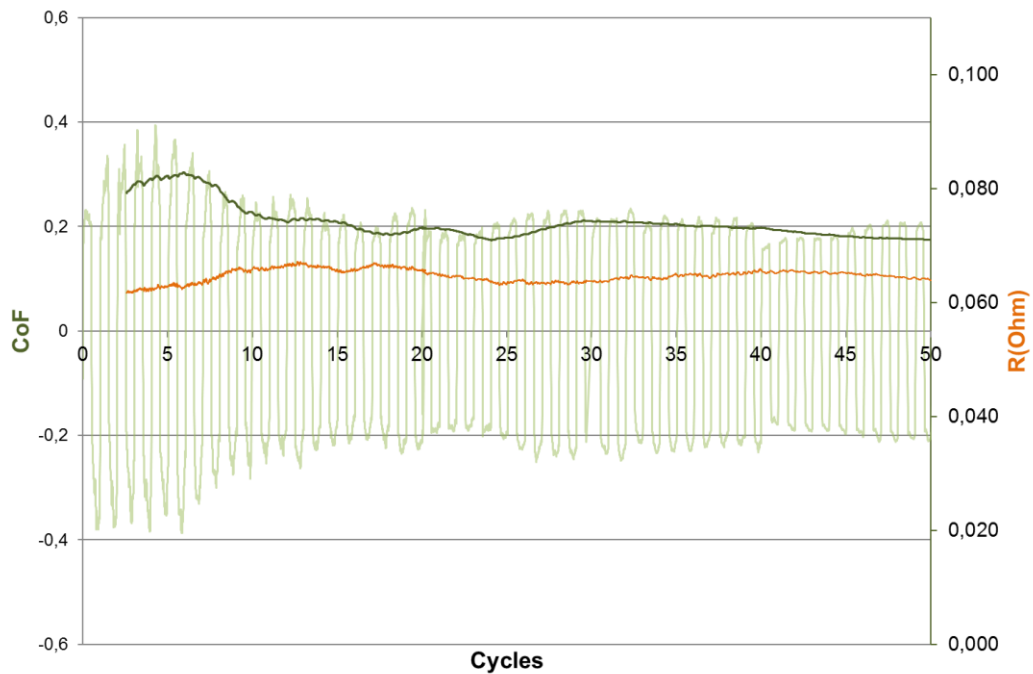
Figure 4.38. Left axis: evolution of the CoF of ref. **Ag80Al20** in air, raw data (light green) and average of 1000 absolute data points (dark green). Right axis: evolution of the ECR of ref. Ag80Al20 in air, average of 1000 data points (orange).

157

Additionally, Figure 4.39 and Figure 4.40 show the evolution of wear in the tests under oil and in air respectively. Wear is represented by the area (μm^2) of the worn-out section and the depth (nm) of the wear track. Each dot in these figures represents a wear measurement point, and the standard deviation value is provided when the measurements corresponding to two tests are available.
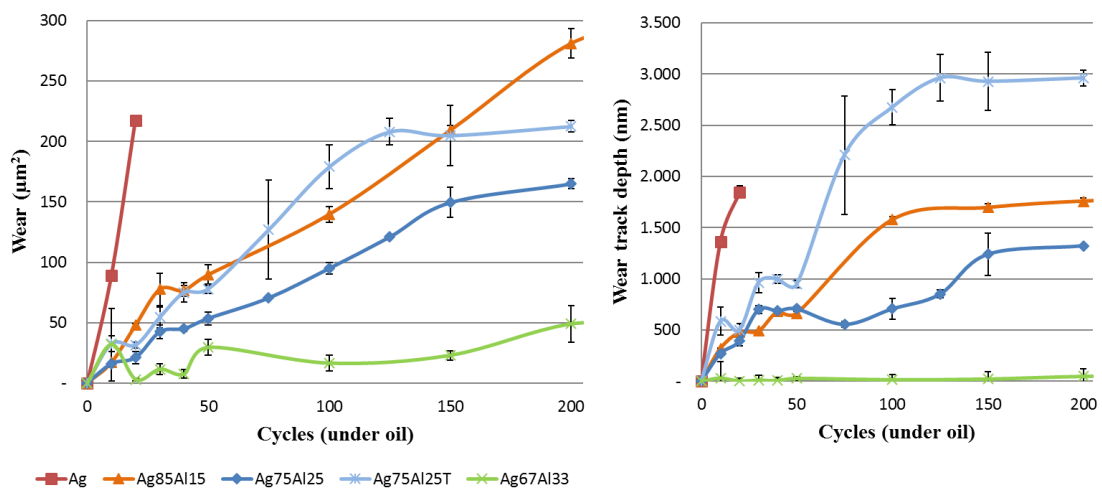
Figure 4.39. Average wear (μm^2; left) and wear track depth (nm; right), as measured by profilometry, vs. number of test cycles, **under oil** test conditions.
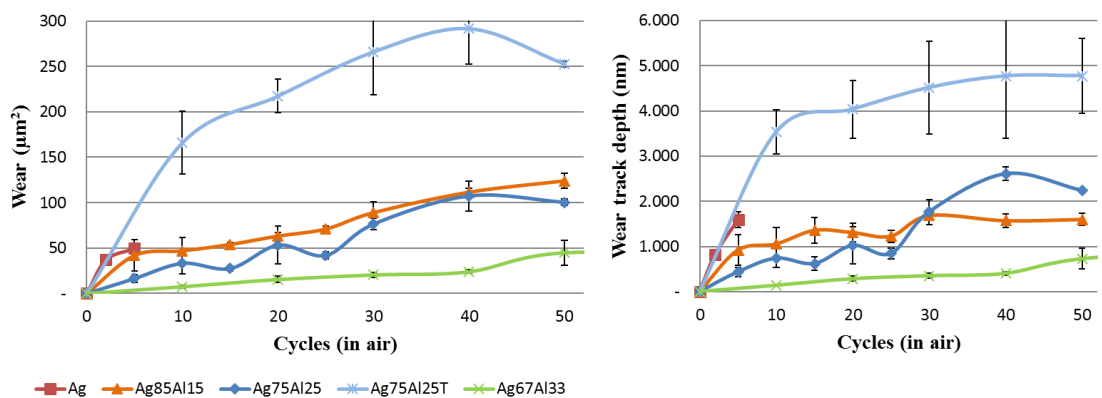
Figure 4.40. Average wear (μm^2; left) and wear track depth (nm; right), as measured by profilometry, vs. number of test cycles, **in air** test conditions.
NOTE: different number of cycles and depth scale than in Figure 4.39.

158

To sum up, comparing the CoF of the coatings in air and under oil, different trends were identified. In the case of ref. Ag78Al22T and Ag63Al37, the CoF under oil was lower than in air. On the other hand, Ag80Al20 showed slightly lower values in air. Ag78Al22 showed similar values in both conditions. This is related to the wear modes identified in each case. Wear rates in air were always clearly higher than under oil for each and every coating (Figure 4.39 and Figure 4.40). This was also evidenced in the scanning electron microscope (SEM) analyses of the wear tracks (Figure 4.33). Concerning dynamic ECR in air, the alloyed coatings showed an upward trend (Ref. Ag, 61mΩ as compared with 63 and 64mΩ for ref. Ag63Al37 and Ag78Al22), especially in the case of ref. Ag80Al20, with 79mΩ (Figure 4.34 to Figure 4.38).

Environmental tests.

Wear is not the only degradation mechanism that the coatings must endure in electrical sliding applications. Reaction with Sulphur present in the oil formulations or with humidity might also degrade the coatings. Alloys with two dissimilar metals in a conductive environment, e.g. under humidity, make up a galvanic couple, which can originate galvanic corrosion. This was in effect observed in the AgAl coatings in **salt spray tests,** following ISO 9227 with a salt solution flow in the 1.05 to 1.85 ml/h range, typically more severe than the field tests, where oxidation of aluminum was observed in the alloyed coatings at 24 and 48 hours (Figure 4.41): grey surfaces for AgAl alloy coatings with larger Al contents as compared with the white surface of ref. Ag.
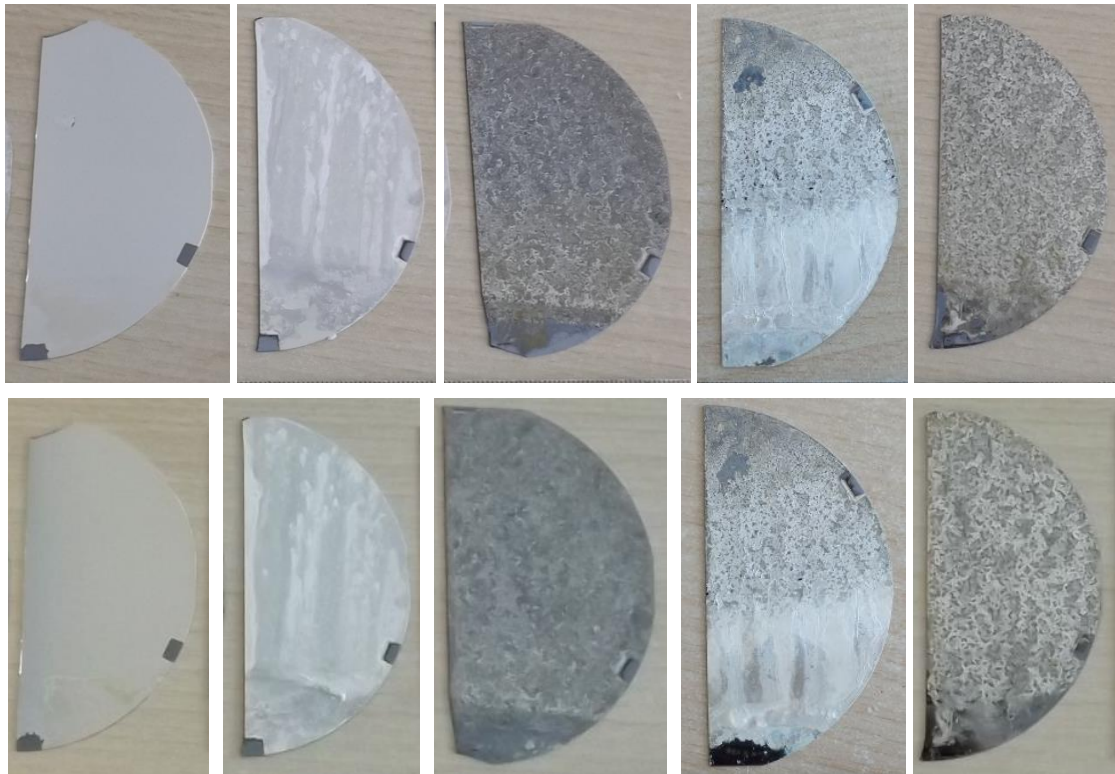
Figure 4.41. Aspect of the coatings on Si substrates after 24 (above) and 48 (below) hours in the salt spray tests: Ref. Ag, Ag80Al20, Ag78Al22T, Ag78Al22 and Ag63Al37 respectively (left to right).

However, sliding electrical contact will typically operate in controlled media, e.g. under insulating oil, not in humidity rich environments.

H$_2$S gas test is an accelerated test to assess the degradation in such an environment. The tarnishing produced by hydrogen sulphide have been reported to result in a surface layer of silver sulphide (Ag$_2$S) of diverse colors (yellow to brown to blue to dark), through reactions such as: $2Ag + H_2S + 1/2O_2 \rightarrow Ag_2S + H_2O$ (Graedel 1992), (Palomar, et al. 2016), (Wan, et al. 2015), (Myers 2009).

In the H$_2$S gas test performed (Figure 2.28), the coatings underwent different visual evolutions (Figure 4.42). The test arrangement, where samples were placed vertically above the solution, caused some of the samples to present a heterogeneous aspect.

Ref. Ag, Ag78Al22 and Ag78Al22T had already developed a tarnished surface in the early stages of the tests, by 24h. On the other hand, ref. Ag63Al37 tarnishing evolved along the test.

Ref. Ag became bluish due to some S uptake, (S:1.1wt% according to the EDS analysis. See spectrum at Figure 4.44,a). Moreover, ref. Ag80Al20 became grey-bluish, with uptake of both oxygen and sulphur (O:9.6-11.9 wt%; S:1.1-1.7 wt%; Al:5.3wt% according to the EDS analysis. See spectrum at Figure 4.44,b).

This was also observed on a larger scale on ref. Ag78Al22T, which showed a darker grey-bluish coloration from early stages, resulting in very little Al surface content and plenty of S uptake (S:10.5wt%; Al:1.25wt%. See spectrum at Figure 4.44,c) (Figure 4.43). Ag78Al22 became brown-bluish with uptake of both O and S (O:8.5wt%; S:1.3wt%; Al:4.4wt%. See spectrum at Figure 4.44,d), more like the surface of ref. Ag80Al20.

On the other hand, Ag63Al37 showed an evolution from light brown to intense blue, due to the progressive oxidation of the surface (O:7.7wt%; S<0.5 wt%; Al:12.3wt%. See spectrum at Figure 4.44,e) (Sampuran-Singh 1976).

Therefore, overall Ag63Al37 showed the highest resistance to Sulphur uptake, tough a gradual oxidation of the surface was observed.

Additionally, the following can also be highlighted:

- Coloring (yellowish/bluish) seems to be caused by a S-Ag reaction;
- darkening by oxidation of Al;
- bluish darkening seems to correspond to Ag-Al oxidation;
- and blistered surfaces are associated to areas rich in S-Ag (though they were not found in the pure Ag coating)

d)

e)
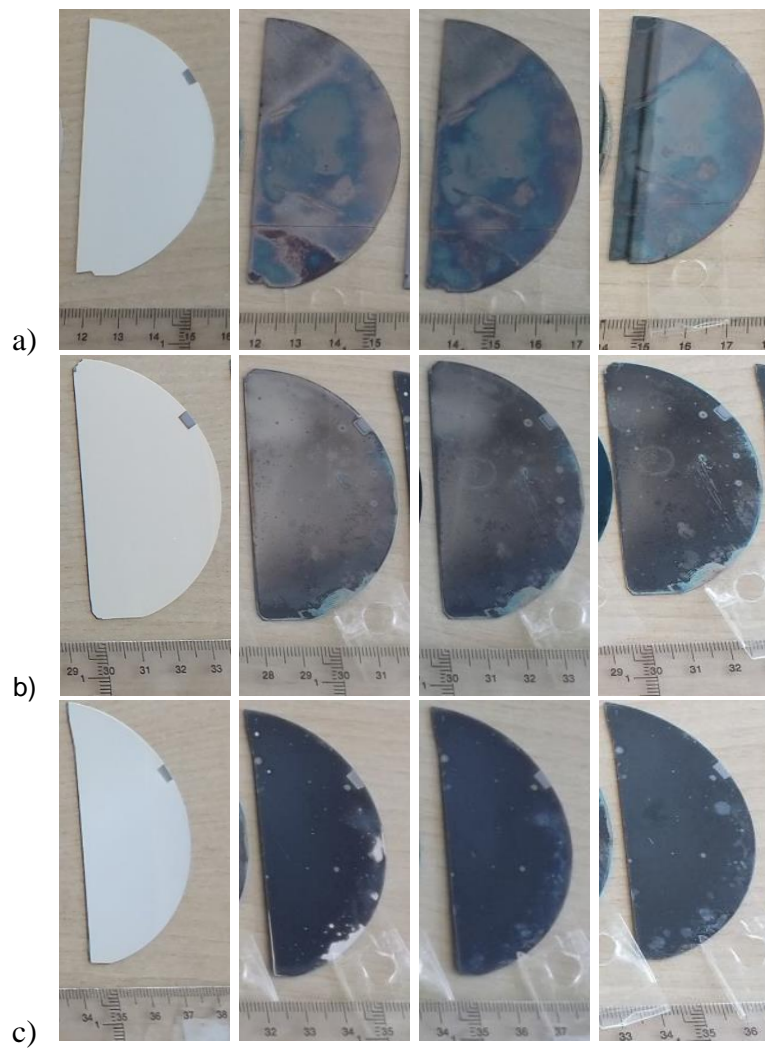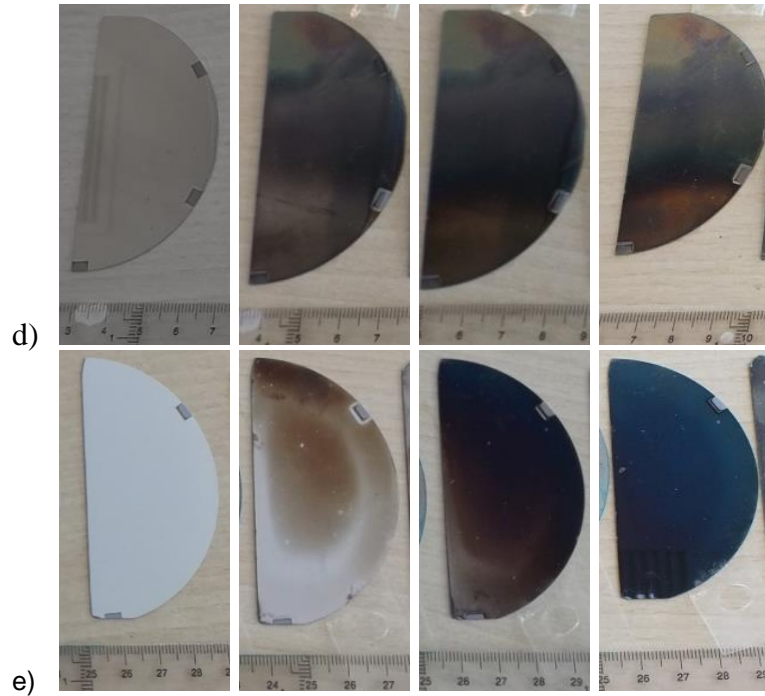
Figure 4.42. Sample a) ref. Ag; b) ref. Ag80Al20; c) ref. Ag78Al22T; d) ref. Ag78Al22;
e) ref. Ag63Al37, initially and after 24h, 48h and 72h of H_2S exposure (left to right).
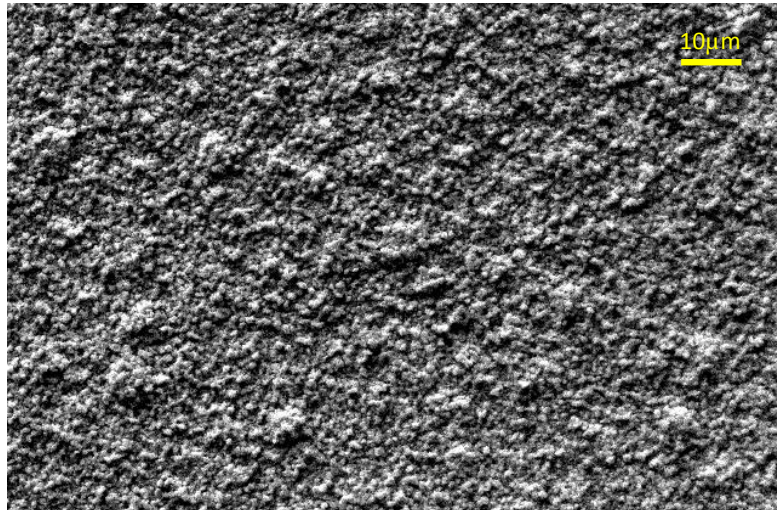
Figure 4.43. Scanning Electron Microscope image of the surface of ref. Ag78Al22T,
after 72 hours of H_2S exposure.
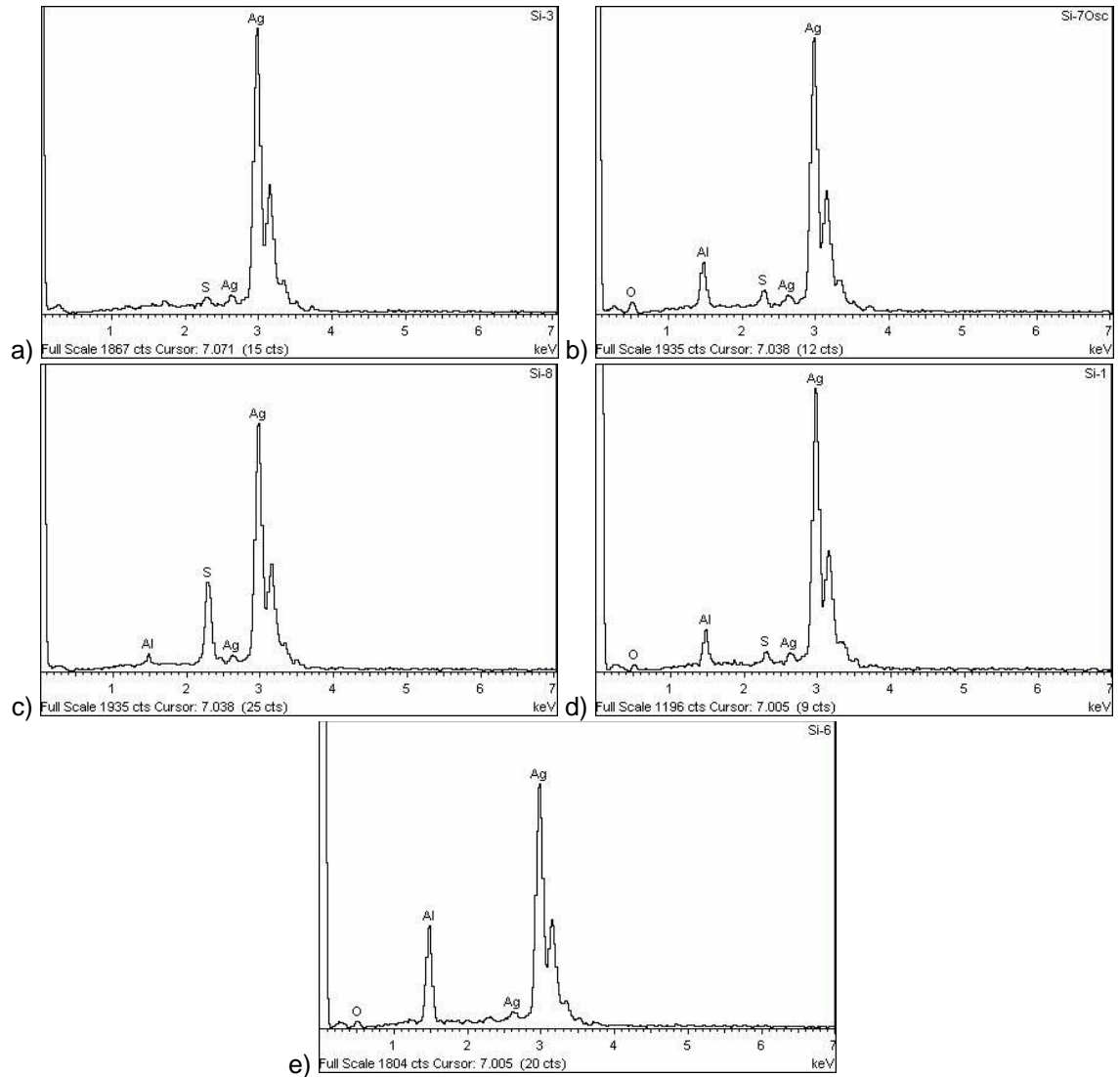
Figure 4.44. EDS spectra of the surface of a) ref. Ag; b) ref. Ag80Al20; c) ref. Ag78Al22T; d) ref. Ag78Al22; e) ref. Ag63Al37, after 72 hours of H_2S exposure.

As a complementary test, an **oil immersion test** was carried out, where the coatings were subjected to repeating thermal cycles for 30 days. The potential effect of the temperature (135ºC) on the coating phases was studied first by XRD (Figure 4.6; black lines in the spectra). It was observed that no changes occurred in ref. Ag, ref. Ag78Al22T, and ref. Ag63Al37. However, ref. Ag80Al20 and Ag78Al22 showed that for Al contents below 25 at%, the FCC phase decomposes to a mixture of Ag(Al) and μ-phase depending on the Ag content, and this should be considered in applications were the coatings are subjected to these temperatures.

After the oil immersion test cycles were completed, samples were removed from the test chamber (Figure 2.29), pictures were taken, and the surfaces were rubbed with dry soft paper tissue, removing the film of unknown products generated on the surface. The oil immersion test showed different degrees of degradation of the coatings (Figure 4.45).

This confirmed the superior resistance of ref. Ag63Al37 to degradation by reaction with components present in the oil, as had also been observed in the H_2S test. Both ref. Ag63Al37 and Ag78Al22 were shown to be prone to oxidation, but reaction with sulfur was limited. The reverse was the case with ref. Ag78Al22T, which showed the poorest performance in both tests. This is related to the high temperature coating deposition, that produced a roughened non-so-compact surface, that did not offer a good barrier protection, while the increase in the specific surface area offered a larger amount of possible reaction sites. The transformation into the μ-phase might have also played a role, though further investigations would be necessary to determine its precise effect.

c)

d)
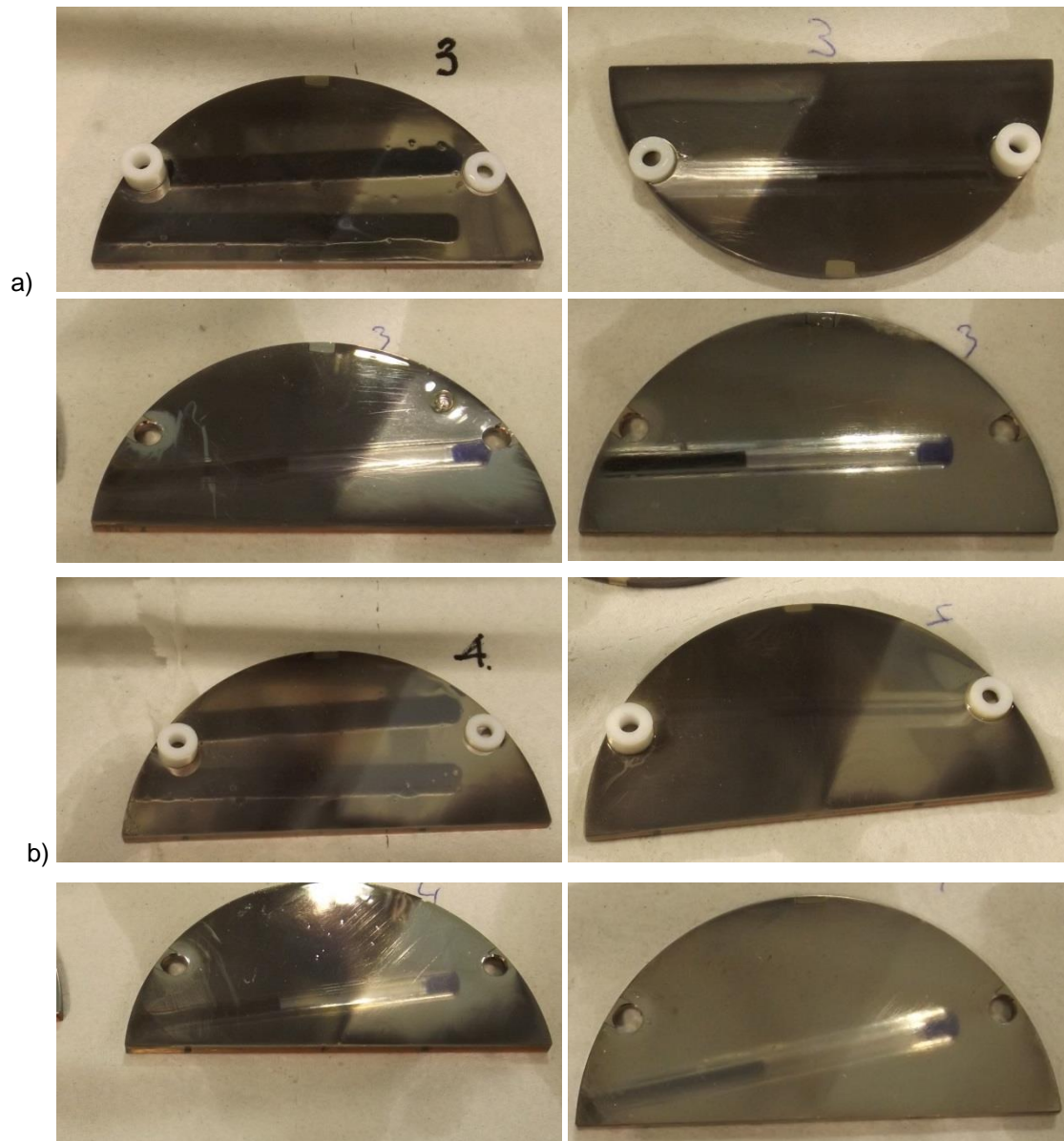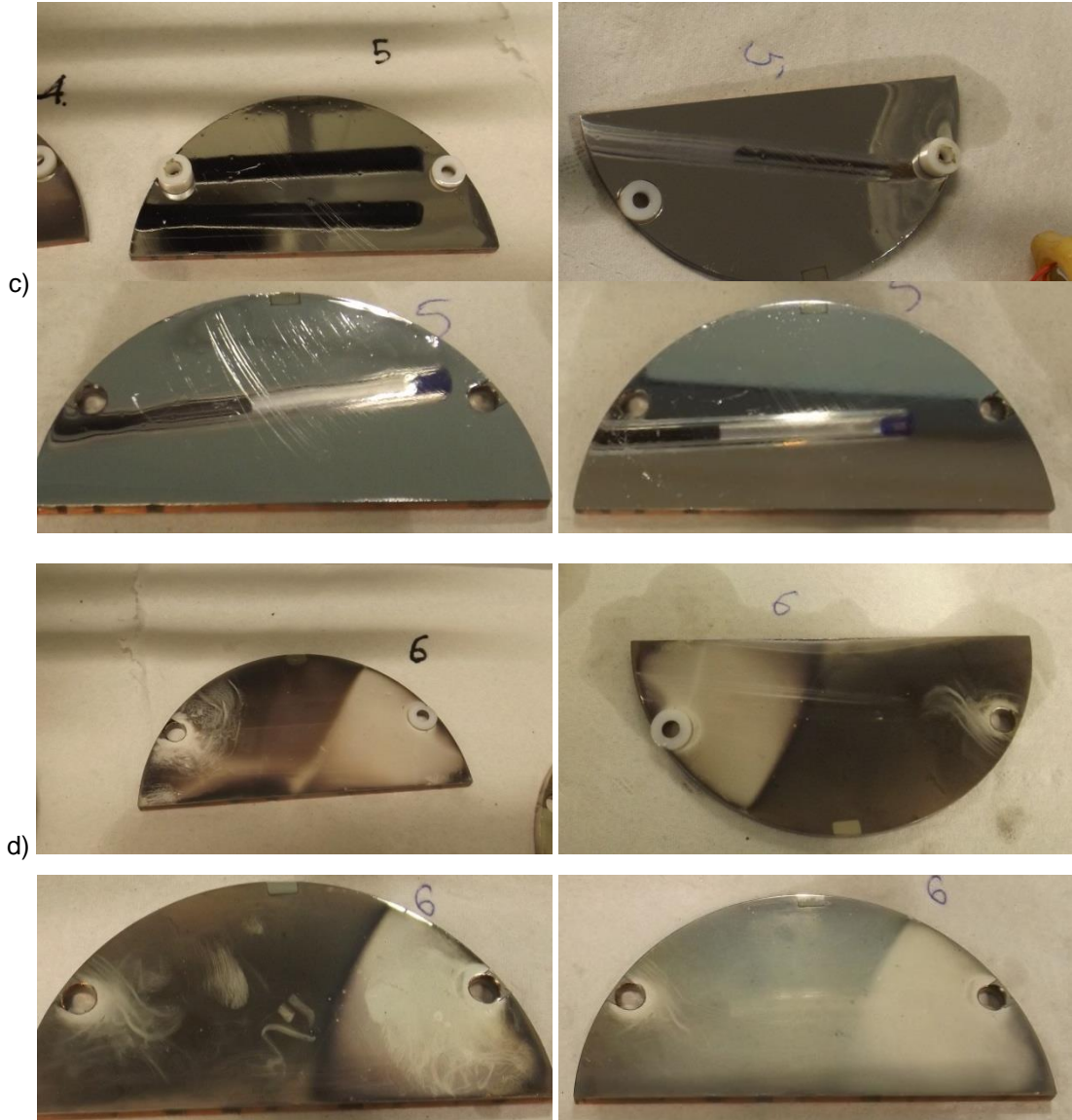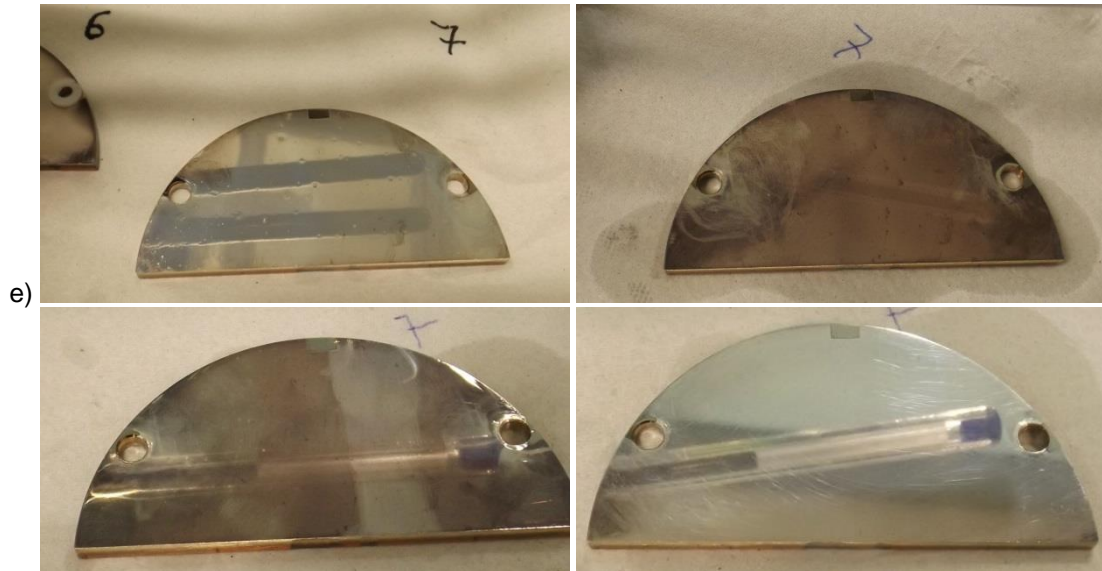
Figure 4.45. Aspect of the coated 3-inch diameter copper half discs samples after 11, 25, 30 test cycles and at the end of the oil immersion test (left to right, top to bottom). a) Ag78Al22; b) Ag80Al20; c) Ag63Al37; d) Ag78Al22T; e) Ag.

At the end of the test, the sample areas that have kept the brigthness were quantified:

Ref. 78Ag22Al ≈ 98%*

Ref. 80Ag20Al ≈ 75%*

Ref. 63Ag37Al ≈ no change

Ref. 78Ag22AlT ≈ 30%*

Ref. Ag ≈ 80%**

*: A light darkening was observed in the "shadowed" area.

**: sample at the top, i.e. no chance of shadowing.

Therefore, in terms of the areas that kept the brightness, i.e. were untarnished, ref. Ag63Al37 showed no change as compared with the initial aspect of the surface. Ref. Ag78Al22 was also mostly untarnished, i.e. 98% of the surface showed no loss of brightness, comparing with 80% in Ag reference. On the other hand, references ref. Ag80Al20 and ref. Ag78Al22T showed lower percentages of untarnished surface, i.e. 75% and 30% respectively.

So the less affected samples were:

Ref. 63Ag37Al < 78Ag22Al < Ag < 80Ag20Al < 78Ag22AlT

Additionally, the degree of degradation in the oil immersion tests was assessed in terms of the evolution of the static electrical contact resistance (ECR) (Figure 4.46, Table 4-4).

Overall, the oil immersion tests caused the **static ECR** of all surfaces to raise. This was observed mainly at low contact loads though, indicating the shallowness of the degradation effect caused by the test. In sliding electrical contacts, it should be expected that some of the components formed at the surface, such as oxides and sulfides, would be removed or worn out, thus minimizing their deleterious effect on the ECR.
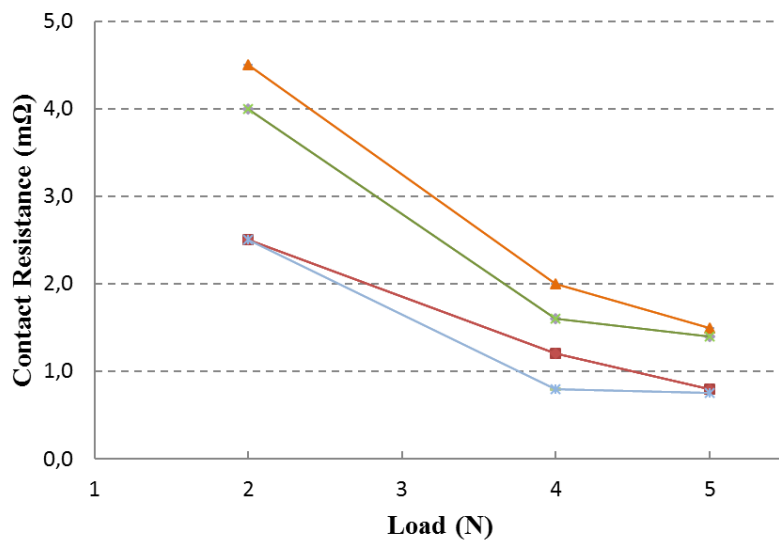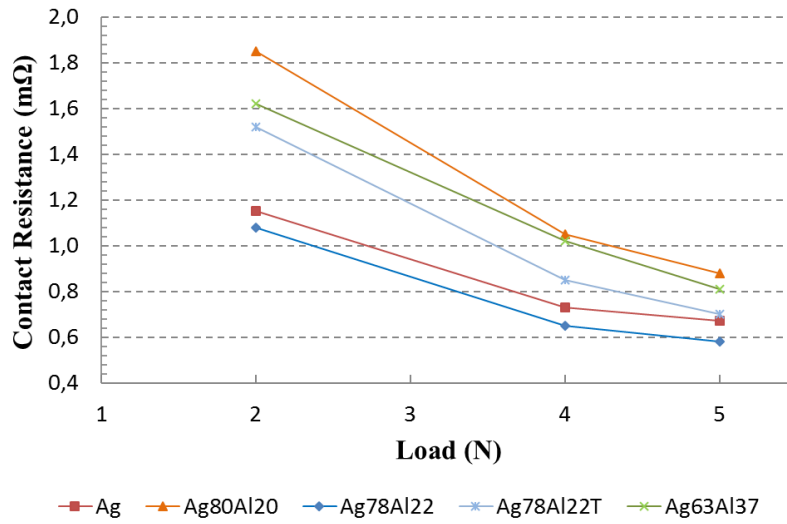
Figure 4.46. Static electrical contact resistance of the coatings, initially (above) and after the oil immersion test (below) (NOTE: different scales).

Along the tribological tests, ECR had also been measured together with the CoF, in the in air tests (Figure 4.34 to Figure 4.38). The average ECR obtained are detailed in Table 4-4 as dynamic ECR. All coatings showed larger ECR values in dynamic conditions than in static conditions. This is caused by a lower contact area due to wear and surface oxidation of the wear tracks, observed by the EDS analyses, during the tribological tests (Taher, et al. 2018). Pure silver, ref. Ag, showed the lowest value, 61mΩ, as no aluminum oxide was present at the surface along the tests. The ECR ranking in static and dynamic was similar, with an order of magnitude larger values in the latter condition.

It can be stated as a summary that sliding electrical contacts require materials that show good electro-tribological properties, together with long term resistance to degradation, either because of wear or reaction with sulfur present in insulating oils. The material typically used, silver, presents good electrical properties but poor tribology, and readily reacts to form deleterious silver sulfides.

On the other hand, silver aluminum alloy coatings have shown in the study presented in this section to improve the tribological properties of silver, both in terms of friction and wear. The latter, is even more remarkable under oil conditions, which corresponds to the operational conditions of many sliding electrical contact applications.

This performance of AgAl coatings is linked to the content of aluminum. The coatings with HCP microstructure over perform those with FCC microstructure. It has also been found that aluminum content can modify the wear mechanism from adhesive to a more erosive/abrasive mode. This is true for different Al percentages if the sliding occurs under oil or in air, occurring at lower Al contents under oil.

Additionally, aluminum content reduces the affinity of the alloy to sulfur. Specially in the case of a 37% of aluminum content, which corresponds to a fully HCP phase and the lowest wear rate observed among the tested alloys, the sulfur intake is greatly minimized (undetectable by EDS), although conversely the proclivity to oxidation rises.

Nonetheless, increasing the Al content results in an increase in the electrical contact resistance, especially in static conditions. This occurs though to a lesser extent in dynamic sliding conditions.

In this case, ECR values have provided insight about the operative performance of the coatings. Use of ECR as a monitoring tool, would have required more extensive studies, as the degradation of the surfaces under oil, because of sulphur and / or oxygen uptake takes much longer than in air conditions.

4.3. DIELECTRIC DLC COATINGS

4.3.1. THE DLC COATINGS.

As mentioned previously, the Diamond Like Carbon coatings were deposited on electrical grade mirror polished copper disks (50mm in diameter and 5 mm thick; Cu-Etp EN-13601 R250; Bronmetal, Spain), and in 8 x 40mm silicon coupons.

Prior to the DLC coating deposition, the copper surface was sputter cleaned with argon. Then, an intermediate 0.1 μm thick WC-6%Co interlayer was deposited to improve the adhesion of the DLC coating to the copper substrate. Subsequently, hydrogenated amorphous carbon (α-C:H) DLC coatings were deposited in a CEMECON CC800/8 plus (Germany) Physical Vapor Deposition Magnetron Sputtering (PVD-MS) unit (Figure 2.13), with acetylene (C_2H_2) as the carbon source gas, at low temperature (<150ºC), for a deposition time of 110 minutes. Coating deposition parameters are detailed in Table 4-5.

Table 4-5. DLC coating deposition parameters.

Reference	V_{BIAS} (V)	Ar:C_2H_2 (mLN)	Pressure (mPa)
#DLC	5-10	100:50	450
#DLCCH	5-10	100:**100**	460
#DLCVB	**150**	100:50	450

Properties of the deposited DLC coatings are detailed in Table 4-6 and Table 4-7. Reference **#DLC** presented a coating thickness of 0.58 μm (including a 0.1 μm thick interlayer), an sp3 ratio of 0.47 and an initial contact angle of 69.4º, that dropped to 63.5º after one minute. The coating surface roughness was Ra 18 nm.

In comparison, coating reference **#DLCCH** was thicker 1.3μm (including a 0.1 μm thick interlayer), presented a lower sp3 ratio of 0.44, but larger contact angle, 78.4º. The coating roughness was similar: Ra 18 nm. Therefore, an increase in acetylene in the

gas mix during the coating deposition, increased the coating thickness, but produced a more hydrophobic and softer coating.

Concerning the **ref. #DLCVB** coating, the thickness was like that of ref. #DLC, i.e. 0.52 µm (including a 0.1 µm thick interlayer), the sp3 ratio at 0.43 was even lower than in ref. #DLCCH, and the contact angle measured was 76.4º. On the other hand, the coating was rougher than the other references, with Ra 81 nm. Therefore, an increase in the applied voltage bias during the coating deposition, increased the coating roughness and the hydrophobicity, but produced an even softer coating.

The differences in the coating compressive residual stresses were also significant, with both higher applied voltage bias and larger acetylene in the gas mix producing less stressed coatings. On the other hand, in all cases the wettability increased with the time (Table 4-6).

Table 4-6. DLC coating characteristics.

Reference	sp3 (%)	e (µm)	Ra (nm)	Residual stress (MPa)	Contact angle (º) t=0	t=60s	Coating life t $_{ABC}$ (cycles)
#DLC	47	0.58	18	-16.9	69.4±1.6	63.5±2.0	48,000
#DLCCH	44	1.33	18	-8.3	78.4±1.9	70.5±0.5	161,000
#DLCVB	43	0.52	81	-2.5	76.4±2.9	65.1±3.9	58,000

Table 4-7. Raman analyses results of the DLC coatings (Robertson 2012) (Ferrari and Robertson 2000).

	D		G				sp3 fraction (%) as per Roberson	
	Centre (cm^{-1})	Area	Centre (cm^{-1})	Area	ID/IG	I(D)/I(G)	**I(D)/I(G)**	G peak position
#DLC	1376	3,19E+06	1548	4,85E+06	0,37	0,66	**0,47**	0,36
#DLCCH	1404	4,83E+06	1553	6,30E+06	0,48	0,767	**0,44**	0,34
#DLCBV	1371	3,84E+06	1547	4,66E+06	0,44	0,82	**0,43**	0,37

NOTE: ID/IG D and G peak intensity ratios.
I(D)/I(G) D and G area ratios.

4.3.2. ELECTRO-TRIBOLOGICAL STUDIES OF THE DLC COATINGS.

The electro-tribology studies in the case of the DLC coatings were performed against 6 mm diameter aluminum (99,7%) balls, on a pin-on-disk (PoD) configuration, in controlled humidity environments, with a Microtest MT4002 tribometer (Microtest S.A. Figure 2.22), the same equipment used in the studies of the coatings and surfaces previously presented.

Also, as in the former tests, the evolution of the Coefficient of friction (CoF) and Electrical Contact Resistance (ECR) were continuously monitored. The main test conditions consisted of a load of 3N and a speed of 50 cm/s. The tests were carried out at room temperature.

Electro-tribological behavior of the different variations of DLC coatings were studied, including different humidity conditions. Unlike in the case of studies of electrically conductive counterparts, the electrical current was not a key parameter in these studies (Chen, et al. 1997), because all studied DLC coatings were dielectric. The evolution of the electrical contact resistance and the coefficient of friction in the tests, typically presented many distinct phases. These are depicted as regions A, B, C, D and E in Figure 4.47, Figure 4.49, and Figure 4.51.

In the case of **ref. #DLCCH**, an initial phase, where the CoF increased and the ECR stayed high (above the measuring limit of the equipment) can be associated to the wear of the aluminum ball and the corresponding enlargement of the contact surface (Region A in Figure 4.47). In the ensuing phase, the contact area and pressure stabilized, a DLC transfer layer formed in the aluminum counterpart (Figure 4.48), some mild adhesive wear occurred, but both the CoF and ECR remained steady (Region B inFigure 4.47).

Next, cracks began to appear in the coating, and the ECR decreased gradually, with the CoF becoming less steady (Region C in Figure 4.47Figure 4.51). As the cracks progressed and the adhesion of aluminum increased, facilitated by the openings and increasing roughness in the outer DLC surface, sections of the coating spalled off, and the ECR began to fell remarkably. In this phase, the surface lost its dielectric character,

and thus could be considered no longer operational in many applications (Region D in Figure). Actually, crack formation and propagation was already identified as one of the potential degradation mechanisms of dielectric DLC coatings in fatigue damage sensors (Wang, et al. 2013).

In the final stage, significant transfer of material between ball and disk occurred, the interlayer and substrate were reached in certain points, which eventually get oxidized. This was accompanied by fluctuations in both the CoF and ECR. The more intense of these involved a drop in the CoF and a surge in the ECR values, which can be ascribed to the transfer and formation of fully covering DLC layers in the aluminum counterparts. Besides, oxidation of the exposed areas in the copper substrate originated the ECR to increase (Region E in Figure 4.47).

Figure 4.47. ECR (Ω; logarithmic scale on the left vertical axis; in blue) and CoF (right vertical axis; in red) evolution of ref. #DLCCH coating against aluminum along the test cycles (horizontal axis). 50% RH. NOTE: Shadowed blue area on the left upper side indicates electric contact resistance values above the upper limit of the ohmmeter.

Figure 4.48. Micrographs of the wear track on the Al ball sliding against coating ref #DLCCH after the electro-tribology test.

Concerning coating **ref. #DLCBV**, the run-up performance (Region A in Figure 4.49) was different to the other coatings, i.e. the CoF did not rise, but decreased. This reflects the softer and rougher character of this coating. In this phase mild wear caused the surface to smoothen, and a graphite rich transfer layer was formed in the aluminum counterpart (Figure 4.50). The lower sp3 content, i.e. more graphitic nature of this coating was actually reflected in a lower CoF as compared with the other coatings all along the test.

Coatings ref. #DLCBV and #DLC being thinner than #DLCCH, phase C was reached in fewer test cycles (Region B-C in Figure 4.49) in these cases. On the other hand, ref. #DLCBV presenting lower internal stresses caused a lesser occurrence of cracks and spalling off of the coating, which translated in a less abrupt drop in the ECR values (Region D-E in Figure 4.49). The fact that ref. #DLCBV and #DLC were thinner also originated an overlap of phases D and E, as the spall off of sections of the coating did reach the interlayer and the substrate easier and faster.

Figure 4.49. ECR (Ω; logarithmic scale on the left vertical axis; in blue) and CoF (right vertical axis; in red) evolution of ref. #DLCVB coating against aluminum along the test cycles (horizontal axis). 50% RH. NOTE: Shadowed blue area on the left upper side indicates electric contact resistance values above the upper limit of the ohmmeter.
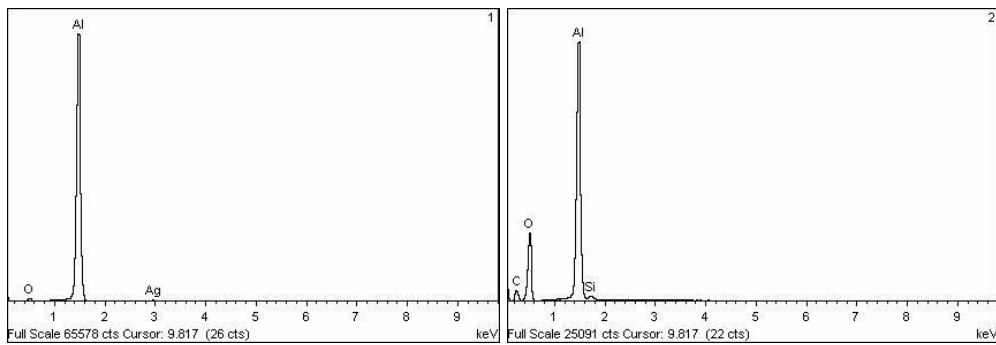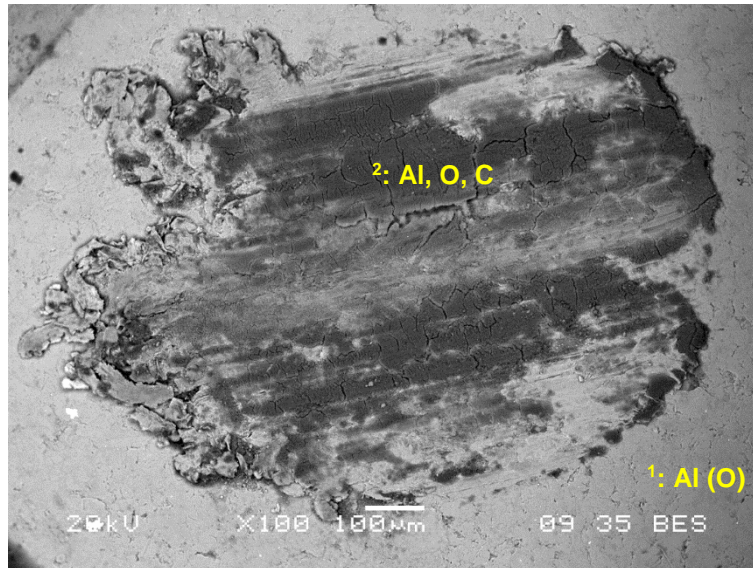
Figure 4.50. SEM image (Backscattering spectrometry) of the wear track on the Al ball against coating ref. #DLCVB (above) and EDS spectra at selected points, outside the wear track (1) and in the wear track (2) (below).

Finally, **ref #DLC** showed a run up and abrupt ECR drop phases like that of ref #DLCCH (Regions A and D in Figure 4.51), but shorter coating life and an overlap of phases D and E like ref. #DLC (Regions B-C and D-E in Figure 4.51).
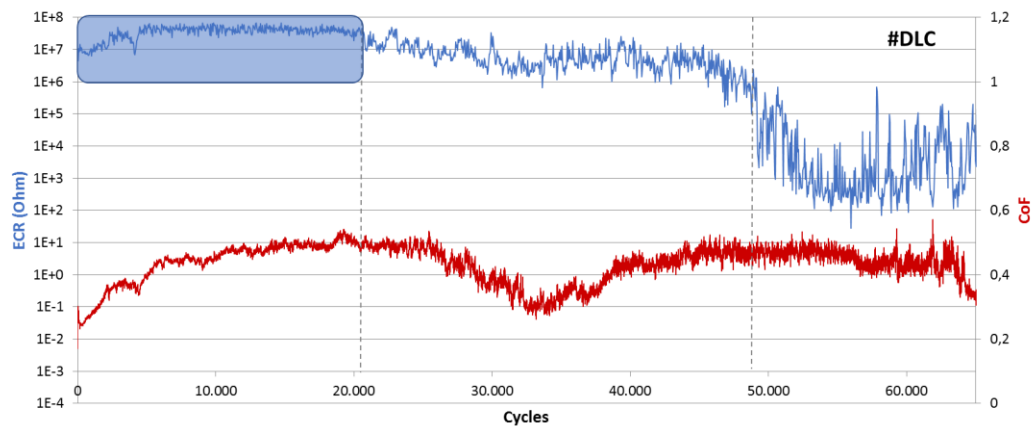
Figure 4.51. ECR (Ω; logarithmic scale on the left vertical axis; in blue) and CoF (right vertical axis; in red) evolution of ref. #DLC coating against aluminum along the test cycles (horizontal axis). 50% RH. NOTE: Shadowed blue area on the left upper side indicates electric contact resistance values above the upper limit of the ohmmeter.

Figure 4.52 to Figure 4.54 and Figure 4.55 to Figure 4.57 show OM and SEM images respectively of the wear tracks on the coatings after the wear tests. The backscattered SEM images in Figure 4.55 to Figure 4.57 show 4 distinct tones: black, corresponding to adhered aluminum, dark grey corresponding to the copper substrate, light grey corresponding to the DLC coating and in white the WC interlayer.

Cracks can be observed (1 in Figure 4.52 to Figure 4.54 and Figure 4.55 to Figure 4.57), especially in ref. #DLCCH and #DLC, which present the largest residual stresses. Actually, the lower the residual stresses the smaller the cracks in the images.

There are also plenty of coating spall offs, that often can be associated with the presence of cracks, which expose either the WC interlayer or the copper substrate (2 and 3 respectively in Figure 4.52 to Figure 4.54 and Figure 4.55 to Figure 4.57).

Finally, lots of adhered aluminum can be observed as well (4 in Figure 4.52 to Figure 4.54 and Figure 4.55 to Figure 4.57).

b
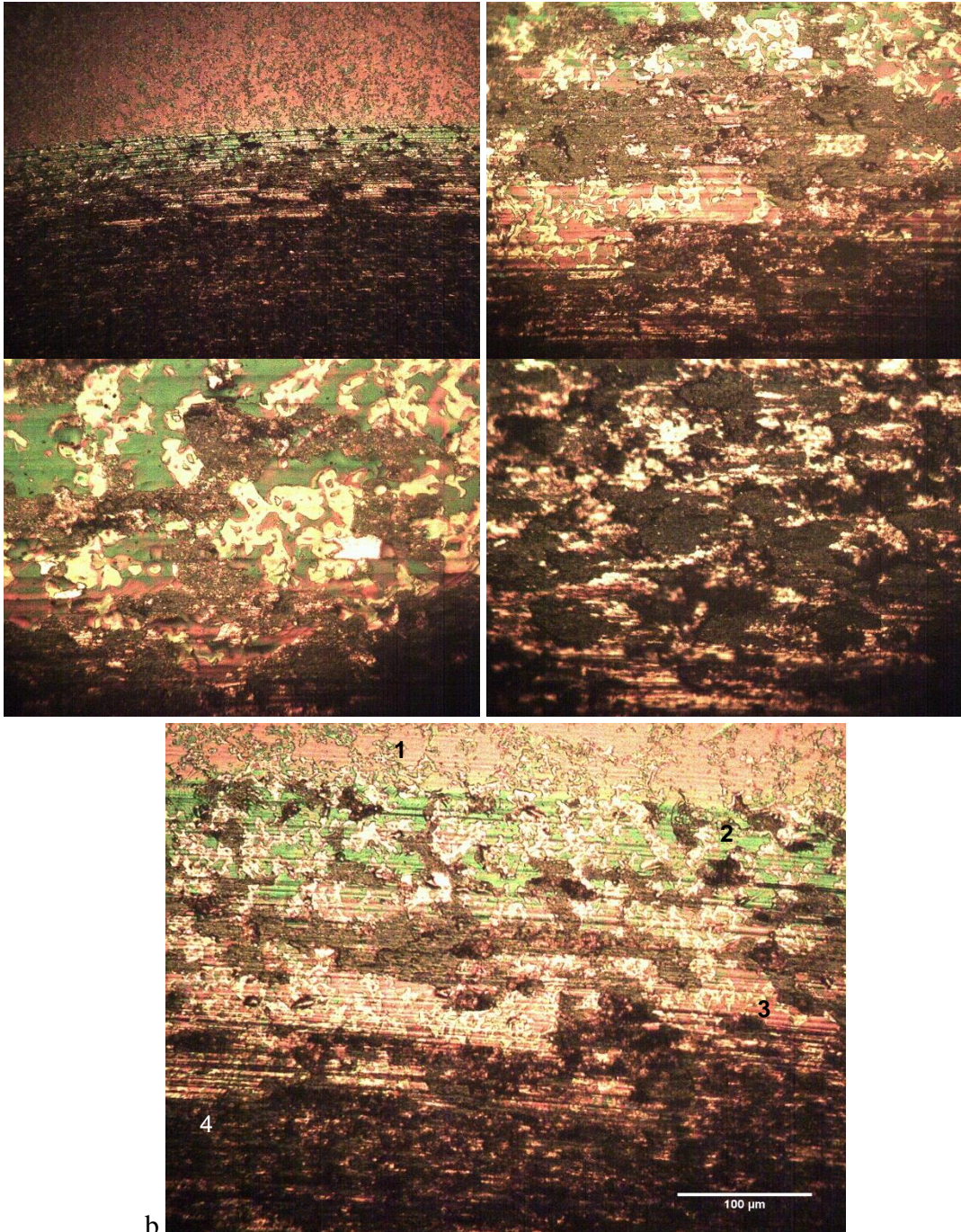
Figure 4.52. Micrographs of the wear track of coating ref. #DLCVB after the electro-tribology test (1: cracks; 2: interlayer; 3: Cu substrate; and 4: Al adhesion).
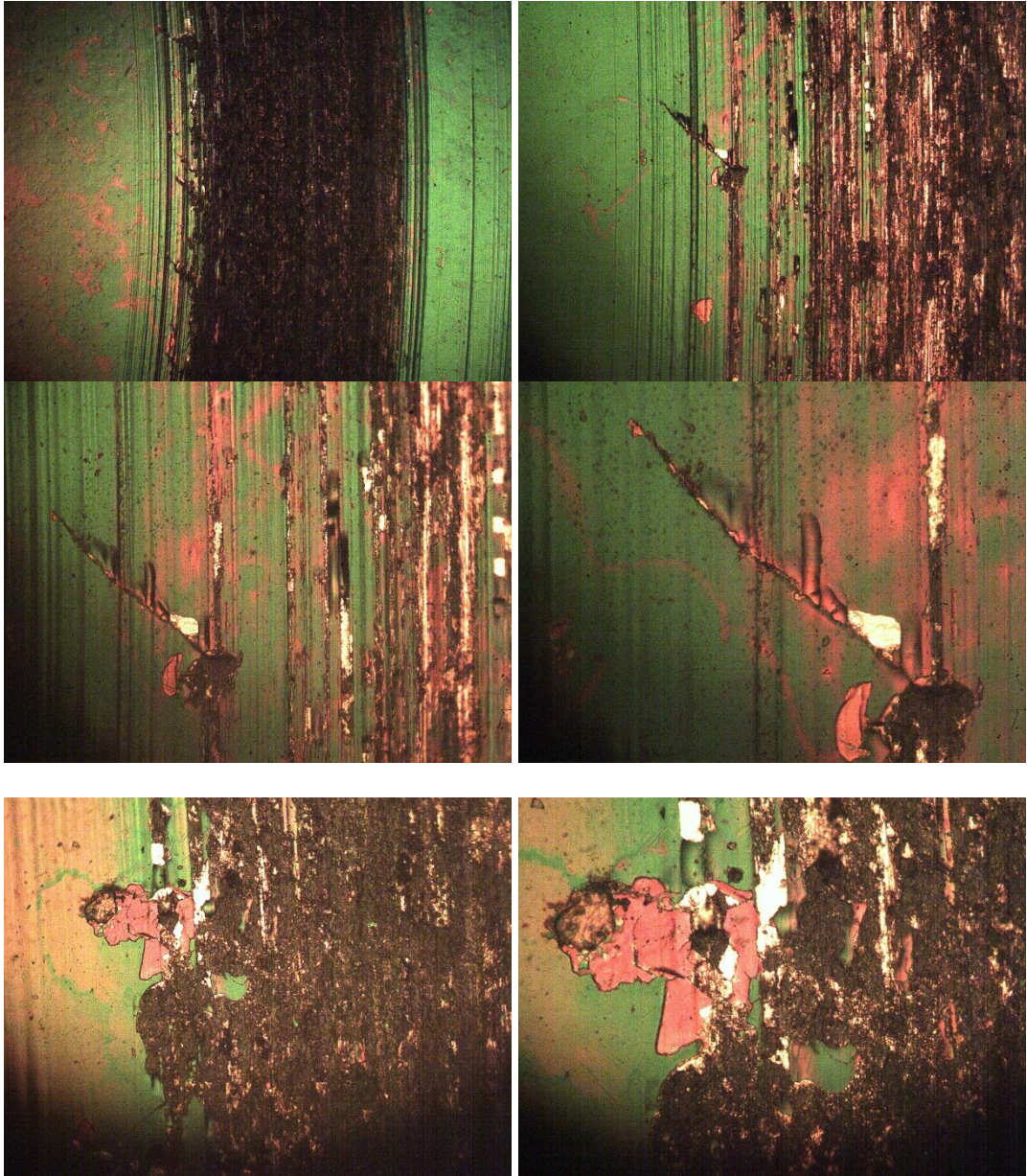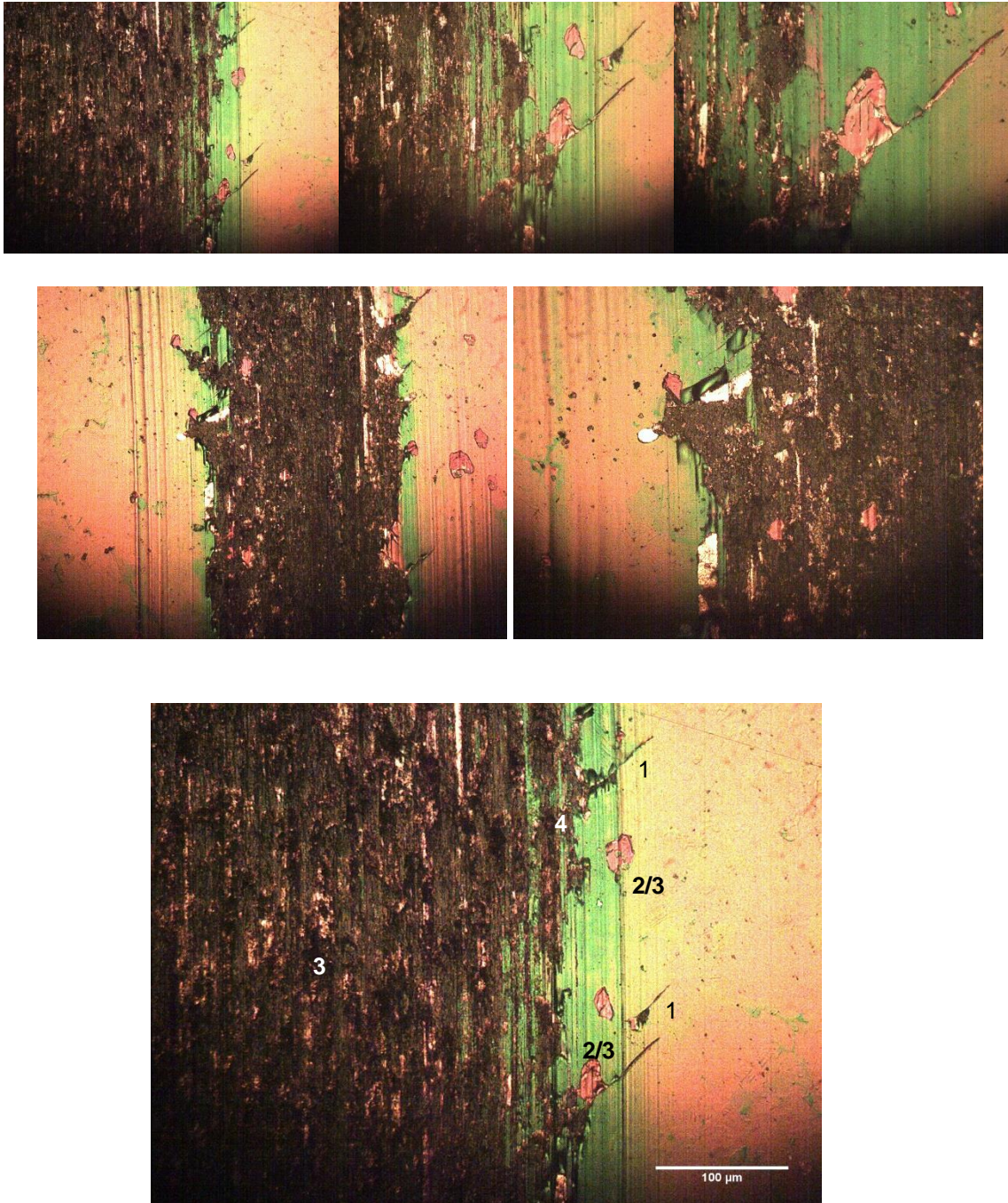
Figure 4.53. Micrographs of the wear track of coating ref #DLCCH after the electro-tribology test (1: cracks; 2: interlayer; 3: Cu substrate; and 4: Al adhesion).
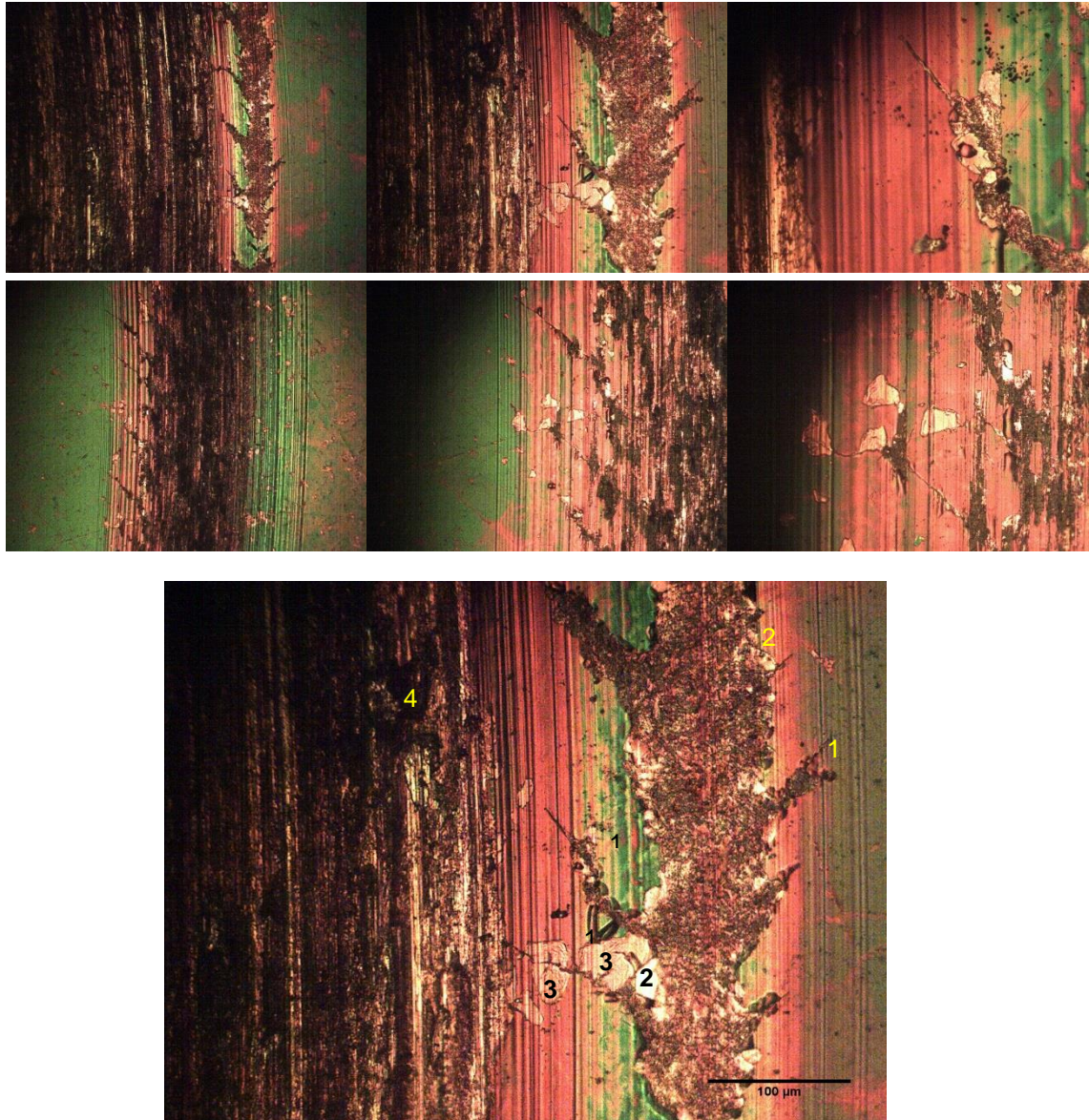
Figure 4.54. Micrographs of the wear track of coating ref. #DLC after the electro-tribology test (1: cracks; 2: interlayer; 3: Cu substrate; and 4: Al adhesion).
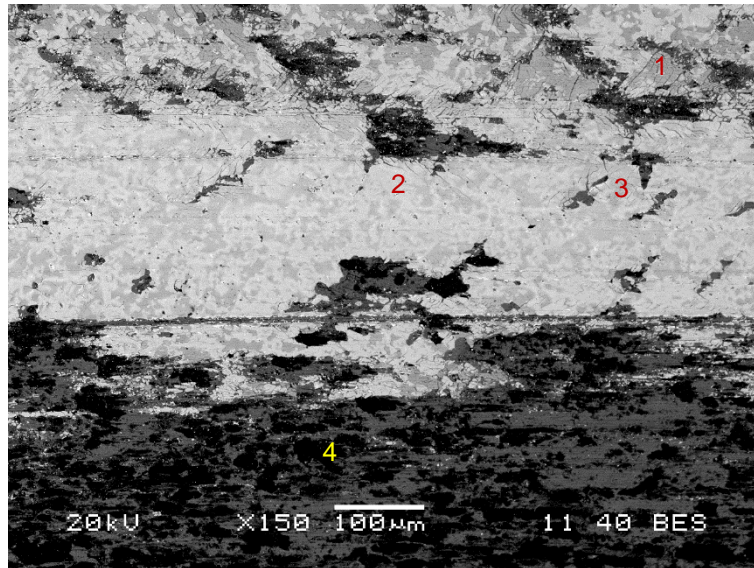
Figure 4.55. Scanning Electron Microscope (Backscattering) images of the wear track of coating ref. #DLCVB after the electro-tribology test (1: cracks; 2: interlayer; 3: Cu substrate; and 4: Al adhesion).
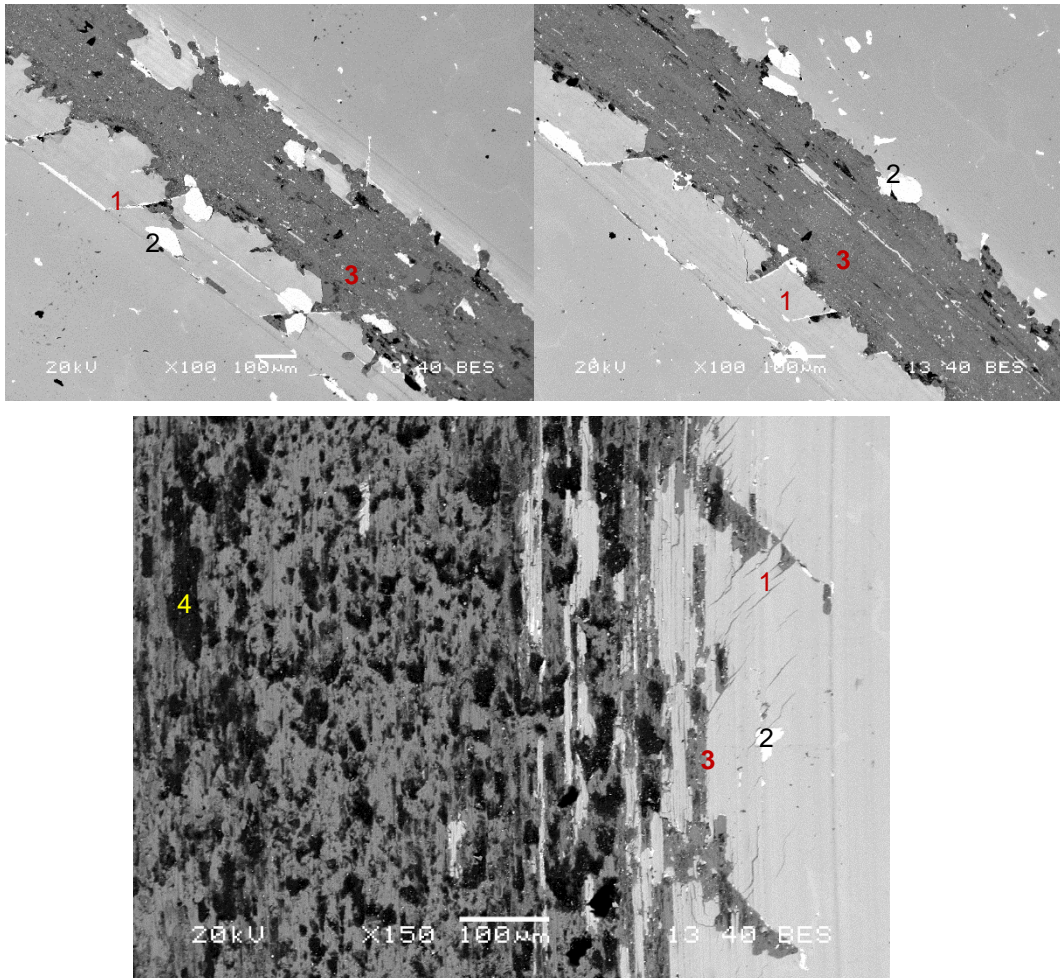
Figure 4.56. Scanning Electron Microscope (Backscattering) images of the wear track of coating ref. #DLCCH after the electro-tribology test (1: cracks; 2: interlayer; 3: Cu substrate; and 4: Al adhesion).
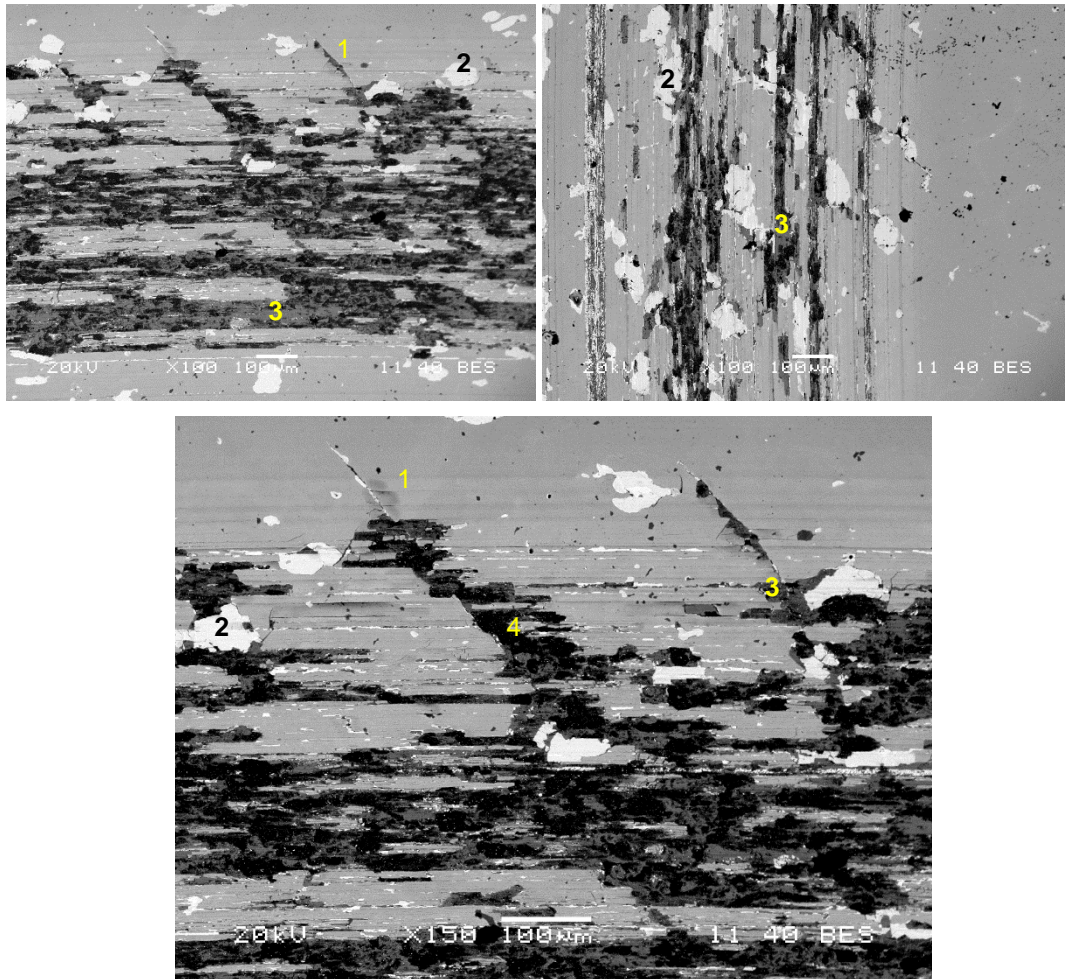
Figure 4.57. Scanning Electron Microscope (Backscattering) images of the wear track of coating ref. #DLCVB (a), #DLCCH (b) and #DLC (c) after the electro-tribology test (1: cracks; 2: interlayer; 3: Cu substrate; and 4: Al adhesion).

Tribological properties of DLC coatings are known to be highly dependent on the relative percentage of **humidity** (%RH) of the surrounding atmosphere (Savage 1948), (Deacon and Goodman 1958) (Grandin and Wiklund 2018). Therefore, the electro-tribology properties of coating ref. #DLC were also studied at different percentages of relative humidity (Figure 4.58, Figure 4.59 and Figure 4.60).

It was found that increasing values of relative humidity caused an extension of the coating life as a dielectric coating in the tested conditions (Figure 4.61). It reached 17,000 cycles at 10% RH (Figure 4.58), but lengthened to 48,000 cycles at 50% RH (Figure 4.51), and to 60,000 cycles at 90% RH (Figure 4.59). On the contrary, lower RH corresponded with lower CoF.

This trend is in accordance with results published elsewhere, which have also observed higher CoF values as the relative humidity increased, although the precise characteristics of the DLC coating and tribological tests conditions were not exactly the same, and overall CoF values were lower (Wang, et al. 2016). One of the reasons argued consists on the deceleration of the graphitization of the coating due to humidity, which prevents formation of hot spots, and blocks the adsorption and diffusion of hydrogen atoms (Luo, Fridrici and Kapsa 2011). The increase of the CoF of hydrogenated DLC coatings in humid air has also been attributed to the increase in the van der Waals bond strength of hydrogen bonding to adsorbed water molecules compared to hydrocarbons (Gardos 1994).
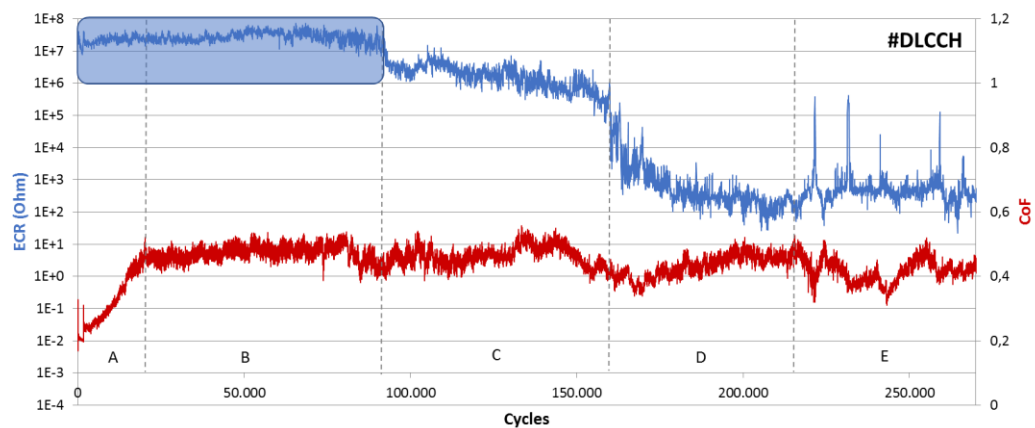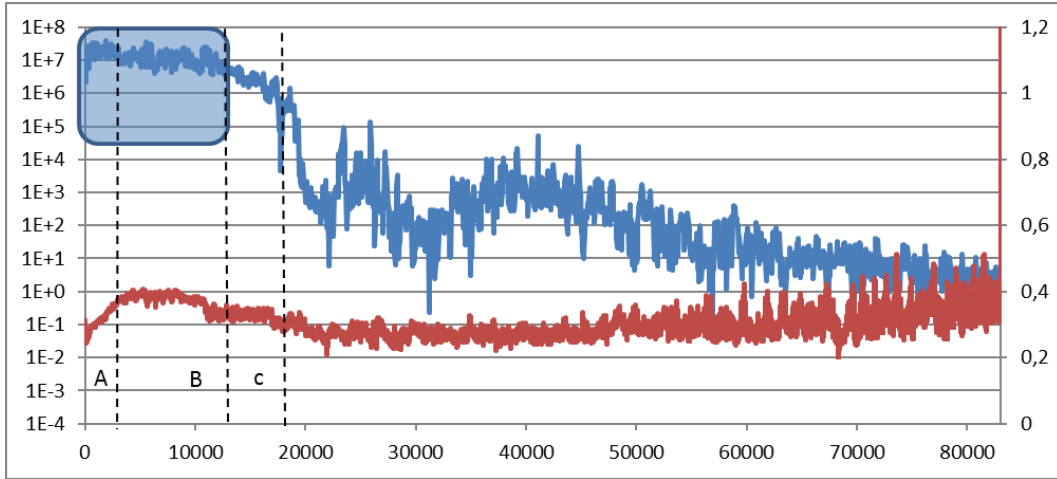
Figure 4.58. ECR (Ω; logarithmic scale on the left vertical axis; above) and CoF (right vertical axis; below) evolution of ref. #DLC against aluminum along the test cycles (horizontal axis), at 10% of relative humidity. Shadowed blue area on the left upper side indicates electric resistance values above the upper limit of the ohmmeter.
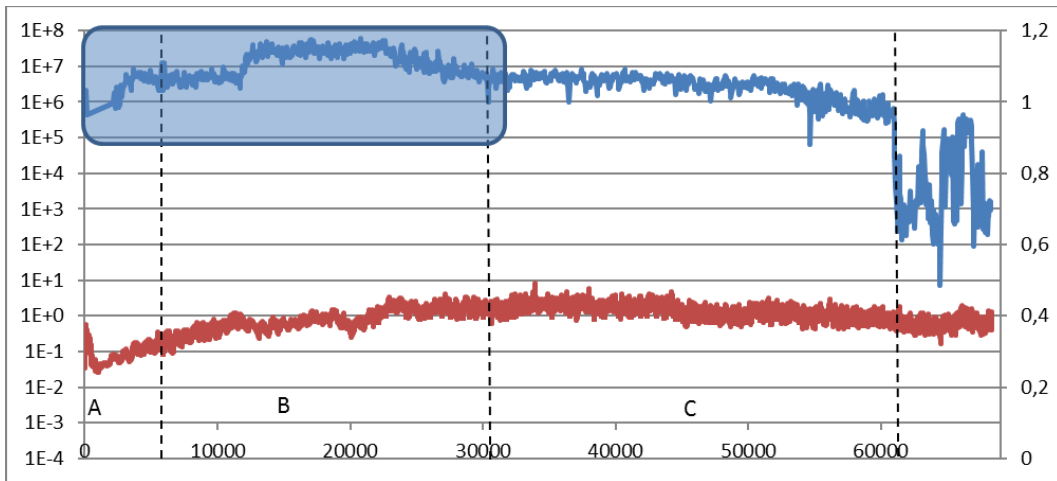
Figure 4.59. ECR (Ω; logarithmic scale on the left vertical axis; above) and CoF (right vertical axis; below) evolution of ref. #DLC against aluminum along the test cycles (horizontal axis), at 90% of relative humidity. Shadowed blue area on the left upper side indicates electric resistance values above the upper limit of the ohmmeter.
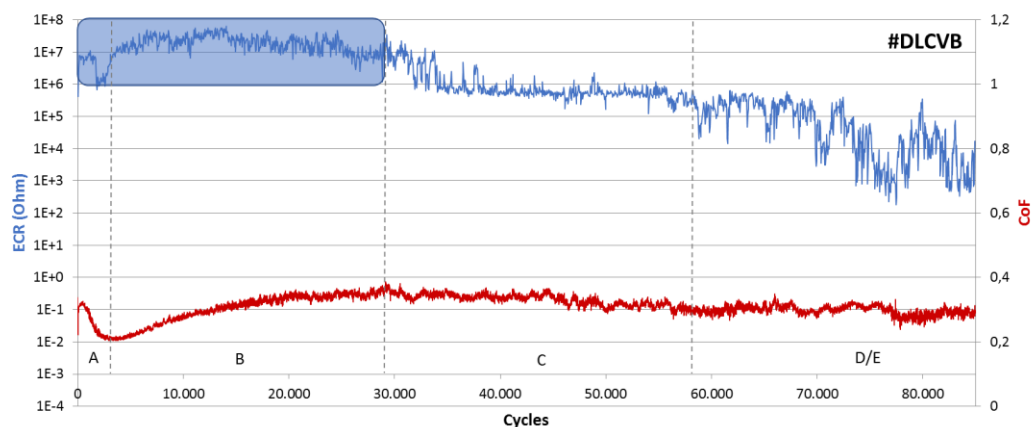
189
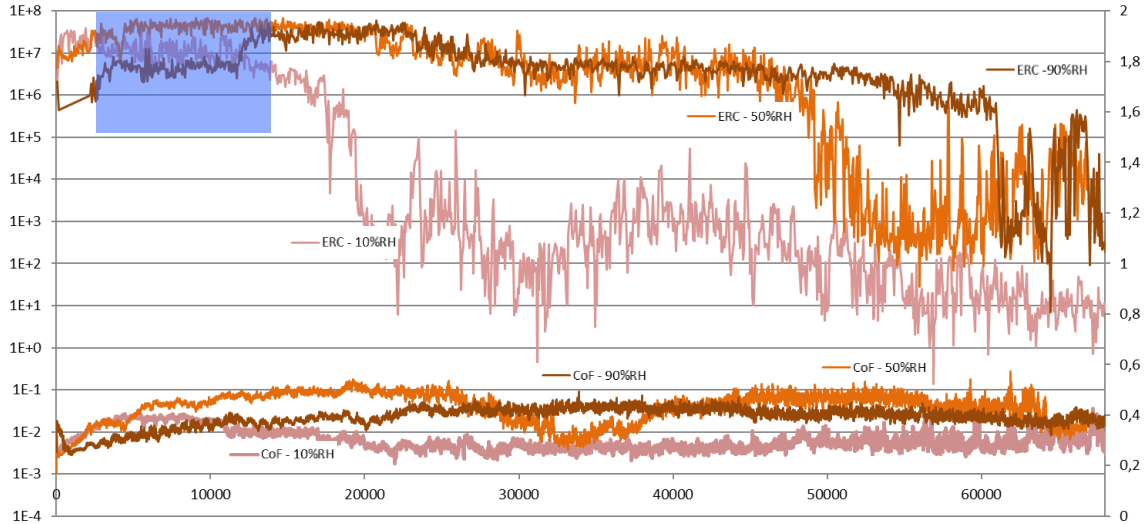
Figure 4.60. ECR (Ω; logarithmic scale on the left vertical axis; above) and CoF (right vertical axis; below) evolution of ref. #DLC coatings against aluminum along the test cycles (horizontal axis), at different relative percentages of humidity: 10% (Figure 4.58), 50% (Figure 4.51) and 90% (Figure 4.59). Shadowed blue area on the left upper side indicates electric resistance values above the upper limit of the ohmmeter.
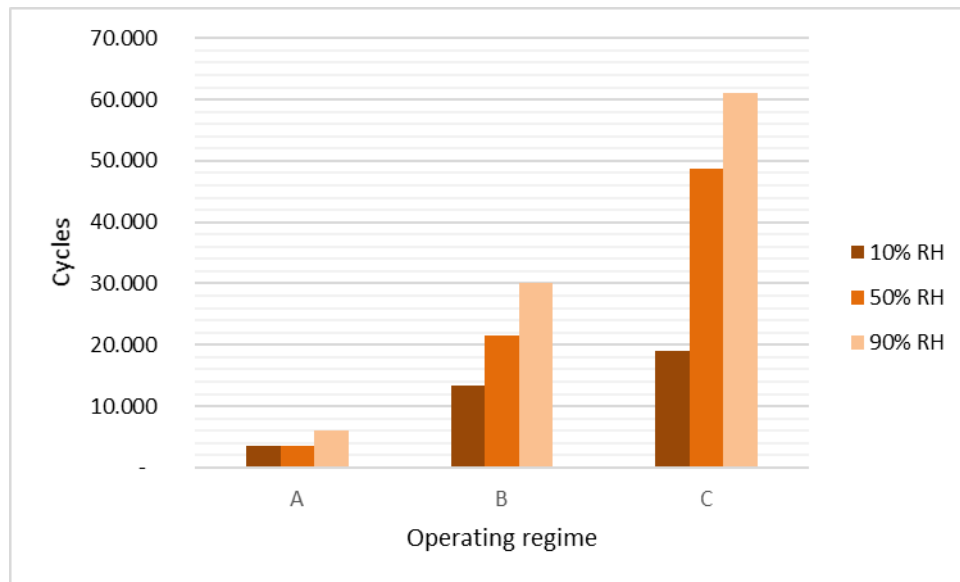
Figure 4.61. Number of cycles (vertical axis) for each operating regime and degree of relative humidity of coating ref. #DLC against aluminum, and trend line (A, B and C as decribed in Figure 4.51, Figure 4.58 and Figure 4.59).

It should also be noted that the CoF values measured in this work are relatively high as compared with values reported elsewhere. One of the reasons might be that the degree of graphitization of the DLC coating has been relatively low, due to the formation of few hot spots because the aluminum counterpart is a good thermal conductor, and the contact load was relatively small (Brizuela, et al. 2002). In this study, where DLC was deposited on copper substrates, the level of oxidation of the outer copper surface, exposed by the wear of the coating, could also have played a role, as the low humidity (10%RH) test have shown both lower CoF and ECR as compared to higher humidity conditions once the coating worn out. Otherwise, the ECR performance and evolution of the coating was qualitatively similar, independent of the relative humidity.

Finally, it could be expected that in more hydrophobic DLCs, such as those of ref. #DLCCH and #DLCVB, the drop in operative life of the coating to occur at higher levels of relative humidity as compared to those of coating #DLC.

To sum up, in this study the DLC coatings have shown to have good electro-tribological features, of potential interest in applications where a dielectric surface is necessary in sliding contact conditions.

ECR have proved to be a good monitoring tool for the status of the DLC coating, independently of the working media, i.e. relative humidity. Formation of cracks, spalling-off of the coating, adhesive wear and surface oxidation are behind the coating degradation when tested against aluminum. This degradation can be tracked by the evolution of the ECR, in such a way that the coating operational life could be defined predictively.

Therefore, electro-tribological data has demonstrated to be potentially useful in the framework of coating development and optimization, as it provides key information about the failure modes. Additionally, it could prove useful in on-line monitoring systems of the degradation of coated parts in operation.

5.   CONCLUSIONS

The **objective** of this thesis has consisted on the development of plasma based surface treatments and coatings with two specific functionalities, supported by electro-tribology studies, as a tool to study the degradation mechanisms of selected surfaces, their operative lives in electrical applications, and eventually explore the potential of electro-tribology as monitoring tool of parts and components in operation.

Improving the tribological properties of two stainless steel alloys and geometries, without compromising their corrosion resistance defined the **first functionality**. Multiple sectors such as aeronautics, marine industry, food and biomedical devices, architecture, chemical processing and a diversity of machinery, consumer goods, etc. could potentially benefit from this functionality. The two alloys studied were an austenitic and a precipitation hardening martensitic stainless steels. The surface treatments developed were based on plasma nitriding, with a combination of Active Screen Plasma and Hollow Cathode effect technologies. The developments focused on the inner diameter surfaces of tube geometries in the first austenitic alloy, and on the other surface of cylindrical geometries in the PH martensitic alloy.

The **second functionality** consisted on dielectric and electrically conductive coatings for electrical sliding applications. Two distinct PVD deposited coatings were studied on Cu substrates for each dielectric and conductive property: DLC coatings and AgAl alloy coatings respectively. Multiple electrical components could benefit from these kinds of

coatings in sliding electrical contacts, including in electrical transformers, engines, transportation vehicles, etc., supporting the developments in the field of smart grids and the electrical car.

In the whole study, the **hypotheses** consisted on i) the assumption that electro-tribology studies will prove useful in the development of the coatings / surfaces, and the monitoring of their operative status; ii) hollow plasma could be useful in reaching valuable compromises between the corrosion resistance and tribological performance of stainless steel alloys; iii) silver-aluminum based coatings could improve the electro-tribological performance of current silver coatings; and iv) DLC based coatings are a promising option for dielectric sliding contacts.

Concerning the **stainless steel** alloys:

- The combination of active screen plasma nitriding with the hollow cathode effect produces thicker nitride layers as compared with conventional plasma nitriding. This hollow cathode has two related main effects: denser plasma and a higher part temperature. This might be beneficial or detrimental for the nitriding of stainless steel with preservation of a good corrosion resistance

- The positive or negative effect depends on the plasma processing conditions, which must be optimized for each geometry or gas mix.

- When the plasma density is high, the process duration short enough, and the process temperature is kept low, nitride layers can still retain good corrosion resistance, as measured by SST. This holds true for both alloys and geometries, and is linked to causing a low level of chromium precipitates in some outer regions of the nitrided layer.

- In the case of the nitrided PH alloy, these surfaces presented steady and high CoF. This could be useful, in applications where rolling regimes are preferred in opposition to sliding regimens.

- Continuous or periodic monitoring of the **ECR** could provide in both cases insightful information about the system status, evolution and conditions of the tribological regime. Eventually it might be a good predictor with respect to the

surface performance, if the conditions of the tribological system are known to a certain extent, because the ECR is sensitive to variations in the humidity, contact pressure, etc. This might prove especially useful on inner geometries, which often does not present an easy inspection access.

Concerning the **sliding electrical coatings**:

- The studies have confirmed that the coating often used in conductive sliding contacts, e.g. transformers, silver, presents good electrical properties but very poor tribology, and readily reacts to form deleterious silver sulfides.

- On the contrary, the silver aluminum alloy coating variations studied have shown much better tribological properties than silver, both in terms of friction and wear.

- This was even more marked in the under oil conditions studied, which corresponds to the operational conditions of many sliding electrical contact applications.

- The performance of AgAl coatings was linked to the content of aluminum. The coatings with larger Al content and HCP microstructure overperformed those with FCC microstructure and lower Al content.

- It was also found that aluminum content in the coating alloy could modify the wear mechanism from adhesive to a more erosive/abrasive mode. This was true for different Al percentages if the sliding occurred under oil or in air, occurring at lower Al contents under oil.

- It was also concluded that the aluminum content in the coating alloy reduces its reactivity with sulphur.

- Overall, among the AgAl studied, the case of a 37% of aluminum content, presented the lowest wear rate and the sulfur intake was minimized.

- On the other hand, the proclivity to oxidation raised, and increasing the Al content in the alloy resulted in an increase in the electrical contact resistance, especially in static conditions, and to a lesser extent in dynamic sliding conditions.

- The DLC coatings studied have also shown to have good dielectric and electro-tribological features.

- Formation of cracks, spalling off of the coating, adhesive wear and surface oxidation were behind the coating degradation (tested against aluminum).

- In both cases though, the electro-tribological performance of the coating has proven to be dependent on the **media**: under oil and in air conditions resulted in different outcomes in the case of the AgAl coatings, and humidity conditioned those obtained in the DLC coatings.

- **ECR** data has provided valuable information about the operational performance of both coatings, complementary to that provided by the CoF.

- Use of ECR as a monitoring tool has shown different results though in each case. ECR have proved to be a good monitoring tool for the status of the DLC coating, independently of the working media, i.e. relative humidity. The degradation of the coating could be tracked by the evolution of the ECR. Potentially, the coating operational life could be defined predictively, if the working conditions were to be known.

- In the case of the AgAl coatings ECR data as a monitoring tool was not proven, as it would have required more extensive studies, because of sulphur and / or oxygen uptake behind the degradation of the coating under oil, takes much longer than in air conditions. …

6.   FUTURE RESEARCH DIRECTIONS

From the results obtained in the study around the two main objectives of the work, development of plasma based surface treatments and coatings with two specific functionalities, and exploring the potential of electro-tribology as a tool, the following topics are suggested for future research:

In the case of the nitrided stainless steel alloys,

- The understanding of why certain regions of the nitrided layer keep enough free Cr should require further research, with the use of additional surface analysis techniques.

- ECR monitoring has been explored on flat surfaces. It should be investigated in more complex configurations, beginning with inner cylinder surfaces.

- Treatments have proved to be quite geometry sensitive. They are also sensitive to the gas mix. Investigations on whether other gas mixes provide more ample treatment windows could be of interest.

- The study of the corrosion resistance should be extended to cases other than the salt spray, and eventually to tribo-corrosion studies.

In the case of the Ag based coatings,

- Like on like electro-tribology studies (i.e. Ag_xAl_y vs. Ag_xAl_y) should provide additional relevant knowledge,

- Considering that some potential applications are subject to a thermal cycle, electro-tribology studies should be expanded to include high temperature tests,

- The potential of other Ag based alloys should also be explored, be it ternary AgAlMe alloys or alloying elements other than Al (Me = Metallic element).

- In the case of the AgAl coatings ECR data as a monitoring tool, more extensive studies would be required, as the degradation of the surfaces under oil, because of sulphur and / or oxygen uptake, takes much longer than in air conditions.

In the case of the DLC dielectric coatings,

- Research into the monitoring capabilities of ERC should be further investigated on complex, no flat, geometries.

- It would also be of interests the performance of the electro-tribological tests with ohmmeters with a higher range of measurements capabilities. It could allow the study of the earlier stages of coating degradation.

Additionally,

- Electro-tribology tests and environmental tests have been carried out separately in this work. As synergetic effects might arise, it would be of interests the undertaking of simultaneous electro-tribo-corrosion studies (with corrosion not only limited to humidity or salt spray).

7. PUBLICATIONS

A number of publications have been prepared along the works related to the thesis, as well as different contributions to scientific international congresses, with poster, oral and invited talks. Details of the contributions are listed next.

Scientific papers in indexed journals (SJR)

- BRACERAS, I.; IBÁÑEZ, I.; DOMÍNGUEZ-MEISTER, S.; URGEBAIN, A.; SÁNCHEZ-GARCÍA, J.A.; LARRAÑAGA, A.; and GARMENDIA, I. Corrosion preserving high density plasma treatment of precipitation hardening stainless steel. Surface and Coatings Technology, 355 (2018) 174–180. ISSN: 02578972.
DOI: 10.1016/j.surfcoat.2018.01.036.

  SJR CiteScore rank (2017): Q1 (17/109) Materials Science, Surfaces, Coatings and Films. CiteScore 2017=3.08. SJR 2017 = 0.928.

- BRACERAS, I.; IBÁÑEZ, I.; DOMÍNGUEZ-MEISTER, S.; SÁNCHEZ-GARCÍA, J.A.; BRIZUELA, M.; LARRAÑAGA, A.; and GARMENDIA, I. Plasma nitriding of the inner surface of stainless steel tubes. Surface and Coatings Technology, 355 (2018) 116–122. ISSN: 02578972.
DOI: 10.1016/j.surfcoat.2018.04.057.

  SJR CiteScore rank (2017): Q1 (17/109) Materials Science, Surfaces, Coatings and Films. CiteScore 2017=3.08. SJR 2017 = 0.928.

- BRACERAS, I.; IBÁÑEZ, I.; TAHER, M.; MAO, F.; DEL BARRIO, A.; SAENZ DE URTURIA, S.; BERASTEGUI, P.; ANDERSSON, A.M.; JANSSON, U. On the Electro-Tribological Properties and Degradation Resistance of Silver-Aluminum Coatings. Wear, 414-415 (2018) 202-211. ISSN: 0043-1648.
DOI: 10.1016/j.wear.2018.08.014

SJR CiteScore rank (2017): Q1 (39/336) Engineering, Mechanics of Materials. CiteScore 2017=3.31. SJR 2017 = 1.386.

- BRACERAS, I.; IBAÑEZ, I.; DOMINGUEZ-MEISTER, S.; VELASCO, X.; BRIZUELA, M.; and GARMENDIA, I. Electro-tribological properties of diamond like carbon coatings. Submitted for publication to an indexed scientific journal.

Contribution to international scientific congresses.

- BRACERAS, I.; DOMÍNGUEZ-MEISTER, S.; IBÁÑEZ, I.; BRIZUELA, M.; and GARMENDIA, I. Electro-tribology of carbonaceous coatings.
  Conference: *Iberian Vacuum Conference, RIVA-X. 8th European Topical Conference on Hard Coatings. Bilbao, Spain, 4-6 October 2017.*
  Type of Participation: Poster

- BRACERAS, I.; IBÁÑEZ, I.; DOMÍNGUEZ-MEISTER, S.; URBEGAIN, A.; BRIZUELA, M.; LARRAÑAGA, A.; and GARMENDIA, I.   Hardening of precipitation hardening stainless steel by Plasma treatment.
  Conference: *Iberian Vacuum Conference, RIVA-X. 8th European Topical Conference on Hard Coatings. Bilbao, Spain, 4-6 October 2017.*
  Type of Participation: Poster

- BRACERAS, I.; IBÁÑEZ, I.; DOMÍNGUEZ-MEISTER, S.; URBEGAIN, A.; SÁNCHEZ-GARCÍA, J.A.; LARRAÑAGA, A.; and GARMENDIA, I. Corrosion preserving high density plasma treatment of precipitation hardening steel.
  Conference: *20th international conference on surface modification of materials by ion beams. Lisbon, Portugal,* 9-14 July 2017*.*
  Type of Participation: Oral

- BRACERAS, I.; IBÁÑEZ, I.; DOMÍNGUEZ-MEISTER, S.; SÁNCHEZ-GARCÍA, J.A.; BRIZUELA, M.; LARRAÑAGA, A.; and GARMENDIA, I. Plasma nitriding of the inner surface of stainless steel pipes.
  Conference: *20th international conference on surface modification of materials by ion beams. Lisbon, Portugal,* 9-14 July 2017*.*
  Type of Participation: Poster

- BRACERAS, I.; DOMÍNGUEZ-MEISTER, S.; IBÁÑEZ, I.; BRIZUELA, M.; CORENGIA, P.; and LARRAÑAGA, A.. Active screen plasma treatment of Cr42Mo4 (AISI 4140) and tribo-corrosion performance.
  Conference: *20th international conference on surface modification of materials by ion beams. Lisbon, Portugal,* 9-14 July 2017*.*
  Type of Participation: Poster

- BRACERAS, I.; DOMÍNGUEZ-MEISTER, S.; IBÁÑEZ, I.; BRIZUELA, M.; CORENGIA, P.; and LARRAÑAGA, A.. Active screen plasma treatment of Cr42Mo4 (AISI 4140) and tribo-corrosion performance.
Conference: *20th international conference on surface modification of materials by ion beams. Lisbon, Portugal,* 9-14 July 2017*.*
Type of Participation: Poster

- BRACERAS, I.; ALVAREZ, N.; MARTINEZ, M.; BRIZUELA, M.; AZKONA, I.; GARMENDIA, I. Plasma Based Wear Resistant Anti-Microbial Surfaces on Medical Devices and Its Monitoring.
Conference: *MRS Materials Reseach Society Fall Meeting & Exhibit 2016. Lisbon, Boston, Massachussets, USA, 27 Nov – 2 Dec, 2016.*
Type of Participation: Invited talk.

- BRACERAS, I.; VELASCO, X.; BRIZUELA, M.; GARMENDIA, I.; and SÁNCHEZ-GARCÍA, J.A. Electro-tribological study of dielectric surfaces.
Conference: *Plasma Surface Engineering 2016. Garmisch-Partenkirchen, Germany, 12-16 September, 2016.*
Type of Participation: Poster

- BRACERAS, I. Plasma-Enhanced Chemical Vapour Deposition PECVD II Session.
Conference: *Plasma Surface Engineering 2016. Garmisch-Partenkirchen, Germany, 12-16 September, 2016.*
Type of Participation: Chairman.

- BRACERAS, I.; SÁNCHEZ-GARCÍA, J.A.; MUSGO, M.; LARRAÑAGA, A.; BRIZUELA, M.; and CORENGIA, P. Active Screen Plasma Nitriding of austenitic stainless steel inner diameters.
Conference: *Plasma Surface Engineering 2016. Garmisch-Partenkirchen, Germany, 12-16 September, 2016.*
Type of Participation: Poster

8. REFERENCES

Acevedo-Hurtado, P.O., P.A. Sundaram, P.G. Caceres-Valencia, E.R. Fachini, C.E. Miller, and B.E. Placzankis. "Characterization of atmospheric corrosion in Al/Ag lap joints." *Corrosion Science* 50 (2008): 3123–3131.

Agoston, A., C. Ötsch, and B. Jakoby. "Viscosity sensors for engine oil condition monitoring—Application and interpretation of results." *Sensors and Actuators A* 121 (2005): 327–332.

André, B., E. Lewin, U. Jansson, and U. Wiklund. "Friction and contact resistance of nanocomposite Ti–Ni–C coatings." *Wear* 270 (2011): 555–566.

Argibay, N., S.V. Prasad, R.S. Goeke, M.T. Dugger, and J.R. Michael. "Wear resistant electrically conductive Au–ZnO nanocomposite coatings synthesized by e-beam evaporation." *Wear* 302 (2013): 955–962.

ASM International Handbook Committee. *ASM Handbook Volume 4: Heat Treating.* Materials Park, Ohio, USA: ASM International, 1991.

—. *ASM Handbook Volume 5: Surface Engineering.* Materials Park, Ohio, USA: ASM International, 1994.

Bader, M.E., R.P. Hall, and G. Strasser. "Integrated Processing Equipment." *Solid State Technology* 33 (1990): 149-154.

Barua, A., H. Kim, and I. Lee. "Effect of the amount of CH4 gas on the characteristics of surface layers of low temperature plasma nitrided martensitic precipitation-hardening stainless steel." *Surface and Coatings Technology* 307 (2016): 1034–1040.

BCC Research. *MFG015G: Physical Vapor Deposition (PVD): Global Markets.* Wellesley, MA, USA: BCC Research, 2016.

Beebe, R.S. "9: Other condition monitoring methods." In *Predicitive Maintenance of Pumps Using Condition Monitoring*, 146-154. Elsevier Science, 2004.

Belin, M. "The wear behavior of a thin MoS2 coating, as studied by triboscopic measurements in friction and electrical contact resistance." In *Lubrication at the Frontier*, by M. Priest P. Ehret L. Flamand G. Dalmaz T.H.C. Childs D. Dowson Y. Berthier C.M. Taylor A Lubrecht J.M. Georges, 439-448. Elsevier Science, 1999.

Ben Amor, Y., et al. "Electrochemical study of the tarnish layer of silver deposited on glass." *Electrochimica Acta* 131 (2014): 89–95.

Bewilogua, K., et al. "Surface technology for automotive engineering." *CIRP Annals - Manufacturing Technology* 58 (2009): 608-627.

Booth, J.E., T.J. Harvey, R.J.K. Wood, and H.E.G. Powrie. "Scuffing detection of TU3 cam–follower contacts by electrostatic charge condition monitoring." *Tribology International* 43 (2010): 113–128.

Bouchoucha, A., S. Chekroud, and D. Paulmier. "Influence of the electrical sliding speed on friction and wear processes in an electrical contact copper–stainless steel." *Applied Surface Science* 223 (2004): 330–342.

Braceras, I., et al. "Corrosion Preserving High Density Plasma Treatment of Precipitation Hardening Stainless Steel." *Surface and Coatings Technology* 355 (2018): 174-180.

Braceras, I., et al. "On the Electro-Tribological Properties and Degradation Resistance of Silver-Aluminum Coatings." *Wear* 414–415 (2018): 202–211.

Braceras, I., et al. "Plasma Nitriding of the Inner surface of Stainless Steel Pipes." *Surface and Coatings Technology* 355 (2018): 116-122.

Braceras, I., I. Ibañez, S. Dominguez-Meister, X. Velasco, M. Brizuela, and I Garmendia. "Electro-tribological properties of diamond like carbon coatings." - , 2019: -.

Braunović, M., V.V. Konchits, and N. K. Myshkin. *Electrical Contacts, Fundamentals, Applications and Technology.* Boca Raton, FL, USA: Taylor & Francis Group, 2006.

Brizuela, M., A. Garcia-Luis, J.L. Viviente, I. Braceras, and J.I. Oñate. "Tribological study of lubricious DLC biocompatible coatings." *Journal of Materials Science: Materials in Medicine* 13 (2002): 1129-1133.

Bronshteyna, L.A., and J.H. Kreiner. "Energy efficiency of industrial oils." *Tribology Transactions* 42, no. 4 (1999): 771–776.

Brühl, S. P., R. Charadia, S. Simison, D.G. Lamas, and A. Cabo. "Corrosion behavior of martensitic and precipitation hardening stainless steels treated by plasma nitriding." *Surface and Coatings Technology* 204 (2010): 3280–3286.

Bucca, G., and A. Collina. "Electromechanical interaction between carbon-based pantograph strip and copper contact wire: A heuristic wear model." *Tribology International* 92 (2015): 47–56.

Budinski, K.G. *Surface Engineering for Wear Resistance.* Prentice-Hall, 1988.

Bundesministerium Für Förschung und Technologie. *Tribologie (Code BMFT-FBT76-38).* Research Report (T76-38) (Code BMFT-FBT76-38), West Germany: Bundesministerium Für Förschung und Technologie, 1976.

Chang, Y.P. "A novel method of using continuous tribo-electrification variations for titanium specimens." *Wear* 262 (2007): 411–423.

Chang, Y-P. "Indirect monitoring of the dynamics at the contact interfaces of a pair of abrading titanium specimens." *Wear* 266 (2009): 1119–1127.

Chang, Y-P., Y-C. Chiou, and R.T. Lee. "Tribo-electrification mechanisms for dissimilar metal pairs in dry severe wear process. Part II. Effect of load." *Wear* 264 (2008): 1095–1104.

Chen, Z., P. Liu, J.D. Verhoeven, and E.D. Gibson. "Electrotribological behavior of Cu-15 vol.% Cr in situ composites under dry sliding." *Wear* 203-204 (1997): 28-35.

Chu, H.Y., and J.F Lin. "Experimental analysis of the tribological behavior of electroless nickel-coated graphite particles in aluminum matrix composites under reciprocating motion." *Wear* 239 (2000): 126–142.

Clarke, A., I.J.J. Weeks, H.P. Evans, and R.W. Snidle. "An investigation into mixed lubrication conditions using electrical contact resistance techniques." *Tribology International* 93 (2016): 709–716.

Corujeira Gallo, S., and H. Dong. "New insights into the mechanism of low-temperature active-screen plasma nitriding of austenitic stainless Steel." *Scripta Materialia* 67, no. 1 (2012): 89-91.

Corujeira Gallo, S., and H. Dong. "Study of active screen plasma processing conditions for carburising and nitriding austenitic stainless Steel." *Surface and Coatings Technology* 203 (2009): 3669-3675.

Dalibon, E.L., V. Trava-Airoldi, L.A. Pereira, A. Cabo, and S.P. Brühl. "Wear resistance of nitrided and DLC coated PH stainless steel." *Surface and Coatings Technology* 255 (2014): 22–27.

Darken, L.S., and R.W. Gurry. *Physical Chemistry of Metals.* New York: McGraw-Hill, 1953.

de Sousa, R.R.M., F.O. de Araujo, J.A.P. da Costa, T. Dumelow, R.S. de Oliveira, and C. Alves. "Nitriding in cathodic cage of stainless steel AISI 316: Influence of sample position." *Vacuum* 83 (2009): 1402-1405.

Deacon, R.F., and J.F. Goodman. "Lubrication by lamellar solids." *Wear* 243A (1958): 464-482.

Dong, H. "S-phase surface engineering of Fe-Cr, Co-Cr and Ni-Cr alloys." *International Materials Reviews* 55 (2010): 65-98.

Dong, H., M. Esfandiari, and X.Y. Li. "On the microstructure and phase identification of plasma nitrided 17-4PH precipitation hardening stainless steel." *Surface and Coatings Technology* 202 (2008): 2969–2975.

Erdemir, A. "Genesis of super low friction and wear in diamondlike carbon films." *Tribology International* 37 (2004): 1005–1012.

Esfandiari, M., and H. Dong. "The corrosion and corrosion–wear behaviour of plasma nitrided17-4PH precipitation hardening stainless steel." *Surface and Coatings Technology* 202 (2007): 466–478.

Fernández de Ara, J., E. Almandoz, J.F. Palacio, and G.G. Fuentes. "Simultaneous ageing and plasma nitriding of grade 300 maraging steel: How working pressure determines the effective nitrogen diffusion into narrow cavities." *Surface and Coatings Technology* 317 (2017): 64–67.

Ferrari, A. C., and J. Robertson. "Interpretation of Raman spectra of disordered and amorphous carbon." *Physical Review B* 61, no. 20 (2000): 14095-14107.

Fiaud, C., and J. Guinement. "The effect of nitrogen dioxide and chlorine on the tarnishing of copper and silver in the presence of hydrogen sulfide." *Proceedings of the Electrochemical Society* 86, no. 6 (1986): 280-304.

Field, S.K., M. Jarratt, and D.G. Teer. "Tribological properties of graphite-like and diamond-like carbon coatings." *Tribology International* 37 (2004): 949–956.

Gardos, M.N. "Tribology and wear behavior of diamond." In *Synthetic diamond: emerging CVD science and technology*, by Dismukes JP (editors) Spear KE, Gardos MN. Tribology and wear behavior of diamond. In: Spear KE, Dismukes JP, editors. Synthetic diamond: emerging CVD science and technology, New York: John Wiley & Sons, Inc; 1994, p. 419. New York, USA: John Wiley & Sons, Inc, 1994.

Glavatskih, S., and E. Höglund. "Tribotronics—Towards active tribology." *Tribology International* 41 (2008): 934–939.

Graedel, T. E. "Corrosion Mechanisms for Silver Exposed to the Atmosphere." *Journal of The Electrochemical Society* 139, no. 7 (1992): 1963–1970.

Grandin, M., and U. Wiklund. "Friction, Wear and tribofilm formation on electrical contact materials in reciprocating sliding against silver-graphite." *Wear* 302 (2013): 1481–1491.

Grandin, M., and U. Wiklund. "Influence of mechanical and electrical load on a copper/copper-graphite sliding electrical contact." *Tribology International* 121 (2018): 1-9.

Grill, A. "Diamond-like carbon: state of the art." *Diamond and Related Materials* 8 (1999): 428-434.

Grill, A. "Electrical and optical properties of diamond-like carbon." *Thin Solid Films* 355-356 (1999): 189-193.

Grill, A. "Tribology of diamondlike carbon and related materials: an updated review." *Surface and Coatings Technology* 91-95 (1997): 507-513.

Hasea, A., and H. Mishina. "Identification and evaluation of wear phenomena under electric current by using an acoustic emission technique." *Tribology International* 127 (2018): 372–378.

He, D.H., and R. Manory. "A novel electrical contact material with improved self-lubrication for railway current collectors." *Wear* 249 (2001): 626–636.

He, D.H., R. Manory, and H. Sinkis. "A sliding wear tester for overhead wires and current collectors in light rail systems." *Wear* 239 (2000): 10–20.

He, M., S. Lee, and C.D. Yeo. "Investigating atomic structure of thin carbon film under mechanical stress and frictional heat generation." *Surface and Coatings Technology* 261 (2015): 79-85.

Helmi Attia, M. "On the fretting wear mechanism of Zr-alloys." *Tribology International* 39 (2006): 1320–1326.

Holt, A.F., et al. "Silver corrosion in transformers, Electrical Insulation and Dielectric Phenomena." *(CEIDP) 2013 IEEE Conference Proceedings*, 2013: 448-451.

Hombo, R., et al. "Tribological and Electrical Contact Behavior of Metal/DLC Nanocomposite Coating on Brass Substrate." *40th Leeds-Lyon Symposium on Tribology & Tribochemistry Forum*, 2013.

Hong, W., W. Cai, S Wang, and M.M. Tomovic. "Mechanical wear debris feature, detection, and diagnosis: A review." *Chinese Journal of Aeronautics* 31, no. 5 (2018): 867–882.

Hoshiyama, Y., R. Mizobata, and H. Miyake. "Mechanical properties of austenitic stainless steel treated by active screen plasma nitriding." *Surface and Coatings Technology* 307, no. B (2016): 1041-1044.

Institute of materials and machine mechanics SAS, v. v. i. *Physical vapor deposition.* 2016. http://www.umms.sav.sk/6493-en/physical-vapor-deposition/ (accessed 10 19, 2018).

International Organization for Standarization. «ISO 9227. Corrosion tests in artificial atmospheres- Salt Spray Tests.» Geneva, Switzerland, 2012.

Janosi, S., Z. Kolozsvary, and A. Kis. "Controlled hollow cathode effect: new possibilities for heating low pressure furnaces." *Metal Science and Heat Treatment* 46, no. 7-8 (2004): 310-311.

Jost, Peter. *Lubrication (Tribology) - A report on the present position and industry's needs.* London, UK.: Department of Education and Science, H. M. Stationary Office., 1966.

Keller, J., V. Fridrici, Ph. Kapsa, and J.F. Huard. "Surface topography and tribology of cast iron in boundary lubrication." *Tribology International* 42 (2009): 1011–1018.

Kim, Y. M., and J. G. Han. "Spectroscopic study for pulsed DC plasma nitriding of narrow deep holes." *Surface and Coatings Technology* 171 (2003): 205-210.

Kimura, Y. "Maintenance tribology: its significance and activity in Japan." *Wear* 207 (1997): 63–66.

Köster, K., P. Kaestner, G. Bräuer, H. Hoche, and M. Oechsner. "Material condition tailored to plasma nitriding process for ensuring corrosion and wear resistance

of austenitic stainless Steel." *Surface and Coatings Technology* 228 (2013): 615-618.

Kusiak, A., Z. Zhang, and A. Verma. "Prediction, operations, and condition monitoring in wind energy." *Energy* 60 (2013): 1-12.

Laporte, J., O. Perrinet, and S. Fouvry. "Prediction of the electrical contact resistance endurance of silver-plated coatings subject to fretting wear, using a friction energy density approach." *Wear* 330-331 (2015): 170–181.

Larisch, B., U. Brusky, and H.J. Spies. "Plasma nitriding of stainless steels at low temperatures." *Surface and Coatings Technology* 116 (1999): 205-211.

Leyland, A., D.B. Lewis, P.R. Stevensom, and A. Matthews. "Low temperature plasma diffusion treatment of stainless steels for improved wear resistance." *Surface and Coating Technology* 62, no. 1–3 (1993): 608-617.

Li, C.X., and T. Bell. "Corrosion properties of active screen plasma nitrided 316 austenitic stainless steel." *Corrosion Science* 46, no. 6 (2004): 1527-1547.

Li, Y., S. Zhang, Y. He, L. Zhang, and L. Wang. "Characteristics of the nitrided layer formed on AISI 304 austenitic stainless steel by high temperature nitriding assisted hollow cathode discharge." *Materials & Design* 64 (2014): 527–534.

Lin, K., X. Li, Y. Sun, X. Luo, and H. Dong. "Active screen plasma nitriding of 316 stainless steel for the application of bipolar plates in proton exchange membrane fuel cells." *International Journal of Hydrogen Energy* 39 (2014): 21470-21479.

Liu, Y., A. Erdemir, and E.I. Meletis. "A study of the wear mechanism of diamond-like carbon films." *Surface and Coatings Technology* 82 (1996): 48-56.

Liu, Y., A. Erdemir, and E.I. Meletis. "An investigation of the relationship between graphitization and frictional behavior of DLC coatings." *Surface and Coating Technology* 86-87 (1996): 564-568.

Liu, Y., A. Erdemir, and E.I. Meletis. "Influence of environmental parameters on the frictional behavior of DLC coatings." *Surface and Coating Technology* 94-95 (1997): 463-468.

Liu, Y., Z. Liu, Y. Xi, and Z. Yao. "Research on an on-line wear condition monitoring system for marine diesel engine." *Tribology International* 33 (2000): 829–835.

Lo, K.H., C.H. Shek, y J.K.L. Lai. «Recent developments in stainless steels.» *Materials Science and Engineering R Reports* 65 (2009): 39–104.

Luo, D.B., V. Fridrici, and Ph. Kapsa. "A systematic approach for the selection of tribological coatings." *Wear* 271 (2011): 2132–2143.

Majdoub, F., M. Belin, J.M. Martin, J. Perret-Liaudet, M. Kano, and K. Yoshida. "Exploring low friction of lubricated DLC coatings in no-wear conditions with a new relaxation tribometer." *Tribology International* 65 (2013): 278-285.

Mao, F., et al. "Combinatorial Study of Gradient Ag−Al Thin Films: Microstructure, Phase Formation, Mechanical and Electrical Properties." *ACS Applied Materials & Interfaces* 8 (2016): 30635-30643.

Mao, F., M. Taher, P. Berastegui, A.M. Andersson, and U. Jansson. "Tuning tribological, mechanical and electrical properties of Ag-X (X=Al, In, Sn) alloys." *Tribology International* 125 (2018): 121-127.

McAlister, A. J. "The Ag−Al (Silver-Aluminum) System." *Bull. Alloy Phase Diagrams* 8, no. 6 (1987): 526-533.

Minfray, C., J.M. Martin, T. Lubrecht, M. Belin, and T. Le Mogne. "A novel experimental analysis of the rheology of ZDDP tribofilms." *Tribological Research and Design for Engineering Systems*, 2003: 807-817.

Mingolo, N., A.P. Tschiptschin, and C.E. Pinedo. "N. Mingolo, A.P. Tschiptschin, C.E. Pinedo, On the formation of expanded austenite during plasma nitriding of an AISI 316L austenitic stainless steel." *Surface and Coatings Technology* 201 (2006): 4215-4218.

Minzari, D., M.S. Jellesen, P. Møller, and R. Ambat. "Morphological study of silver corrosion in highly aggressive sulfur environments." *Engineering Failure Analysis* 18, no. 8 (2011): 2126-2136.

Muhl, S., and A. Pérez. "The use of hollow cathodes in deposition processes: A critical review." *Thin Solid Films* 579 (2015): 174–198.

Myers, M. "The Performance Implications of Silver as a Contact Finish in Traditionally Gold Finished Contact Applications." *Proceedings of the 55th IEEE HOLM 2009 Conference on Electrical Contacts*, 2009.

Naeem, M., M. Shafiq, M. Zaka-ul-Islam, N. Nawaz, J.C. Díaz-Guillén, and M. Zakaullah. "Effect of cathodic cage size on plasma nitriding of AISI304 steel." *Materials Letters* 181 (2016): 78–81.

Nedfors, N., D. Primetzhofer, L. Wang, J. Lud, L. Hultmand, and U. Jansson. "Characterization of magnetron sputtered Cr–B and Cr–B–C thin films for electrical contact applications." *Surface and Coatings Technology* 266 (2015): 167–176.

Nie, M., and L. Wang. "Review of condition monitoring and fault diagnosis technologies for wind turbine gearbox." *Procedia CIRP* 11 (2013): 287–290.

Nikolov, K., K. Bunk, A. Jung, P. Kaestner, G. Bräuer, and C.P. Klages. "High-efficient surface modification of thin austenitic stainless steel sheets applying short-time plasma nitriding by means of strip hollow cathode method for plasma thermochemical treatment." *Vacuum* 110 (2014): 106-113.

Nikolov, K., K. Köster, P. Kaestner, G. Bräuer, y C.P. Klages. «Strip hollow cathode method for plasma thermochemical treatment for surface modification of thin metal strips: Plasma nitriding of austenitic stainless steel sheets for bipolar plates.» *Vacuum* 102 (2014): 31-37.

Nygren, K., M. Samuelsson, A. Flink, H. Ljungcrantz, A. Kassman Rudolphi, and U. Jansson. "Growth and characterization of chromium carbide films deposited by high rate reactive magnetron sputtering for electrical contact applications." *Surface and Coatings Technology* 260 (2014): 326–334.

Oñate, J.I., et al. "Wear reduction effect on ultra-high-molecular-weight polyethylene by application of hard coatings and ion implantation on cobalt chromium alloy, as measured in a knee wear simulation machine." *Surface and Coatings Technology* 142-144 (2001): 1056-1062.

Ou, K.L., H.H. Chou, C.M. Liu, and P.W. Peng. "Surface modification of austenitic stainless steel with plasma nitriding for biomedical applications." *Surface and Coatings Technology* 206 (2011): 1142–1145.

Palomar, T., B. Ramírez Barat, E. García, and E. Cano. "A comparative study of cleaning methods for tarnished silver." *Journal of Cultural Heritage* 17 (2016): 20-26.

Pantazopoulos, G., et al. "Sliding wear behaviour of a liquid nitrocarburised precipitation-hardening (PH) stainless steel." *Surface and Coatings Technology* 187 (2004): 77– 85.

Pinedo, C.E., et al. "Low temperature active screen plasma nitriding of 17–4 PH stainless steel." *Surface and Coatings Technology* 308 (2016): 189–194.

Podgornik, B., and J. Vižintin. "Tribology of thin films and their use in the field of machine elements." *Vacuum* 68, no. 1 (2002): 39-47.

Rigou, V.I., G. Marginean, D. Frunzăverde, and C.V. Câmpian. "Silver based composite coatings with improved sliding wear behavior." *Wear* 290–291 (2012): 61–65.

Robertson, J. "Diamond-like amorphous carbon." *Materials Science and Engineering: R: Reports* 37, no. 4–6 (2012): 129-281.

Rudolphi, A.K., and S. Jacobson. "Stationary loading, fretting and sliding of silver coated copper contacts - influence of corrosion films and corrosive atmosphere." *Tribology International* 30, no. 3 (1997): 165-175.

Salameh, J.P., S. Cauet, E. Etien, and A. Sakout. "Gearbox condition monitoring in wind turbines: A review." *Mechanical Systems and Signal Processing* 111 (2018): 251–264.

Sampuran-Singh, K. V. Anand. "Electrochemical properties of dielectric films of aluminium oxide deposited on silicon." *Thin Solid Films* 37 (1976): 453-460.

Savage, R.H. "Graphite lubrication." *Journal of Applied Physics* 19 (1948): 1-10.

Shen, L., L. Wang, and J.J. Xu. "Plasma nitriding of AISI 304 austenitic stainless steel assisted with hollow cathode effect." *Surface and Coatings Technology* 228 (2013): S456–S459.

Simonovic, K., and M. Kalin. "Experimentally derived friction model to evaluate the anti-wear and friction-modifier additives in steel and DLC contacts." *Tribology International* 111 (2017): 116–137.

Song, J., and V. Schinow. "Correlation between friction and wear properties and electrical performance of silver coated electrical connectors." *Wear* 330-331 (2015): 400–405.

Sun, Y. "Y.Sun, Tribocorrosive behavior of low temperature plasma-nitrided PH stainless steels liding against alumina under linear reciprocation with and without transverse oscillations." *Wear* 362-363 (2016): 105–113.

Taher, M., F. Mao, P. Berastegui, A.M. Andersson, and U.. Jansson. "The Influence of Chemical and Phase Composition on Mechanical, Tribological and Electrical Properties of Silver-Aluminum Alloys." *Tribology International* 119 (2018): 680-687.

Takeno, T., H. Saito, M. Goto, J. Fontaine, H. Miki, and M. Belin. "Deposition, structure and tribological behavior of silver–carbon nanocomposite coatings." *Diamond & Related Materials* 39 (2013): 20–26.

Tandon, N., K.M. Ramakrishna, and G.S. Yadava. "Condition monitoring of electric motor ball bearings for the detection of grease contaminants." *Tribology International* 40 (2007): 29–36.

Torres Pérez, A., G. García-Atance Fatjó, M. Hadfield, and S. Austen. "A model of friction for a pin-on-disc configuration with imposed pin rotation." *Mechanism and Machine Theory* 46, no. 11 (2011): 1755–1772.

«Tribology Science Industrial Application Status and Development Strategy. The investigation on position and function of tribology in industrial energy conservation, consumption and emission reduction.» Report of 2 year Chinese Investigation, 2009.

Trinh, K.E., A. Tsipenyuk, M. Varenberg, A. Rosenkranz, N. Souza, and F. Mücklich. "Wear debris and electrical resistance in textured Sn-coated Cu contacts subjected to fretting." *Wear* 344-345 (2015): 344-345.

Tzanakis, I., M. Hadfield, B. Thomas, S.M. Noya, I. Henshaw, and S. Austen. "Future perspectives on sustainable tribology." *Renewable and Sustainable Energy Reviews* 16 (2012): 4126–4140.

Vakis, A.I., et al. "Modeling and simulation in tribology across scales: An overview." *Tribology International* 125 (2018): 169–199.

Vetter, J. "60 years of DLC coatings: Historical highlights and technical review of cathodic arc processes to synthesize various DLC types, and their evolution for industrial applications." *Surface and Coating Technology* 257 (2014): 213–240.

Wahl, K.J., M. Belin, and I.L. Singer. "A triboscopic investigation of the wear and friction of MoS2 in a reciprocating sliding contact." *Wear* 214 (1998): 212-220.

Wan, Y., X. Wang, X. Wang, Y. Li, H. Sun, and K. Zhang. "Determination and Generation of the Corrosion Compounds on Silver Exposed to the Atmospheres." *International Journal of Electrochemical Science* 10 (2015): 2336-2354.

Wang, F., Z. Lu, L. Wang, G. Zhang, and Q. Xu. "Effect of tribochemistry on friction behavior of fluorinated amorphous carbon films against aluminum." *Surface and Coatings Technology* 304 (2016): 150–159.

Wang, P., T. Takagi, T. Takeno, and H. Miki. "Early fatigue damage detecting sensors. A review and prospects." *Sensors & Actuators, B* 198 (2013): 46–60.

Wikipedia. n.d. https://en.wikipedia.org/wiki/Plasma_(physics) (accessed August 13, 2018).

Yang W.J., Zhang M. , Zhao Y.H. , Shen M.L. , Lei H. , Xu L. , Xiao J.Q. ,Gong J. ,Yu B.H. , Sun C. "Enhancement of mechanical property and corrosion resistance of 316 L stainless steels by low temperature arc plasma nitriding." *Surface and Coatings Technology* 298 (2016): 64-72.

Yang, J.B., C.B. Lin, T.C. Wang, and H.Y. Chu. "The tribological characteristics of A356.2Al alloy/Gr(p) composites." *Wear* 257 (2004): 941–952.

Ye, Z., H. Moon, M.H. Lee, and A. Martini. "Size and load dependence of nano scale electric contac tresistance." *Tribology International* 71 (2014): 109–113.

Yu, Q., G. Huang, M. Cai, F. Zhou, and W. Liu. "In situ zwitterionic supramolecular gel lubricants for significantly improved tribological properties." *Tribology International* 95 (2016): 55–65.

Zagonel, L., C. Figueroa, R. Droppajr, and F. Alvarez. "Influence of the process temperature on the steel microstructure and hardening in pulsed plasma nitriding." *Surface and Coatings Technology* 201, no. 1-2 (2006): 452-457.

Zhang, M., X. Wang, X Fu, and Y. Xia. "Performance and anti-wear mechanism of CaCO3 nanoparticles as a green additive in poly-alpha-olefin." *Tribology International* 42 (2009): 1029–1039.

Zhang, S.W. *Current industrial activities in China and green tribology.* London, UK.: Institution of Engineering & Technology, 2009.

Zhu, X., C. Zhong, and J. Zhe. "Lubricating oil conditioning sensors for online machine health monitoring – A review." *Tribology International* 109 (2017): 473–484.